Synthesis and Reactivity of Low Valent Main Group Element Complexes

Terry Chu

Chemistry

A thesis

Submitted to the Faculty of Graduate Studies

In partial fulfillment of the requirements for the

Degree of Doctor of Philosophy

Department of Chemistry

Faculty of Mathematics and Science

Brock University

St. Catharines, Ontario

Abstract

The β-diketiminate aluminum(I) complex NacNacAl (**III-1**) was shown to activate a range of substrates containing robust single and double bonds. Compound **III-1** oxidatively adds a variety of H–X bonds (X = H, B, Al, C, Si, N, P, O) to give a series of four-coordinate aluminum hydride derivatives including the first example of an aluminum boryl hydride. In the case of Al–H addition, the reaction was shown to be in equilibrium and reversible. Furthermore, cleavage of aryl and alkyl C–F bonds, the latter a rare reaction with only a handful of examples in the literature, was observed with **III-1**. Robust C–O and C–S bonds were also activated by **III-1** along with RS–SR and R_2P–PR_2 bonds. All novel aluminum complexes were characterized by spectroscopic methods and X-ray diffraction analysis for the majority of them. Activation of the C=S or P=S bonds in a thiourea or phosphine sulfide, respectively, was accomplished by **III-1** to give the first examples of Lewis base-stabilized monomeric terminal aluminum sulfides. The nature of the Al=S bond was examined computationally as well as experimentally. Related reaction with a urea derivative gave an unexpected aluminum hydride while reaction of **III-1** with phosphine oxides gave a putative aluminum oxide as a result of P=O bond cleavage. However, the aluminum oxo promptly deprotonates a neighbouring molecule to furnish an aluminum hydroxide as the isolated product.

Reduction of the cationic germanium(II) complex **IV-1** affords the formally zero valent germanium complex **IV-4** stabilized by the bis(imino)pyridine platform. Compound **IV-4** was fully characterized by spectroscopic methods and X-ray diffraction analysis. The molecule has a singlet ground state and DFT studies revealed partial delocalization of one of the germanium lone pairs into the ligand framework. Complex

IV-4 was unreactive towards H–X bond activation, the lack of reactivity ascribed to the large singlet-triplet energy gap calculated. The same bis(imino)pyridine ligand was also used to prepare reduced zinc complexes. Monoreduction of the zinc dichloride precursor gave the formally Zn(I) compound **IV-6**. Further reduction of **IV-6** in the presence of DMAP gave the formally zero valent zinc complex **IV-9**. Both compounds were fully characterized by spectroscopic methods, DFT calculations, and X-ray diffraction analysis which revealed that both zinc atoms are four-coordinate and adopt unusual square planar and see-saw geometry, respectively.

Acknowledgements

First and foremost, I would like to thank my supervisor Dr. Georgii Nikonov for the opportunity to work in his research group. Your enthusiasm and insatiable desire for chemisty is an inspiration and I hope some of that has rubbed off on me during my time in the group. Thank you for giving me the opportunity to grow and develop as a chemist.

I would like to thank my graduate committee members Dr. Heather Gordon and Dr. Tony Yan for their helpful suggestions and support. Dr. Theocharis Stamatatos and Dr. Paul Zelisko are acknowledged for their participation in my candidacy examination. Thank you to Dr. Joffre Mercier for helping convince me to come to Brock and for being a friendly face on and off campus. This thesis would not have been possible without the excellent staff members at Brock. Many, many thanks are extended to Jordan and John Vandenhoff from the glassblowing shop, Steve Crumb from the machine shop, and Irene Palumbo, Jenn Roberts, and Alison Moffat from the Science Stores. Special thanks to Razvan Simionescu for his expertise and invaluable assistance with all things related to NMR.

A number of collaborators must be thanked for their role in bringing this thesis to fruition. Thank you to Dr. Art van der Est and Dr. Prashanth Poddutoori for acquiring, analyzing, and interpreting the EPR data. I am appreciative of the computational studies performed by Lee Belding, Dr. Travis Dudding, and Dr. Sergei Vyboishchikov which were crucial in order to get a better understanding of the molecules prepared for this thesis. I am grateful to Dr. Ilya Korobkov, Dr. Bulat Gabidullin, Dr. Judith Howard, and Dr. Lyudmila Kuzmina for their role in collecting and solving absolutely vital X-ray diffraction data.

I would like to extend my gratitude to the former and current members of the Nikonov lab for their comraderie and friendship: Dr. Tori Lee, Courtney Boone, Van Hung Mai, Yaroslav Boyko, Kostya Piatrou, Iryna Alshakova, Minh Tho Nyugen, Kayla Jakobsson, and John Lortie. In particular, I want to thank Dr. Kseniya Revunova and Nick McLeod for all the excellent times we had together. Other members of the Brock chemistry department must also be thanked for their support and friendship: Dr. Emma Stares, Majeda Al Hareri, Zemane W'Giorgis, Kassandra Emberson, Dr. Sergey Vshyvenko, Dr. Vimal Varghese, and Dr. Sam Mula. You have all made a big impact in my life!

Finally, I must thank my parents, Colin and Tania, and my sister Teena for their endless support and unending love. None of this would be possible without you.

Table of Contents

Abbreviations

$\{^1H\}$	proton decoupled
°C	degrees Celsius
δ	chemical shift
$\Delta H^{\ddagger}$	activation enthalpy
$\Delta S^{\ddagger}$	activation entropy
3c-4e	three centreed-four electron bonding
Å	Angström
Ar	2,6-diisopropylphenyl
atm	atmosphere (1 atm = 1 bar, 760 mm Hg, 101.3 kPa, 14.969 psi)
Bn	benzyl
br	broad (NMR)
*c*AAC	cyclic alkyl amino carbene
Cp*	η^5-C_5Me_5
Cy	cyclohexyl
d	doublet (NMR)
DCM	dichloromethane
DFT	density functional theory
Dipp	2,6-diisopropylphenyl
DMAP	4-dimethylaminopyridine
e	electron
Et	ethyl
g	gram(s)
h	hour(s)
hept	heptet (NMR)
HOMO	highest occupied molecular orbital
Hz	Hertz
^{i}Pr	isopropyl
IR	infrared spectroscopy
J	coupling constant (NMR)
k	reaction rate constant
K	Kelvin

LUMO	lowest unoccupied molecular orbital
M	central metal atom in a complex
m	*meta*
m	multiplet (NMR)
Me	methyl
Mes	mesityl
MHz	megahertz
mmol	millimol(s)
MO	molecular orbital
NacNac	*β*-diketiminate
NHC	N-heterocyclic carbene
NMR	nuclear magnetic resonance
o	*ortho*
p	*para*
Ph	phenyl
q	quartet (NMR)
RT	room temperature
s	singlet (NMR)
t	triplet (NMR)
^{t}Bu	*tert*-butyl
THF	tetrahydrofuran
TMS	trimethylsilyl
Tol	tolyl
Tripp	2,4,6-triisopropylphenyl
VT	variable temperature

List of Figures

List of Schemes

List of Tables

I. Introduction

Interest in main group chemistry has undergone a significant surge in the last twenty years. This resurgence is due to advances in ligand design and synthetic methodologies that have allowed for the synthesis and isolation of novel main group complexes that were previously too reactive to handle and store under ambient conditions.[1-6] With access to these complexes, novel reactivity that was previously unknown for main group elements has been demonstrated. Of particular note are low valent main group complexes that have displayed reactivity that was previously pertinent only to transition metal complexes. This particular aspect is of great relevance as main group complexes could come to replace transition metal complexes, a desirable goal due to the recognized toxicity and scarcity of the late transition metals, as catalysts for a variety of chemical transformations in the future.[7]

The contents of this thesis are divided into two major sections. The first involves the activation of robust single and double bonds by a low valent aluminum complex. The *β*-diketiminate aluminum(I) complex was first reported by Roesky and co-workers sixteen years ago[8] and ample reactivity of the molecule have been subsequently reported.[5] However, a noted absence was the reactivity of the aluminum(I) complex towards compounds with σ-bonds. As such, the oxidative addition of various H–X (X = H, B, Al, C, Si, N, P, and O), C–Y (Y = F, O, S), RS–SR, and $R_2P–PR_2$ bonds by the aluminum(I) complex will be presented. As well, cleavage of E=S and E=O (where E is carbon or phosphorus) bonds by the Al(I) species will also be discussed.

The second half of the thesis entails the synthesis and characterization of novel low valent germanium and zinc complexes. While divalent germanium complexes are

well known in the literature,[5,6] recent reports have disclosed the preparation of germanium complexes in the zero valent oxidation state stabilized by carbene-based ligands.[9,10] With the idea of extending this chemistry towards different ligand environments in the hope of engendering original structural features and modes of reactivity, the synthesis and characterization of a Ge(0) complex stabilized by the bis(imino)pyridine ligand will be presented. Furthermore, the chemistry will be extended to zinc and the preparation of monomeric, formally Zn(I) and Zn(0) bis(imino)pyridine complexes will be discussed.

The following historical section of the present thesis includes an account of bond activation by main group complexes as well as an overview of the chemistry of aluminum in the +1 oxidation state. This is followed by the detailed summary of compounds with heavier Group 14 elements in the zero valent oxidation state.

II. Historical

II.1 Bond Activation by Main Group Element Complexes

Historically there has been a sharp divide between the reactivity of transition metal compounds and main group element compounds. Due to the presence of partially occupied valence d orbitals that are often relatively close in energy, the chemistry of the transition metals is viewed to be richer than that of the main group elements. It is well known that transition metal complexes often interact with small molecules such as CO, C_2H_4, or H_2 and can mediate activation of robust bonds.[11] While there are exceptions, main group compounds are generally not known to participate in such reactions. Recent advances in the last 20 years have started to change this viewpoint due to the availability of main group compounds that were previously thought to be unstable. These include compounds with multiple bonds between heavier main group elements,[3,4] stable low-valent derivatives with open coordination sites,[5,6] and stable paramagnetic compounds with unpaired electrons centreed on heavier main group elements[1] or stable singlet diradicaloid electron configurations.[2] Common to all of these new species is the presence of frontier orbitals with small energy separations, a feature more often associated with transition metal complexes. This has resulted in the ability of many main group compounds to exhibit behaviour akin to transition metal complexes, particularly the ability to activate robust bonds.[7] This portion of the historical will give an overview of the various bond activations that have been mediated by main group element complexes. Outside the purview of this literature review is the chemistry of Frustrated Lewis Pairs (FLP) first reported by Stephan and co-workers.[12,13] In this thesis, focus is placed on bond activation by single-site main group complexes whereas FLP systems generally employ

an intermolecular pair of sterically hindered Lewis acid and base to promote bond activation and catalysis. FLP chemistry has recently been extensively reviewed.[14-16]

II.1.1 H–H Bond Activation

Activation of dihydrogen by transition metal complexes has been studied comprehensively for many decades.[17] On the other hand, the same reaction with main group elements and their compounds is poorly studied, with scattered reports of vapor phase reactions of dihydrogen with heavier group 13 elements, typically upon photoactivation, with the products trapped in a frozen matrix.[18-20] Only within the last decade has activation of dihydrogen been realized with main group element complexes in solution and in the solid state, first demonstrated by Power and co-workers in 2005.[21] Since then the activation of dihydrogen has been expanded to a multitude of complexes with main group elements spanning Groups 13 to 15.

II.1.1.1 Group 13 Complexes

Piers and co-workers reported the rapid reaction of hydrogen with the highly Lewis acidic, antiaromatic perfluoropentaphenylborole (**II-1**) in both solution and solid state (Scheme 1).[22] The products, *cis*- and *trans*- isomers of boracyclopent-3-ene (**II-2**), are the result of the addition of hydrogen atoms to the carbons α to boron in **II-1**. The mechanism was probed via kinetic studies and DFT calculations and was revealed to begin with 1,2-addition of dihydrogen across the B–C_α bond of **II-1** followed by 1,2-hydride migration to give *cis*-**II-2** or a kinetically competitive pathway involving ring opening, during which rotation about the B–C_α bond is unrestricted, followed by rapid cyclization and 1,2-hydride migration to give the *trans* isomer of **II-2**.[23]

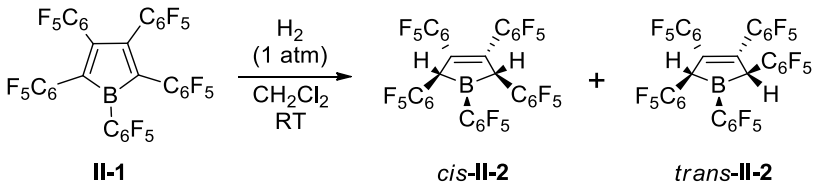

Scheme 1. Activation of H_2 by perfluoropentaphenylborole **II-1**.

In 2014, the groups of Bertrand and Stephan reported the isolation of a *c*AAC-aminoborylene adduct (**II-3**) which featured an allenic structure, supported by the crystal structure obtained from X-ray diffraction analysis.[24] Compound **II-3** readily activates dihydrogen leading to the *c*AAC-borane adduct (**II-4'**), which was unstable and rearranged to the final product **II-4** through a 1,2-hydride migration (Scheme 2). The two-step process was supported by calculations, with both steps being strongly exergonic ($\Delta G = -18$ and -12 kcal mol^{-1}, respectively).

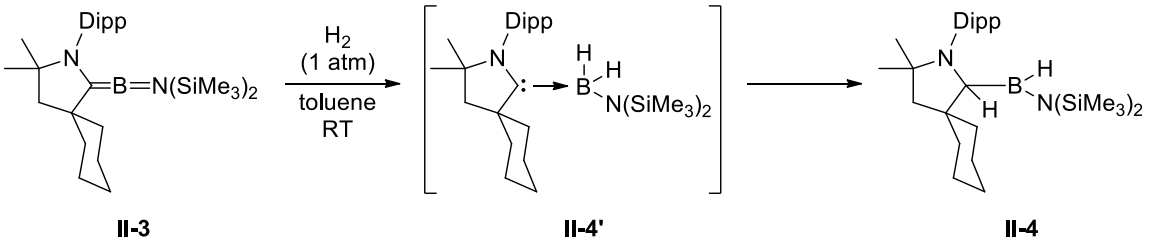

Scheme 2. H_2 activation by *c*AAC-aminoborylene adduct **II-3**.

Gallium containing compounds have also been shown to activate dihydrogen. Utilizing the digallane species $Ar^{Dipp}Ga{=}GaAr^{Dipp}$ (**II-5**, Ar^{Dipp} = 2,6-(2,6-$^{i}Pr_2C_6H_3)_2C_6H_3$), which partly dissociates into monomeric $Ar^{Dipp}Ga$: in solution, reaction with H_2 gave a dimeric gallium hydride derivative, $\{Ar^{Dipp}Ga(\mu\text{-}H)H\}_2$ (**II-6**) with two bridging and two terminal hydrogen atoms (Scheme 3).[25] As both the dimeric and monomeric forms are present in solution, theoretical calculations were carried out to determine which form is activating dihydrogen. The calculations revealed that the activation energy for the reaction of $Ar^{Dipp}Ga$: with H_2 is approximately 50 kcal mol^{-1}.

Such a significant barrier effectively ruled out the pathway involving digallane dissociation. Instead, it was shown that the mechanism starts with the addition of one equivalent of H_2 to **II-5** to give the 1,2-dihydride intermediate ($Ar^{Dipp}HGaGaHAr^{Dipp}$) that reacted further with another equivalent of H_2, resulting in cleavage of the Ga–Ga bond and formation of two equivalents of $Ar^{Dipp}GaH_2$. Subsequent dimerization of the two monomeric units led to the formation of **II-6**.[26]

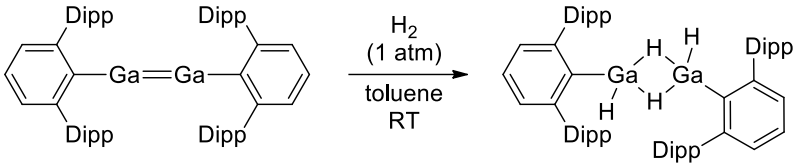

II-5 **II-6**

Scheme 3. Dihydrogen activation by digallane **II-5**.

The gallium(I) β-diketiminate compound NacNacGa (**II-7**; NacNac = $[ArNC(Me)CHC(Me)NAr]^-$, Ar = 2,6-$^{i}Pr_2C_6H_3$) also reacts with dihydrogen to give the gallium dihydride $NacNacGaH_2$ (**II-8**).[27] The closely related zwitterionic gallium(III) species NacNac'Ga^{t}Bu (**II-9**; NacNac' = $[ArNC(=CH_2)CH=C(Me)NAr]^{2-}$), prepared via dehydrohalogenation of NacNacGaBr(^{t}Bu) with $K[CH_2(SiMe_3)_2]$, also reacts with H_2. DFT calculations revealed that the HOMO primarily resides on the terminal carbon of the exocyclic alkene moiety while the LUMO is dominated by Ga 4p character. Consistent with the calculations, reaction of **II-9** with dihydrogen afforded the 1,4-addition product NacNacGaH(^{t}Bu) (**II-10**) as shown in Scheme 4.[28]

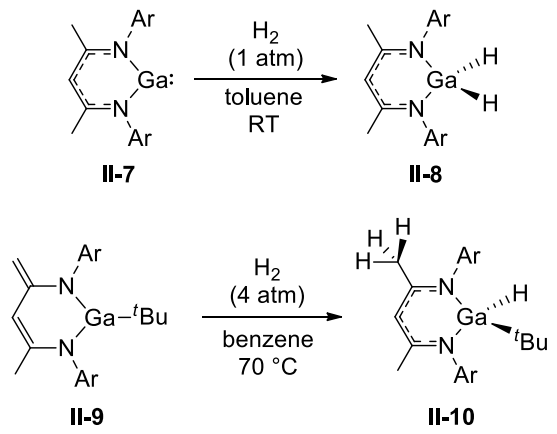

Scheme 4. 1,1- and 1,4-addition of H_2 by *β*-diketiminate gallium complexes.

II.1.1.2 Group 14 Complexes

Singlet carbenes contain a vacant orbital and a lone pair of electrons in a non-bonding orbital, a situation reminiscent of the frontier molecular orbitals of transition metal fragments. Thus, it was proposed that carbenes could exhibit reactivity similar to the transition metals. Although typical Arduengo-type N-heterocyclic carbenes, either with saturated or unsaturated rings, do not react with H_2, both the cyclic alkyl amino carbene **II-11** and the acyclic alkyl amino carbene **II-13** activate the H–H bond to give the alkane products **II-12** and **II-14**, respectively, at 35 °C (Scheme 5).[29] Theoretical studies revealed that the difference in reactivity between the two types of carbenes is correlated to their singlet-triplet energy gap, calculated to be 46 kcal mol^{-1} for *c*AACs versus 68 kcal mol^{-1} for NHCs. Calculations also showed that activation of dihydrogen by the singlet carbene proceeded via a heterolytic mechanism. The initial step is the donation of electron density from the carbene lone pair to the antibonding σ* orbital of H_2, leading to elongation and polarization of the H–H bond and asymmetric carbon–hydrogen distances in the transition state. Afterwards, the hydridic end of $H^{\delta+}$–$H^{\delta-}$ attacks

the positively polarized carbene centre, resulting in complete scission of the H–H bond to give the alkane products.

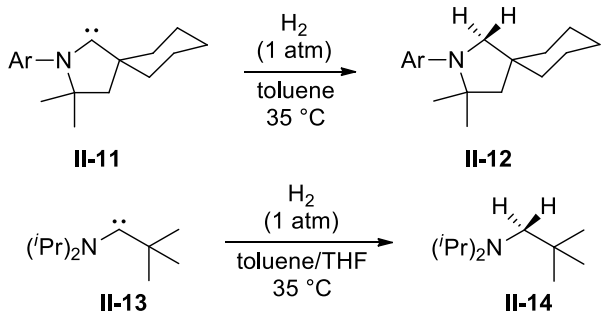

Scheme 5. Activation of H_2 by cyclic (**II-11**) and acylic (**II-12**) alkyl amino carbenes.

Silylenes have also been demonstrated to activate dihydrogen. The groups of Aldridge, Jones, and Mountford have synthesized the stable mixed amido boryl silylene Si(B(NArCH–)$_2$)(N(SiMe$_3$)Ar) (**II-15**) and revealed the facile activation of dihydrogen in benzene (proceeding even at 0 °C) to give the dihydrosilane H_2Si(B(NArCH–)$_2$)(N(SiMe$_3$)Ar) (**II-16**), in quantitative yield (Scheme 6).[30] The production of **II-16** from **II-15** is the first experimentally observed activation of H_2 by a silylene. Thermodynamically, the activation of H_2 is calculated to be strongly exergonic (ΔG = −29.2 kcal mol^{-1}), while kinetically the computed value of $\Delta G^{\ddagger}$ (23.3 kcal mol^{-1}) is consistent with the observed activation at or below room temperature.

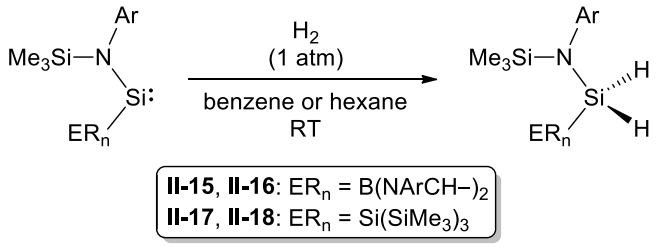

Scheme 6. Dihydrogen activation by silylenes **II-15** and **II-17**.

Similarly, the silyl coordinated silylene $Si(Si(SiMe_3)_3)(N(SiMe_3)Ar)$ (**II-17**), prepared by the same groups, can also split dihydrogen at room temperature in hexane to give the corresponding dihydrosilane $H_2Si(Si(SiMe_3)_3)(N(SiMe_3)Ar)$ (**II-18**).[31]

In 2005, Power and co-workers reported the facile activation of H_2 by the germanium alkyne analogue $Ar^{Dipp}GeGeAr^{Dipp}$ (**II-19**), the first instance of H–H bond activation by a main group element complex in the condensed phase.[21] Compound **II-19** reacts directly with dihydrogen in hexane at room temperature and atmospheric pressure to yield a mixture of hydrogenated products **II-20** to **II-22**, the ratio of the products controlled by the equivalents of H_2 in the reaction (Scheme 7). Based on the products observed, initial addition of H_2 to **II-19** affords the digermene **II-20**, which reacts further with a second equivalent of H_2 to give the digermane **II-21**. The production of **II-22**, which has no Ge–Ge bond, may be accounted for by the fact that digermene **II-20** exists in an equilibrium with either monomeric $Ar^{Dipp}HGe$: or the bridged isomer $Ar^{Dipp}Ge(\mu\text{-}H)_2GeAr^{Dipp}$. The Ge–Ge bond is absent in both germanium species and reaction with H_2 would produce the primary germane **II-22**.

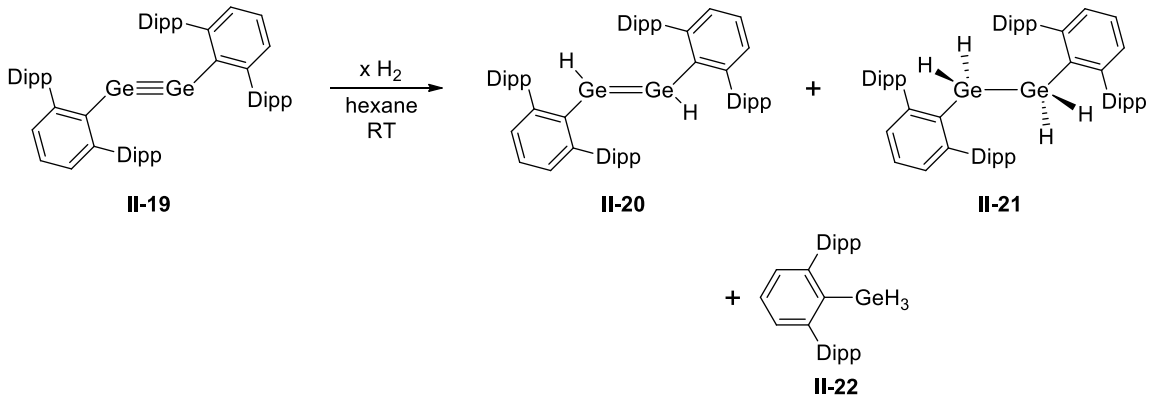

II-19 **II-20** **II-21** **II-22**

Scheme 7. Multiple additions of H_2 to digermyne **II-19** to give digermene (**II-20**), digermane (**II-21**), and primary germane (**II-22**).

Jones and co-workers later extended the activation of dihydrogen by germanium alkyne analogues to the amido-digermyne L^1GeGeL^1 (**II-23**; L^1 = N(Ar*)($SiMe_3$), Ar* = 2,6-[C(H)Ph_2]$_2$-4-MeC_6H_2) (Scheme 8).[32] Compound **II-23** reacted readily with H_2 at room temperature in solution to give the stable germanium hydride $L^1GeGe(H_2)L^1$ (**II-24**). Remarkably, activation of H_2 in solution was observed to occur at temperatures as low as −10 °C, while activation in the solid state was noted at 20 °C to afford **II-24** in greater than 95% yield after 1 hour. In contrast to **II-19**, compound **II-23** did not react with further equivalents of dihydrogen even upon heating to 100 °C. Theoretical calculations by Frenking revealed that addition of H_2 to **II-23** gives the singly bridged species, $L^1Ge(\mu\text{-}H)GeHL^1$, which rearranges through a low activation pathway to the symmetrically hydrogenated compound $L^1HGeGeHL^1$ and then to the most stable isomer **II-24**, which was isolated.[33] The second addition of H_2 would result in cleavage of the Ge–Ge bond, yielding L^1GeH and L^1GeH_3, however the calculations suggested that the second addition is thermodynamically unfavourable.

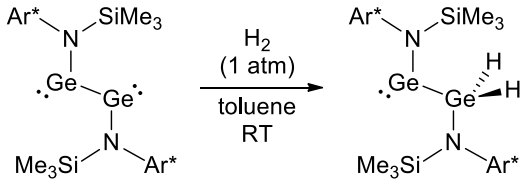

II-23 **II-24**

Scheme 8. Activation of H_2 by amido-digermyne **II-23**.

By increasing the steric bulk on the amido ligand, Jones *et al*. isolated the amido-digermyne L^2GeGeL^2 (**II-25**; L^2 = N($Ar^{\#}$)(Si^iPr_3), $Ar^{\#}$ = 2,6-[C(H)Ph_2]$_2$-4-^{i}PrC_6H_2), which unlike **II-23** features a Ge–Ge multiple bond.[34] Compound **II-25** was also capable of activating dihydrogen, generating the hydrido-digermene $L^2HGeGeHL^2$ (**II-26**) within 20 minutes at room temperature (Scheme 9). The reaction also takes place at −10 °C,

proceeding to completion within 1 hour. Similar to **II-23**, no evidence for the formation of di- or tri-hydrogenation products was observed even with excess H_2 at elevated temperatures. The reaction profile for the addition of H_2 to **II-25** was calculated and found to be similar to the hydrogenation reaction of **II-23**.[35]

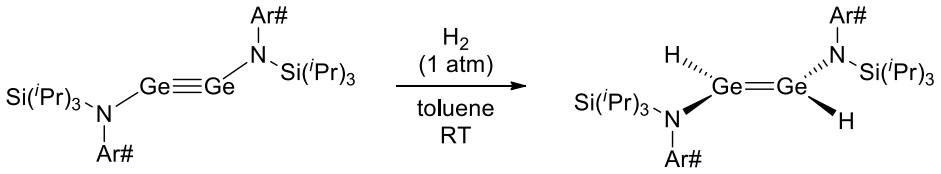

II-25 **II-26**

Scheme 9. Dihydrogen activation by amido-digermyne **II-25**.

Power's group also reported that dihydrogen activation could be accomplished by using sterically bulky divalent two-coordinate germylenes.[36] Treatment of the germylene $GeAr^{Mes}_2$ (**II-27**; Ar^{Mes} = 2,6-(2,4,6-$Me_3C_6H_2$)$_2C_6H_3$) with H_2 afforded the tetravalent germanium dihydride $Ar^{Mes}_2GeH_2$ (**II-28**) in high yield. The reaction of the more sterically encumbered $GeAr^{Dipp}_2$ (**II-29**) with dihydrogen gave the trihydride germane $Ar^{Dipp}GeH_3$ (**II-22**) along with HAr^{Dipp} elimination (Scheme 10). Calculations suggested that reaction with H_2 proceeded via interaction of the σ orbital of H_2 with the empty 4p orbital at the germanium atom along with back donation from the Ge lone pair to the H_2 σ* orbital. In the case of **II-27**, H–H bond cleavage results in the energetically favored product **II-28**. For **II-29**, the initial steps are identical, however the two large Ar^{Dipp} groups introduce sufficient strain such that elimination of HAr^{Dipp} is the preferred pathway along with production of monomeric $Ar^{Dipp}HGe$:, which then reacts further with H_2 to give the final product **II-22**.

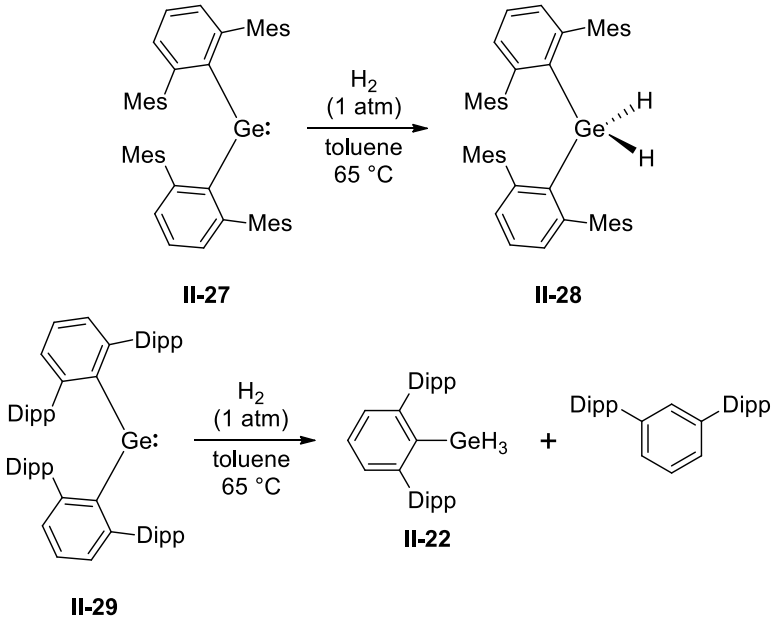

Scheme 10. H–H bond cleavage by diaryl germylenes **II-27** and **II-29**.

Akin to their germanium congeners, distannynes are also able to activate dihydrogen. As seen in Scheme 11, the tin analogue of **II-19**, $Ar^{Dipp}SnSnAr^{Dipp}$ (**II-30**), reacts with H_2 to give the symmetrically bridged Sn(II) hydride $Ar^{Dipp}Sn(\mu\text{-}H)_2SnAr^{Dipp}$ (**II-31**).[37] Using the bulkier terphenyl ligand, reaction of $Ar^{Dipp*}SnSnAr^{Dipp*}$ (**II-32**; Ar^{Dipp*} = 2,6-(2,4,6-$^{i}Pr_3C_6H_2)_2$-3,5-$^{i}Pr_2$-C_6H) with dihydrogen gave the kinetically and thermodynamically more stable isomer $Ar^{Dipp*}SnSn(H_2)Ar^{Dipp*}$ (**II-33**). Unlike the reactions with digermynes, no further reaction with H_2 was observed to give distannenes or distannanes. Calculations performed by Wang and Schleyer revealed that activation of H_2 by **II-30** leads to $Ar^{Dipp}Sn(\mu\text{-}H)SnHAr^{Dipp}$ which promptly isomerizes to $Ar^{Dipp}HSnSnHAr^{Dipp}$.[38] The latter subsequently dissociates into two equivalents of $Ar^{Dipp}HSn$: which then dimerizes to give **II-31**.

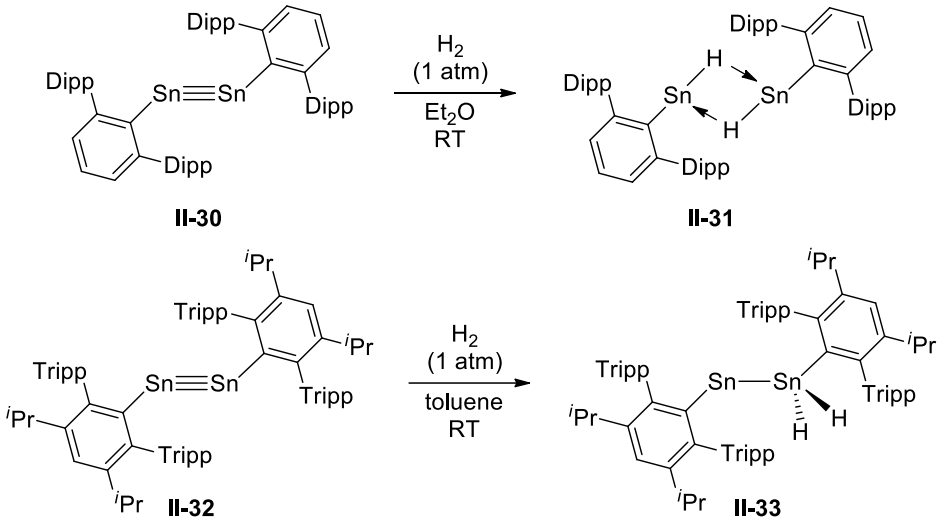

Scheme 11. Activation of H_2 by distannynes **II-30** and **II-32**.

Utilizing the bulky amido ligand L^2, Jones and co-workers were able to prepare distannyne L^2SnSnL^2 (**II-34**), the tin analogue of **II-25** which can also activate dihydrogen (Scheme 12).[39] The reaction is, however, slower compared to **II-25**, proceeding to 70% completion after 24 hours to yield an isomer of the digermene **II-26**, $L^2Sn(\mu\text{-}H)_2SnL^2$ (**II-35**).

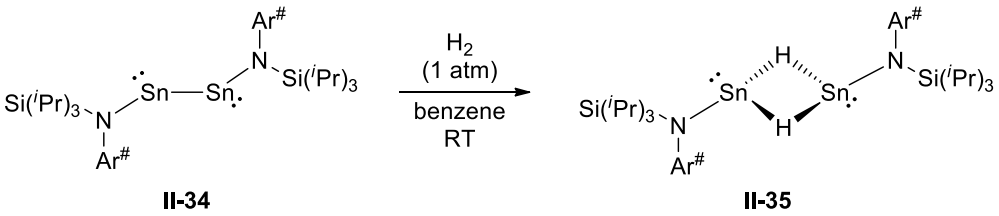

Scheme 12. Dihydrogen activation by amido-distannyne **II-34**.

Divalent, di-coordinate stannylenes have also been demonstrated to react directly with H_2. Whereas no reaction was observed between H_2 and $SnAr^{Mes}_2$ (**II-36**) even upon heating to 70 °C, the more sterically crowded derivative $SnAr^{Dipp}_2$ (**II-37**) reacted readily with H_2 (Scheme 13).[40] In contrast with the germanium analogue, the product obtained was not a Sn(IV) species, but instead arene elimination was observed along with the

Sn(II) hydride $\{Ar^{Dipp}Sn(\mu\text{-}H)\}_2$ (**II-31**). DFT calculations revealed a similar reaction pathway to the one described above for the germanium diaryls.[36]

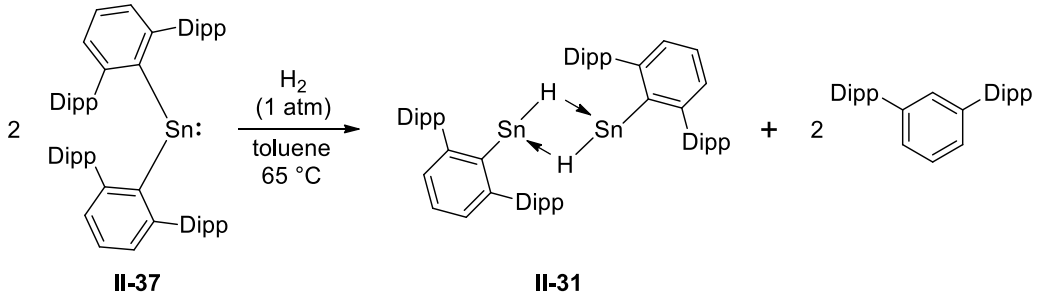

II-37 **II-31**

Scheme 13. Activation of dihydrogen by diaryl stannylene **II-37**.

Recently, oxidative addition of H_2 by the bis(boryl) stannylene complex $Sn(B(NArCH\text{–})_2)_2$ (**II-38**) was reported by the Aldridge, Jones, and Mountford groups (Scheme 14).[41] The reaction occurs readily at room temperature and under 1 atmosphere of H_2 pressure and to give $H_2Sn(B(NArCH\text{–})_2)_2$ (**II-39**) and represents the first example of simple oxidative addition of H_2 to a monometallic Sn(II) system to generate a Sn(IV) product.

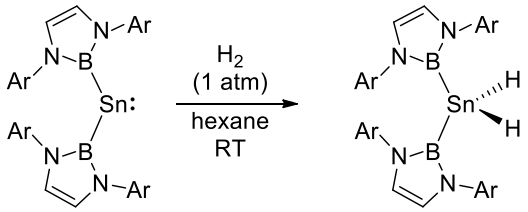

II-38 **II-39**

Scheme 14. Oxidative addition of H_2 by bis(boryl) stannylene **II-38**.

The activation of dihydrogen has since been extended to main group clusters. Tuononen and Power revealed that the tin cluster $Sn_{8(}Ar^{Mes})_4$ (**II-40**) reacts with excess H_2 to afford the tetrameric tin hydride $(HSnAr^{Mes})_4$ (**II-41**) after stirring for 4 hours at 60 °C (Scheme 15).[42] Calculations showed that tin cluster **II-38** has frontier molecular orbitals with both electron donating and accepting features, necessary prerequisites for

bond activation. The Gibbs energy of activation was found to be 32 kcal mol^{-1}, in accord with the higher temperature and excess dihydrogen needed in order for the reaction to proceed.

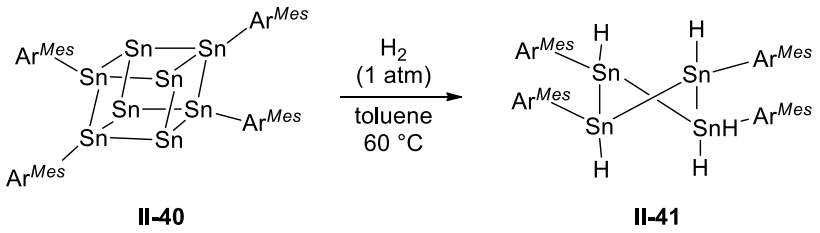

II-40 **II-41**

Scheme 15. Dihydrogen activation by tin cluster **II-40**.

II.1.1.3 Group 15 Complexes

Stephan and co-workers reported in 2014 that the aromatic heterocycle 2,4,6-tri-*tert*-butyl-1,3,5-triphosphabenzene (**II-42**) is reduced under 4 atmospheres of H_2 to give isomeric [3.1.0]bicyclo reduction products (**II-43a** and **II-43b**), with the structure of the major isomer confirmed by X-ray crystallography (Scheme 16).[43] NMR studies revealed that the reaction proceeds via a reversible 1,4-addition of H_2, confirmed via *para*-hydrogen experiments, to generate intermediate conformational isomers of 1,3,5-triphosphacyclohexa-1,4-dienes (**II-43a'** and **II-43b'**). The hydrogenated intermediates then undergo an irreversible suprafacial hydride shift concurrent with P–P bond formation to give the final, isolated products. DFT calculations revealed that facile distortion of the planar triphosphabenzene to a boat-conformation provides the requisite combination of vacant acceptor (C–P π^* orbital localized on phosphorus) and donor (C–P π orbital localized on carbon) orbitals that allows for the polar addition of dihydrogen to the hexadiene intermediates.

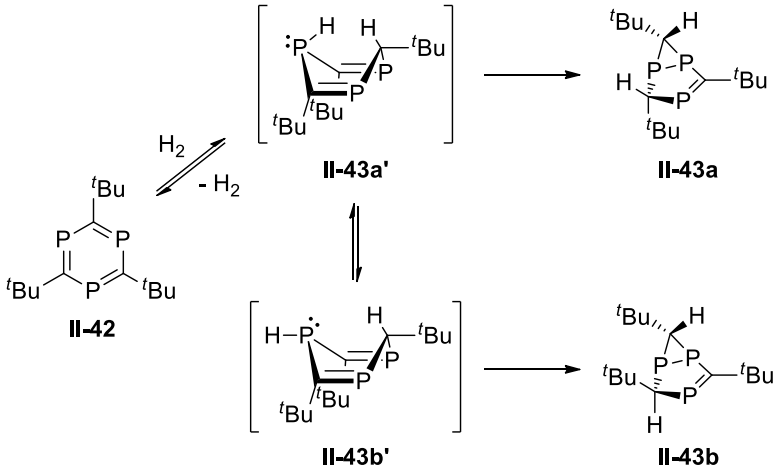

Scheme 16. Activation of H_2 by triphosphabenzene **II-42**.

II.1.2 N–H Bond Activation

Unlike the activation of dihydrogen, activation of N–H bonds are more difficult for transition metal complexes since Lewis basic amines tend to favor the formation of classical Werner-type complexes. In fact, the first example of ammonia activation by a transition metal complex was only reported in 2005 by Hartwig and co-workers.[44] After Bertrand reported the activation of ammonia by nucleophilic carbenes in 2007,[29] a plethora of main group element complexes have been shown to promote N–H bond activation with many substrates, including alkyl and aryl amines as well as the parent or substituted hydrazines.

II.1.2.1 Group 13 Complexes

Reaction of digallane **II-5** with ammonia at room temperature afforded $Ar^{Dipp}HGa(\mu\text{-}NH_2)_2GaHAr^{Dipp}$ (**II-44**) with the gallium centres symmetrically bridged by two NH_2 units and each bound to a terminal hydride (Scheme 17).[25]

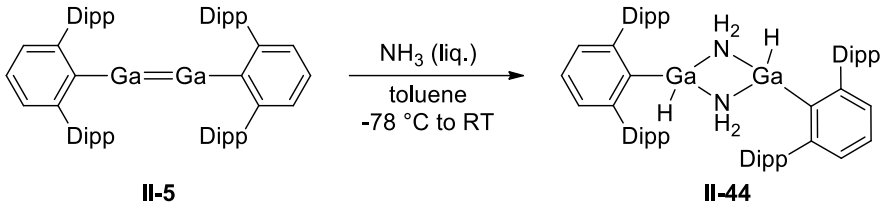

II-5 **II-44**

Scheme 17. Ammonia activation by digallane **II-5**.

Ammonia activation is also observed with zwitterionic **II-9** to produce the 1,4-addition product NacNacGaNH$_2$(^{t}Bu) (**II-45**),[28] while oxidative addition of the N–H bond in diethylamine occured with **II-7** to give the gallium hydrido amido complex NacNacGaH(NEt$_2$) (**II-46**) (Scheme 18).[27]

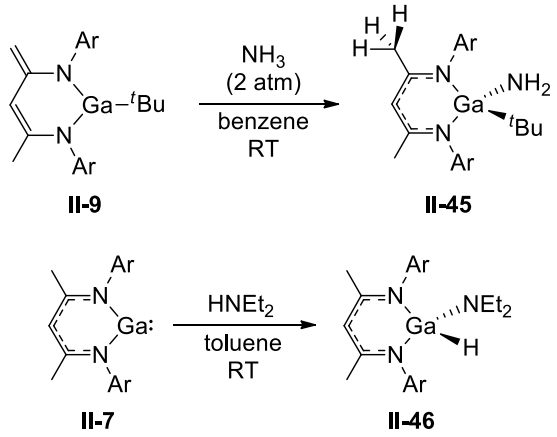

II-9 **II-45**

II-7 **II-46**

Scheme 18. Activation of NH_3 and diethylamine by *β*-diketiminate gallium complexes.

II.1.2.2 Group 14 Complexes

Cyclic (**II-11**) and acylic (**II-12**) alkyl amino carbenes readily react with ammonia to give the N–H activated products **II-47** and **II-48**, respectively (Scheme 19).[29] The mode of activation was calculated to be very similar to that observed with H_2.

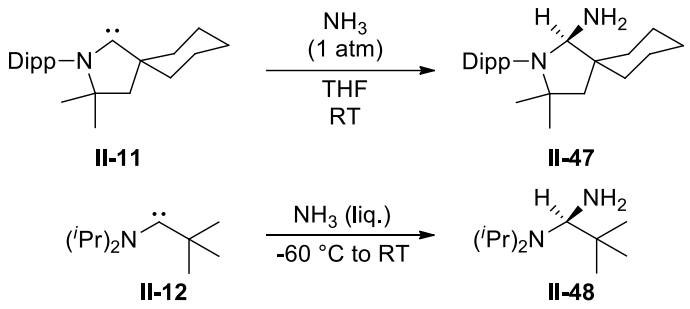

Scheme 19. Oxidative addition of ammonia by alkyl amino carbenes to give **II-47** and **II-48**.

Although carbenes derived from imidazoles were known to be inert towards ammonia,[45] recent reports have demonstrated the ability of imidazolin-2-ylidenes to activate NH_3. Reaction of **II-49** with ammonia gave **II-50** (Scheme 20).[46] Remarkably, the ammonia activation was found to be reversible, as addition of sulfur to **II-50** at low temperature resulted in formation of the corresponding thiourea along with free ammonia, observed as a triplet at −0.17 ppm in the ^{1}H NMR spectrum, upon warming. Ammonia was also observed in the headspace of a standing solution of **II-50** in benzene via gas chromatography and high-resolution mass spectrometry. Compound **II-49** also activates the N–H bond of a wide variety of *para*-substituted anilines with either electron-donating or electron-withdrawing substituents.

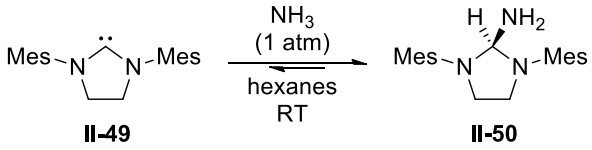

Scheme 20. Activation of ammonia by NHC **II-49**.

Utilizing the photoswitchable NHC **II-51**, the Bielawski group has demonstrated the on-demand reversible activation of ammonia.[47] While addition of gaseous NH_3 to a solution of **II-51** did not result in any reaction, **II-51** was consumed along with concomitant appearance of **II-52** after the sample was subjected to UV radiation (λ = 313

nm) for 30 minutes (Scheme 21). Irradiation of the sample resulted in photoisomerization of **II-51** into the ring-closed form which readily activates ammonia to give **II-52**, confirmed by an independent reaction of pre-irradiated **II-51** with NH_3. Subsequent irradiation with visible-light ($\lambda > 500$ nm) for 100 minutes resulted in the regeneration of **II-51** along with liberated NH_3, confirmed by high-resolution mass spectrometric analysis of the reaction-mixture headspace.

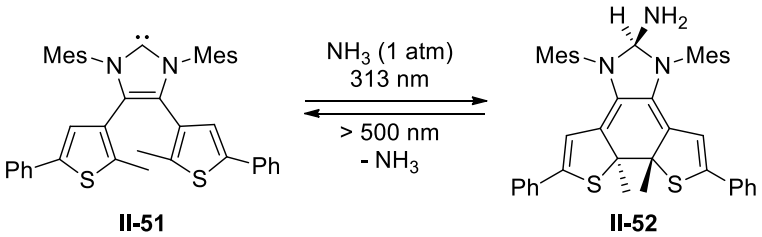

II-51 **II-52**

Scheme 21. Photoswitchable ammonia activation by **II-51**.

Cyclic diamido carbenes **II-53** and **II-55** have also been shown to activate ammonia to give cyclic amines **II-54** and **II-56**, respectively (Scheme 22).[48,49] In a subsequent paper, activation of N–H bonds by **II-53** was extended to a wide variety of alkyl and aryl amines, while the mechanism of N–H activation by diamido carbenes was probed by treating **II-53** with electron-rich and electron-deficient *para*-substituted anilines.[46] The corresponding Hammett plot featured a negative slope, consistent with the buildup of positive charge at the amine nitrogen atom and therefore an electrophilic role can be ascribed to **II-53**, in contrast with the nucleophilic pathway proposed for *c*AACs. On the other hand, insertion of **II-53** into diarylamines was fastest when they were electron deficient. This suggests that **II-53** is ambiphilic and activates the N–H bonds of acidic or basic amines through nucleophilic or electrophilic pathways, respectively.

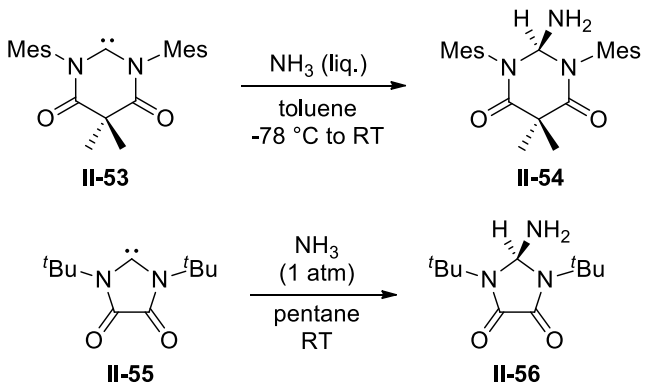

Scheme 22. Ammonia activation by cyclic diamido carbenes **II-54** and **II-55**.

Silylenes are particularly effective in the activation of N–H bonds. Utilizing the silylene NacNac'Si (**II-57**), Roesky and co-workers demonstrated the activation of ammonia to give the 1,1-addition product, NacNac'SiH(NH_2) (**II-58**).[50] Sicilia and co-workers examined the reaction of **II-57** with ammonia computationally and found that formation of the 1,4-addition product is kinetically more favorable than the 1,1-addition product due to the higher energy barrier for the latter process (48.7 kcal mol^{-1} for 1,1-addition versus 26.6 kcal mol^{-1} for 1,4-addition).[51] However, when the free energy profiles were calculated for the reaction of **II-57** with two equivalents of ammonia, since the reaction was performed with excess ammonia, a significant decrease in the energy barrier to 15.3 kcal mol^{-1} was found for the 1,1-addition product due to the assistance of the second molecule of ammonia, consistent with the results reported. Analogous activation of the N–H bond in hydrazine and *N*-methyl hydrazine was also reported by Roesky with **II-57** to give **II-59** and **II-60**, respectively (Scheme 23).[52]

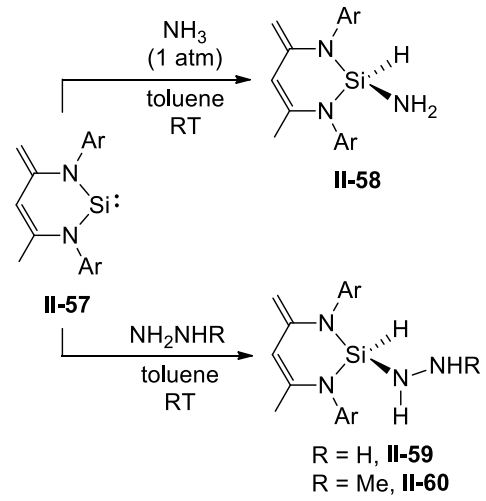

Scheme 23. Activation of ammonia and hydrazines by zwitterionic silylene **II-57**.

With the $Ni(CO)_3$ adduct of **II-57** (**II-61**), Driess and co-workers were able to selectively activate ammonia, isopropylamine, and phenylhydrazine in a 1,4 fashion in toluene to yield the corresponding *β*-diketiminate Si(II)–$Ni(CO)_3$ complexes **II-62** to **II-64** (Scheme 24).[53] Though the mechanism is unclear, the authors proposed that selective 1,4-addition is due to increased acidity of the N–H protons upon coordination of the substrate with **II-61**. Intermolecular deprotonation of the N–H bond with a second molecule of **II-61** by the exocyclic methylene group followed by proton migration afforded the products observed.

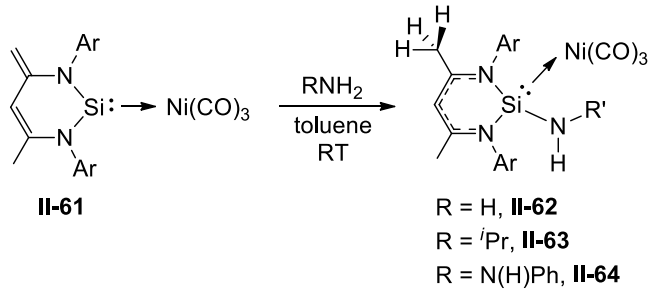

Scheme 24. 1,4-addition of ammonia, amine, and hydrazine by silylene **II-61**.

Lewis base-stabilized silanone NacNac'Si=O(DMAP) (**II-65**) also reacts with gaseous ammonia (Scheme 25).[54] The expected product, silahemiaminal **II-66**, was found

to be in equilibrium with the silanoic amide tautomer **II-66'**. The equilibrium between **II-66** and **II-66'** is dependent on both the polarity of the solvent as well as the concentration of the solution.

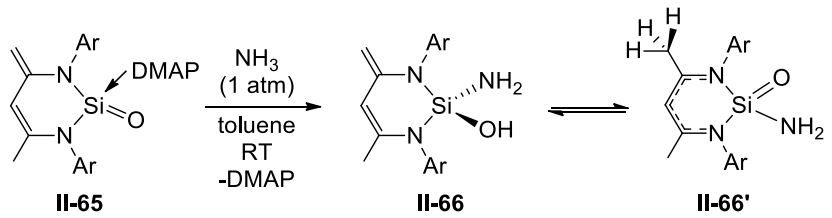

Scheme 25. Ammonia activation by Lewis base-stabilized silanone **II-65**.

The germanium analogue of **II-57** (**II-67**) also activates ammonia at room temperature to give **II-68** (Scheme 26).[55] Unlike **II-57**, 1,4-addition of ammonia was observed in the reaction with **II-68**. According to DFT calculations, the 1,4-addition product was kinetically (barrier heights of 27.5 and 67.9 kcal mol^{-1} for the 1,4- and 1,1-addition, respectively) and thermodynamically (the 1,4-addition product was calculated to be more stable than the 1,1-addition product by 13.6 kcal mol^{-1}) more favorable.[51] On top of that, formation of the stronger C−H bond in **II-68** versus formation of the Ge−H bond in the putative 1,1-addition product could be another driving force for the selectivity observed. The addition of hydrazine to **II-68** also occurs in a similar fashion to give the germanium hydrazide **II-69**.[56] A related six-membered, zwitterionic N-heterocyclic germylene (**II-70**) was prepared by Driess and co-workers and was also found to activate NH_3 to give the 1,4-addition product **II-71** (Scheme 26).[57]

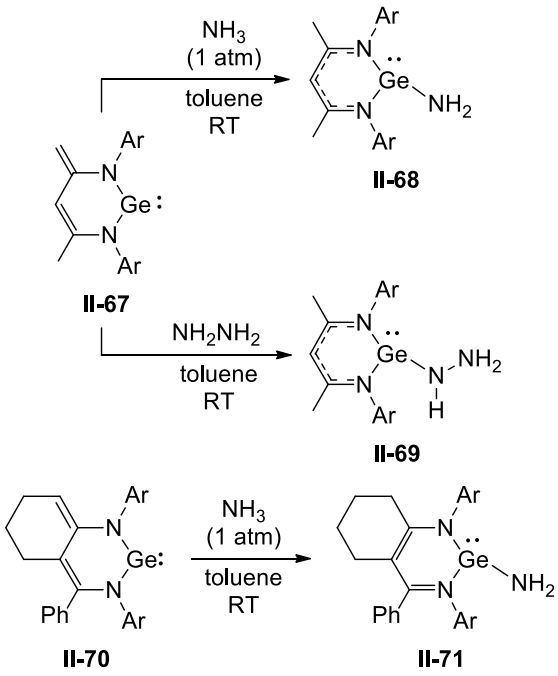

Scheme 26. Activation of ammonia and hydrazine with N-heterocyclic germylenes **II-67** and **II-70**.

Diaryl germylenes **II-27** and **II-29** also react with ammonia to give the corresponding Ge(IV) products $Ar^{Mes}_2GeH(NH_2)$ (**II-72**) and $Ar^{Dipp}_2GeH(NH_2)$ (**II-73**), respectively (Scheme 27).[36] Calculations revealed that the pathway involving a single NH_3 molecule had a high energy barrier in which a transition state could not be located. As an excess of ammonia was utilized in the reaction, an alternative scenario involving two NH_3 molecules were considered in the calculations. In the calculated structure, one molecule of ammonia is coordinated to the empty 4p orbital on germanium via the lone pair while the second NH_3 molecule solvates the coordinated ammonia via intermolecular N--H interactions. The oxidative addition pathway was found to be 5.7 kcal mol^{-1} lower in energy than the alternative elimination pathway, even though the products $Ar^{Mes}GeNH_2$ and HAr^{Mes} are more energetically favored than **II-72**. Not only that, **II-27** can also activate the N–H bonds of hydrazine and *N*-methyl hydrazine to give the first

Ge(IV) hydrazides $Ar^{Mes}_2GeH(NHNH_2)$ (**II-74**) and $Ar^{Mes}_2GeH(NHNHMe)$ (**II-75**), Scheme 27.[58] DFT calculations of the mechanism of N–H bond activation revealed that the reaction proceeds via an intermolecular proton transfer, mediated by a second equivalent of hydrazine that has formed an adduct with **II-27** beforehand via a dative Ge–N bond. As such, when N,N-dimethyl hydrazine was used, only an adduct with **II-27** was obtained.

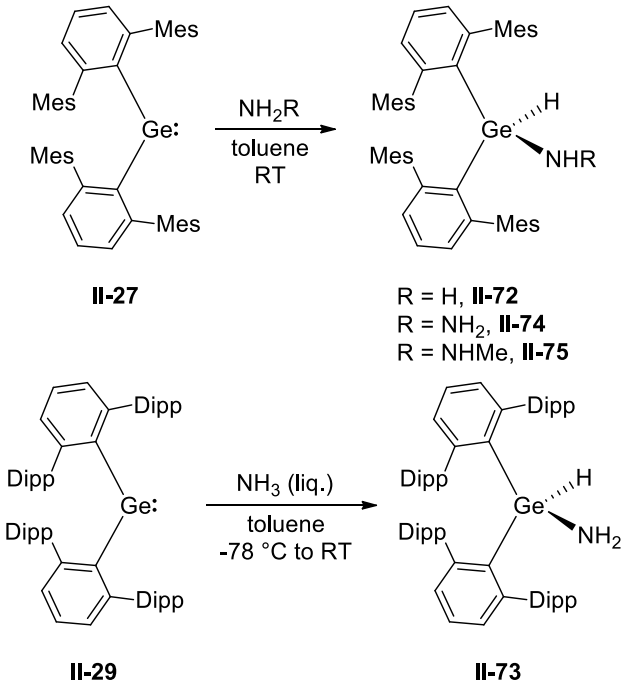

Scheme 27. N–H bond activation of ammonia and hydrazines with diaryl germylenes **II-27** and **II-29**.

Similarly, the diaryl stannylenes **II-36** and **II-37** can react with NH_3 to furnish the amido bridged complexes $Ar^{Mes}Sn(\mu\text{-}NH_2)_2SnAr^{Mes}$ (**II-76**) and $Ar^{Dipp}Sn(\mu\text{-}NH_2)_2SnAr^{Dipp}$ (**II-77**), respectively, along with elimination of the respective aryl ligand (Scheme 28).[36,40] Unlike the germylene analogues, the oxidative addition product, $Ar^{Mes}_2SnH(NH_2)$, is energetically disfavored by 2.2 kcal mol^{-1}, whereas the elimination of HAr^{Mes} and production of **II-70** is strongly favored by 20.3 kcal mol^{-1}.[36]

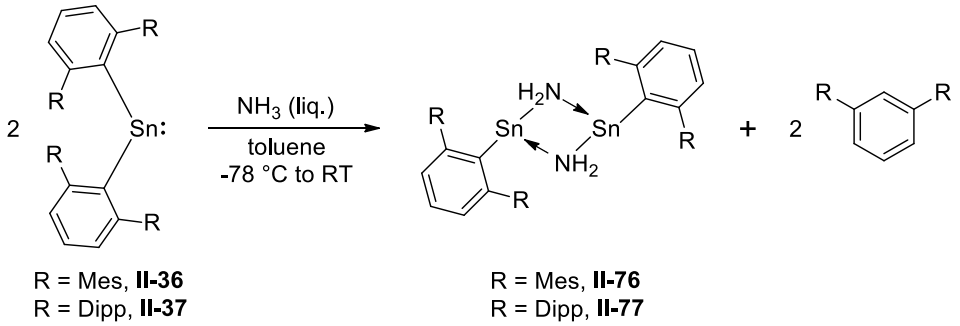

Scheme 28. Ammonia activation by diaryl stannylenes **II-36** and **II-37**.

Activation of ammonia has also been demonstrated by bis(boryl) stannylene **II-38** (Scheme 29).[41] Addition of excess ammonia to a benzene solution of **II-38** yielded the ammonia adduct **II-78** followed by generation of the amidotin(IV) hydride $(NH_2)SnH(B(NArCH–)_2)_2$ (**II-79**).

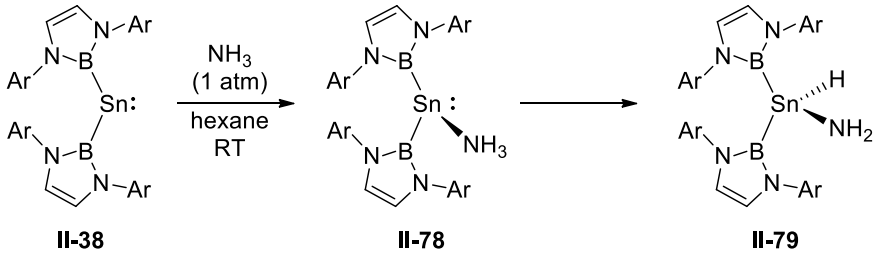

Scheme 29. Formation of NH_3 adduct **II-78** from **II-38** followed by N–H bond activation to give **II-79**.

II.1.2.3 Group 15 Complexes

Recently, Radosevich and co-workers have reported the activation of N–H bonds with tricoordinate phosphorus compound **II-80**.[59] Initially prepared by Arduengo,[60] **II-80** displays an unusual planar T-shaped geometry at phosphorus with the tridentate O,N,O-donors occupying three adjacent coplanar sites. Condensation of NH_3 onto a solid sample of **II-80** produced the pentacoordinate hydrido amido phosphorus species **II-81**. Related addition of alkyl and aryl amines to **II-80** occurs readily at room temperature to give the corresponding phosphorus compound **II-82**, with the bulkier aryl amines requiring

heating to 55 °C to complete the reaction (Scheme 30). The authors concluded, based on kinetic studies coupled with DFT calculations, that the mechanism of N–H bond activation by **II-80** is an entropically controlled, stepwise process initiated by electrophilic activation of the amine substrate to give a phosphoranide intermediate. The second step is a rate-determining amine-assisted proton transfer to furnish the final hydrido amido products.

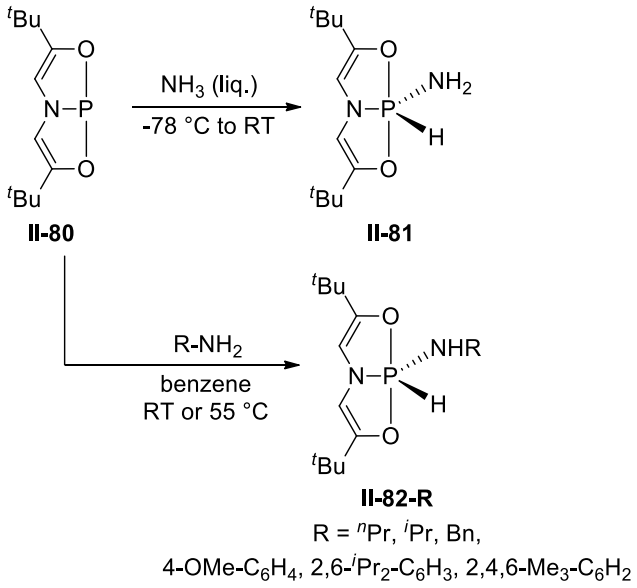

Scheme 30. Activation of ammonia and alkyl and aryl amines by **II-80**.

Shortly thereafter, Kinjo *et al*. reported the preparation of a diazaphosphapentalene derivative **II-83** featuring a bent geometry with two phosphorus atoms at the bridgehead.[61] At ambient temperature, gaseous ammonia was activated by **II-83** to give the 1-aza-2,3-diphospholene derivative **II-84**, formally the product of σ-bond methathesis between an N–H bond of ammonia and an endocyclic P–N bond of **II-83** (Scheme 31). Unlike the activation of ammonia by **II-80**, kinetic studies revealed that the reaction is first order in **II-83** and ammonia.

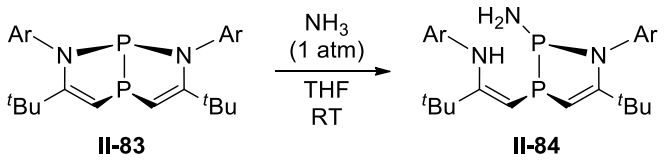

Scheme 31. N–H bond cleavage by **II-83** to give **II-84**.

Utilizing a similar strategy, Radosevich and co-workers synthesized the chelated σ^3-phosphorus triamide (**II-85**) with an exaggerated C_s distortion.[62] Compound **II-85** was demonstrated to activate ammonia as well as alkyl and aryl amines to pentacoordinate P(V) compound **II-86** (Scheme 32). Monitoring the reaction by multinuclear NMR spectroscopy along with kinetic studies revealed that N–H bond activation proceeded via a stepwise mechanism, starting with 1,2-addition across a phosphorus–amide bond followed by subsequent intramolecular σ^3-P to σ^5-P tautomerization. Interestingly, the oxidative addition of *tert*-butyl amine was found to be reversible. Refluxing a toluene solution of **II-86-^{t}Bu** under a dynamic nitrogen sweep gave **II-85** via reductive elimination.

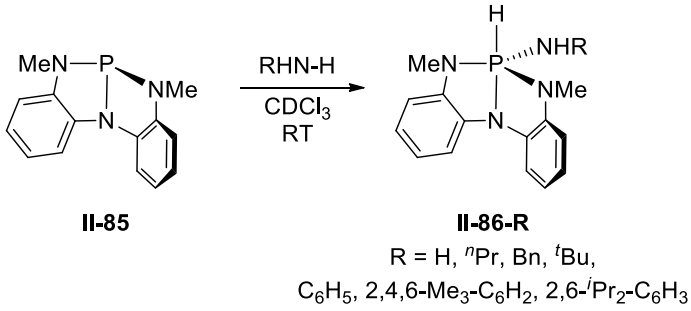

Scheme 32. Ammonia and akyl and aryl amine activation by **II-85**.

Most recently, Aldrige and Goicoechea reported the preparation of tridentate phosphorus compound **II-87** supported by the *N*,*N*-bis(3,5-di-*tert*-butyl-2-phenoxy)amide ligand.[63] While compound **II-87** is closely related to **II-80**, the molecular structure was found to be more akin to the bent structures observed for **II-83** and **II-85**. Like the other

tricoordinate phosphorus species above, facile activation of gaseous ammonia at room temperature was also performed with **II-87** to give **II-88** (Scheme 33).

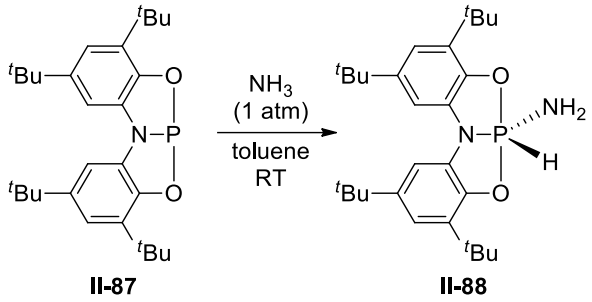

Scheme 33. Activation of ammonia by **II-87**.

II.1.3 O–H and S–H Bond Activation

Activation of O–H and S–H bonds has been shown with many main group element complexes and provides a facile route to well-defined complexes bearing a terminal OH or SH group. Activation of both water and methanol occurred upon reaction with NacNacGa (**II-7**) and the corresponding complexes **II-89** and **II-90** were isolated.[27] Gallium complex **II-9** activates hydrogen sulfide to give the 1,4-addition product **II-91**, akin to the products of dihydrogen and ammonia activation (Scheme 34).[28]

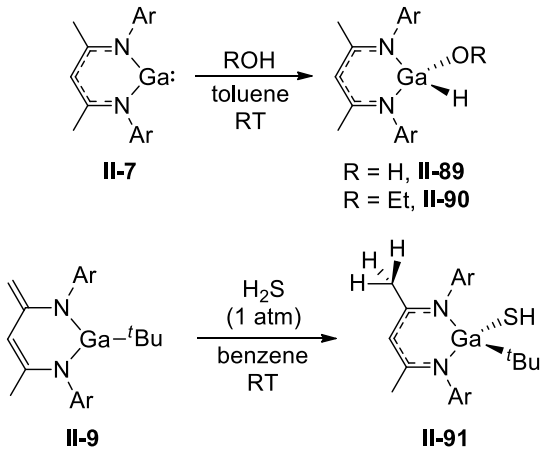

Scheme 34. O–H and S–H bond activation by gallium complexes **II-7** and **II-9**.

The addition of water to silylene **II-57** in a 2:1 ratio affords the donor-stabilized siloxysilylene **II-92** (Scheme 35).[64] Although the mechanism is unknown, the authors reasoned that the reaction could proceed via O–H bond activation to give the hydroxosilylene, NacNacSiOH, as a result of 1,4-addition or the silanol NacNac'SiH(OH), the expected product of 1,1-addition, followed by reaction with the second equivalent of **II-51**. The reaction of **II-57** with hydrogen sulfide gas at low temperature resulted in the formation of donor-stabilized silathioformamide **II-93** (Scheme 35).[53] Analogous to the reaction with water, two possible intermediates were proposed. The silathioformamide, NacNac'SiH(SH), could result from 1,1-addition followed by proton migration to the exocyclic methylene group. Alternatively, 1,2-addition would give the amino(mercapto)silylene, NacNacSiSH, with subsequent protonation of the Si(II) lone pair to give **II-93**. Attempts to observe an intermediate by low temperature NMR spectroscopy was unsuccessful so DFT calculations were performed. The authors found that the two postulated intermediates are practically isoenergetic while the tautomer **II-93** is favored by −23 kcal mol^{-1}.

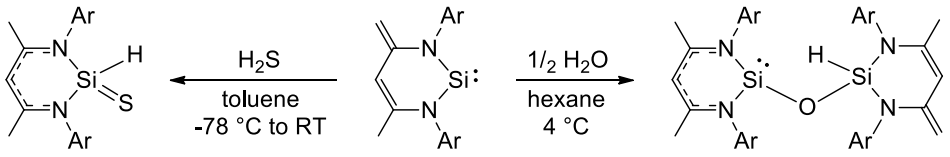

Scheme 35. Activation of H_2O and H_2S by zwitterionic silylene **II-57**.

Dialkyl germylene $Ge(CH(SiMe_3)_2)_2$ **II-94** was found by Lappert and co-workers to oxidatively add the O–H bond of ethanol to give $(CH(SiMe_3)_2)_2GeH(OH)$ (**II-95**) at room temperature.[65] Similarly, diaryl germylene $GeAr^{Mes}_2$ (**II-27**) reacts with water or methanol to give the Ge(IV) insertion product $Ar^{Mes}_2GeH(OH)$ (**II-96**) and

$Ar^{Mes}_2GeH(OMe)$ (**II-97**), respectively (Scheme 36). The mechanism of O–H bond insertion, discerned via DFT calculations, was found to be catalytic, aided by a second molecule of water,[66] paralleling the mechanism calculated for the insertion of **II-27** into the N–H bond of NH_3.[36]

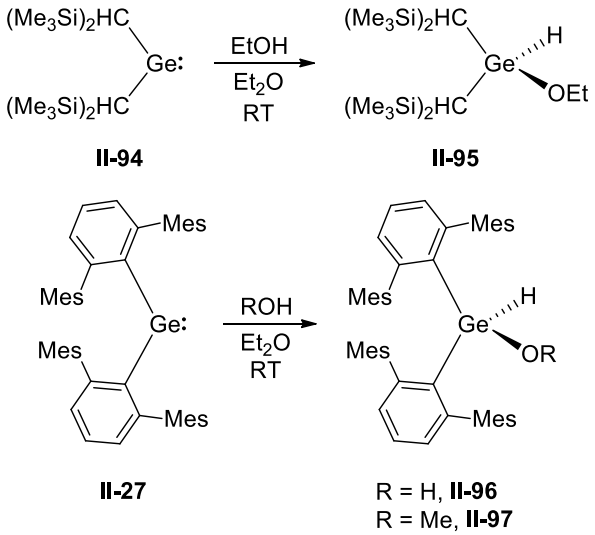

Scheme 36. O–H bond activation by dialkyl (**II-94**) and diaryl germylene (**II-27**).

Germylene **II-67** reacts with H_2O at room temperature to form NacNacGeOH (**II-98**) while reaction with phenol and pentafluorophenol gave the corresponding aryloxides **II-99** and **II-100**, respectively (Scheme 37).[67]

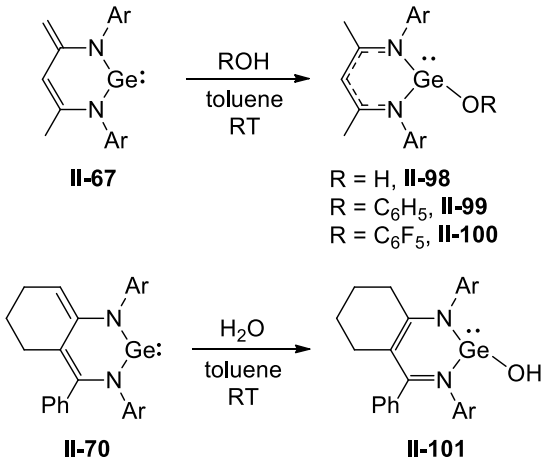

Scheme 37. Activation of water and phenols by germylenes **II-67** and **II-70**.

N-heterocyclic germylene **II-70** similarly reacts with water at room temperature to give germylene hydroxide **II-101** (Scheme 37).[57]

Dialkyl and diaryl stannylenes activate O–H bonds as well. Using Lappert's stannylene, $Sn(CH(SiMe_3)_2)_2$ (**II-102**), Pörschke and co-workers reported the addition of water and methanol to yield hydroxyl and methoxy diorganostannanes $(CH(SiMe_3)_2)_2SnH(OH)$ (**II-103**) and $(CH(SiMe_3)_2)_2SnH(OMe)$ (**II-104**), respectively (Scheme 38).[68] In contrast, reaction of the diaryl stannylene **II-36** with water or methanol produces the Sn(II) species $Ar^{Mes}Sn(\mu\text{-}OH)_2SnAr^{Mes}$ (**II-105**) and $Ar^{Mes}Sn(\mu\text{-}OMe)_2SnAr^{Mes}$ (**II-106**), respectively, along with elimination of HAr^{Mes} (Scheme 38). Calculations suggest that arene elimination proceeds via a one-step σ bond metathesis, with a cyclic transition state in which a hydrogen from a coordinated water molecule is transferred to the aryl substituent,[66] akin to the mechanism calculated for the reaction of **II-36** with NH_3.[36]

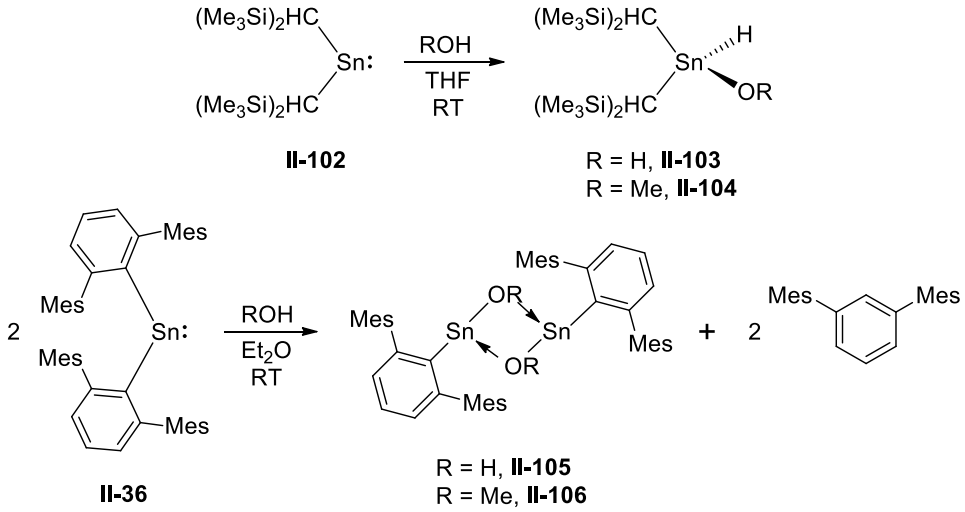

Scheme 38. O–H bond activation by dialkyl (**II-102**) and diaryl stannylene (**II-36**).

The bis(boryl) stannylene **II-38** readily undergoes oxidative addition with water to give $(OH)SnH(B(NArCH\text{–})_2)_2$ (**II-107**) under ambient conditions (Scheme 39).[41]

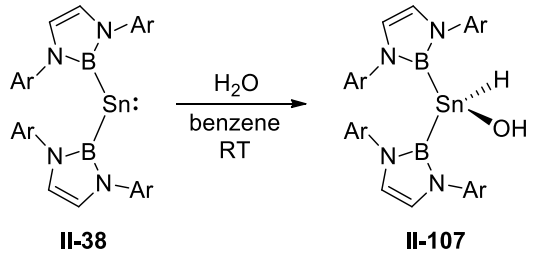

Scheme 39. Insertion of **II-38** into the O–H bond of water.

Analogous to the activation of N–H bonds, triamido phosphorus complex **II-85** can likewise activate the O–H bonds of alkyl and aryl alcohols to give **II-108** (Scheme 40).[62] The same mechanism was found to be operative as the one proposed for N–H bond activation. The activation of *tert*-butyl alcohol was also found to be reversible, giving back **II-85** upon refluxing a toluene solution of **II-108-^{t}Bu** under a nitrogen sweep.

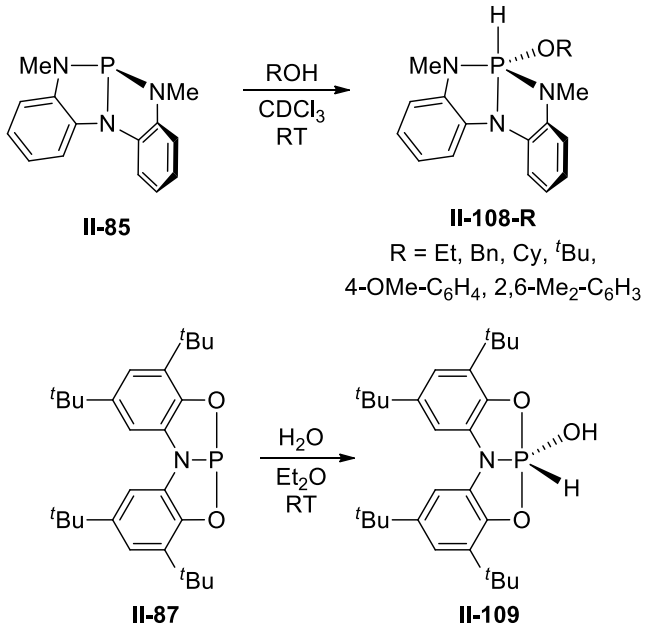

Scheme 40. Oxidative addition of O–H bonds in water and alcohols by the phosphorus complexes **II-85** and **II-87**.

Phosphorus(III) complex **II-87** similarly reacts with water to give the P(V) species **II-109** (Scheme 40).[63]

II.1.4 C–H Bond Activation

Activation of C–H bonds has emerged as an attractive method for transforming abundant starting materials into value added products with the potential to streamline synthetic strategies, increase atom economy, and minimize waste.[69] Recent work has revealed such chemistry to be effected by main group element complexes. α-C–H activation of THF with the in-situ generated bis-carbene Al(I) complex **II-110**, obtained from the reaction of the bromo precursor with potassium hydride, was reported recently by Driess and co-workers with concomitant elimination of H_2 and production of metalated compound **II-111** (Scheme 41).[70] DFT calculations were performed and revealed the mechanism to begin with THF coordination followed by H–H interaction between the Al–H and C–H moieties and subsequent elimination of dihydrogen through a five-membered-ring transition state. The resulting zwitterion then undergoes a barrierless rearrangement to the isolated product.

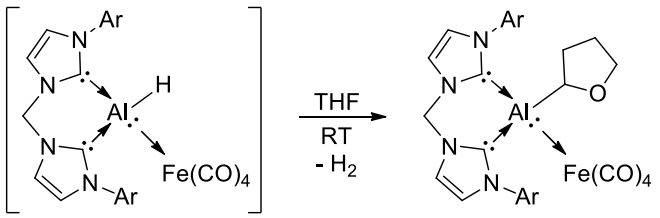

II-110 **II-111**

Scheme 41. C–H bond activation by in-situ generated Al(I) hydride **II-110**.

C–H bond activation has been demonstrated with an anionic gallium(I) N-heterocylic carbene analogue by the Jones group.[71] Reaction of **II-112** with $[HC(N(Mes)CH–)_2]Cl$ yielded the gallium hydride **II-113** as a result of oxidative insertion of the Ga(I) centre into the imidazolium C–H bond, the first example of such a reaction with gallium (Scheme 42).

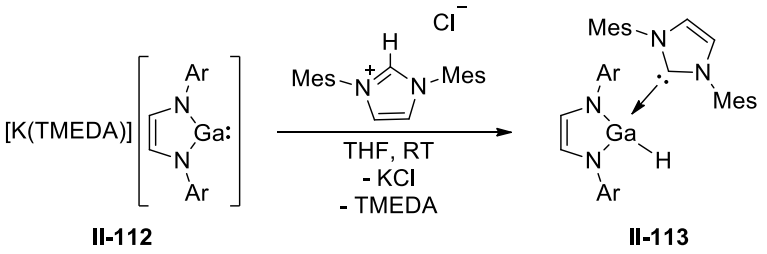

Scheme 42. C–H activation by anionic gallium(I) compound **II-112**.

Activation of acidic C–H bonds by N-heterocyclic carbenes was first reported by Arduengo and co-workers.[72] Reaction of **II-49** with acetylene gave the C–H insertion product **II-114**. Activation of the C–H bonds of methyl phenyl sulfone and acetonitrile by **II-49** proceeded smoothly at room temperature to give **II-115** and **II-116**, respectively. It should be noted that the analogous unsaturated carbene 1,3-diadamantyl-imidazol-2-ylidene failed to react with CH_3CN, only giving the solvate as the product. Although a longer reaction time was needed, **II-49** reacts with chloroform at room temperature to give the C–H activated product **II-117** (Scheme 43).

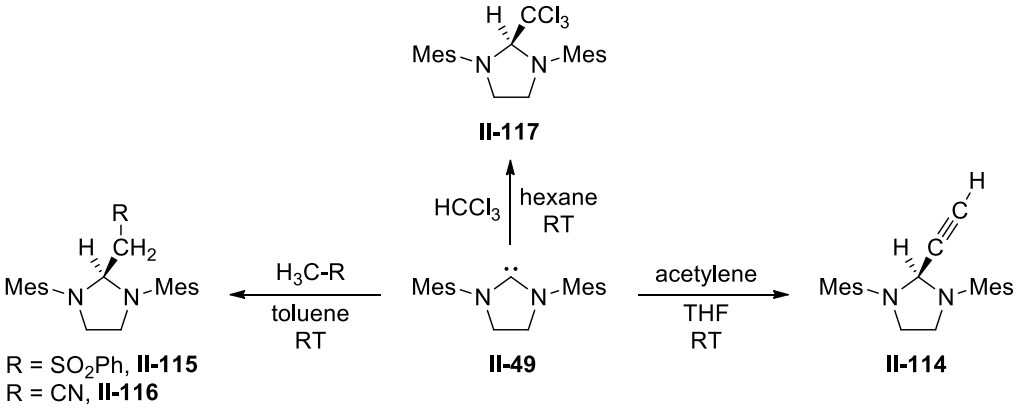

Scheme 43. Activation of acidic C–H bonds by **II-49**.

Utilizing ring-expanded NHCs, Whittlesey *et al*. demonstrated the activation of non-acidic C–H bonds.[73] Compounds **II-118** and **II-120** display a significantly wider N–C–N angle than **II-49** which in turn considerably increases their basicity. As such, heating a solution of **II-118** or **II-120** at 70 °C resulted in the intramolecular activation of

a methyl group in the flanking N-aromatic rings to furnish **II-119** and **II-121**, respectively (Scheme 44).[74] The reactivity demonstrated is reminiscent of the well-established *ortho*-metalation of aryl rings by low oxidation state or highly Lewis acidic transition metal compounds.

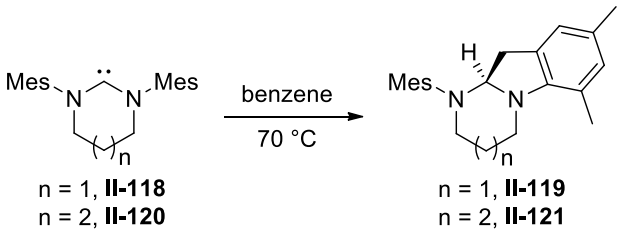

Scheme 44. Intramolecular C–H activation by ring-expanded NHCs **II-118** and **II-120**.

Triazole based N-heterocyclic carbenes have also been used to activated C–H bonds. Reaction of **II-122** with acetonitrile at high temperatures resulted in the production of C–H activated product **II-123** (Scheme 45).[75]

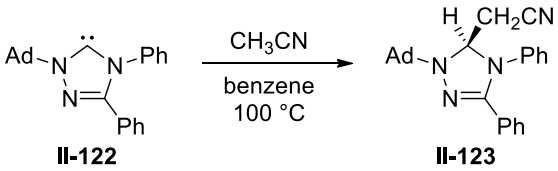

Scheme 45. Activation of acetonitrile by triazole based N-heterocylic carbene **II-122**.

Aryl amino carbenes have been shown by the Bertrand group to readily activate C–H bonds.[76] Carbene **II-124**, generated at low temperature, is stable for days at −50 °C but undergoes an intramolecular C–H insertion reaction upon warming to room temperature to produce **II-125**. Furthermore, biaryl amino carbenes **II-126** and **II-128** spontaneously rearranges into the aminofluorene isomer **II-127** and aminodibenzofluorene isomer **II-129** at low temperature (Scheme 46).[77] DFT calculations were performed to shed further insight into the rearrangements. Both **II-126** and **II-128** were predicted to have a singlet ground state with the corresponding triplet state higher in

energy by 17.9 kcal mol^{-1} and 16.0 kcal mol^{-1}, respectively. Consistent with the spontaneous rearrangement of **II-126** to **II-127** at low temperature, the reaction was predicted to be highly exothermic (ΔG = −36.2 kcal mol^{-1}) with a transition state located 17.0 kcal mol^{-1} above **II-126**. Similar values were also predicted for the rearrangement of **II-128** to **II-129** (ΔG = −27.4 kcal mol^{-1}, $\Delta G^{\ddagger}$ = 27.5 kcal mol^{-1}).

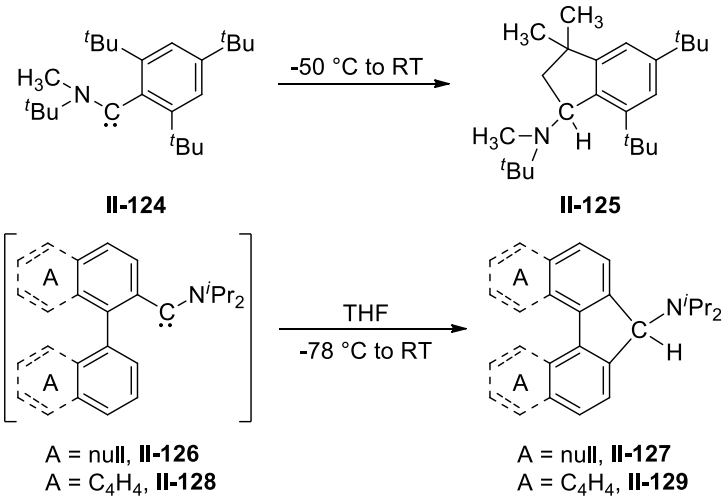

Scheme 46. Intramolecular C–H activation by aryl amino carbenes **II-124**, **II-126**, and **II-128**.

Diamido carbenes prepared by Bielawski and co-workers are also reactive towards C–H bond activation (Scheme 47).[78]

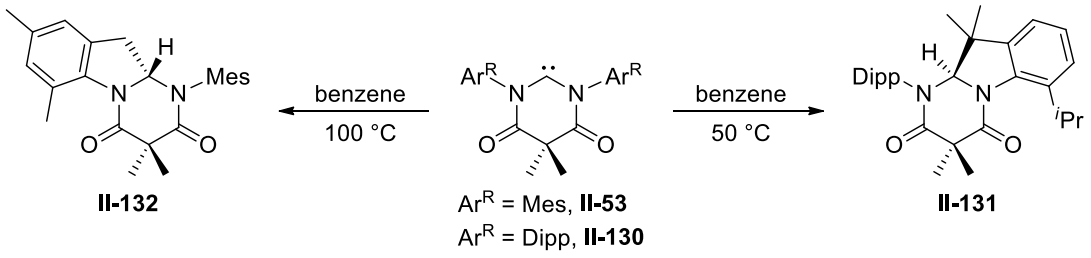

Scheme 47. Thermolysis of **II-53** and **II-130** to give cyclometalated products **II-131** and **II-132**.

Initial studies revealed that **II-130** reacts with its pendant arylisopropyl group upon heating to 50 °C to give the cyclometalated product **II-131**. The more stable diamido

carbene **II-53** only undergoes intramolecular C–H activation upon heating at 100 °C for several hours to furnish **II-132**.[79]

Additionally, **II-53** undergoes intermolecular C–H activation with a range of electron-rich or electron-deficient *para*-substitued tolyl derivatives (Scheme 48) along with secondary benzylic C–H bonds as well as primary C–H bonds of α-carbonyl substrates at high temperature.[79] Tertiary C–H bonds were not activated presumably due to steric hindrance. Data from the activation of the toluene derivatives allowed for the construction of a Hammett plot with a linear, positive slope, reflecting the buildup of negative charge at the benzylic carbon atom. Therefore, the intermolecular C–H insertion was consistent with a step-wise process wherein **II-53** functioned as nucleophile and polarized the C–H bond prior to insertion.

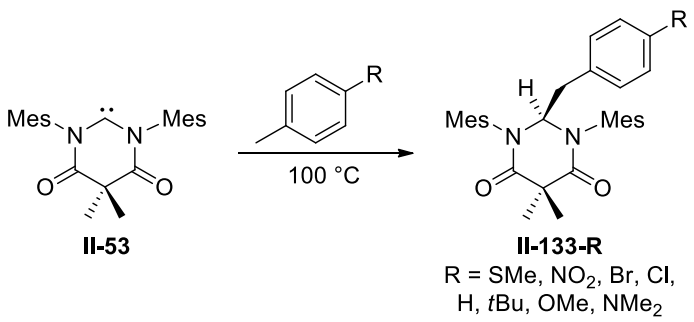

Scheme 48. C–H activation of para-substituted tolyl derivatives by **II-53**.

In addition to the C–H activated product **II-134**, the formally hydrogenated diamino carbene **II-135** was produced along with benzene in the reaction of **II-53** with 1,4-cyclohexadiene (Scheme 49).[79] This reaction constituted the first transfer hydrogenation of a hydrocarbon by a carbene.

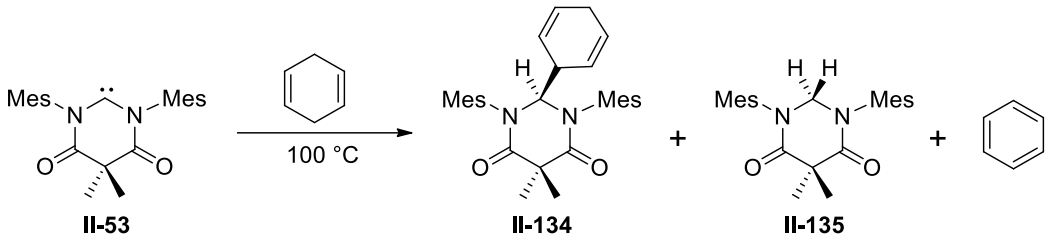

Scheme 49. Transfer hydrogenation of 1,4-cyclohexadiene by **II-53**.

The ability of **II-55** to activate C–H bonds has also been disclosed. As summarized in Scheme 50, **II-55** inserts into the C–H bonds of various tolyl derivatives upon heating at 80 °C.[49] Compound **II-55** was also found to insert into the α-C–H bond of THF affording the resulting product **II-137**, the least acidic C–H bond activated by a stable carbene to date (Scheme 50).

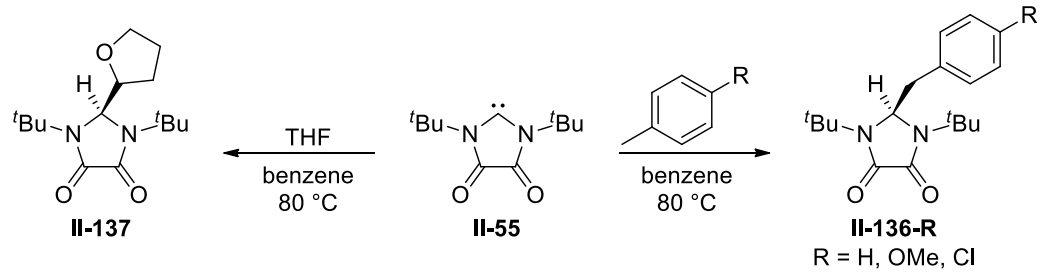

Scheme 50. Activation of C–H bonds by **II-55**.

Very recently, a cyclic alkyl amido carbene was prepared by the Bielawski group.[80] Carbene **II-138**, generated in-situ at ambient temperature, immediately rearranged into the C–H insertion product **II-139** (Scheme 51), similar to the rearrangements observed with **II-53** and **II-130** upon heating.

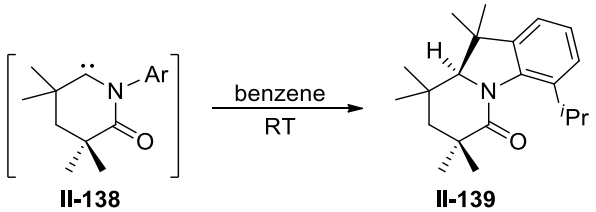

Scheme 51. Intramolecular C–H activation by cyclic alkyl amido carbene **II-138**.

Driess and co-workers reported the reaction of acetylene and phenylacetylene with silylene **II-57** to give the 1,1-addition product **II-140** and **II-141**, respectively, at room temperature.[81] Theoretical calculations gave a prohibitively high barrier for the direct C–H insertion of 41.3 kcal mol^{-1}. Instead they proposed a two-step mechanism, starting with deprotonation of the alkyne by the basic exocylic methylene group of **II-57** followed by hydrogen migration to the silicon atom. Silylene **II-57** can also selectively activate the C–H bond in pentafluorobenzene and trifluorobenzene to give **II-142** and **II-143**, respectively (Scheme 52).[82]

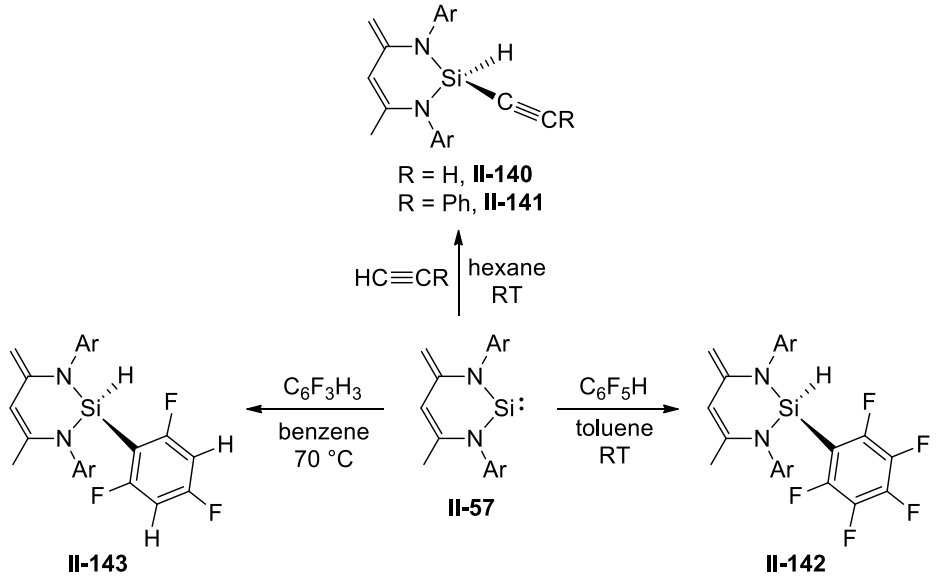

Scheme 52. Activation of C–H bonds by silylene **II-51**.

The same group also found that the NHC adduct of **II-57** (**II-144**) undergoes slow rearrangement via intramolecular C–H activation above −20 °C to give the silyl hydride **II-145** (Scheme 53).[83] While the mechanism is currently unknown, two pathways were proposed. The first involved deprotonation of an N-methyl group of the NHC ligand by the nucleophilic exocyclic methylene group of **II-57** followed by H[1,4]- and Si[1,3]-

shifts to give **II-145**. The second pathway proceeds via direct addition of the C–H bond to the Si(II) centre followed by cleavage of the dative Si–C bond to yield **II-145**.

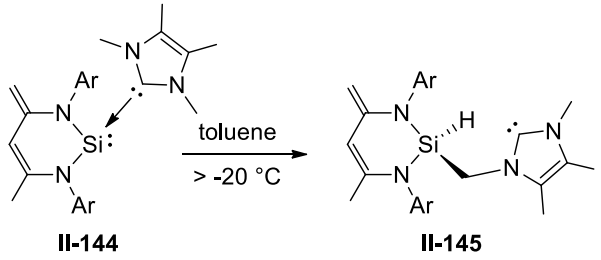

II-144 **II-145**

Scheme 53. C(sp^3)–H activation by silylene **II-144**.

Thermolysis of both the amido boryl silylene **II-15** and silyl coordinated silylene **II-17** resulted in sluggish intramolecular C–H activation of one of the isopropyl groups on a 2,6-diisopropylphenyl ring to give cyclo-metalated species **II-146** and **II-147**, respectively (Scheme 54).[30,31]

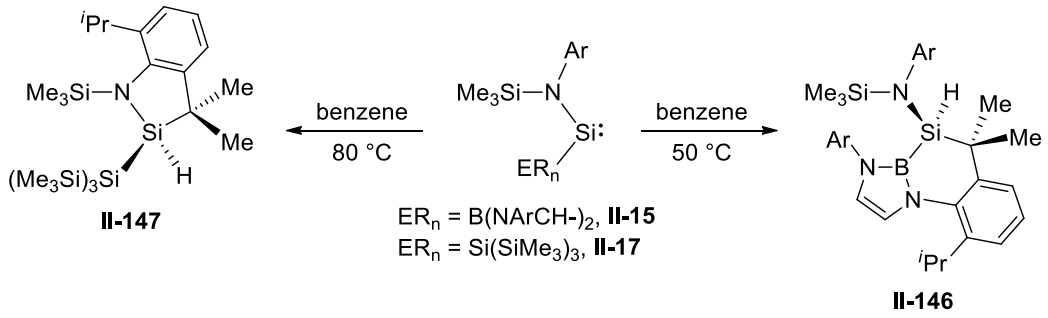

II-147 **II-146**

Scheme 54. Intramolecular C–H activation by silylenes **II-15** and **II-17**.

Kinetically stabilized 1,2-dihydrosilylenes (**II-148**) reported by Tokitoh *et al*. have been shown to isomerize to a similar cyclo-metalated product **II-149** (Scheme 55).[84] The isomerization ensues via an initial 1,2-hydrogen migration to form the intermediate silyl silylene **III-132'** followed by subsequent insertion of the silylene moiety into the benzylic C–H bonds of the sterically demanding $CH(SiMe_3)_2$ groups.

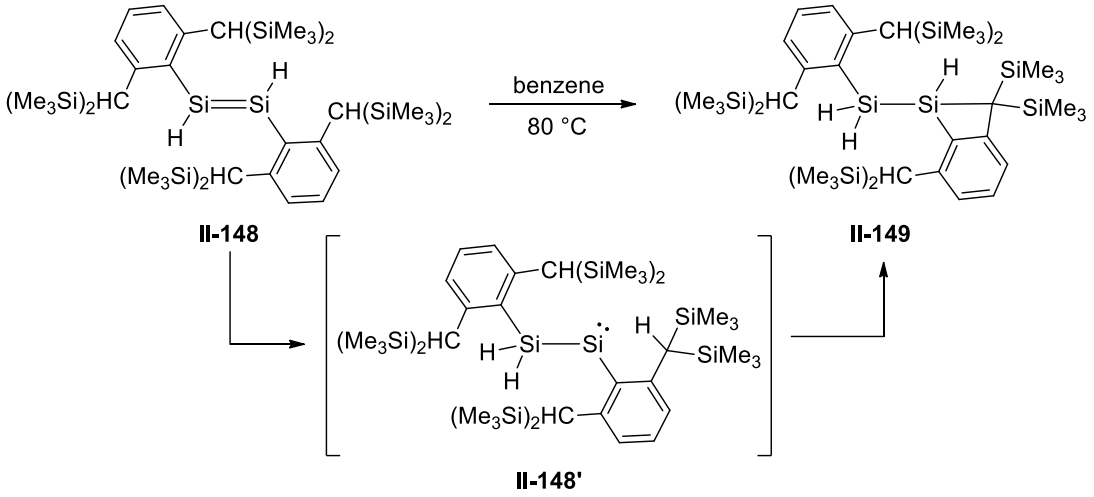

Scheme 55. Thermal isomerization of **II-148** to give **II-149**.

Germylene **II-67** has also demonstrated the ability to activate the C–H bond of phenylacetylene to give **II-150**, however the reaction is accompanied by formation of the [2+4] cycloaddition product.[85] In a separate report, the reaction of **II-67** with trimethylsilyl diazomethane resulted in C–H bond cleavage to furnish the diazogermylene NacNacGeC(N_2)$SiMe_3$ (**II-151**) after three days at room temperature (Scheme 56).[86]

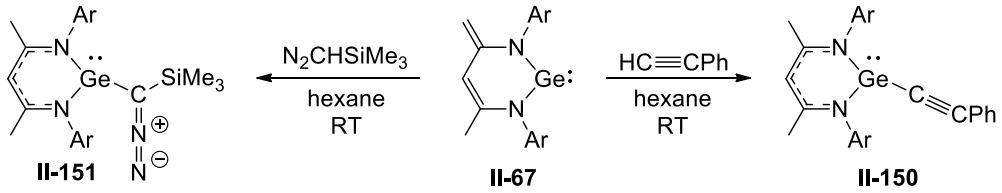

Scheme 56. C–H activation by germylene **II-67**.

A series of C–H activation reactions using dimetallynes with cyclic olefins has been reported by the Power group.[87] Treatment of digermyne (**II-19**) and distannyne (**II-30**) with cyclopentadiene at room temperature gave the corresponding germanium (**II-152**) and tin (**II-153**) aryl cyclopentadienyl species along with evolution of hydrogen gas (Scheme 57). The less reactive cyclopentene did not react with **II-30** but two equivalents of cyclopentene reacted with **II-19** to give the same Cp-containing species **II-152** along

with a complex mixture of products. Finally, no reaction was observed between cyclohexadiene with **II-30** but reaction of **II-19** with 4 equivalents of cyclohexadiene gave a mixture of the known hydride (**II-20**), benzene, and novel germanorbornene **II-154** (Scheme 57). The products obtained are highly unusual as dimetallynes have been shown earlier to undergo cycloadditions with alkenes.[88] In a subsequent paper, experimental evidence suggests the 1,2-addition of the doubly allylic C–H bond of cyclopentadiene across the M≡M bond is the reaction mechanism, while in the case of cyclopentene an oxidative dehydrogenation is proposed to occur first.[89]

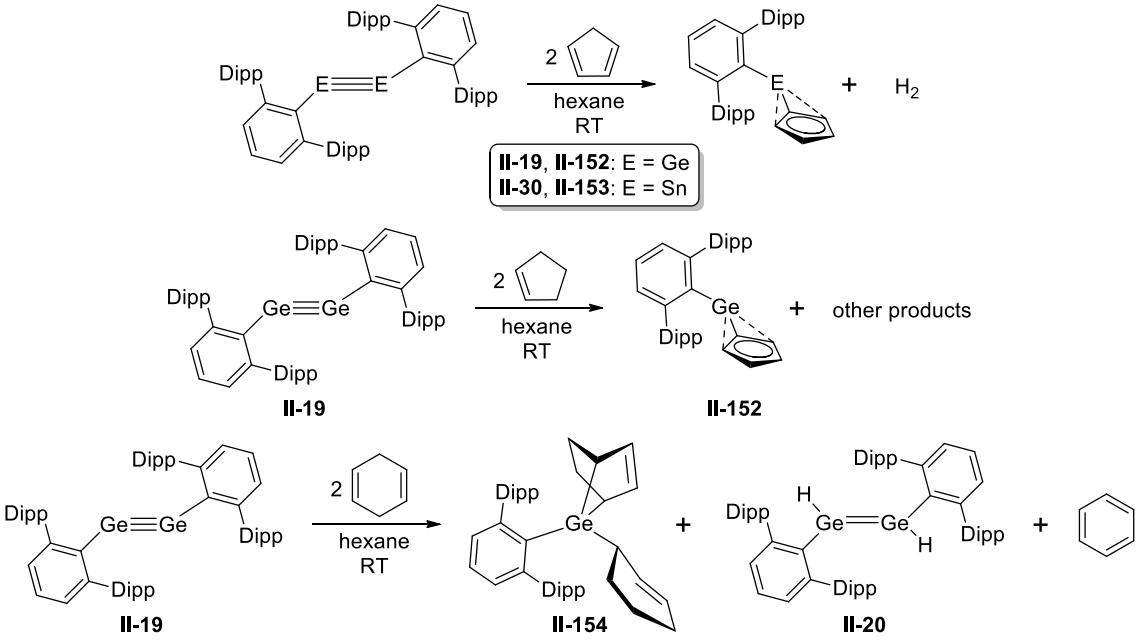

Scheme 57. Activation of C–H bonds in cyclic olefins by dimetallynes **II-19** and **II-30**.

Similarly, amido-digermyne **II-25** reacts with an excess of 1,3-cyclohexadiene to afford the 1,4-bis(germylene)-substituted carbocycle **II-155**.[90] Upon heating, compound **II-155** yielded benzene and the hydrido-digermene **II-26** (Scheme 58). Overall, the process can be considered as the C–H activation of 1,3-cyclohexadiene by **II-25** or the transfer hydrogenation of **II-25** by 1,3-cyclohexadiene. The mechanism of the reaction

was probed with quantum mechanical calculations and revealed that addition of **II-25** to 1,3-cyclohexadiene occurs in parallel with cleavage of the Ge–Ge bond followed by step-wise *β*-hydride elimination to give **II-26** and benzene.

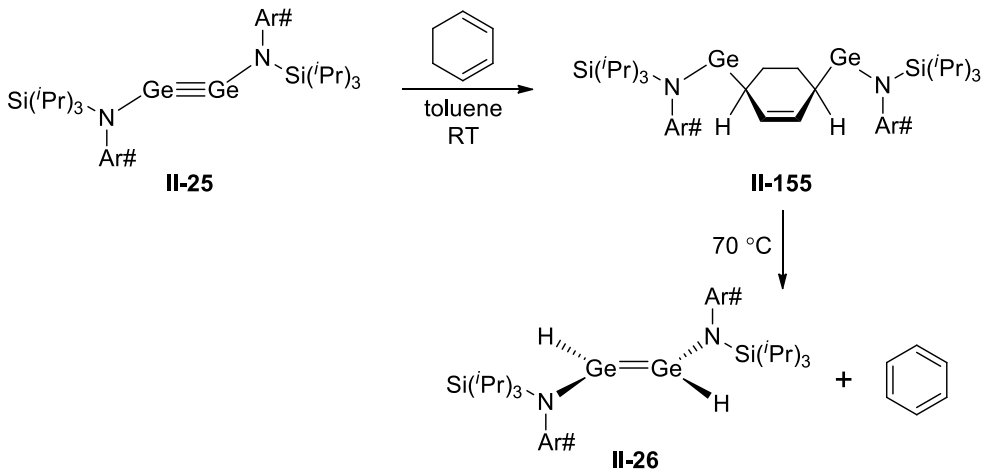

Scheme 58. Reaction of **II-25** with 1,3-cyclohexadiene.

Finally, the adduct between diaryl germylene **II-27** and *tert*-butyl isocyanide (**II-156**) undergoes C–H activation upon heating to give the Ge(IV) hydride cyanide complex **II-157** and isobutene in nearly quantitative yield (Scheme 59).[91]

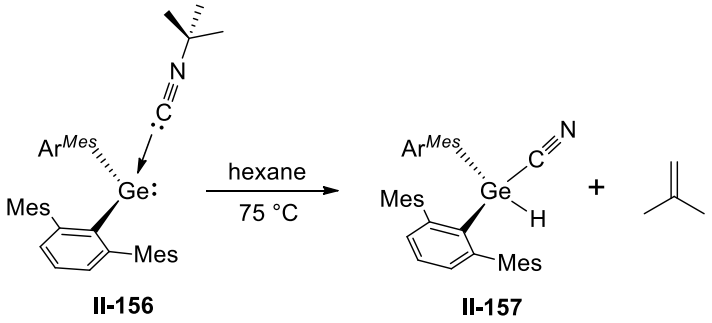

Scheme 59. Intramolecular C–H activation upon heating of **II-156** to give **II-157** and isobutylene.

DFT calculations were used to elucidate a plausible mechanism for the reaction. Direct deprotonation of the *tert*-butyl group led to a prohibitively high energy for the transition state. As such, Power and co-workers considered a concerted mechanism which led to a

transition state, with an activation energy of 29 kcal mol^{-1}, for heterolytic C–N bond cleavage along with the formation of a formally anionic germanium centre and a *tert*-butyl cation. The subsequent reaction path is exothermic by 9 kcal mol^{-1} and led to the complete dissociation of the *tert*-butyl cation coupled with simultaneous C–H proton transfer to germanium.

II.1.5 Si–H and Sn–H Bond Activation

Despite the analogy between H–H and Si–H activation, only a handful of reports regarding silane activation by main group metal complexes are found in the literature. Facile splitting of the Si–H bond of triethylsilane was demonstrated by Braunschweig and co-workers with pentaphenylborole (**II-158**).[92] As such, addition of the silane to a solution of **II-158** resulted in quantitative yield of the kinetic product *trans*-**II-159**. Conversion to the thermodynamic product *cis*-**II-159** was accomplished by heating a solution of *trans*-**II-159** at 60 °C for 3 days (Scheme 60).

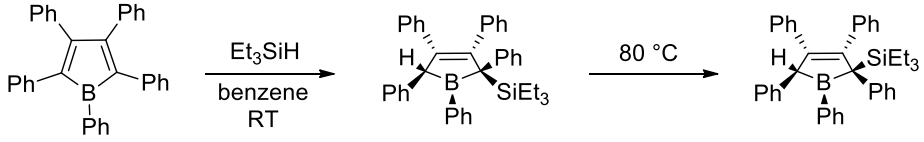

II-158 *trans*-**II-159** *cis*-**II-159**

Scheme 60. Activation of triethylsilane by pentaphenylborole **II-158**.

Analogous to the mechanism for H_2 addition to **II-1**, the addition of triethylsilane was proposed to occur via 1,2-addition across the B–C_α bond to give a ring opened 1-bora-2,4-pentadiene product that subsequently undergoes ring closure followed by 1,2-hydride migration to give the final product. Unlike the addition of dihydrogen, activation of triethylsilane is highly selective under ambient conditions as a consequence of restricted rotation in the ring opened intermediate due to the bulky phenyl and triethylsilyl groups.

Therefore, interconversion between the two rotamers is disfavored and *trans*-**II-159** is formed exclusively.

Contrary to the addition of protic bonds to **II-9**, addition of hydridic SiH_4 gives rise to **II-160** with a backbone appended SiH_3 moiety and a hydride bound to gallium (Scheme 61).[28]

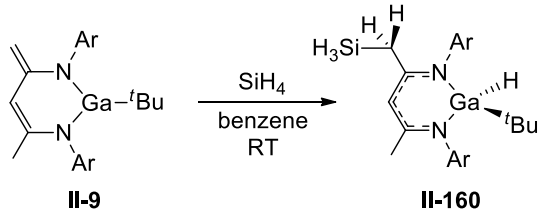

II-9 **II-160**

Scheme 61. 1,4-addition of SiH_4 across gallium complex **II-9**.

Bertrand and co-workers have revealed that cyclic alkyl amino carbene **II-11** is also capable of activating a series of silanes to give silyl hydride **II-161**, with reaction conditions dependent on the steric bulk of the substituents on the substrate.[93] While N-heterocyclic carbenes are inert towards the activation of dihydrogen, carbene **II-162** reacted with phenylsilane at room temperature to afford the Si–H insertion product **II-163** (Scheme 62).

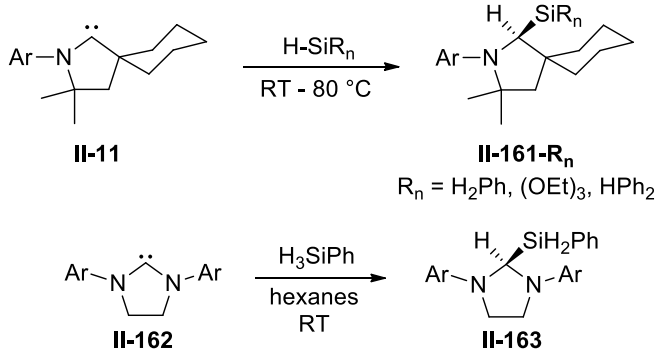

II-11 **II-161-R_n**

R_n = H_2Ph, $(OEt)_3$, HPh_2

II-162 **II-163**

Scheme 62. Activation of silanes by carbenes **II-11** and **II-162**.

On the other hand, reaction of unsaturated N-heterocyclic carbene **II-164** with phenyl silane at high temperature resulted in C–N bond cleavage and ring expansion to

give **II-165** (Scheme 63).[94] Though it wasn't observed directly, the reaction is proposed to go through the Si–H activation intermediate **II-165'** followed by insertion of the silyl group into the C–N bond. The final step of the reaction sequence involves hydrogen atom transfer from the silicon atom to the carbon atom to give **II-165** as the final product.

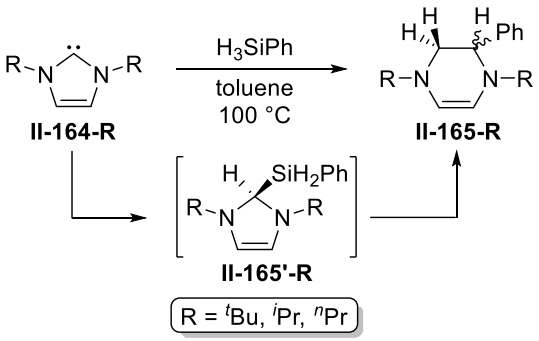

Scheme 63. Si–H bond activation by NHC **II-164** on-route towards C–N bond cleavage and ring expansion.

Bond activation by diamido carbene **II-53** has also been extended to silanes.[95] At room temperature, **II-53** cleaves the Si–H bond of a variety of alkyl, aryl, and alkoxy silanes while activation of trichlorosilane required heating to 60 °C to furnish the corresponding silyl hydride **II-166** (Scheme 64).

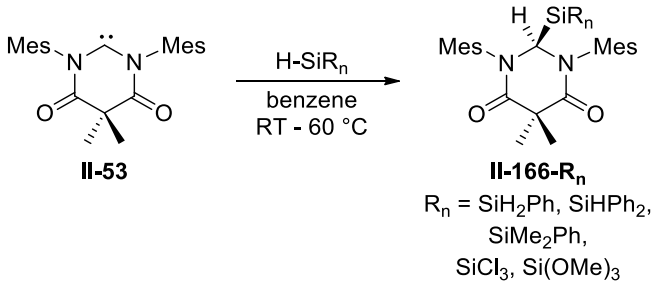

Scheme 64. Activation of silanes by diamido carbene **II-53**.

Bis(boryl) stannylene **II-38** reacted readily with silanes to yield silyltin(IV) hydrides, the first example of Si–H oxidative addition across a Sn(II) centre (Scheme 65).[41]

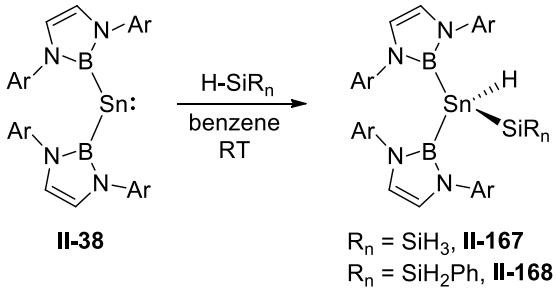

Scheme 65. Silane activation by bis(boryl) stannylene **II-38**.

A single example of Sn–H bond activation is reported in the literature. As shown in Scheme 66, reaction of triphenyltin hydride with NacNacGa (**II-7**) gave the 1,1-addition product NacNacGaH($SnPh_3$) (**II-169**).[27]

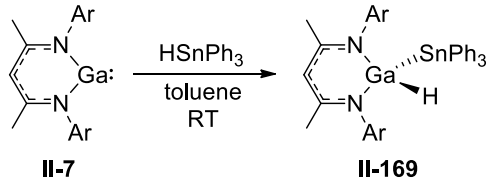

Scheme 66. 1,1-addition of the Sn–H bond across the Ga(I) centre in **II-7**.

II.1.6 B–H and Al–H Bond Activation

Only a few examples of B–H bond activation by a main group element complex has been reported in the literature, all utilizing compounds with low valent Group 14 centres. Cyclic alkyl amino carbene **II-11** has been shown to activate pinacolborane to give **II-170**,[93] while the first example of 1,1-insertion of BH_3 into a carbene was reported by the groups of So and Mézailles.[96] Using the stable carbenoid **II-171**, addition of $BH_3{\cdot}SMe_2$ resulted in the formation of compound **II-172** after one night at room temperature. Compound **II-172** was found to be monomeric in solution but dimerizes upon crystallization. DFT calculations revealed that addition of BH_3 to **II-171** is highly exergonic with a calculated ΔG value of −59.5 kcal mol^{-1}. Later it was shown that diamido carbene **II-53** reacts readily with borane-dimethyl sulfide to yield the Lewis base

stabilized hydrido boryl complex **II-173**.[97] Lastly, stannylene **II-38** reacts with borane-trimethylamine to furnish the B−H addition product **II-174**.[41] The four reactions are summarized in Scheme 67.

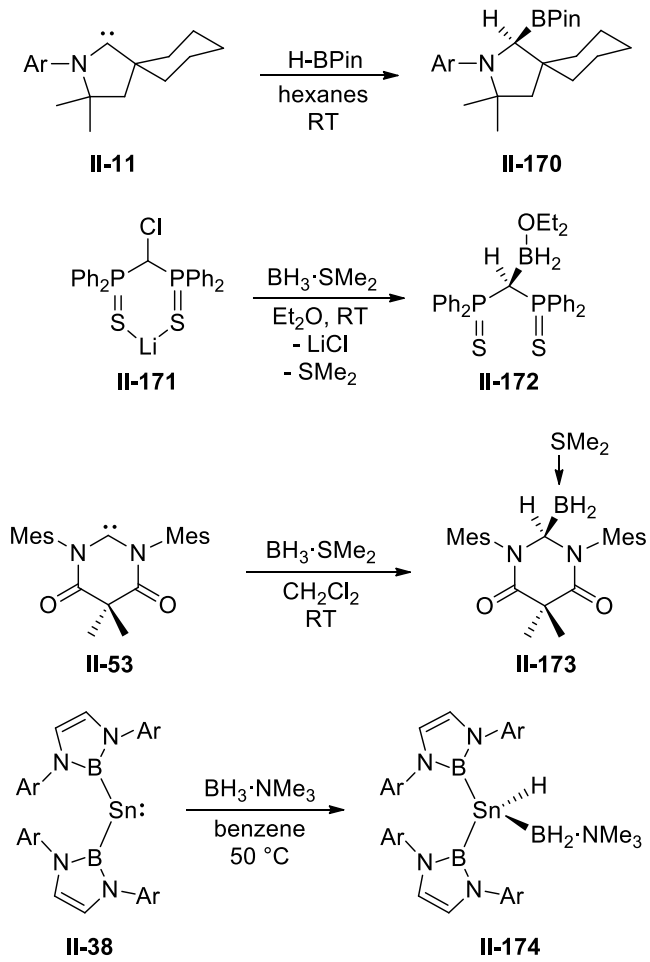

Scheme 67. B–H bond activation by main group element complexes.

One example of Al–H bond activation was found in the literature. Reaction of silylene **II-57** with one equivalent of alane-trimethylamine at room temperature resulted in production of the 1,1-insertion product **II-175** (Scheme 68).[98]

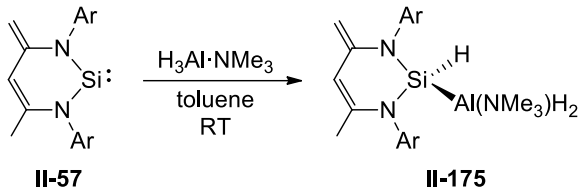

Scheme 68. Al–H bond activation by **II-57**.

II.1.7 P–H and As−H Bond Activation

The first instance of P–H bond activation by a main group element complex was shown by the reaction of Ga(I) compound **II-7** with diphenylphosphine to furnish the hydrido gallium phosphide **II-176** (Scheme 69).[27]

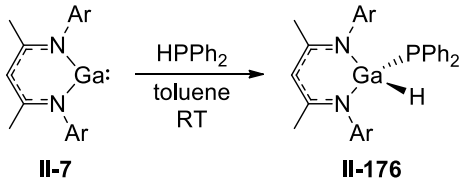

Scheme 69. Activation of diphenylphosphine by **II-7**.

Following that report, Bertrand utilized *c*AACs **II-11** and **II-178** to activate the P–H bonds of phenyl and diphenylphosphine, respectively.[93] NHC **II-162** can also activate phenylphosphine to give hydrido phosphide **II-180** (Scheme 70).

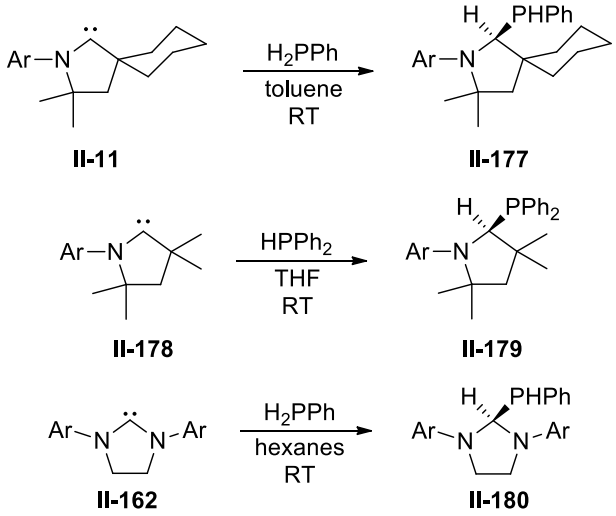

Scheme 70. Phosphine activation by carbenes.

Primary phosphines were smoothly activated by **II-53** at room temperature, while secondary phosphines required elevated temperature to complete the reaction to give the respective hydrido phosphide derivatives (Scheme 71).[99]

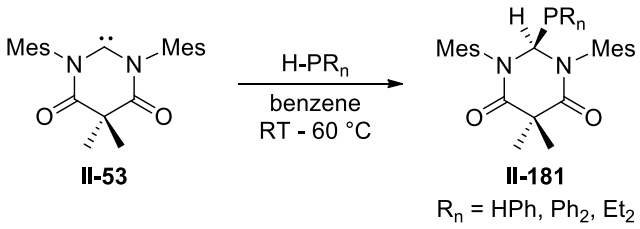

Scheme 71. Activation of primary and secondary phosphines by **II-53**.

The parent phosphine PH_3 reacted with silylene **II-57** to give the 1,1-addition product NacNac'SiH(PH_2) (**II-182**), proceeding slowly with an excess of phosphine in the reaction.[100] In contrast, reaction of **II-57** with AsH_3 proceeds rapidly to give the arsasilene **II-183**. Interestingly, solvation of isolated crystals of **II-183** leads to an equilibrium mixture with its tautomer, the 1,1-addition product **II-183'**. The authors eventually discovered that **II-183'** is the initial product obtained from the reaction of **II-57** with arsine, as formation of **II-183'** starts at −50 °C while production of arsasilene **II-183** only occurs upon warming above −30 °C (Scheme 72). The drastic difference in reactivity between PH_3 and AsH_3 is ascribed to the higher Bronsted acidity of AsH_3 versus PH_3 which facilitates As–H activation by **II-57**.

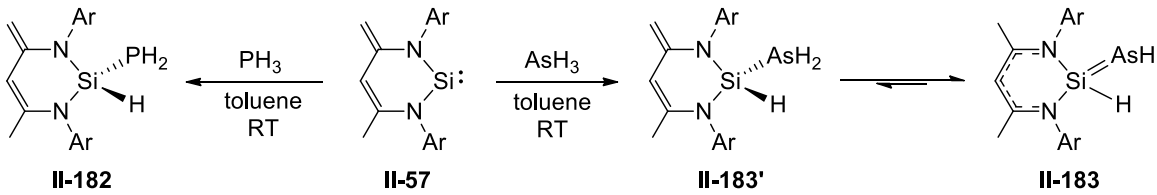

Scheme 72. PH_3 and AsH_3 activation by silylene **II-57**.

The first example of P–H bond activation by germanium and tin was reported by Ragogna and co-workers.[101] Reaction of diaryl germylene **II-27** and stannylene **II-36** with an excess of PH_3 (80 psi) gave both the 1,1-addition product, **II-184** and **II-185**, as well as the arene elimination product **II-186** and **II-187** (Scheme 73).

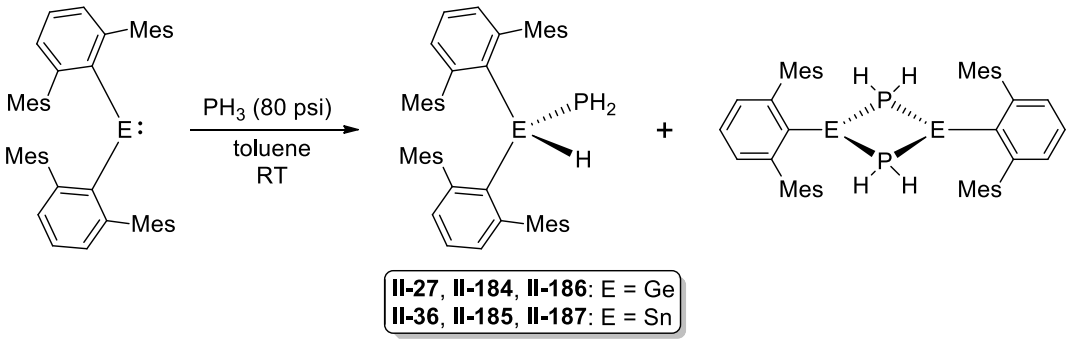

Scheme 73. Activation of PH_3 by low coordinate diaryl tetrylenes **II-27** and **II-36**.

II.1.8 C–F Bond Activation

As carbon forms the strongest single bond with fluorine, the activation of C–F bonds is unsurprisingly challenging and typically requires the application of highly elaborate transition metal complexes and/or forcing conditions. Recent reports have delineated the ability of main group metal complexes to cleave such bonds. Activation of pentafluoropyridine and octofluorotoluene by ethyl dithiocarbamate **II-188** was reported in 2012 by Bertrand and co-workers.[102] In both cases, selective activation of the C–F bond at the *para*-position was observed accompanied by ring closure to give compounds **II-189** and **II-190**. In a later paper, insertion of the *para*-C–F bond of pentafluoropyridine into *c*AAC **II-191** at room temperature to give adduct **II-192** was discovered by the same group (Scheme 74).[103]

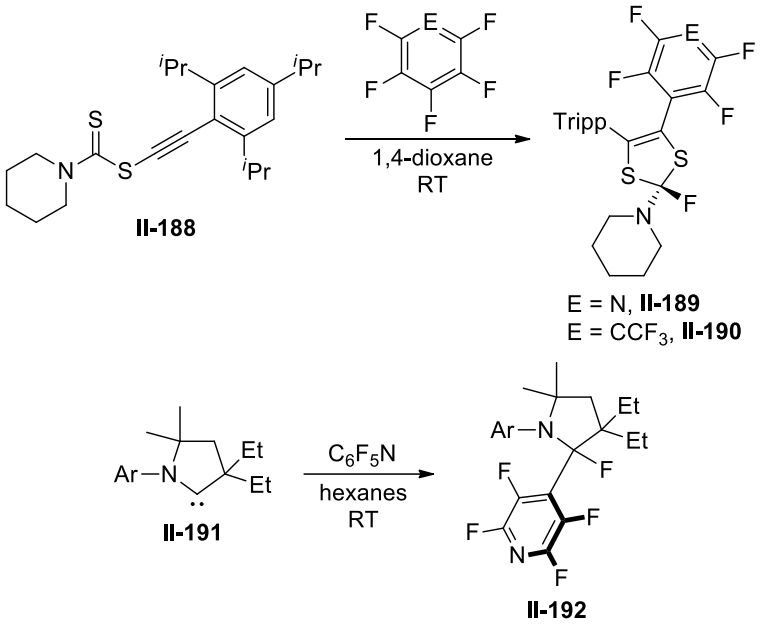

Scheme 74. C–F bond activation with carbamate **II-188** and carbene **II-191**.

Utilizing two-coordinate silylene **II-57** and three-coordinate chloro silylene **II-193**, Roesky and co-workers have revealed the activation of a variety of aryl C–F bonds.[82] Both compounds were able to activate hexafluorobenzene to give the corresponding silicon(IV) fluorides **II-194** and **II-195**. When **II-57** and **II-193** are treated with pentafluoropyridine and octafluorotoluene, regioselective activation at the *para*-position led to the formation of complexes **II-196** to **II-199**. As mentioned earlier, selective addition of the C–H bond of pentafluorobenzene was observed with **II-57**. With **II-193**, selective insertion into the *para*-C–F bond occurred to give **II-200**. The authors attributed the regioselectivity to the poorer stability of penta-coordinate silicon hydrides compared to penta-coordinate silicon fluorides. The reactivity of silylenes **II-57** and **II-193** are summarized in Scheme 75.

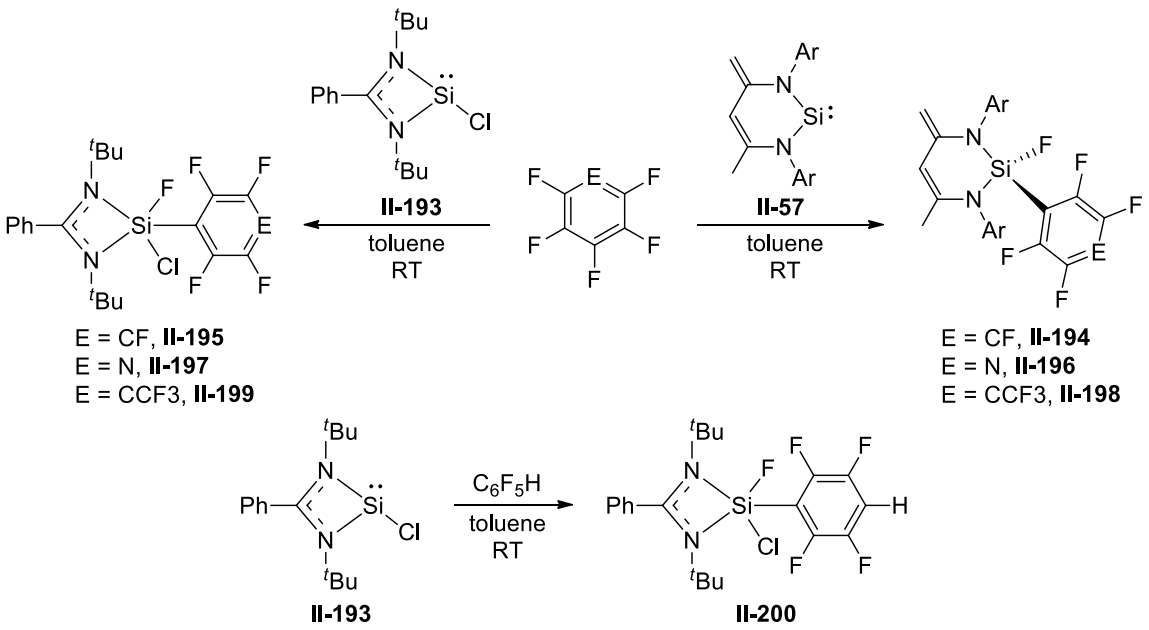

Scheme 75. Aryl C–F bond activation by silylenes **II-57** and **II-193**.

As shown by Tacke *et al*., bis-amidinate silylene **II-201** oxidatively adds hexafluorobenzene to give **II-202** at room temperature.[104] The related germylene amido **II-203** reacts with pentafluoropyridine at room temperature to give cleanly the *para*-C–F activated product **II-204** (Scheme 76).[105]

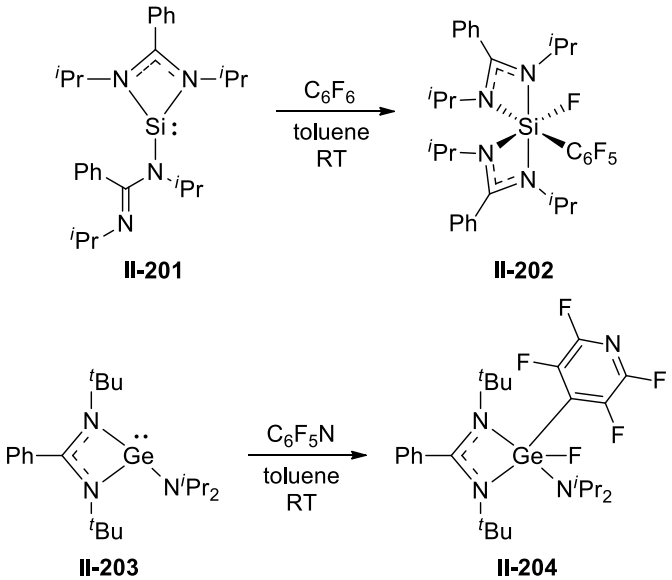

Scheme 76. Activation of C–F bonds by silylene (**II-201**) and germylene (**II-203**) amidinate complexes.

Even more challenging than aryl C–F bond activation is the activation of alkyl C–F bonds and, in particular, mono-activation of the CF_3 group. Treatment of **II-57** and **II-193** with $PhN=C(CF_3)_2$ resulted in difluorinated alkene products **II-205** and **II-206** formed by the selective activation of one of the carbon–fluorine bonds rather than the three-memebered silacycle as a result of [1+2]-cycloaddition (Scheme 77).[106]

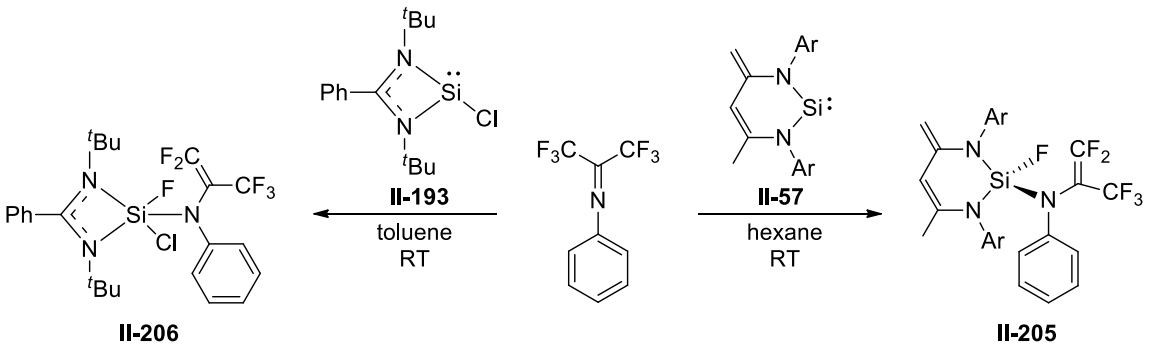

Scheme 77. Selective mono-activation of a CF_3 group by silylenes **II-57** and **II-193**.

II.1.9 C–X (X = Cl, Br, I) Bond Activation

Related activation of weaker C–X bonds (X = Cl, Br, and I) by main group metal complexes has also been demonstrated. *β*-Diketiminate stabilized gallium(I) complex **II-7** has been shown to activate the C–Cl bond of *tert*-butyl chloride to give **II-207** by Fischer and co-workers. (Scheme 78).[107]

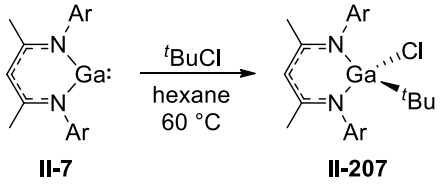

Scheme 78. C–Cl bond activation by gallium(I) complex **II-7**.

The indium analogue of **II-7**, NacNacIn (**II-208**), can activate primary, secondary, and tertiary alkyl iodides, as well as secondary and tertiary alkyl bromides (Scheme 79).[108] Mechanistically, rapid recombination of indium and carbon-centreed radicals upon

homolytic cleavage of the C–X bond was proposed for these reactions, based on the observation of a weak but perisistent EPR signal at −83 °C in the reaction of **II-208** with methyl iodide.

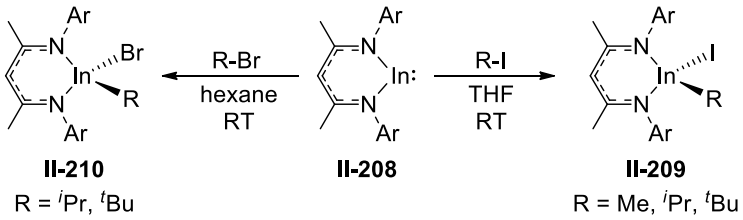

Scheme 79. C–X bond activation by NacNacIn (**II-208**).

A series of haloalkanes were reacted with silylene **II-57** by Driess and co-workers (Scheme 80).[109] The reaction of **II-57** with methyl iodide furnishes solely the 1,1-insertion product NacNac'SiI(Me) (**II-211**). In addition, **II-57** readily inserts into the aliphatic C–Br bond of benzyl bromide, yielding the 1,1-insertion product NacNac'SiBr(CH_2Ph) (**II-212**). Dichloromethane reacts with **II-57** over the course of several weeks to afford the 1,1-insertion product NacNac'SiCl(CH_2Cl) (**II-213**) while the reaction with CH_2ClI was much faster and is complete within 8 hours, leading to the iodo(chloromethyl)silane **II-214** exclusively. Reaction of **II-57** with dibromomethane affords the 1,1-insertion product NacNac'SiBr(CH_2Br) (**II-215**) with concomitant production of the dibromosilane NacNac'$SiBr_2$. Treatment of **II-57** with perhalogenated hydrocarbons also affords the respective 1,1-insertion products. Reaction of $CHCl_3$ and $MeCCl_3$ with **II-57** gave the chloro(dichloroalkyl)silane **II-216** along with a small amount of the dichlorosilane NacNac'$SiCl_2$. With regards to the mechanism, Driess proposed that the reaction occurs via the 1,4-addition (kinetic) product followed by rearrangement to the thermodynamic 1,1-insertion product, in accord with previous DFT

calculations, which suggested that addition of electrophiles to **II-57** leads to the 1,4-addition product due to the zwitterionic character of **II-57**.[110]

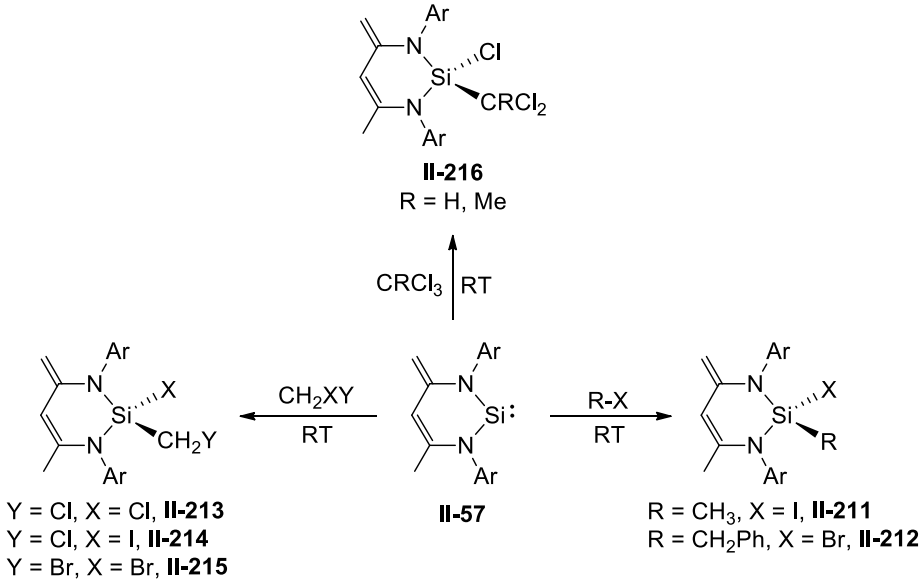

Scheme 80. C–X bond activation by silylene **II-57**.

Stannylenes are also capable of activating C–X bonds (Scheme 81).

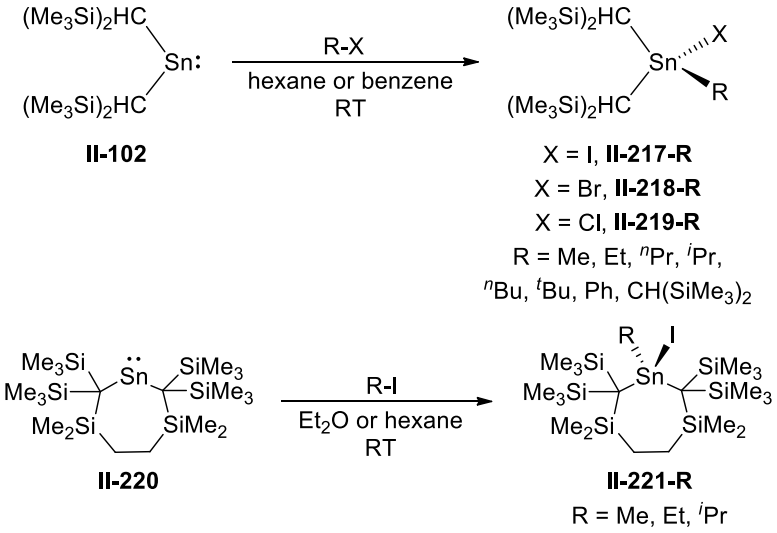

Scheme 81. Activation of C–X bonds by stannylenes **II-102** and **II-220**.

Lappert has shown that stannylene **II-102** can undergo oxidative addition with a variety of alkyl and aryl halide to give the Sn(IV) complexes $(CH(SiMe_3)_2)_2SnRX$ (**II-217** X = I, **II-218** X = Br, **II-219** X = Cl).[111] The relative rates of reaction decreased in the sequence

I > Br > Cl. As reported by the groups of Eaborn and Smith, cyclic stannylene **II-220** can similarly activate alkyl iodides to give complex **II-221**.[112,113]

II.1.10 C–O Bond Activation

The activation of C–O bonds is highly desirable, with many precedents for the cleavage of more reactive allylic and benzylic C(sp^3)–O bonds by transition metal complexes. On the other hand, examples of alkyl C(sp^3)–O bond cleavage are scarce in the literature. Driess and co-workers revealed that if the bis-carbene Al(I) complex **II-110** is generated with potassium triethylborohydride in THF, the reaction afforded the THF-ring-opened complex **II-222** as the product (Scheme 82).[70] DFT calculations suggested that the reaction starts with activation of the Al–H bond by the Lewis acid BEt_3, formed in-situ from K[$HBEt_3$]. Interaction of the aluminum centre with THF further weakens the Al–H bond, leading to the rate-determining aluminum hydride bond scission. Subsequent hydride transfer from the $HBEt_3^-$ anion to the THF molecule triggers the C–O bond cleavage, leading to the stable, isolated product **II-222**.

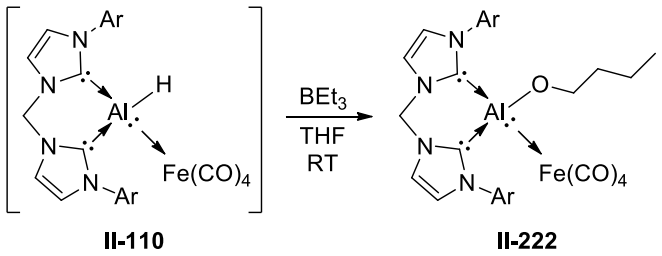

Scheme 82. Ring-opening of THF via C–O bond cleavage by **II-110**.

II.2 Aluminum in the +1 Oxidation State

Aluminum, the most abundant metal in the Earth's crust, exhibits a vast array of chemistry in the trivalent state, the most stable oxidation state for the element.[114,115] There has also been significant interest in the chemistry of the lower oxidation states of

aluminum, particularly the monovalent state as it is expected to be far more accessible than the +2 oxidation state. This portion of the historical will be focused on monomeric Al(I) compounds and their subsequent reactivity starting with a short summary of the chemistry of aluminum(I) halide and stable, tetrameric aluminum(I) compounds.

Low valent aluminum chemistry has been known since 1948, with monochloro aluminum, AlCl, among the first to be reported in 1948 by Klemm *et al*., prepared by reacting elemental chlorine and aluminum metal at 1000 °C.[116] Klemm also showed that aluminum(I) halides are thermodynamically unstable under standard conditions as they disproportionate into aluminum metal and aluminum(III) halides.[116] Despite their instability, aluminum(I) halides can be trapped and studied in solid argon matrices and are entropically favored in the gas phase at high temperatures and low pressures. Preparative routes to gaseous AlX include synproportionation reactions between AlX_3 and molten aluminum metal or the reaction of HX (X = Cl, Br, or I) or CHF_3 (as an HF equivalent) with molten aluminum metal at high temperatures (about 800–1000 °C).[117] By using cryochemical methods and preparing metastable solutions of AlX at −78 °C, Schnöckel and co-workers were able to study the reactivity of aluminum(I) halides.[117]

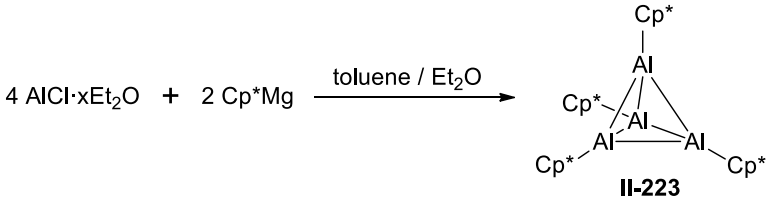

Scheme 83. Synthesis of $(Cp^*Al)_4$ **II-223**.

It wasn't until 1991 when the first aluminum(I) compound that was stable under normal conditions was prepared by Schnöckel (Scheme 83).[118] The organometallic Al(I)

compound $(Cp^*Al)_4$ (**II-223**) was prepared by a salt metathesis reaction between $MgCp^*_2$ and a metastable solution of AlCl in a diethyl ether/toluene mixture.

An alternative preparation, reported by Roesky and co-workers, involved the reduction of $[Cp^*AlCl(\mu\text{-}Cl)]_2$ with potassium or sodium/potassium alloy in toluene.[119] Compound **II-223** was structurally characterized and found to be tetrameric in the solid state. However, at temperatures above 30 °C there exists an equilibrium between tetrameric $(Cp^*Al)_4$ and monomeric Cp*Al.[120,121] As expected, Cp*Al is monomeric in the gas phase as determined by means of gas-phase electron diffraction.[122] After the initial synthesis of **II-223**, other stable tetrameric Al(I) complexes with σ-bonded substituents such as bulky silyl ($Si(^tBu)_3$,[123] $SiMe_3$[124]) and alkyl ligands ($C(SiMe_3)_3$[125]) were prepared. The reactivity of these tetrameric species is well established and has been extensively reviewed.[126-128]

II.2.1 Monomeric Aluminum(I) Compounds

In an effort to access monomeric Al(I) species, Roesky and co-workers reasoned that utilizing the sterically bulky bidentate *β*-diketiminate ligand should afford the necessary steric stabilization to prevent oligomerization.[8] Accordingly, they prepared the *β*-diketiminato aluminum diiodide complex $NacNacAlI_2$ (**II-224**), which upon reduction with two equivalents of potassium metal at room temperature gave NacNacAl (**II-225**), the first example of a well-defined monomeric aluminum(I) derivative (Scheme 84). A closely related analogue of **II-225** was later prepared by the Cui group utilizing the ^{t}BuNacNac ligand (^{t}BuNacNac = $[ArNC(^tBu)CHC(^tBu)NAr]^-$), following the same synthetic strategy of reducing the diiodide precursor, ^{t}BuNacNacAlI$_2$ (**II-226**), with two equivalents of potassium to give ^{t}BuNacNacAl (**II-227**).[129] The remarkable thermal

stability of complexes **II-225** and **II-227**, with decomposition temperatures above 150 °C, is attributed to the kinetic protection of the metal centres afforded by the steric bulk of the *β*-diketiminate ligand. X-ray crystallographic analyses of the heterocycles revealed a planar AlN_2C_3 ring. As well, the two complexes are rare examples of two-coordinate aluminum centres.

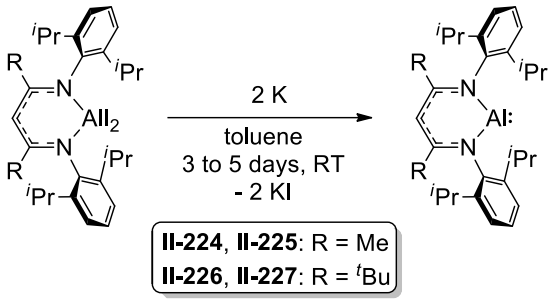

Scheme 84. Preparation of *β*-diketiminate Al(I) complexes **II-225** and **II-227**.

Theoretical studies on **II-225** revealed that it has both Lewis acidic as well as Lewis basic character due to the sp-like hybridized singlet lone pair of electrons and an empty p-orbital at the aluminum centre.[8] This duality was demonstrated by the reaction between **II-225** and tris(pentafluorophenyl)borane (Scheme 85).[130] The product of the reaction, **II-228**, was crystallographically characterized and revealed to be the Lewis acid/base adduct with the aluminum centre acting as a σ-donor to the Lewis acidic boron centre. Concomitantly, the aluminum atom accepts electron density from one of the *ortho*-fluoro substituents of a pentafluorophenyl ring, resulting in elongation of the C–F bond (1.414(6) Å) relative to the remaining 14 C–Fs (average distance of 1.355 Å). This interaction is strong enough to persist in solution, with nine partly overlapping resonances in the ^{19}F NMR spectrum, indicative of a distorted $B(C_6F_5)_3$ group due to the Al–F interaction.

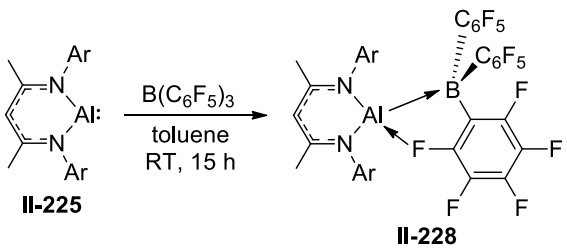

Scheme 85. Ambiphilic behavior of **II-225** displayed upon reaction with $B(C_6F_5)_3$.

With their singlet lone pairs, complexes **II-225** and **II-227** can be viewed as being isolobal to N-heterocyclic carbenes and thus have potential to exhibit carbene-like reactivity or act as strong reducing agents. The latter reactivity is exemplified by the reaction of **II-225** with p-block elements. The Al(I) centre is readily oxidized with elemental oxygen to give the oxide-bridged species $[NacNacAl(\mu\text{-}O)_2]$[131] (**II-229**), while the corresponding reaction with elemental sulfur gave the S_3 bridged complex $[NacNacAl(\mu\text{-}S_3)_2]$ (**II-230**) with a central Al_2S_6 ring described as a homobimetallic derivative of the S_8 crown.[132] Similarly, the partial reduction of P_4 with **II-225** led to the P_4^{4-} bridged species $(NacNacAl)_2(\mu\text{-}P_4)$ (**II-231**) which was formed upon insertion of the aluminum centre into two P–P edges of the P_4 tetrahedron (Scheme 86).[133]

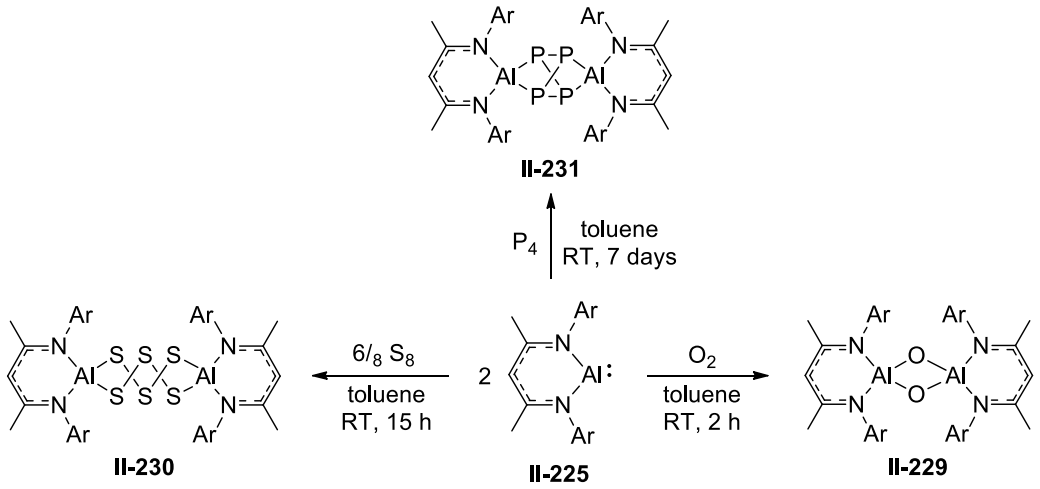

Scheme 86. Reaction of **II-225** with the p-block elements.

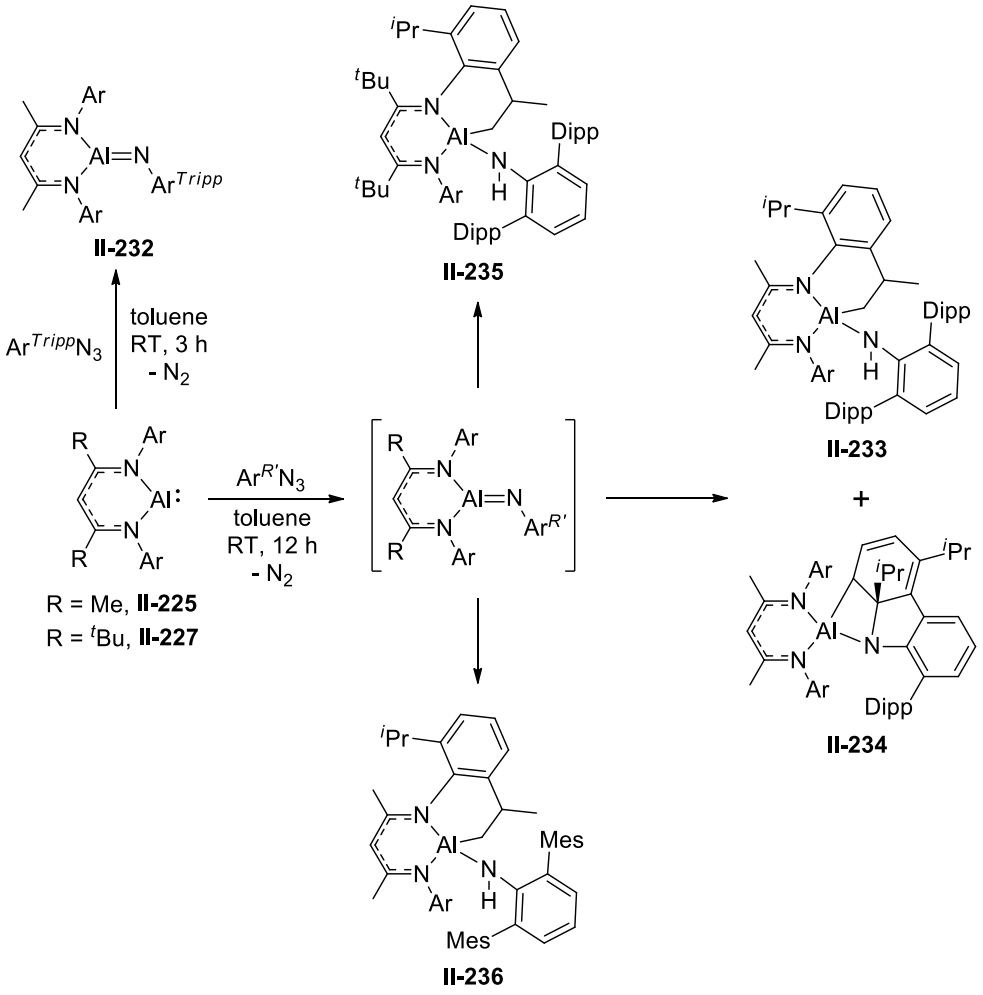

Scheme 87. Reaction of **II-225** and **II-227** with terphenyl azides.

The carbene-like ability of **II-225** and **II-227** to undergo cycloaddition reactions, along with their reducing power, has led to the two complexes being particularly reactive towards unsaturated substrates, most prominently with organic azides (Scheme 87).[134] Treatment of **II-225** with $Ar^{Tripp}N_3$ (Ar^{Tripp} = 2,6-(2,4,6-$^{i}Pr_3C_6H_3)_2C_6H_3$) afforded the first monomeric aluminum imide NacNacAl=NAr^{Tripp} (**II-232**) along with elimination of N_2. When a slightly less bulky terphenyl azide, $Ar^{Dipp}N_3$, was reacted with **II-225**, it was presumed that a similar monomeric aluminum imide was formed initially as an intermediate that subsequently isomerizes to give a mixture of an aluminum alkyl amide, **II-233**, as a result of intramolecular C–H activation, and compound **II-234**, the product of

a formal [2+2] cycloaddition of the Al=N moiety and an aryl substituent on nitrogen. Heating the reaction mixture to 50 °C for 24 hours converted all of **II-234** to **II-233**.[135] The reaction of **II-227** with $Ar^{Dipp}N_3$ gave **II-235**[129] while the reaction of **II-225** with $Ar^{Mes}N_3$ yielded **II-236**,[131] with both reactions proceeding through an assumed aluminum imide intermediate.

Reaction of **II-225** with smaller azides RN_3, where R is $SiMe_3$, $SiPh_3$, and 1-adamantyl, in a 1:2 ratio, led to the novel aluminum analogue of tetrazole NacNacAl[$(NR)_2N_2$] (**II-237**).[136,137] The reaction proceeded via an intermediate aluminum imide that undergoes a [2+3] cycloaddition with the second equivalent of azide to give the isolated product (Scheme 88).

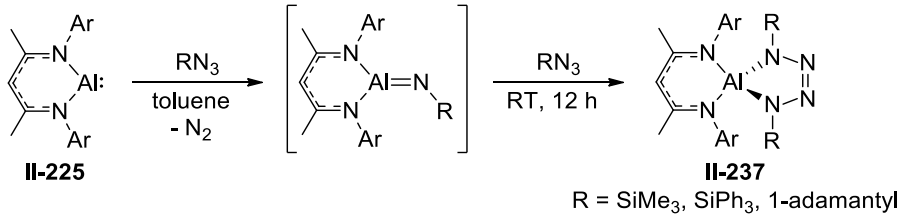

Scheme 88. Reaction of **II-225** with silyl and alkyl azides.

Related reaction of **II-225** with $^tBuSi(N_3)_3$ gave **II-238**.[137] The authors deduced that the production of **II-238** starts with the initial elimination of N_2 to furnish the Al=N intermediate which rearranges to the aluminum silyl imide via migration of an azido group. Finally, the silyl imide intermediate undergoes a [2+2] cycloaddition with itself to give the final, isolated product (Scheme 89).

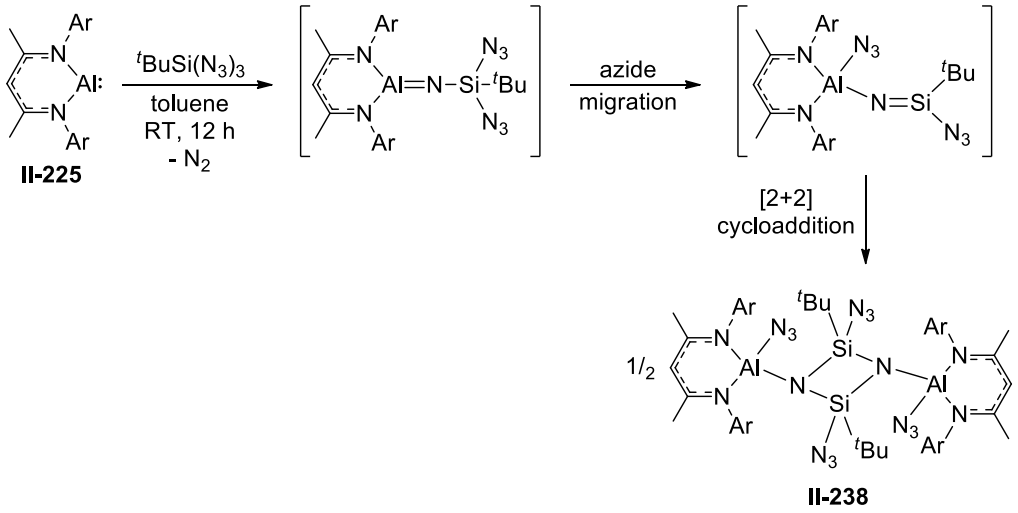

Scheme 89. Reaction of **II-225** with $^{t}BuSi(N_3)_3$ to give **II-238**.

Compounds **II-225** and **II-227** have also demonstrated interesting reactivity with other N-unsaturated substrates. When **II-225** is treated with two equivalents of diphenyldiazomethane, dinitrogen elimination occurs at elevated temperatures to give the diiminyl aluminum compound NacNacAl(N=CPh$_2$)$_2$ (**II-239**).[138] It was assumed that the formation of **II-239** starts with the initial generation of Ph$_2$C=N–N=CPh$_2$ followed by its oxidative addition to **II-225**. The reaction of **II-225** with azobenzene yielded **II-240**, likely via a three-membered AlN$_2$ [2+1] cycloaddition intermediate. Due to the highly strained nature of the ring, the intermediate rearranges to the final product by cleaving the N–N bond concurrently with migration of a hydrogen atom from the *ortho* position of one of the adjacent phenyl rings. Calculations estimated that **II-240** is 76 kcal mol^{-1} lower in energy than the initial cycloaddition intermediate.[139] Reaction of **II-227** with two equivalents of a bulky isonitrile, CNAr^{Dipp}, afforded two different products, **II-241** and **II-242**, depending on the reaction conditions. Both are proposed to form via an initial C–C coupling of the isonitrile molecules, giving intermediates that then undergo a C–H

activation reaction, in the case of **II-241**, or a C–N cleavage of the NacNac ligand followed by a subsequent insertion reaction to produce **II-242** (Scheme 90).[129]

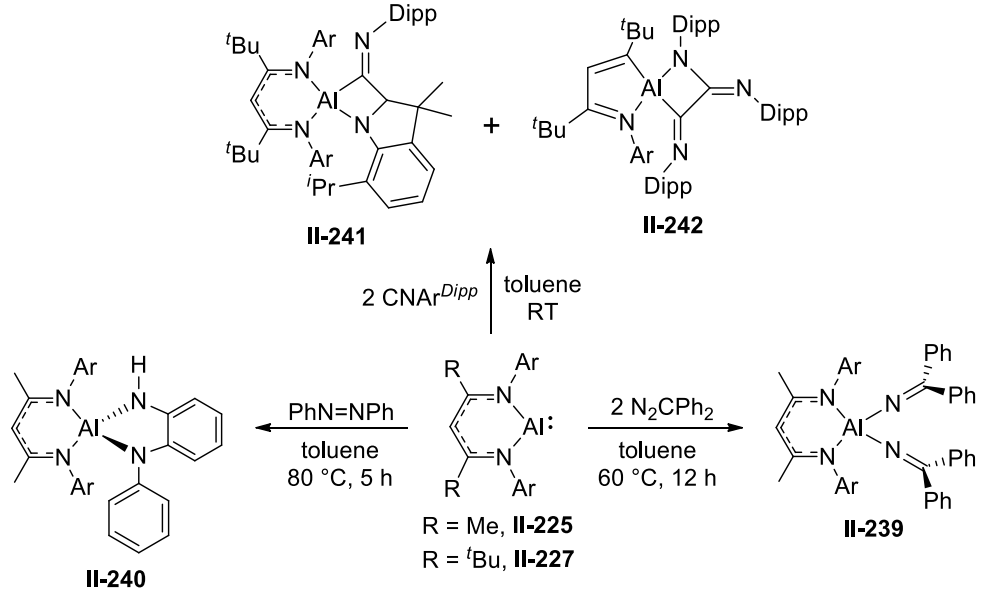

Scheme 90. Reaction of **II-225** and **II-227** with diphenyldiazomethane, azobenzene, and terphenyl isonitrile.

Complex **II-225** readily undergoes cycloaddition at low temperature with acetylene to yield the structurally characterized alumocyclopropene complex NacNacAl(η^2-C_2H_2) (**II-243**).[140] Reaction of **II-225** with other substituted alkynes and diynes (PhC≡CH, MeC≡CMe, and ($Me_3SiC{\equiv}C–)_2$) formed similar alumocyclopropene derivatives (Scheme 91).[141] It is worth noting that **II-225** does not react with bis(trimethylsilyl)acetylene, however the corresponding alumocyclopropene derivative can be obtained via the co-reduction of **II-224** and $Me_3SiC{\equiv}CSiMe_3$ with potassium metal.[142]

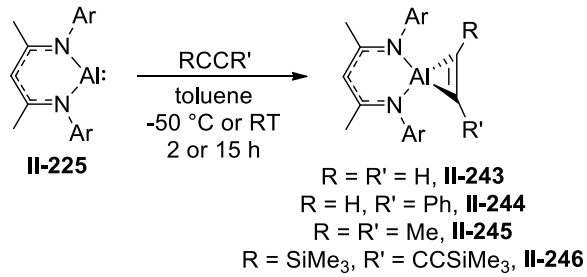

Scheme 91. Cycloaddition of alkynes with **II-225** to give alumocyclopropene derivatives.

Reaction of **II-225** with NHCs at high temperature lead to the attack of the NHC at the aluminum centre followed by hydrogen migration from one of its backbone methyl substituents to give the NHC-coordinated aluminum hydride **II-247**.[138] Remarkably, reaction of **II-227** with an NHC yielded the stable, monomeric aluminum imide **II-248** as a result of ring-contraction (Scheme 92).[143] Compound **II-248** represents the first structurally characterized monomeric iminoalane.

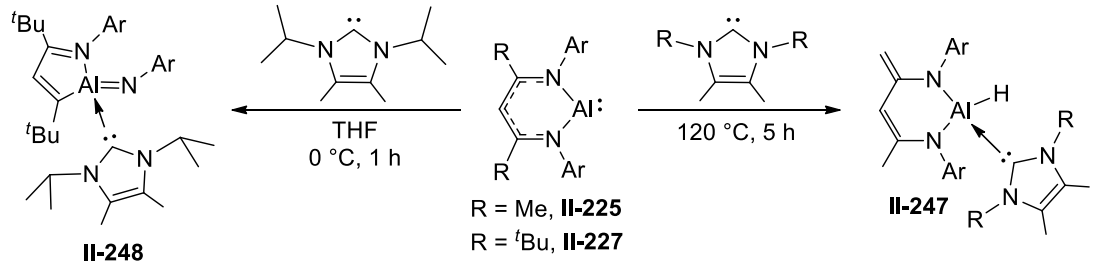

Scheme 92. Reaction of **II-225** and **II-227** with N-heterocyclic carbenes.

Though not as extensively studied, complexes **II-225** and **II-227** also revealed noteworthy reactivity towards compounds with σ-bonds. Oxidative addition of water was observed with **II-227** to give ^{t}BuNacNacAlH(OH) (**II-249**).[129] In contrast, elimination of water and dihydrogen occurs in the reaction of **II-225** with two equivalents of $PhB(OH)_2$, affording the spirocylic complex NacNacAl(OB(Ph)O–)$_2$ (**II-250**) as the final product, containing an unprecedented AlB_2O_3 ring (Scheme 93).[144] DFT calculations supported a concerted mechanism driven by the exothermic formation of the Al–O bonds.

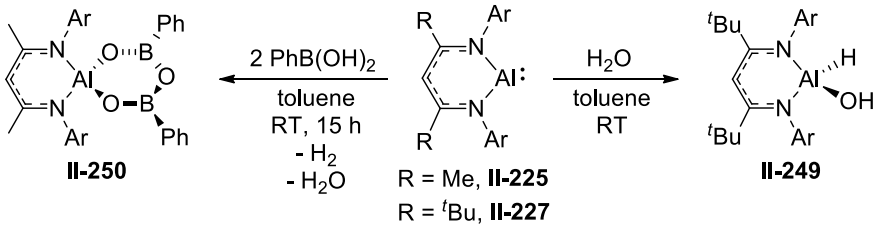

Scheme 93. Reaction of **II-225** and **II-227** with phenylboronic acid and H_2O, respectively.

Kinjo and co-workers have reported the oxidative addition of the C–O bond in an oxazolylidene ring by **II-225** to give the ring expanded compound **II-251** (Scheme 94).[145] However, the reaction is specific to this particular substrate, as reaction of **II-225** with 4,4-dimethyl-2-oxazoline and 3,4,4-trimethyl-2-oxazolinium iodide gave complex mixtures of products.

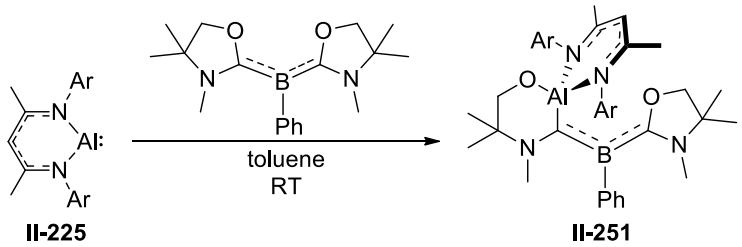

Scheme 94. C–O bond oxidative addition by **II-225**.

Recently, Schultz *et al*. described the insertion of **II-225** into the Bi–C bond of $BiEt_3$ to yield NacNacAlEt($BiEt_2$) (**II-252**) at elevated temperature.[146] In a subsequent paper, reaction of **II-225** with E_2Et_4 (E = Sb, Bi) resulted in oxidative cleavage of the E–E bond to give compound **II-253** at ambient temperature (Scheme 95).[147]

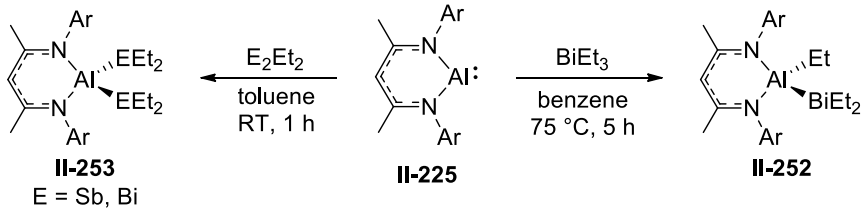

Scheme 95. Oxidative addition of Bi–C and E–E (E = Sb, Bi) bonds by **II-225**.

II.3 Heavier Group 14 Elements in the Zero Valent Oxidation State

Compounds with divalent Group 14 elements are well known in the literature and extensively studied. Recently, the synthesis and characterization of complexes with heavier Group 14 elements in the formal oxidation state of zero have been accomplished. These novel species can be categorized into two groups. The first are di- or trinuclear complexes stabilized by carbenoid ligands with the earliest example of such compounds reported by Robinson and co-workers in 2008.[148] Reduction of the neutral hyper-valent silicon-carbene adduct **II-254** with four equivalents of potassium graphite gave the stable carbene-stabilized bis-silylene, **II-255**, in 23 % yield with the silicon atoms in the formal oxidation state of zero (Scheme 96). In the crystal structure, the silicon atoms are two-coordinate and the Si–Si bond length is consistent with previously reported disilene complexes. In contrast to disilenes with three-coordinate silicon atoms (in the +2 oxidation state), the silicon atoms in **II-255** have *trans*-bent geometries with C–Si–Si bond angles of 93.37(5)°, consistent with the predominantly 3p-character of the Si–Si bonding orbitals and mainly 3s-character of the silicon lone-pair molecular orbitals. DFT calculations support this description, with the HOMO corresponding to the Si–Si π bond, while the HOMO−1 is primarily the Si–Si σ bond. The HOMO−2 was found to be one of the two nonbonding lone-pair molecular orbitals.

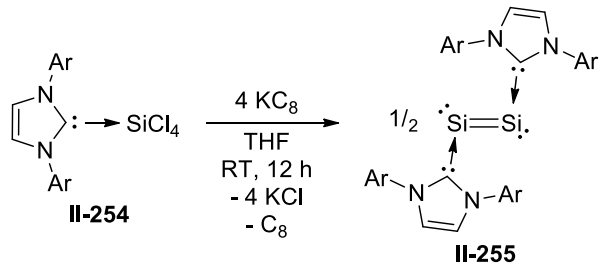

Scheme 96. Preparation of silicon(0) dimer **II-255**.

Shortly thereafter, the germanium analogue of **II-255** was prepared by the Jones lab.[149] Treatment of the dichlorogermylene-carbene adduct **II-256** with one equivalent of the *β*-diketiminate stabilized magnesium(I) dimer gave the dimeric germanium(0) dimer **II-257** with a low yield of 20 % (Scheme 97). The X-ray crystal structure of **II-257** was determined and found to be isomorphous with that of **II-255**. The germanium atoms are two-coordinate with a Ge–Ge internuclear distance that is close to the average bond length of other crystallographically characterized digermenes while the carbene ligands are nearly orthogonal to the Ge_2 fragment with a C–Ge–Ge bond angle of 89.87(8)°. DFT calculations were performed and a similar electronic structure and bonding situation was found compared to **II-255**.

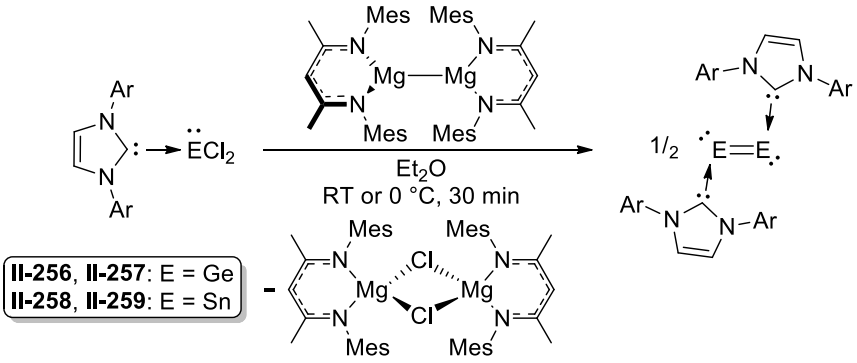

Scheme 97. Preparation of germanium(0) (**II-257**) and tin(0) dimer (**II-259**).

The tin derivative of **II-255** and **II-257** was prepared by reduction of **II-258** with the magnesium(I) reagent to give **II-259** (Scheme 97).[150] Unlike **II-255** and **II-257** (decomposition temperature of 209 °C[148] and 162–165 °C,[149] respectively), **II-259** decomposes slowly in the solid state at room temperature and rapidly at 50 °C, while in solution the compound decomposes to elemental tin and free carbene at 20 °C. Despite its low stability, an X-ray crystal structure analysis of **II-259** was carried out and its molecular structure is nearly equivalent with the lighter congeners with a *trans*-bent

geometry of the carbene ligands that are nearly orthogonal to the Sn_2 fragment (C–Sn–Sn = 91.82(8)°). The Sn–Sn bond length lies within the range found for three-coordinate, doubly bonded distannenes. Moreover, DFT calculations revealed that the Sn=Sn fragment is constructed from a σ-bond (HOMO−1) and an out-of-plane π-bond (HOMO), while the Sn lone-pairs (HOMO−2 and HOMO−3) are high in s-character. Attempts to generate the lead analogue using the same methodology led to the immediate deposition of lead metal and free carbene.

Recently, a triatomic silicon(0) cluster was reported by Roesky and co-workers.[151] Reduction of the tetrachlorosilane-carbene adduct **II-260** with potassium graphite in a 3:12 molar ratio furnished the complex **II-261** (Scheme 98). The crystal structure of **II-262** revealed a triangular Si_3 unit coordinated to three *c*AAC ligands oriented in a propeller fashion with respect to the Si_3 moiety. Each silicon atom is in the formal oxidation state of zero and adopts a three-coordinate trigonal pyramidal geometry with a lone pair of electrons considered as the fourth coordination site. According to DFT calculations, the cyclic Si_3 fragment features three Si–Si σ-bond orbitals, while the C–Si bonds are composed of a C→Si σ-donor bond orbital along with a π-type C←Si back-bonding interaction.

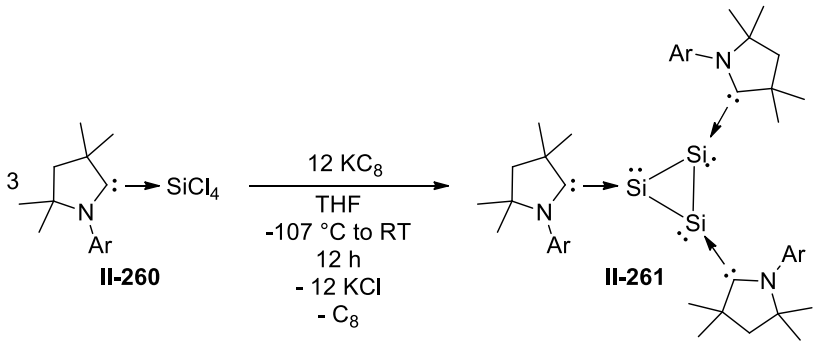

Scheme 98. Prepartion of trimeric silicon(0) cluster **II-262**.

A single example of an N-heterocyclic silylene-stabilized digermanium(0) complex was reported by So and co-workers.[152] Reduction of the silicon(II)–germanium(II) adduct **II-262** with two equivalents of potassium graphite gave a 20 % yield of the digermanium(0) complex **II-263** (Scheme 99). The X-ray crystal structure of **II-263** revealed that the SiGeGeSi skeleton has a *trans*-bent (Ge–Ge–Si = 91.95(6)°) and planar geometry, similar to the one observed for **II-257** and a Ge–Ge bond length that is comparable to typical Ge–Ge bond lengths in digermenes. DFT calculations indicated that the HOMO is a Ge–Ge π-orbital interacting with the empty p orbital on the silicon atoms. The HOMO−1 is located primarily on the Ge–Ge σ orbital whereas the HOMO−2 is the donor–acceptor interaction between the lone-pair orbitals on the silicon atoms and the vacant p-orbitals on the germanium atoms while the HOMO−3 is found primarily on the lone-pair orbitals of the germanium centres.

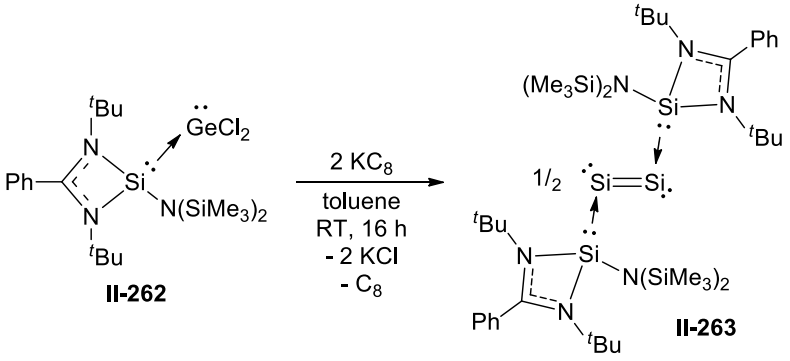

Scheme 99. Preparation of silylene stabilized germanium(0) dimer **II-263**.

The second group of compounds that contain Group 14 elements in the zero valent oxidation state are the so-called ylidones. First proposed by Frenking *et al*. based on calculations for allenes that deviate significantly from the expected linear geometry,[153-155] the central atom E retains its valence electrons as two lone pairs while the bond between the two donor ligands and the formally zero valent E can be best

described in terms of donor–acceptor interactions (Scheme 100). In this description, the bent molecular geometry is a consequence of the two lone pairs of electrons on the central atom and two dative electron pairs from the donor ligands in accordance with the VSEPR theory. Experimental verification of bent allenes, also known as carbodicarbenes, has since been provided by Bertrand and Fürstner.[156,157] Calculations have been extended to the heavier allene analogues and the bent molecular geometry was similarly predicted. Furthermore, these compounds are predicted to possess two lone-pair molecular orbitals with π and σ geometry at the E(0) atom which also accounts for the significant values calculated for the first and second proton affinities.[158-160]

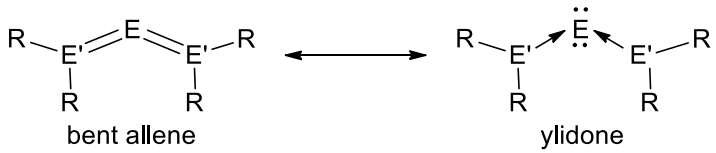

Scheme 100. Bent allene versus ylidone.

The ylidone descriptor has been used to explain the bent structures observed for the stable heavier allene analogues prepared by Kira and Wiberg. Trisilallene **II-265** was prepared by reduction of **II-264** with four equivalents of potassium graphite.[161] Trigermaallene **II-267** and 1,3-digerma-2-silaallene **II-269** were prepared in the same manner using the appropriate reagent (**II-266** or **II-268**),[162] while the 2-germadisilaallene **II-271** was prepared by reduction of a 2:1 mixture of dialkylsilylene **II-270** and $GeCl_2$·dioxane.[163] Tristannaallene **II-273** was prepared by the reduction of diamido stannylene **II-272** with sodium metal (Scheme 101).[164]

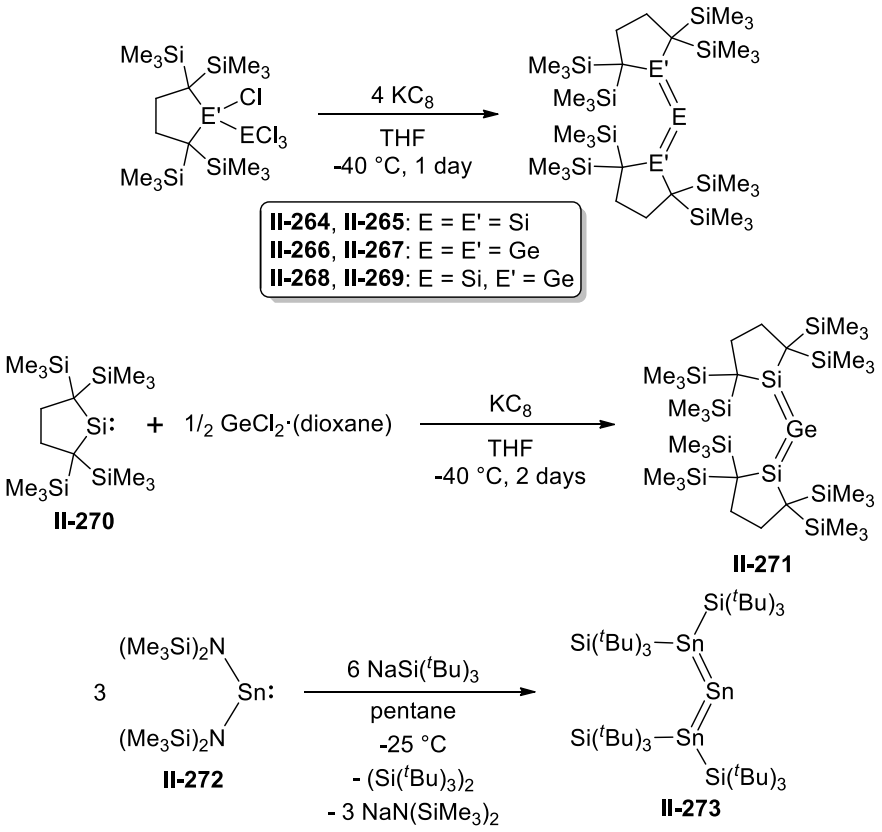

Scheme 101. Preparation of heavier allene analogues.

All the heavier allene analogues are non-linear with E–E–E bond angles ranging from 122 to 156°. Alternative to the calculations performed by Frenking, Kira rationalized the strongly bent structure of these compounds to the Jahn–Teller distortion associated with effective π–σ* mixing based on results from DFT calculations.[165]

The preparation of silylones and germylones with carbenes as the donor ligands has since been pursued with the first carbene-stabilized silylone prepared by the Roesky group in 2013.[166] Reduction of the dichlorosilylene carbene adduct **II-274** with two equivalents of potassium graphite gave the siladicarbene **II-275** in nearly quantitative yield (Scheme 102). Consistent with the silylone description, the silicon atom in **II-275** is two-coordinate and adopts a bent geometry with a C–Si–C bond angle of 117.70(8)°. DFT calculations predicted that the triplet form of **II-275** is between 17.2 to 18.5 kcal

mol^{-1} higher in energy than the singlet form, depending on the level of theory used in the calculation. Consistent with the results, no signals were observed in the EPR spectrum of **II-275**. The molecular orbitals also exhibit features expected for a silylone. The HOMO−1 is a σ lone pair at the silicon atom while the HOMO is a π-type orbital with significant Si–C π bonding. Another support for the assignment of **II-275** as a silylone are the large values predicted for the first and second proton affinities, 272.2 and 186.7 kcal mol^{-1}, respectively. In a subsequent paper, an experimental and theoretical charge density study performed by the same authors further confirmed the assignment of **II-275** as a silylone.[167]

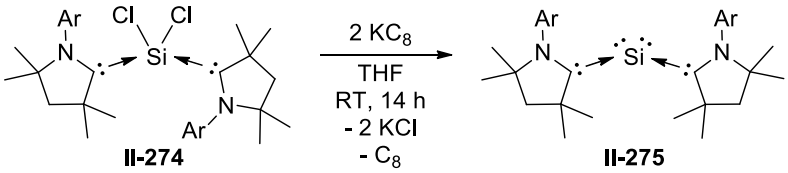

Scheme 102. Preparation of siladicarbene **II-275**.

With siladicarbene **II-275** in hand, Roesky and co-workers were interested in examining the reactivity of the molecule. No reaction was observed with hydrogen, ammonia, or carbon dioxide, however reaction with a sub-stoichiometric amount of potassium resulted in the production **II-276**, an isomer of **II-275** with a six-membered cyclic silylene ring containing a three-coordinate silicon atom (Scheme 103).[168] With regards to the mechanism, the authors proposed the formation of a radical anion intermediate via one-electron transfer from potassium to **II-275**, which was experimentally confirmed by EPR spectroscopy. According to DFT studies, the radical electron resides on one of the carbene carbon atoms and subsequently abstracts H$^{\bullet}$ from an adjacent isopropyl group on an N-aromatic ring, generating a carbon radical that reacts with the central silicon atom, forming a new Si–C bond. The intermediate is then

oxidized to **II-276** along with simultaneous reduction of another equivalent of **II-275** to start a new cycle, consistent with the fact that only a sub-stoichiometric amount potassium was necessary in the reaction.

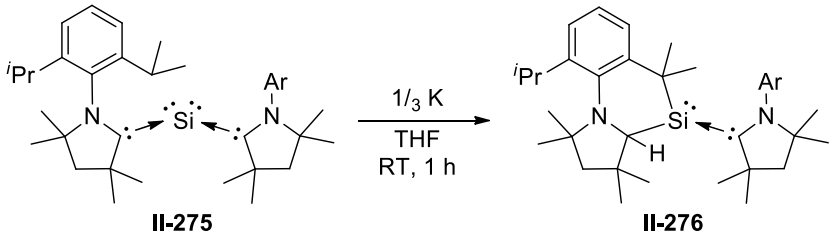

Scheme 103. Reduction of **II-275** with potassium to give **II-276**.

The germanium analogue of **II-275** was accessed through a different route as reduction of the germanium analogue of **II-274** did not furnish the desired product.[10] Instead, reaction between a 1:2:2.1 molar ratio of $GeCl_2$·dioxane, *c*AAC, and KC_8 gave the germadicarbene **II-277** (Scheme 104). Compound **II-277** is EPR silent, confirming that the ground state is a singlet akin to **II-275**. Similarly, the crystal structure of **II-277** revealed a two-coordinate germanium atom with a C–Ge–C bond angle of 114.71(6)°. Consistent with the absence of a resonance in the EPR spectrum, the singlet state for **II-277** was calculated to be between 16 to 18 kcal mol^{-1} more stable than the triplet state, depending on the method utilized. The shapes of the orbitals are also display typical features expected for a ylidone, with the HOMO−1 a σ-type lone pair orbital located on the germanium atom while the HOMO is a π-type orbital with the largest contribution on germanium. Finally, large values of 265.8 kcal mol^{-1} for the first proton affinity and 180.4 kcal mol^{-1} for the second proton affinity were computed, in accord with the assignment of **II-277** as a germylone.

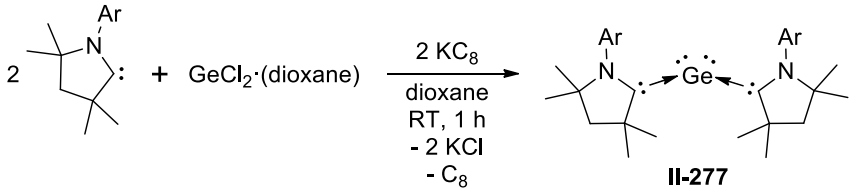

Scheme 104. Preparation of germadicarbene **II-277**.

Utilizing a chelating bis-N-heterocylic carbene ligand, Driess and co-workers have reported the preparation of cyclic sila- and germadicarbene complexes, **II-279** and **II-281**, respectively.[9,169] Reduction of the cationic chloro silylene (**II-278**) and germylene (**II-280**) precursor with two equivalents of sodium napthalenide yielded the corresponding ylidones in moderate yields (Scheme 105). X-ray diffraction analysis revealed that the silicon and germanium atoms are two-coordinate with acute C–E–C bond angles of 89.1(1)° for **II-279** and 86.5(1)° for **II-281** and shorter E–C bond lengths relative to the chloro precursors. DFT calculations were carried out to gain further insights into the electronic structures of **II-279** and **II-281**. In both complexes, the singlet state is lower in energy with similar singlet-triplet energy gaps of 33.0 and 33.2 kcal mol^{-1} calculated for **II-279** and **II-281**, respectively. Furthermore, **II-279** and **II-281** exhibited similar frontier molecular orbitals, with the HOMO a π-type orbital at the Group 14 centre whereas the HOMO−1 represents the σ lone-pair orbital at silicon or germanium. Associated with the HOMO is a E–C π back-bonding interaction that could account for the shorter E–C inter-nuclear distances observed. Consistent with the description of **II-279** and **II-281** as ylidones, large first (281.7 kcal mol^{-1} for **II-279** and 279.6 kcal mol^{-1} for **II-281**) and second (189.4 and 175.0 kcal mol^{-1} for **II-279** and **II-281**, respectively) proton affinity values were calculated.

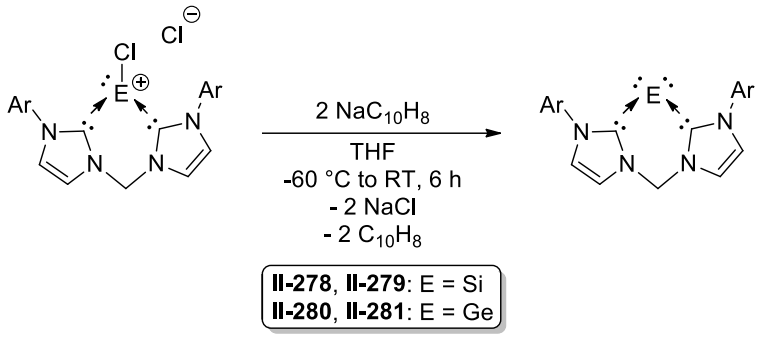

Scheme 105. Preparation of bis-NHC stabilized silylone (**II-279**) and germylone (**II-281**).

In comparison with **II-275**, the larger proton affinity values suggest that **II-279** has stronger silylone character with a more nucleophilic silicon site due to the stronger σ-donating but weaker π-accepting character of the bis-NHC ligand. Accordingly, treatment of **II-279** with elemental sulfur furnished the monomeric silicon disulfide complex **II-282** (Scheme 106).[170] DFT calculations showed that the electronic structure of **II-282** is best described with semi-polar Si–S bonds displaying moderate p_π–p_π bonding character along with delocalization of positive charge into the bis-carbene ligand framework.

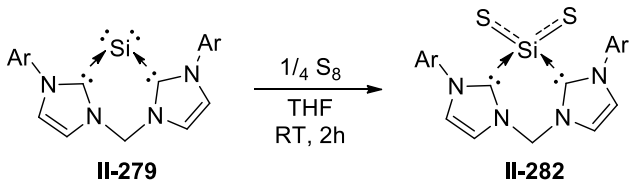

Scheme 106. Reaction of **II-279** with S_8 to give silicon disulfide complex **II-282**.

In an interesting variation, Kinjo and co-workers have utilized an imino-N-heterocylic carbene to stabilize a Ge(0) complex (Scheme 107).[171] Reduction of the chlorogermyliumylidene ion (**II-283**) with excess potassium graphite furnished the first dicoordinate germylone supported by a carbene and an imine ligand (**II-284**). Similar to **II-281**, an acute C–Ge–N bond angle of 80.59(6)° was found in **II-284** along with a shortened Ge–C bond length compared to the corresponding distance in **II-283**. The

HOMO is primarily a Ge–C π-bonding orbital which exhibits antibonding conjugation with the N=C(^{t}Bu) π-orbital in the C_2N_2Ge ring, consistent with delocalization of electron density into the five-membered ring. Meanwhile, the HOMO−1 is a σ-type lone-pair orbital at the germanium atom according to DFT calculations.

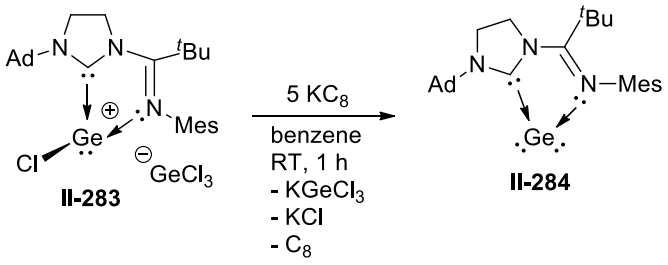

Scheme 107. Preparation of germylone **II-284**.

In accord with the nucleophilic character of **II-284**, reaction with one or two equivalents of methyl trifluoromethanesulfonate gave the corresponding monocationic or dicationic species **II-285** and **II-286**, respectively.[171,172] As well, **II-284** can donate electron density to Group VI transition metals. Reaction of **II-284** with a stoichiometric amount of $M(CO)_5(THF)$ (M = Cr, Mo, W) gave the adduct **II-287**, the first examples of germylone-transition metal complexes (Scheme 108).[172] DFT calculations were performed and the HOMO of **II-287** is nearly identical to the HOMO of **II-284**. Interestingly, the HOMO−2 represents a d-orbital of the transition metal in a π-bonding interaction with the germanium atom via back-donation. Donation of a σ-type lone pair from the germanium atom to the transition metal atom is found in HOMO−7.

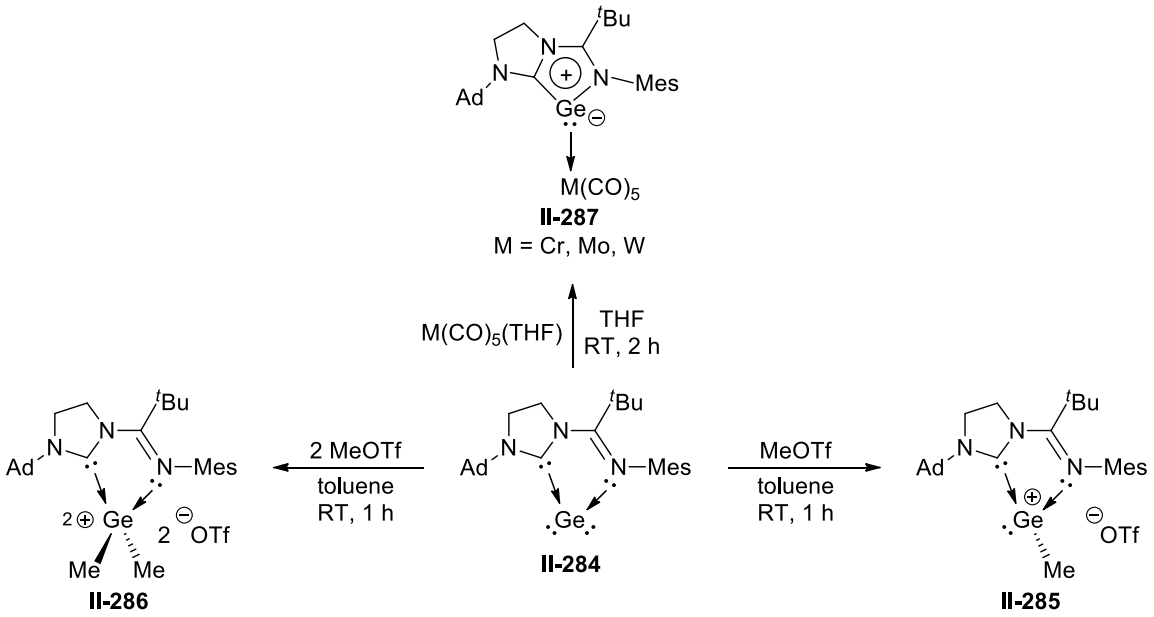

Scheme 108. Reactivity of **II-284** towards electrophiles and metal carbonyls.

III. Activation of Robust Single and Double Bonds by *β*-Diketiminate Aluminum(I) Complex

III.1 Introduction

Significant efforts are underway to replace catalysts based on the late transition metals, due to their recognized toxicity and significant costs as a result of their scarcity. A potential wellspring are complexes of the main group elements as they are less toxic, relatively, and significantly more abundant in the Earth's crust.[7] This promising potential has led to a renewed vigour and interest in main group chemistry, particularly main group complexes in reduced oxidation states in order to mimic reactivity that has so far been exclusive to transition metals.[6,173,174] As highlighted in Chapter II, significant advances have been achieved in recent years and novel modes of reactivity have been shown that were once thought to be impossible for main group complexes. In particular this chapter will focus on the low-valent Al(I) complex NacNacAl (**III-1**, NacNac = $[ArNC(Me)CHC(Me)NAr]^-$ and Ar = 2,6-^{i}Pr$_2$C$_6$H$_3$).

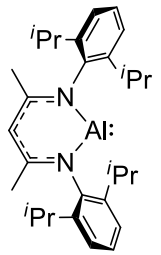

III-1

Complex **III-1** was first reported by Roesky and co-workers in 2000 and can be classified as an aromatically stabilized carbenoid featuring an aluminum-based lone pair and an accessible antibonding π* (Al–N) orbital.[8] Since the initial report, a wealth of reactivity has been observed with **III-1**, typically involving activation of element–element bonds and reaction with unsaturated substrates such as alkenes, alkynes, azides, and diazenes.[5]

In contrast, before the start of this project there were scant reports on the reactivity of **III-1** towards compounds with σ-bonds. The frontier molecular orbitals of **III-1** are reminiscent of those found on transition metal centres[175,176] and should therefore be amenable for activation of robust σ-bonds. This analogy prompted the start of this project to study oxidative reactions mediated by **III-1**.

The first section of this chapter involves the activation of a variety of robust H–X bonds by **III-1**. The second section sees the oxidative addition chemistry of **III-1** extended to C–X bonds, where X is fluorine, oxygen, and sulfur. The third portion will present the addition of functionalized element–element bonds across the aluminum centre. The final sections will outline the activation of multiple bonds by **III-1**, first C=S and P=S bonds followed by C=O and P=O bonds in the last section.

III.2 Activation of H–X Bonds

III.2.1 Synthesis of H–X Bond Activation Products

Firstly, the reaction between **III-1** and dihydrogen was investigated (Scheme 109). No H–H bond activation was observed at room temperature after a solution of **III-1** in benzene was charged with 4 atm of H_2. However, a reaction was noted upon heating the solution at 70 °C overnight, cleanly furnishing the known aluminum dihydride NacNacAlH_2 (**III-2**) with ^{1}H and ^{13}C NMR chemical shifts that are consistent with previously reported spectroscopic data.[177]

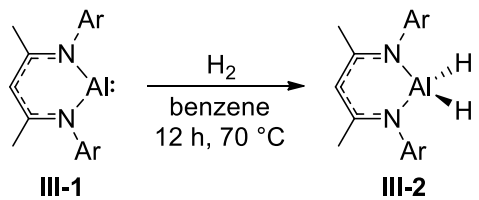

III-1 III-2

Scheme 109. Activation of H_2 by **III-1** to give NacNacAlH_2 (**III-2**).

Buoyed by this result and given the analogy between H–H and Si–H activation,[178] the addition of silanes to **III-1** was attempted (Scheme 110). Phenylsilane readily adds to **III-1** at room temperature after stirring overnight to give the novel aluminum silyl hydride NacNacAlH(SiH_2Ph) (**III-3**), while addition of the bulkier methylphenylsilane required heating at 70 °C overnight to produce NacNacAlH(SiHMePh) (**III-4**). Compounds **III-3** and **III-4** are rare examples of silyl hydride derivatives of aluminum, with only one other example reported by Driess and co-workers, NacNac'SiH($AlH_2(NMe_3)$) (NacNac' = $[ArNC(=CH_2)CH=C(Me)NAr]^{2-}$).[98]

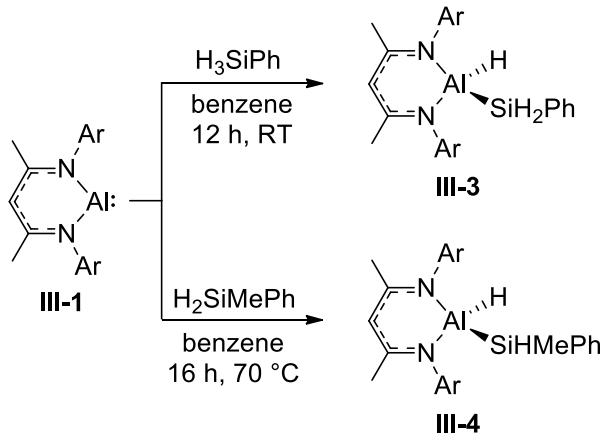

Scheme 110. Activation of silanes by **III-1** to give NacNacAlH(SiH_2Ph) (**III-3**) and NacNacAlH(SiHMePh) (**III-4**).

Given the diagonal analogy between silicon and boron, reaction between **III-1** and boranes was studied (Scheme 111). Pinacolborane adds to **III-1** over the course of 3 hours at room temperature to cleanly yield the first example of an aluminum boryl hydride, NacNacAlH(BPin) (**III-5**). The chemistry of boron substituted compounds of aluminum is mainly represented by carborane and borohydride derivatives. Most relevant are the first boryl substituted aluminum compounds, (THF)$Me_2AlB(ArNCH–)_2$ and ((μ-Me)$MeAlB(ArNCH–)_2)_2$ that were recently prepared by the Anwander group from the reaction of trimethylaluminum with Yamashita's borylide, $[Li(THF)_2][B(ArNCH–)_2]$.[179]

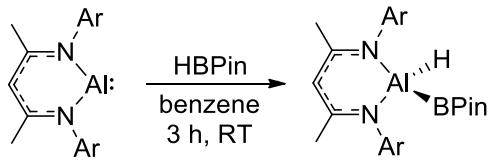

III-1 **III-5**

Scheme 111. Activation of HBPin by **III-1** to give NacNacAlH(BPin) (**III-5**).

Related oxidative addition of **III-2** to **III-1** results in formation of the dimer (NacNacAl(H)–)$_2$ (**III-6**) in approximately 50% yield at room temperature (Scheme 112). In an attempt to push the reaction to completion, the reaction mixture was heated to 50 °C. Surprisingly, complex **III-6** disproportionates back to a mixture of **III-1** and **III-2**, indicative of an entropy-driven reaction. Moreover, returning the solution back to room temperature results in clean reproduction of the initial mixture of **III-1**, **III-2**, and **III-6** without any side products. Therefore, an equilibrium mixture exists between the three species in solution. Thermodynamic parameters of the equilibrium (ΔH = −10.0(7) kcal mol^{-1} and ΔS = −31.3(2) cal mol^{-1}) were extracted from the van't Hoff plot generated from the equilibrium constants obtained from ^{1}H NMR spectra recorded at temperatures ranging from 295.1 to 348.1 K (Figure 1). This dynamic process is of interest as a proof of principle for reductive elimination from an aluminum centre, a key step in many transition metal catalyzed reactions but an uncommon reaction for main group complexes. Previously, Beachley and co-workers reported the synthesis of organometallic Ga(I)[180] and In(I)[181] compounds via elimination of tetramethylsilane from KM(CH_2SiMe_3)$_3$H (M = Ga or In). However, these results were not reproducible and the proposed decomposition likely follows a more complicated pathway rather than a simple reductive elimination.[182]

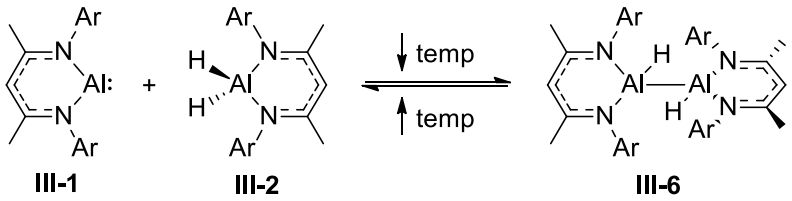

Scheme 112. Equilibrium between **III-1**, **III-2**, and **III-6**.

More recently, Fischer *et al*. have reported the reductive elimination of Cp*H from Cp^*AlH_2 to furnish the Al(I) compound Cp*Al, with the three species in equilibrium in toluene at 110 °C.[183]

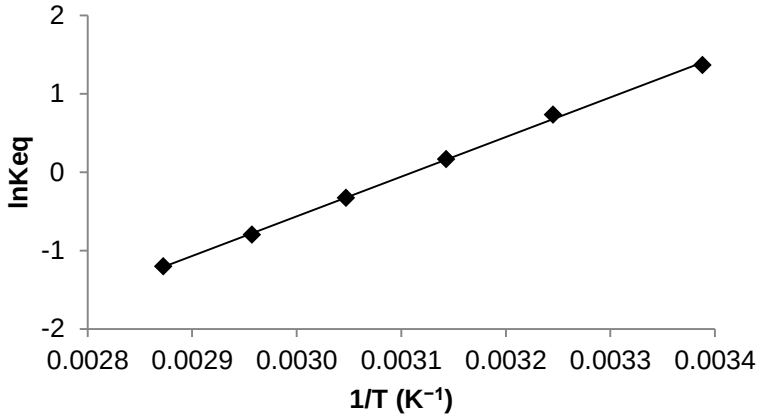

Figure 1. van't Hoff plot of the equilibrium between **III-1**, **III-2**, and **III-6** (R^2 = 0.999).

While aryl and olefinic sp^2 and alkynyl sp C–H bonds are resistant towards oxidative addition with **III-1**, especially since alkenes and alkynes readily undergo cycloadditions with **III-1**,[5] it was hypothesized that C–H bonds on cyclopentadiene and its derivatives could be more amenable towards addition across **III-1** (Scheme 113). Reaction between **III-1** and cyclopentadiene results in similar π-complexation observed with alkenes previously. On the other hand, the sterically encumbered pentamethylcyclopentadiene underwent C–H bond oxidative addition over the course of 3 days at 70 °C to give the alkyl hydride derivative NacNacAlH(Cp*) (**III-7**).

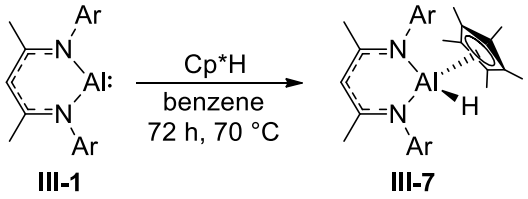

Scheme 113. Activation of Cp*H by **III-1** to give NacNacAlH(Cp*) (**III-7**).

Next, the addition of amines to **III-1** was investigated. No reaction was observed between **III-1** and 2,6-diisopropylaniline or 2,6-dimethylaniline, even at elevated temperatures, likely due to the significant steric bulk from the NacNac ligand and the substrates preventing close approach of the N–H bond to the aluminum centre. Using *tert*-butylamine instead, oxidative addition resulted in production of aluminum amido hydride NacNacAlH(NH^{t}Bu) (**III-8**) after stirring the mixture for 3 days at room temperature, while addition of the more acidic aniline gave NacNacAlH(NHPh) (**III-9**) in 16 hours at room temperature (Scheme 114). Many aluminum amido hydride complexes are known in the literature, with the closest analogue to **III-8** and **III-9** being NacNacAlH(NHAr) reported by Roesky and co-workers, obtained via reaction between **III-2** and 2,6-diisopropylaniline at elevated temperatures.[137]

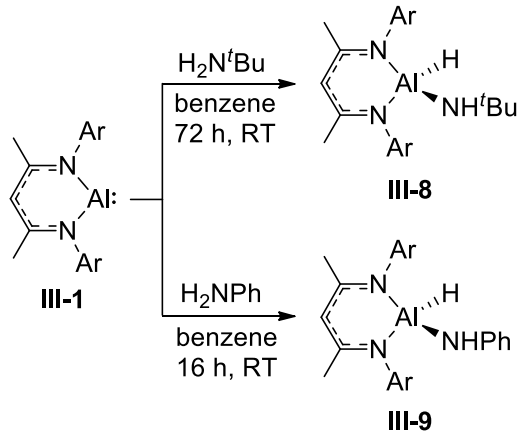

Scheme 114. Activation of amines by **III-1** to give NacNacAlH(NH^{t}Bu) (**III-8**) and NacNacAlH(NHPh) (**III-9**).

Related addition of a less polar but weaker P–H bond of diphenylphosphine occurs readily at room temperature and affords a phosphide hydride derivative of aluminum, NacNacAlH(PPh_2) (**III-10**), as seen in Scheme 115.

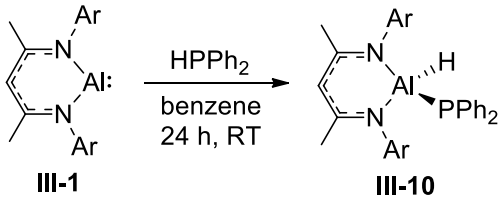

III-1 III-10

Scheme 115. Activation of diphenylphosphine by **III-1** to give NacNacAlH(PPh_2) (**III-10**).

Finally, as outlined in Scheme 116, the reaction of **III-1** with isopropanol occurs smoothly at room temperature over the course of 16 hours to furnish the hydrido alkoxy product NacNacAlH(O^iPr) (**III-11**). Although many hydrido alkoxides of four-coordinate aluminum are known, most of them are aluminate compounds with bulky aryloxide ligands. Therefore, compound **III-11** represents a rare example of a neutral, monomeric hydrido alkoxy aluminum species.

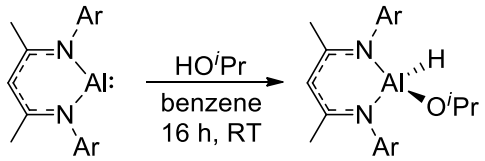

III-1 III-11

Scheme 116. Activation of isopropanol by **III-1** to give NacNacAlH(O^iPr) (**III-11**).

III.2.2 Spectroscopic Characterization of H–X Bond Activation Products

All the novel complexes prepared have been fully characterized by multinuclear NMR and IR spectroscopy. In the ^1H NMR spectrum, all the complexes, except **III-4** and **III-6**, display a pattern of signals indicative of C_s symmetry in solution.

Table 1. Spectroscopic data for NacNacAlH(X) complexes

	^{1}H NMR chemical shifts				IR frequency (cm^{-1})
Compound	**H_L** [a]	**Me_L** [b]	**CH ^{i}Pr** [c]	**CH_3 ^{i}Pr** [d]	**Al–H**
III-3	4.93	1.54	3.42, 3.35	1.43, 1.17, 1.13, 1.11	1785
III-4	4.93	1.56, 1.53	3.46, 3.23	1.52, 1.44, 1.39, 1.16, 1.13, 1.09, 0.82	1785
III-5	5.00	1.59	3.50	1.53, 1.43, 1.19	1795
III-6	4.69	1.50, 1.31	3.77, 3.67, 3.53, 2.95	1.74, 1.50, 1.21, 1.12, 1.09, 0.90, 0.84	1778, 1772
III-7	4.90	1.44	3.57, 3.16	1.44, 1.15, 1.03	1802
III-8	4.86	1.57	3.46, 3.31	1.44, 1.15, 1.11	1812
III-9	5.07	1.56	3.36, 3.17	1.44, 1.14, 1.03, 0.96	1854
III-10	4.92	1.51	3.69, 3.21	1.64, 1.12, 1.08, 1.00	1778
III-11	4.87	1.57	3.40	1.52, 1.41, 1.15	1824

^{1}H NMR spectra were accumulated in C_6D_6 at room temperature. [a] Ligand backbone proton. [b] Ligand backbone methyl. [c] Heptet. [d] Doublet.

As such, all the complexes exhibit a duo of heptets, ranging from 3.70 to 3.10 ppm, coupled to a quartet of doublets, typically found between 1.60 to 1.00 ppm (Table 1) due to the inequivalent isopropyl groups on the aromatic rings. On occasion the heptets and doublets have overlapped into multiplets resulting in fewer than expected number of multiplets. On top of that, two singlets are found at ~5 and ~1.5 ppm that correlate to the C*H* and methyl protons in the framework of the NacNac ligand, respectively. The Al–H signals cannot be observed directly by ^{1}H NMR spectroscopy because of quadrupolar broadening due to the ^{27}Al centre (nuclear spin = 5/2) but the presence of the hydride is confirmed by the IR stretches observed at approximately 1800 cm^{-1} (Table 1).

More specifically, the protons on the phenylsilyl group in **III-3** gives rise to a doublet at 3.87 ppm ($^{3}J_{\text{H–H}}$ = 2.8 Hz) that is correlated in the ^{1}H–^{29}Si HSQC spectrum with an upfield signal at −74.0 ppm in the ^{29}Si NMR spectrum. Furthermore, a stretch at 2065 cm^{-1} was found in the IR spectrum for the Si–H bond in **III-3**. In the case of **III-4**, addition of methylphenylsilane results in a chiral centre at the resulting silyl group leading to the observed C_1 symmetry in solution. As such, four separate heptets are present for the isopropyl methine protons, however, three have overlapped into a multiplet at 3.46 ppm with the fourth heptet close by at 3.23 ppm ($^{3}J_{\text{H–H}}$ = 6.8 Hz). Accordingly, eight doublets integrating to three protons each coupled to a heptet are expected to be observed. However, only seven doublets are seen between 1.60 and 0.75 ppm as two have overlapped to give a larger doublet that integrates to six protons. Two singlets at 1.55 and 1.53 ppm integrating to three protons each are assigned to the inequivalent methyl groups in the NacNac framework while a third singlet at 4.93 ppm correlates to the C*H* proton. The methylphenylsilyl moiety in **III-4** manifests as a doublet

of quartets ($^3J_{H–H}$ = 5.1 Hz, $^3J_{H–H(Al)}$ = 6.6 Hz) for the Si*H* proton while the methyl group is found as a doublet at −0.14 ppm ($^3J_{H–H}$ = 5.1 Hz). In the IR spectrum, the band at 2065 cm^{-1} is assigned to the Si–H bond.

The boryl ligand in **III-5** gives rise to the ^{11}B NMR resonance at 34.9 ppm, consistent with a three-coordinate boron centre that compares well with the ^{11}B NMR chemical shift of 31.9 and 27.9 ppm reported by Anwander and co-workers for their aluminum boryl complexes.[179] The ^{1}H NMR spectrum for **III-6** is complicated by the presence of **III-1** and **III-2**, however the pattern of signals observed is consistent with either C_2 or C_i symmetry in solution. Therefore, four heptets at 3.77, 3.67, 3.53, and 2.95 ppm ($^3J_{H–H}$ = 6.1, 6.9, 6.9, and 6.6 Hz, respectively) and eight doublets between 1.8 and 0.8 ppm are assigned to the isopropyl methine and methyl protons, respectively, on the aryl rings. Similar to **III-4**, the backbone methyls are inequivalent and are assigned to the two singlets at 1.51 and 1.31 ppm. The γ-proton in the ligand backbone is found as a singlet at 4.69 ppm. Unlike the other complexes, two bands at 1778 and 1772 cm^{-1} are attributed to the Al–H bonds.

The methyl groups of the Cp* ligand in **III-7** gives rise to a singlet at 1.48 ppm as a result of a fast haptotropic shift. The N*H* signals in **III-8** and **III-9** were observed as broad singlets at −0.03 and 3.27 ppm, respectively. Furthermore, the *tert*-butyl protons in **III-8** manifest as a singlet integrating to nine protons at 0.90 ppm, while signals for the para and meta protons on the amido phenyl group are observed as a multiplet at 6.68 ppm and a doublet at 6.38 ppm ($^3J_{H–H}$ = 7.8 Hz), respectively, in **III-9**.

Table 2. Selected bond lengths and angles of NacNacAlH(X) complexes.

	Lengths, Å				Angles, °		
Compound	**Al–N1**	**Al–N2**	**Al–X**	**N_2C_3–Al**	**N1–Al–N2**	**N1–A–X**	**N2–Al–X**
III-3	1.899(1)	1.902(1)	2.4523(7)	0.676	96.42(6)	119.19(4)	107.54(4)
III-4	1.904(2)	1.910(2)	2.4548(7)	0.748	95.67(6)	111.94(5)	115.06(5)
III-5	1.910(1)	1.910(1)	2.124(2)	0.749	95.12(5)	119.19(6)	110.66(6)
III-7	1.9552(11)	—	2.0906(11)	0.847	93.57(7)	117.77(5)	—
III-8	1.9078(10)	—	1.7900(18)	0.613	94.66(6)	111.95(5)	—
III-9	1.890(4)	1.901(3)	1.826(4)	0.436	96.3(2)	113.2(2)	113.7(2)
III-10	1.896(1)	1.907(1)	2.3970(5)	0.571	95.42(6)	112.03(4)	111.55(4)
III-11	1.895(2)	1.898(1)	1.695(1)	0.499	96.11(6)	109.58(7)	110.23(7)

The presence of the phosphide ligand in **III-10** is supported by the upfield ^{31}P NMR signal at −67.9 ppm while the isopropoxide moiety in **III-11** is established with the presence of a heptet at 3.90 ppm ($^{3}J_{H–H}$ = 6.1 Hz) coupled to a doublet at 0.72 ppm ($^{3}J_{H–H}$ = 6.0 Hz).

III.2.3 Structural Characterization of H–X Bond Activation Products

Along with spectroscopic methods, all the complexes were also structurally characterized by X-ray diffraction analysis (Table 2). In all cases, the central aluminum atom is four-coordinate, bound to two nitrogen atoms from the nearly planar NacNac ligand and a hydride, while the fourth position is a ligand derived from the bond that was activated. The aluminum centre lies out of the plane defined by the N_2C_3 atoms of the NacNac ligand, ranging from 0.436 Å at the shortest to 0.847 Å at the longest, with a distance of 0.642 Å as the average. Another prominent feature of these structures is the significant distortion of the N_2AlHX fragment from tetrahedral geometry, such that the average N–Al–N bond angle is significantly smaller (95.41°) than the average N–Al–X bond angle (113.33°). The average Al–N distance found in the structures, 1.909 Å (ranging from 1.890(4) to 1.955(1) Å), is shorter than the corresponding distance in **III-1** (1.957(2) Å)[8] but comparable with other four-coordinate NacNac ligated aluminum complexes (1.906 Å on average).[a]

In particular, the crystal structures of **III-3** (Figure 2) and **III-4** (Figure 3) displays Al–Si bond distances of 2.4523(7) and 2.4548(7) Å, respectively. Both distances are comparable to the corresponding distance in NacNac'SiH(AlH_2(NMe_3)) of 2.487(1) Å[98] and the average Al–Si distance of a four-coordinate aluminum centre (2.466 Å).[a]

[a] Based on a search in the Cambridge Crystallographic Data Centre.

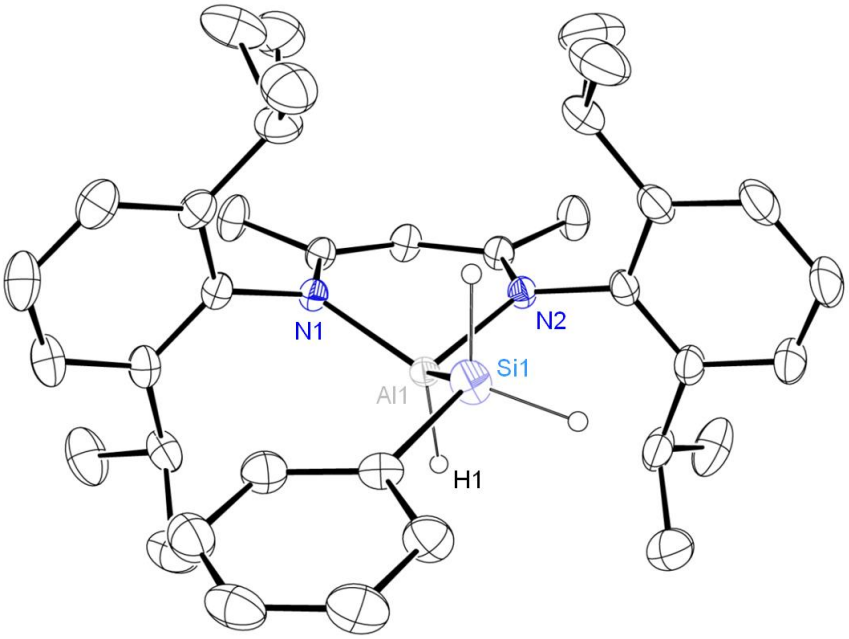

Figure 2. Molecular structure of NacNacAlH(SiH_2Ph) (**III-3**). Thermal ellipsoids are shown at 30% and the hydrogen atoms, except the aluminum hydride and silyl protons, are removed for clarity.

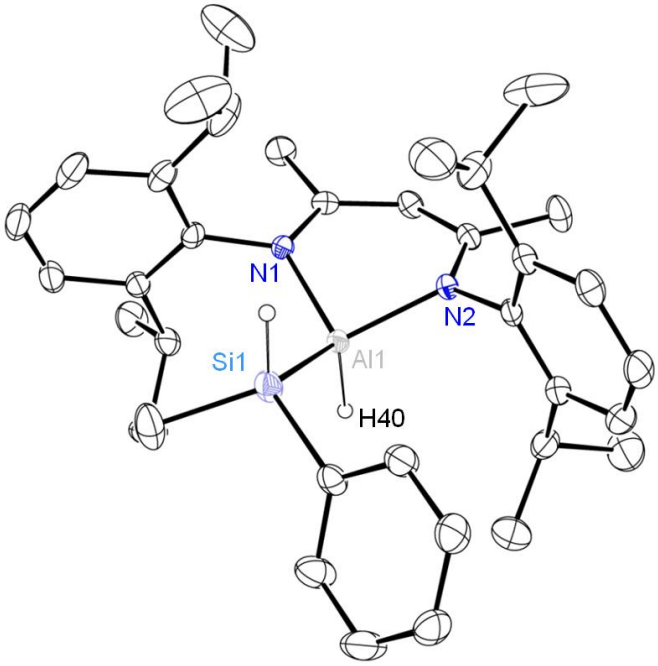

Figure 3. Molecular structure of NacNacAlH(SiHMePh) (**III-4**). Thermal ellipsoids are shown at 30% and the hydrogen atoms, except the aluminum hydride and silyl proton, are removed for clarity.

The structure of **III-5** is shown in Figure 4. The Al–B single bond distance of 2.124(2) Å is comparable to the respective distance in (THF)Me_2AlB(ArNCH–)$_2$ (2.150(2) Å) and ((μ-Me)MeAlB(ArNCH–)$_2$)$_2$ (2.119(3) Å).[179] Comparatively longer are the distances found in the donor-acceptor aluminum–boron bonds of Lewis adducts between nucleophilic Al(I) species and electrophilic boranes, ranging from 2.115(2) to 2.183(5) Å.[130,184,185]

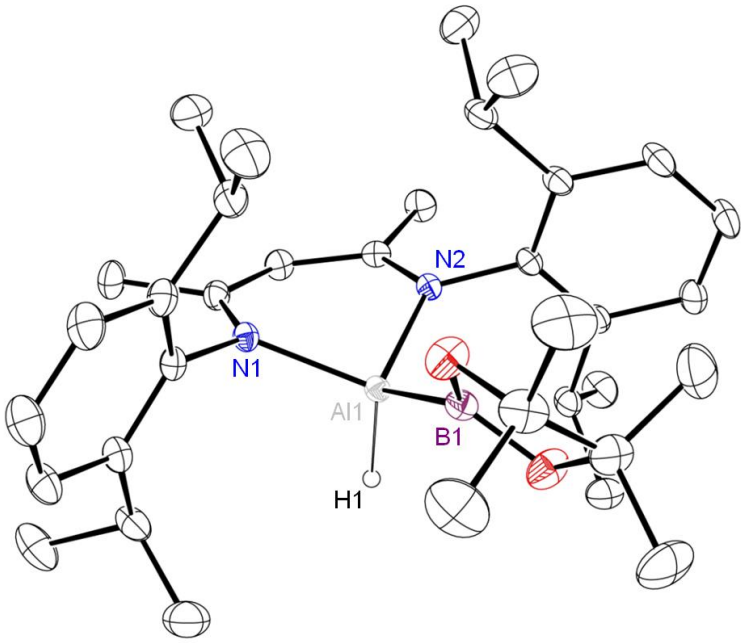

Figure 4. Molecular structure of NacNacAlH(BPin) (**III-5**). Thermal ellipsoids are shown at 30% and the hydrogen atoms, except the aluminum hydride, are removed for clarity.

The molecular structure of **III-7** (Figure 5) contains a crystallographically imposed mirror plane running through the centre of the molecule and perpendicular to the NacNac ligand. Interestingly, the structure revealed an η^1 coordination mode of the Cp* ligand with a long distance of 2.0906(19) Å between Al1 and C1, longer than the average distance (1.981 Å) in four-coordinate aluminum hydrido alkyl compounds by 0.109 Å.[186,187] Such an elongated Al–C bond distance along with the acute C2–C1–Al1 bond

angle of 96.97(10)° indicates that there is significant p-character on the carbon atom in the bonding interaction between aluminum and the Cp* ring and consistent with the facile haptotropic shift of the ligand observed by ^{1}H NMR spectroscopy. The significant steric strain imposed by the Cp* ligand and the bulky aromatic groups on the NacNac ligand also results in the extended Al1–N1 bond length of 1.9552(11) Å, significantly longer than the average distance of 1.909 Å in this series of crystal structures.

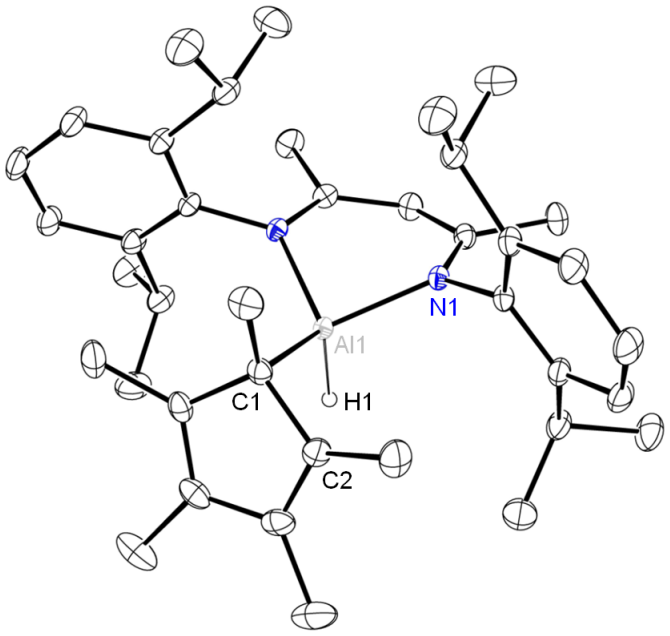

Figure 5. Molecular structure of NacNacAlH(Cp*) (**III-7**). Thermal ellipsoids are shown at 30% and the hydrogen atoms, except the aluminum hydride, are removed for clarity. A mirror plane runs through Al1 and C1, thus the left side of the molecule is a reflection of the right side.

The crystal structures of **III-8** and **III-9** are shown in Figure 6 and Figure 7, respectively. The two structures are closely related to each other with similar Al–NHR bond distances of 1.7900(18) Å for **III-8** and 1.826(4) Å for **III-9** and both are comparable to the respective distance of 1.817(2) Å found in NacNacAlH(NHAr).[137]

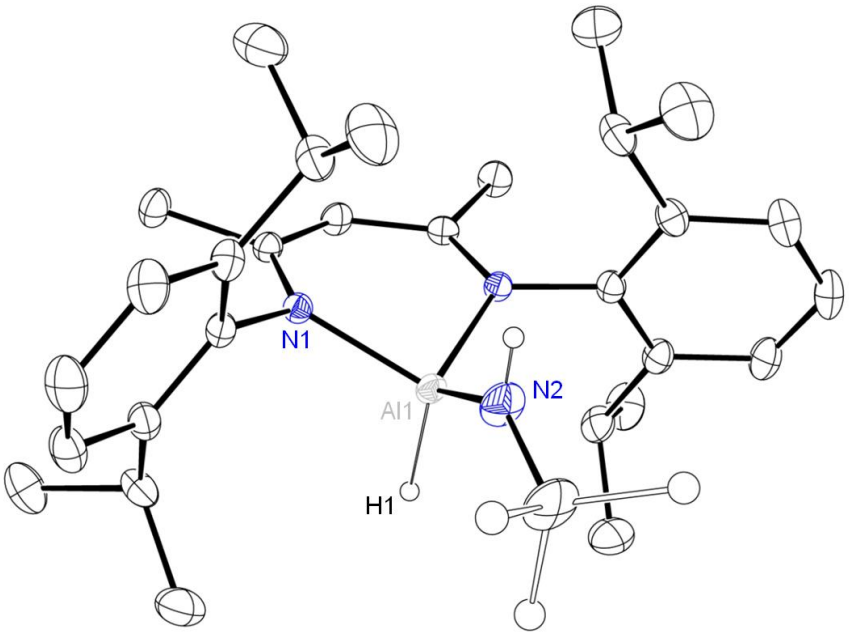

Figure 6. Molecular structure of NacNacAlH(NH^{t}Bu) (**III-8**). Thermal ellipsoids are shown at 30% and the hydrogen atoms, except the aluminum hydride and amido proton, are removed for clarity. The *tert*-butyl group on N2 is rotationally disordered and a mirror plane runs through Al1 and N2, thus the left side of the molecule is a reflection of the right side.

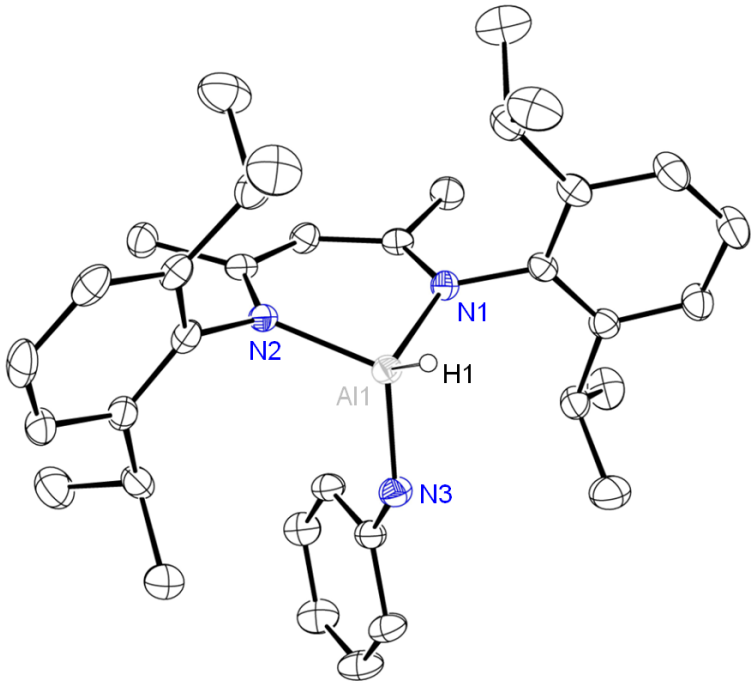

Figure 7. Molecular structure of NacNacAlH(NHPh) (**III-9**). Thermal ellipsoids are shown at 30% for one of two independent molecules and the hydrogen atoms, except the aluminum hydride and amido proton, are removed for clarity.

The molecular structure of **III-10** (Figure 8) revealed an Al1–P1 bond distance of 2.3970(5) Å that is on par with the average Al–P bond distance found for neutral four-coordinate aluminum hydrido phosphides (2.375 Å)[188-194] and four-coordinate phosphide hydride aluminates (2.403 Å).[195,196]

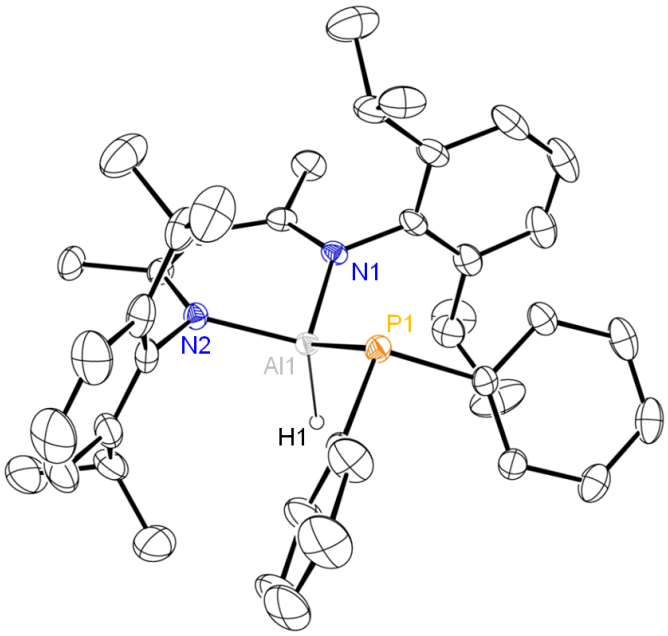

Figure 8. Molecular structure of NacNacAlH(PPh_2) (**III-10**). Thermal ellipsoids are shown at 30% and the hydrogen atoms except the aluminum hydride are removed for clarity.

Finally, the structure of **III-11** displayed an Al1–O1 bond distance of 1.695(1) Å (Figure 9). The distance measured is shorter than the average Al–O distance in neutral, monomeric four-coordinate hydrido aryloxy aluminum compounds (1.723 Å)[197-199] but comparable with the Al–O distance in monomeric four-coordinate aryloxide hydride aluminates (1.712 Å).[200]

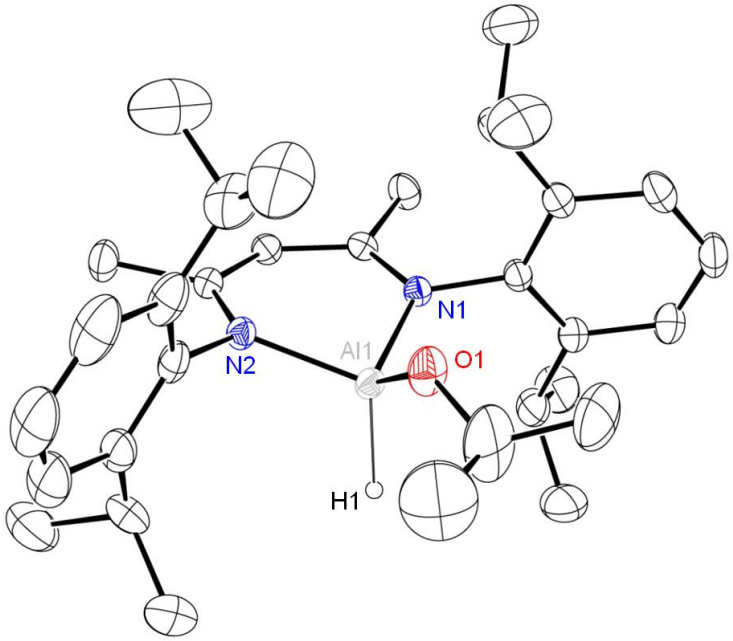

Figure 9. Molecular structure of NacNacAlH(O^{i}Pr) (**III-11**). Thermal ellipsoids are shown at 30% and the hydrogen atoms except the aluminum hydride are removed for clarity.

III.3 Activation of C–X Bonds

After successfully activating a variety of H–X bonds with **III-1**, activation of C–X bonds were considered, starting with carbon–fluorine bonds. C–F bond activation is particularly challenging as fluorine forms the strongest single bond to carbon, with a bond dissociation energy of 115.9 kcal mol^{-1}. In addition to the thermodynamic stability of fluorocarbons, they are also poor Lewis bases, making their activation kinetically unfavourable.[201] In transition metal chemistry, activation of the C–F bond in polyfluorinated aromatics is much more facile compared to fluorobenzene. This fact can be attributed to the decreasing strength of the bond, along with lower barriers for C–F activation upon increasing fluorination. Thus, DFT calculations revealed that the C–F bond energy in C_6F_6 is 127.1 kcal mol^{-1} compared to 132 kcal mol^{-1} in C_6H_5F, whereas the corresponding activation barriers for addition to a ruthenium complex are 34.6 and

44.9 kcal mol^{-1}, respectively.[202] Additionally, the position of the surrounding fluorine atoms has an activating effect on a given C–F bond and follows the order *ortho* > *meta* > *para*.[203] Accordingly, the same trend was observed for the reactions of **III-1** with fluoroarenes. Addition of hexafluorobenzene to **III-1** results in facile addition of the aryl C–F bond at room temperature within 20 minutes to give NacNacAlF(C_6F_5) (**III-12**). Next, pentafluorobenzene was reacted with **III-1** and C–F bond activation occurs exclusively at the *para* position to furnish the aluminum aryl fluoride derivative NacNacAlF(3-C_6HF_4-1,2,4,5) (**III-13**) after 20 minutes at room temperature. Activation of the 1,2,3,4 isomer of tetrafluorobenzene occurs strictly at the 2-position to give NacNacAlF(2-$C_6H_2F_3$-1,3,4) (**III-14**), however, the reaction requires a significantly longer reaction time of 16 hours at room temperature. The selectivity observed is due to the two *ortho* fluorine atoms flanking the 2-position. On the other hand, addition of the 1,2,4,5 isomer of $C_6H_2F_4$ requires extended heating at elevated temperatures (70 °C, 48 hours) to give exclusively the C–F activation product, NacNacAlF(2-$C_6H_2F_3$-1,4,5) (**III-15**). Further decrease of the extent of fluorination in the starting fluoroarene necessitates more forcing reaction conditions. Thus, addition of 1,2,3-trifluorobenzene at both the 1- and 2-positions gave a mixture of NacNacAlF(2-$C_6H_3F_2$-1,3) (**III-16-1**) and NacNacAlF(1-$C_6H_3F_2$-2,3) (**III-16-2**) after heating the reaction at 80 °C for 4 days in a 3:1 ratio. As previously observed, activation at the 2-position is favored due to the presence of two *ortho* fluorine atoms. The 1,3,5 isomer of trifluorobenzene is even less reactive due to the absence of activating fluorine atoms at the *ortho* position. Therefore, activation of the C–F bond occurs sluggishly at 100 °C over the course of 4 days to yield NacNacAlF(1-$C_6H_3F_2$-3,5) (**III-17**) along with an unknown by-product. Finally,

prolonged heating of **III-1** in the presence of fluorobenzene (days at 100 °C) resulted only in decomposition of **III-1** and no evidence of any aluminum fluoride derivatives was observed. A summary of the aryl C–F bond activations facilitated by **III-1** is given in Scheme 117. During the course of this thesis a closely related report from the Crimmin lab disclosed C–F and C–O bond activation of similar substrates with **III-1**.[204]

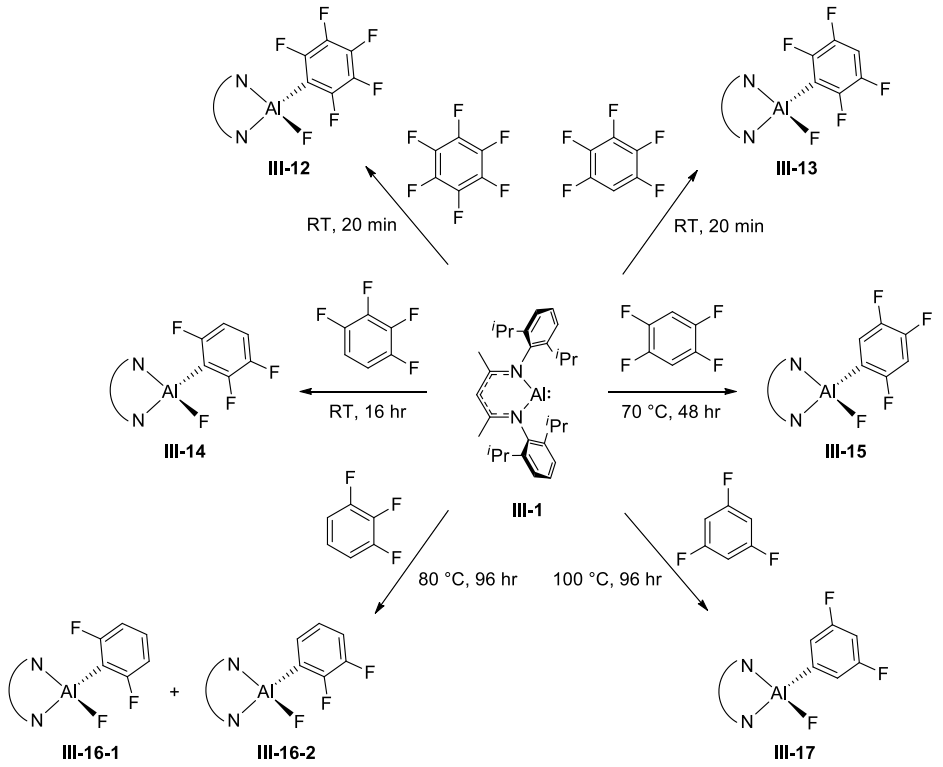

Scheme 117. Summary of C(sp^2)–F bond activation by **III-1**.

Unsurprisingly, compounds **III-12** to **III-16** gave a very similar set of signals in their ^{1}H NMR spectra, the main difference being additional signals in the aromatic region for the protons on different fluoroarene ligands. As such, the compounds displayed a pattern of signals consistent with C_s symmetry. The methine protons on the isopropyl groups on the aromatic rings are present at approximately 3.50 and 3.00 ppm and are coupled to four doublets between 1.50 and 0.50 ppm from the methyl protons. A singlet observed at ~5 ppm is attributed to the backbone C*H* proton while the singlet at ~1.5 ppm

integrates to six and is assigned to the methyl groups in the ligand framework. Due to the complicated mixture of signals in the ^{1}H NMR spectrum of **III-17**, its identity was confirmed via ^{19}F NMR spectroscopy. In the ^{19}F NMR spectrum, the terminal aluminum fluoride is found upfield at approximately −170 ppm while the fluorine atoms on the aromatic ring follow the expected pattern of increasingly upfield chemical shifts at the *ortho*, *para*, and *meta* position.

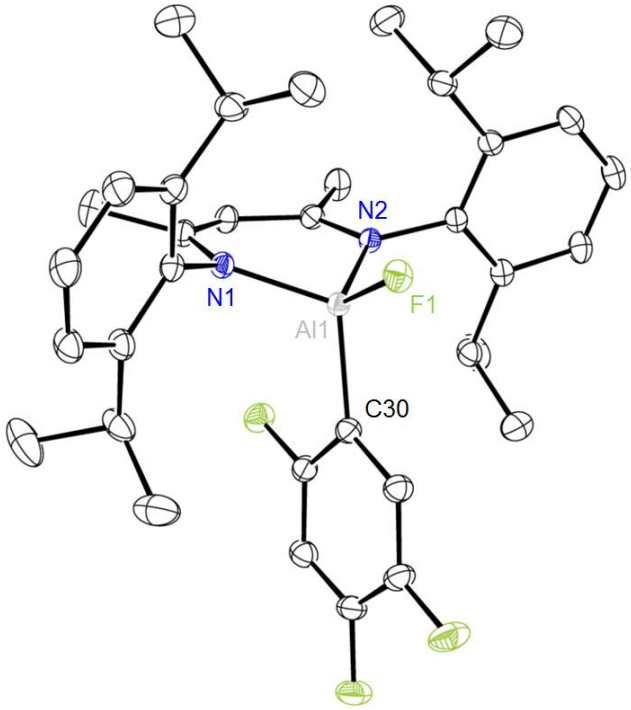

Figure 10. Molecular structure of NacNacAlF($C_6F_3H_2$) (**III-15**). Thermal ellipsoids are shown at 30% and the hydrogen atoms are removed for clarity.

Table 3. Selected bond lengths and angles for complex **III-15**.

	Lengths, Å			**Angles, °**	
A1–N1	1.883(1)	Al1–F1	1.6641(6)	N1–A1–N2	98.27(4)
Al1–N2	1.8814(9)	Al1–C30	1.972(1)	F1–Al1–C30	108.24(4)

The crystal structure of **III-15**, obtained via X-ray diffraction analysis, is shown in Figure 10. As expected, the aluminum centre is a distorted tetrahedron sitting 0.496 Å

below the plane defined by the NacNac ligand. The $C_6F_3H_2$ ring is nearly perpendicular with an angle of 87.59° between the N_2C_3 plane and the plane defined by the aromatic ring. The aluminum–fluorine and aluminum–carbon bond lengths in **III-15** take values of 1.6641(6) and 1.972(1) Å, respectively. These values are consistent with those found in the closely related complexes ^{Mes}NacNacAl$(C_6F_5)_2$ (1.9946(2) and 2.0198(2) Å) and ^{Mes}NacNacAlF_2 (1.6637(8) and 1.6647(8) Å), where ^{Mes}NacNac is [Ar'NC(Me)CHC(Me)NAr']$^-$ and Ar' = 2,4,6-$Me_3C_6H_2$.[205] The Al–N distances of 1.883(1) and 1.8814(9) Å are marginally shorter than the average distances (1.909 Å) observed in the structures reported in the previous section. The structure of **III-15** is also very similar to the structure of **III-12** reported by Crimmin and co-workers in their communication.[204]

Encouraged by these results, the activation of the more challenging C(sp^3)–F bond was attempted (Scheme 118). A search of the literature revealed only one example of formal C(sp^3)–F addition to a metal centre reported by Goldman and co-workers in 2011.[206] Remarkably facile addition of 1-fluoropentane to **III-1** was observed at room temperature within minutes to furnish the aluminum alkyl fluoride derivative NacNacAlF(C_5H_{11}) (**III-18**). Oxidative addition of the secondary alkyl C–F bond of fluorocyclohexane also occurs at room temperature within minutes to give the complex NacNacAlF(C_6H_{11}) (**III-19**). The formation of complexes **III-18** and **III-19** represents the first examples of direct alkyl–fluorine bond oxidative addition to any metal centre regardless of its position in the periodic table.[207,208] In the ^{1}H NMR spectra, both complexes have inequivalent isopropyl moieties on the aromatic rings, indicative of C_s symmetry in solution. Similar to the products of aryl C–F bond activation, both

compounds displayed two heptets at approximately 3.60 and 3.20 ppm coupled to four doublets ranging from 1.50 to 1.00 ppm. For **III-18**, the methylene unit directly bonded to the aluminum centre gives rise to a multiplet at −0.12 ppm while the terminal methyl group in the alkyl chain is assigned to the triplet at 0.72 ppm ($^3J_{H–H}$ = 7.1 Hz). The remaining protons in the alkyl chain are found as broad signals in the region between 1.20 and 0.90 ppm. In complex **III-19**, a multiplet at −0.26 ppm is assigned to the methine proton on the carbon directly bonded to the aluminum metal while the protons on the remaining CH_2 links are observed as multiplets between 1.40 and 0.60 ppm.

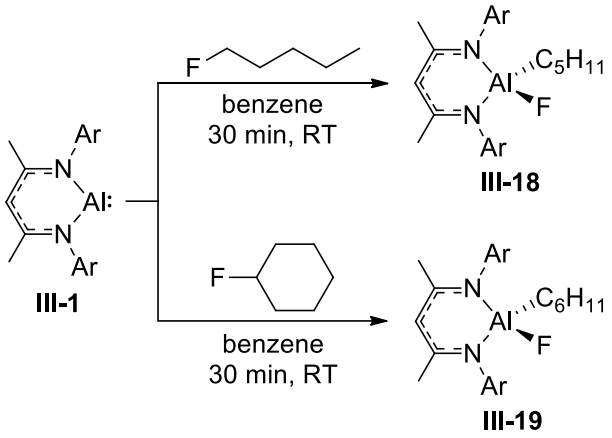

Scheme 118. Activation of 1-fluoropentane and fluorocyclohexane by **III-1** to give NacNacAlF(C_5H_{11}) (**III-18**) and NacNacAlF(C_6H_{11}) (**III-19**).

The crystal structures of **III-18** (Figure 11) and **III-19** (Figure 12, with a crystallographically imposed mirror plane bisecting the structure) are closely related. Both exhibit a distorted tetrahedral geometry around the aluminum atom sitting 0.546 Å and 0.547 Å below the plane of the NacNac ligand for **III-18** and **III-19**, respectively. The Al–N bond lengths are approximately 1.90 Å in both complexes, consistent with the corresponding distance in **III-15**. The Al1–C30 distance for **III-18** is 1.969(2) Å, nearly equivalent with the Al1–C16 distance of 1.9739(16) Å in **III-19**.

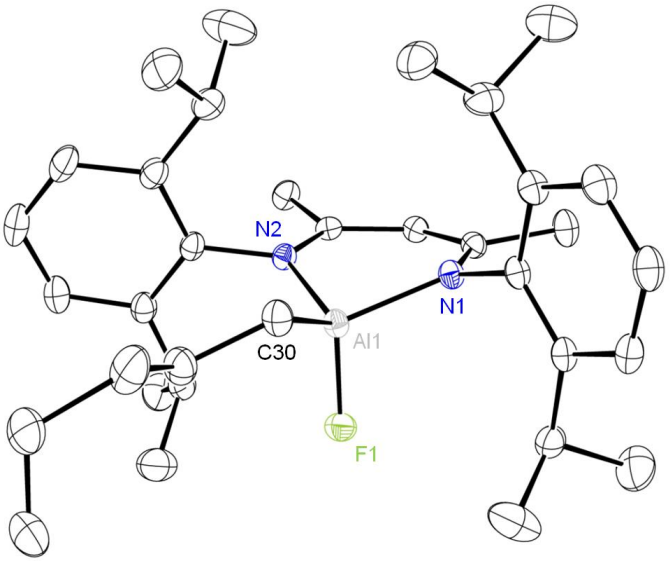

Figure 11. Molecular structure of NacNacAlF(C_5H_{11}) (**III-18**). Thermal ellipsoids are shown at 30% and the hydrogen atoms are removed for clarity. The two final carbon atoms in the alkyl chain are disordered but only one position is shown for clarity.

Table 4. Selected bond lengths and angles for complex **III-18**.

	Lengths, Å				**Angles, °**
A1–N1	1.896(1)	Al1–F1	1.670(1)	N1–A1–N2	96.21(5)
Al1–N2	1.893(1)	Al1–C30	1.969(2)	F1–Al1–C30	110.88(6)

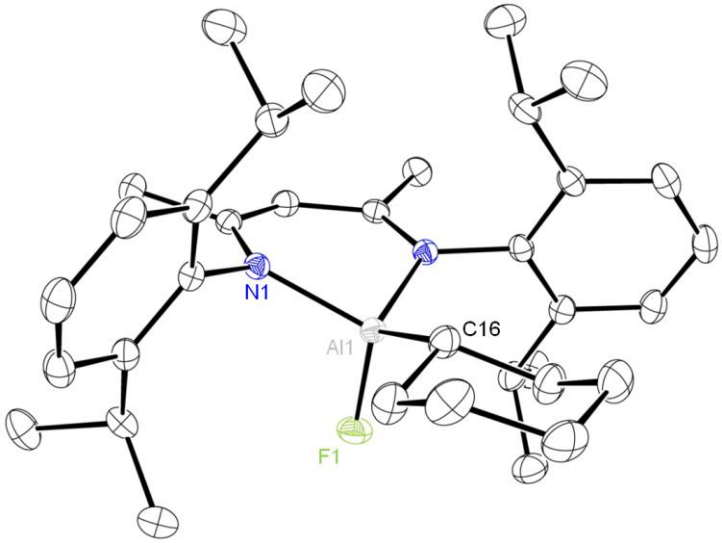

Figure 12. Molecular structure of NacNacAlF(C_6H_{11}) (**III-19**). Thermal ellipsoids are shown at 30% and the hydrogen atoms are removed for clarity. A mirror plane runs through Al1, F1 and C16, thus the left side of the molecule is a reflection of the right side.

Table 5. Selected bond lengths and angles for complex **III-19**.

Lengths, Å				Angles, °	
A1–N1	1.8984(9)	Al1–C16	1.9739(16)	N1–A1–N1a	95.28(5)
Al1–F1	1.6687(10)			F1–Al1–C16	113.80(6)

The Al–F bonds are also nearly equivalent, with bond lengths of 1.670(1) and 1.6687(10) Å for **III-18** and **III-19**, respectively. Both Al–C and Al–F distances measured in **III-18** and **III-19** are also comparable with the respective distance in **III-15**.

In their report on C(sp^3)–F oxidative addition by an iridium pincer complex, Goldman and co-workers proposed that the addition proceeded through a multistep pathway starting with C–H activation followed α-fluorine migration and subsequent hydride migration.[206] In order to determine whether **III-1** activated the C–F bond in a multistep fashion or a concerted, single step mechanism, a kinetic study on the addition of 1,2,3,4-tetrafluorobenzene was performed. Measuring the reaction rate at 295.1 K under pseudo-first-order conditions established the first-order dependence in **III-1**.

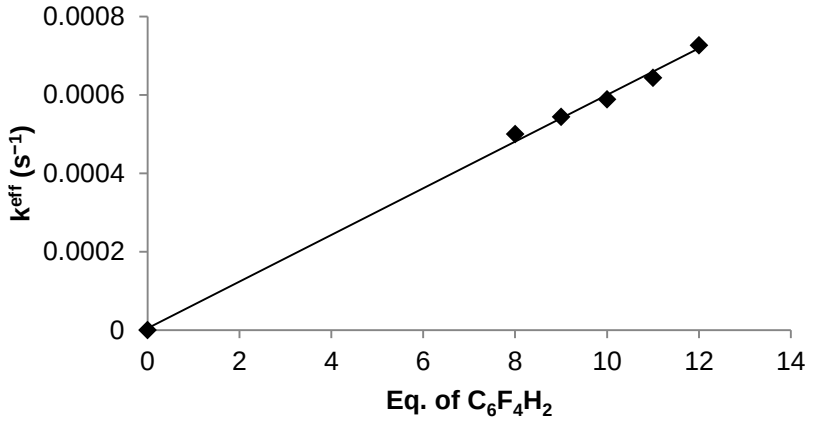

Figure 13. Plot of the pseudo-first-order rate constant for the formation of **III-14** as a function of equivalents of 1,2,3,4-tetrafluorobenzene (R^2 = 0.997).

Repeating the experiment with varying amounts of the substrate (8 to 12 equivalents) allowed for the plot of effective reaction constant, k^{eff}, versus equivalent of substrate to

be constructed (Figure 13). The linear correlation observed in the plot thus established first-order dependence in the substrate. Therefore, the overall reaction is second-order and points to a simple one-step C–F oxidative addition pathway. From a series of kinetic measurements in the temperature range of 264.1 to 303.1 K with 10 equivalents of 1,2,3,4-tetrafluorobenzene, an Eyring plot was created and the activation parameters $\Delta H^{\ddagger}$ = 13.6(2) kcal mol^{-1} and $\Delta S^{\ddagger}$ = −27.2 cal K^{-1}·mol^{-1} were extracted (Figure 14). In accord with the concerted oxidative addition mechanism, the large and negative entropy of activation obtained points to a highly ordered transition state for the reaction.

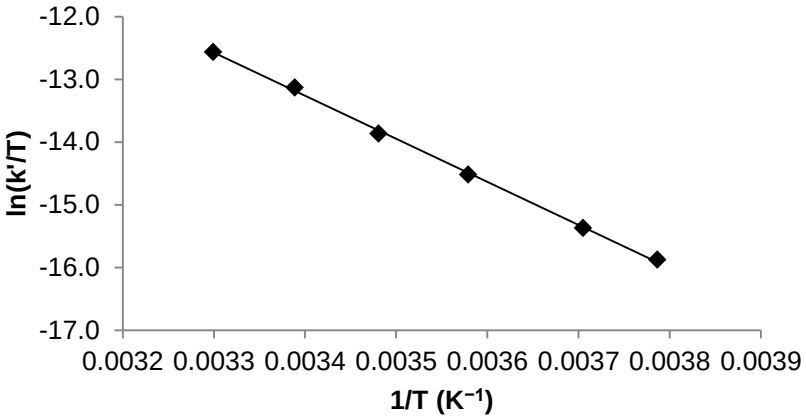

Figure 14. Eyring plot for the formation of **III-14** (10 equivalents of 1,2,3,4-tetrafluorobenzene) (R^2 = 0.999).

The realization of C–F bond activation by **III-1** suggested that the weaker C–O bond (85.5 kcal mol^{-1}) should be similarly activated by **III-1**. Initial experiments with diethyl ether showed no reaction even at elevated temperatures whereas heating a mixture of **III-1** and anisole to 100 °C resulted in partial addition across the O–CH_3 bond. However, the reaction was accompanied by significant thermal decomposition of **III-1** and it was presumed that the reaction may be sensitive to the steric bulk of the substrate being activated. Therefore, THF was chosen as the substrate due to its smaller steric

profile and the possibility that opening of the THF ring could provide an extra driving force for the reaction (Scheme 119). As hoped, reaction of **III-1** with THF resulted in insertion of the aluminum centre into the C–O bond to give the cyclic alkoxide derivative NacNacAl(–$OCH_2CH_2CH_2CH_2$–) (**III-20**) at room temperature. Consistent with the expected C_s symmetry of the product, the ^{1}H NMR spectrum of **III-20** displayed two heptets at 3.80 and 3.15 ppm ($^3J_{H–H}$ = 6.8 and 6.9 Hz, respectively) coupled to four doublets at 1.47 ($^3J_{H–H}$ = 6.6 Hz), 1.32 ($^3J_{H–H}$ = 6.8 Hz), 1.14 ($^3J_{H–H}$ = 6.8 Hz), and 1.04 ppm ($^3J_{H–H}$ = 6.8 Hz) for the inequivalent isopropyl groups on the aromatic rings. The cyclic alkoxide moiety gives rise to a triplet at 0.05 ppm ($^3J_{H–H}$ = 6.9 Hz) for the Al–CH_2 protons while the signal for the Al–OCH_2 protons are found as a multiplet at 4.16 ppm. Signals for the remaining methylene protons are found overlapping with the singlet at 1.56 ppm, corresponding to the methyl protons in the NacNac framework, and the doublet at 1.32 ppm.

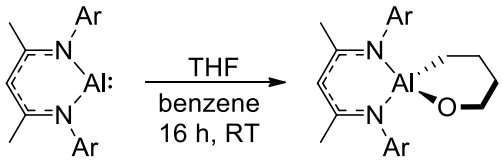

III-1 **III-20**

Scheme 119. Activation of THF by **III-1** to give NacNacAl(–$OCH_2CH_2CH_2CH_2$–) (**III-20**).

The crystal structure of **III-20**, determined by X-ray diffraction analysis, revealed two, almost perpendicular five- and six-membered alumocycles with a dihedral angle of 88.70° between the two rings (Figure 15). A distorted tetrahedral geometry was observed for the aluminum atom that sits 0.470 Å below the N_2C_3 plane of the NacNac ligand.

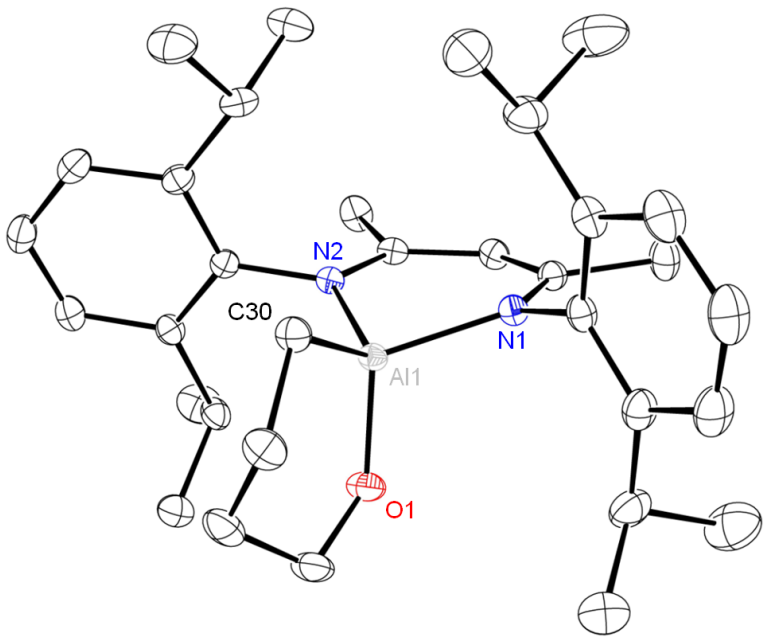

Figure 15. Molecular structure of NacNacAl(–$OCH_2CH_2CH_2CH_2$–) (**III-20**). Thermal ellipsoids are shown at 30% and the hydrogen atoms are removed for clarity.

Table 6. Selected bond lengths and angles for complex **III-20**.

Lengths, Å				**Angles, °**	
A1–N1	1.898(1)	Al1–O1	1.722(1)	N1–A1–N2	96.05(4)
Al1–N2	1.908(1)	Al1–C30	1.956(1)	O1–Al1–C30	107.78(5)

The Al1–O1 distance of 1.722(1) Å and Al1–C30 distance of 1.956(1) Å are comparable to the corresponding distances of 1.7507(13) and 1.9498(17) Å, respectively, in the related 2,3-dibenzohydrofuran derivative ^{Mes}NacNacAl(–O(C_6H_4)CH_2CH_2–).[209] Unremarkable Al–N distances of 1.898(1) and 1.908(1) Å were found for **III-20**.

A logical extension of the chemistry is the activation of the C–S bond (65 kcal mol^{-1}) by **III-1** which should be similarly feasible. Stirring a mixture of **III-1** and diethyl sulfide at 50 °C overnight resulted in formation of the unsymmetrically substituted alkyl thiolate aluminum complex NacNacAlEt(SEt) (**III-21**), the first example of C(sp^3)–S oxidative addition mediated by a main group element (Scheme 120). Two distinct ^{i}Pr

groups were observed in the ^{1}H NMR spectrum at 3.79 ppm ($^{3}J_{H–H}$ = 6.8 Hz) and 3.31 ppm ($^{3}J_{H–H}$ = 6.8 Hz) coupled to four doublets at 1.60, 1.35, 1.25, and 1.08 ppm ($^{3}J_{H–H}$ = 6.6, 6.8, 6.8, and 6.8 Hz, respectively), consistent with C_s symmetry. The ethyl group gives rise to a quartet and triplet at 0.06 ($^{3}J_{H–H}$ = 8.1 Hz) and 0.94 ppm ($^{3}J_{H–H}$ = 8.1 Hz), respectively, while the quartet at 2.68 ppm ($^{3}J_{H–H}$ = 7.4 Hz) and triplet at 1.35 ppm (overlapped with a doublet) is assigned to the ethyl sulfide moiety.

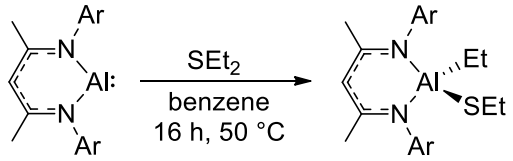

III-1 **III-21**

Scheme 120. Carbon–sulfur bond activation by **III-1** to give NacNacAlEt(SEt) (**III-21**).

The crystal structure of **III-21** (Figure 16), with a crystallographically imposed mirror plane bisecting the molecule, revealed a four-coordinate aluminum centre in a distorted tetrahedral geometry. Consistent with the structures presented earlier in the chapter, the aluminium atom is found 0.584 Å below the plane consisting of the nitrogen and carbon atoms of the NacNac framework. A bond distance of 2.2239(8) Å was found for the Al1–S1 bond and is comparable to the distances reported in the related bis-thiolate compound NacNacAl(SH)$_2$ (2.223(1) and 2.217(1) Å).[210] The Al1–C18 distance of 1.995(2) Å is analogous to the corresponding distances of 1.980(4) and 1.974(4) Å measured in the related complex $^{t\text{Bu}}$NacNacAlEt$_2$ (where $^{t\text{Bu}}$NacNac is [ArNC(^{t}Bu)CHC(^{t}Bu)NAr]$^{-}$) reported by Cui and co-workers,[129] while the Al–N1 bond length was found to be 1.9110(12) Å, consistent with the other structures reported earlier in the chapter.

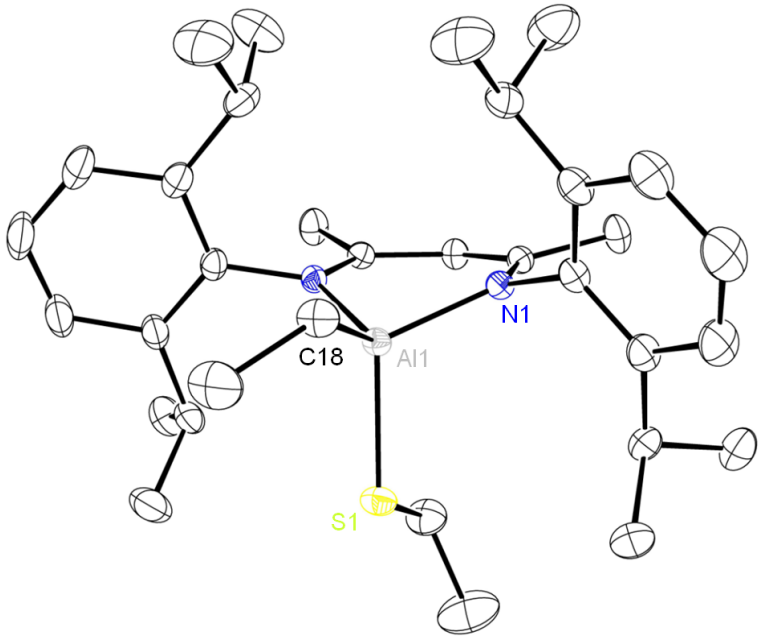

Figure 16. Molecular structure of NacNacAlEt(SEt) (**III-21**). Thermal ellipsoids are shown at 30% and the hydrogen atoms are removed for clarity. The aluminum–ethyl and sulfur–ethyl groups are disordered over two positions related by the crystallographic mirror plane but only one is shown.

Table 7. Selected bond lengths and angles for complex **III-21**.

Lengths, Å		**Angles, °**	
Al1–N1	1.9110(12)	N1–A1–N1a	96.61(7)
Al1–S1	2.2239(8)	S1–Al1–C18	105.89(7)
Al1–C18	1.995(2)		

Finally, cleavage of the C–N and C–P bond was attempted. Unfortunately, even after prolonged heating (days) at 90 °C, no productive chemistry towards bond cleavage was observed in the reaction between **III-1** and N,N-dimethylaniline or triethyl phosphine, likely due to significant steric congestion in the putative transition states.

III.4 Activation of Functionalized E–E Bonds

Following on the successful activation of C–X bonds by **III-1**, activation of functionalized element–element bonds was studied. The investigation started with the

reaction of **III-1** with diphenyl disulfide (Scheme 121). The sulfur–sulfur bond was readily cleaved at room temperature within 3 hours to cleanly furnish the symmetrically substituted bis(phenylsulfido) aluminum complex NacNacAl(SPh)$_2$ (**III-22**). The same reactivity has been observed previously with other low-valent main group species such as silylenes,[211,212] germylenes,[213-217] stannylenes,[213,217-219] and plumbylenes[220] as well as low-valent antimony and bismuth complexes.[221,222] FLPs have also effected the cleavage of the S–S bond in disulfides.[223,224] The ^{1}H NMR spectrum of **III-22** is consistent with C_{2v} symmetry in solution with a single heptet at 3.33 ppm ($^3J_{H–H}$ = 6.7 Hz) that is coupled to two doublets at 1.44 and 1.02 ppm ($^3J_{H–H}$ = 6.6 and 6.8 Hz, respectively). As well, two singlets are observed at 5.15 and 1.53 ppm for the backbone C*H* and methyl protons, respectively.

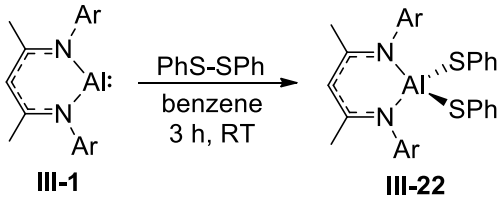

III-1 **III-22**

Scheme 121. Activation of diphenyl disulfide by **III-1** to give NacNacAl(SPh)$_2$ (**III-22**).

The structure of **III-22**, shown in Figure 17, was confirmed by X-ray diffraction analysis. The coordination geometry around the aluminum centre is a distorted tetrahedron with the atom sitting 0.420 Å below the N_2C_3 skeleton of the NacNac ligand. The Al–S bond lengths 2.2220(6) and 2.2199(6) Å are essentially identical to each other and similar to the distance found in **III-21** and the corresponding Al–SPh distance in a three-coordinate (2.225(1) Å)[225] and five-coordinate (2.274(3) Å)[226] aluminum complex. The metrical parameters are also comparable to the respective bond distances of 2.237(1) and 2.245(1) Å[227] in the dimeric bis-sulfide species [NacNacAl(μ-S)]$_2$ as well as the Al–S

linkages in [NacNacAl(μ-S_3)$_2$AlNacNac] (2.223(1) and 2.248(1) Å),[132] obtained upon reaction of **III-1** with S_8. The Al–N distances of 1.895(1) and 1.893(1) Å are comparable to the average Al–N distance (1.909 Å) observed in the other NacNac ligated aluminum complexes reported in section III.2.

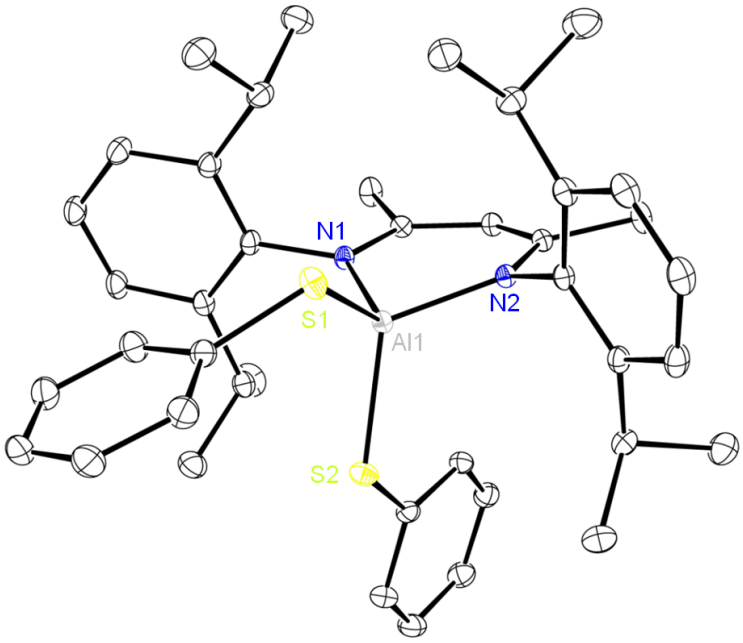

Figure 17. Molecular structure of NacNacAl(SPh)$_2$ (**III-22**). Thermal ellipsoids are shown at 30% and the hydrogen atoms are removed for clarity.

Table 8. Selected bond lengths and angles for complex **III-22**.

	Lengths, Å			**Angles, °**	
A1–N1	1.895(1)	Al1–S1	2.2220(6)	N1–A1–N2	97.09(6)
Al1–N2	1.893(1)	Al1–S2	2.2199(6)	S1–Al1–S2	102.77(2)

Next, activation of the phosphorus–phosphorus bond in a disphosphine was attempted (Scheme 122). Reaction of **III-1** with the bulky tetraphenyl diphosphine resulted in cleavage of the P–P bond over the course of 3 days at 70 °C to cleanly furnish the novel aluminum bis(diphenyl phosphido) complex NacNacAl(PPh_2)$_2$ (**III-23**). While there are many examples of low-valent main group complexes activating white

phosphorus,[228-230] including **III-1**,[133] the production of **III-23** is the first example of a main group complex activating the P–P bond in a diphosphine. Interestingly, despite the symmetric substitution pattern at the aluminum centre, two different ^{i}Pr groups are present in the molecule as two heptets at 3.79 and 3.65 ppm ($^{3}J_{H–H}$ = 6.5 and 6.6 Hz, respectively) are observed in the ^{1}H NMR spectrum coupled to four doublets at 1.61, 1.09, 1.03, and 0.98 ppm ($^{3}J_{H–H}$ = 6.7, 6.8, 6.5, and 6.6 Hz, respectively), consistent with C_s symmetry in solution. Furthermore, two singlets at −36.8 and −50.0 ppm were present in the proton decoupled ^{31}P NMR spectrum.

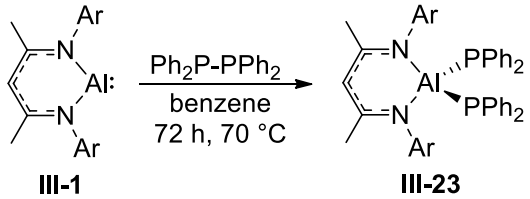

III-1 **III-23**

Scheme 122. Activation of tetraphenyl diphosphine by **III-1** to give NacNacAl(PPh_2)$_2$ (**III-23**).

The non-equivalency of the phosphido groups in bis(phosphide) complexes has precedence, for example, in the structure of $Cp_2Hf(PEt_2)_2$ reported by Baker *et al.*[231] A significant difference in the Hf–P bond distances as well as the geometry around the phosphorus atom was observed (2.488(1) Å, trigonal planar vs. 2.682(1) Å, pyramidal) that was attributed to the donation of the lone pair on one phosphorus centre into a vacant orbital on hafnium. However, such a difference in coordination geometry around the two phosphorus atoms was not observed in **III-23**, as seen in its molecular structure determined by X-ray diffraction (Figure 18). Both P1 and P2 exhibit trigonal pyramidal geometry with average bond angles of 108.8° and 109.0°, respectively, while the Al–P bonds in **III-23** (2.3775(5) and 2.3979(5) Å) are slightly different but both are comparable to the respective distance of 2.3971(6) Å found in **III-10**. Similar to the other

structures discussed, a distorted tetrahedral geometry is seen at the aluminum centre. Due to the large diphenyl phosphide groups, the aluminum atom sits 0.685 Å below the plane defined by the N_2C_3 framework of the ligand, even farther than the corresponding distance of 0.571 Å in the closely related hydrido phosphido complex **III-10**. Similarly, an expansion of the bite angle is noted in **III-23** compared to **III-10** (98.80(5) vs. 95.42(6)°) due to the increased steric pressure.

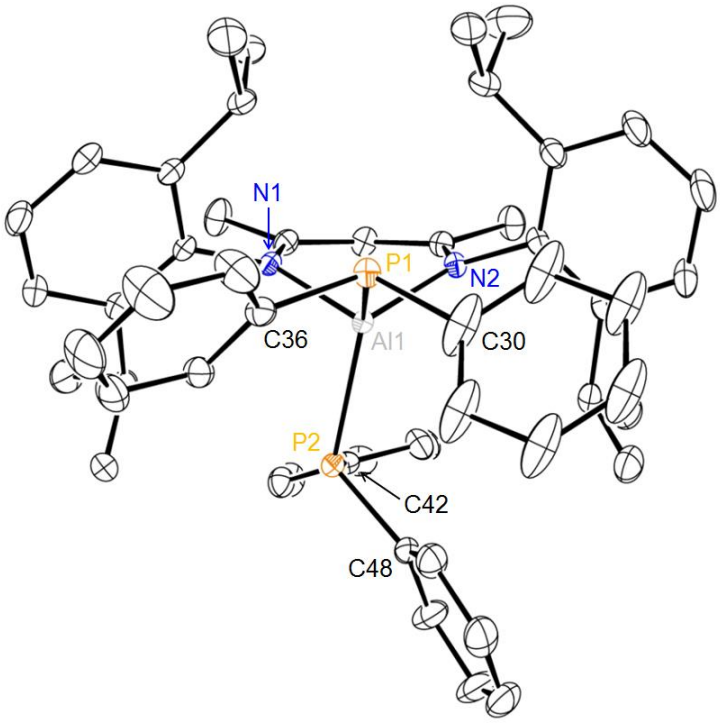

Figure 18. Molecular structure of NacNacAl$(PPh_2)_2$ (**III-23**). Thermal ellipsoids are shown at 30% and the hydrogen atoms are removed for clarity. One phenyl ring bonded to P1 is disordered over two positions but only one is shown.

Table 9. Selected bond lengths and angles for complex **III-23**.

Lengths, Å			**Angles, °**		
Al1–N1	1.925(1)	N1–A1–N2	98.80(4)	C30–P1–C36	105.5(1)
Al1–N2	1.903(1)	P1–A1–P2	124.87(2)	Al1–P2–C42	107.87(4)
Al1–P3	2.3775(5)	Al1–P1–C30	112.5(1)	Al1–P2–C48	116.19(5)
Al1–P4	2.3979(5)	Al1–P1–C36	108.44(5)	C42–P2–C48	103.00(6)

Therefore, based on the metrical parameters, the observed C_s symmetry in complex **III-23** is strictly due to the significant steric bulk afforded by the diphenyl phosphide ligands, resulting in restricted movement and rotation around the aluminum centre.

In order to probe whether dynamic behaviour in **III-23** can be observed and studied, a variable-temperature NMR spectroscopy study was performed. As illustrated in Figure 19, two septets are observed for the inequivalent methine protons on the isopropyl group in the slow-exchange regime. As the temperature is raised, the signals merge and the pattern of the isopropyl moieties morph into a single heptet, consistent with an average C_{2v} symmetry for the molecule in the fast-exchange regime. From the ^{1}H NMR data, the barrier for this process was found to have a $\Delta G^{\ddagger}$ value of 17.0 kcal mol^{-1} at the coalescence temperature of 70 °C. Similar dynamic behaviour has been observed by Piers and co-workers in bisalkyl scandium complexes, $^{t\text{Bu}}$NacNacScR$_2$ (R = Cl, Me, Et, Bz, CH_2CMe_3, CH_2SiMe_3), however lower coalescence temperatures ranging from –60 to 30 °C were found.[232]

Further attempts at E–E bond activations included reacting **III-1** with bis(pinacolato)diboron and hexamethyldisilane. Unfortunately, in both cases no bond activation was observed even after heating for days at 90 °C. Obstruction by the sterically bulky diisopropylphenyl groups on the NacNac ligand is likely limiting the approach of the B–B or Si–Si bond and preventing their reaction with the aluminum centre.

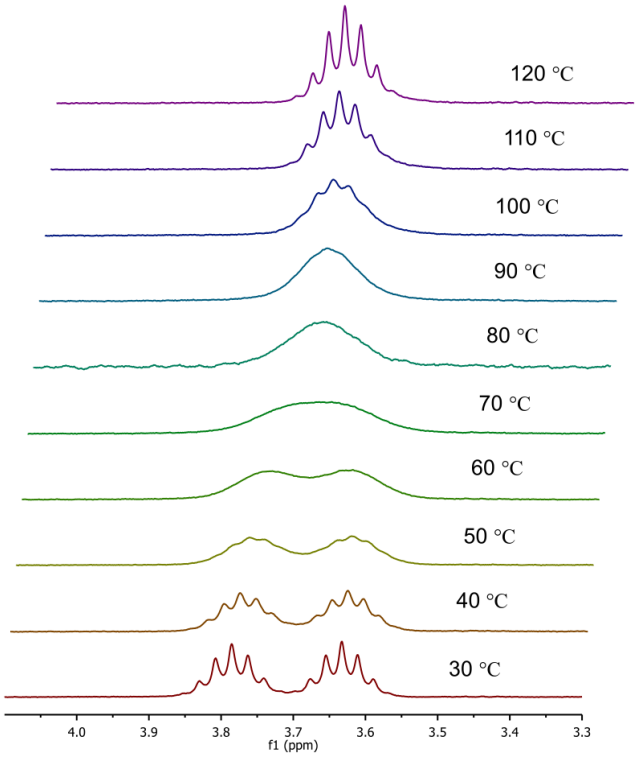

Figure 19. Series of ^{1}H NMR spectra of **III-23** (300 MHz, toluene-d_8), depicting the coalescence temperature and dynamic behaviour of the molecule.

III.5 Activation of C=S and P=S Bonds

Now that the ability of **III-1** to oxidatively add very strong σ C–O and C–F bonds has been demonstrated, it was thought that perhaps **III-1** can also mediate oxidative addition of substrates with multiple bonds. Complete oxidative addition of $R_nX{=}YR_m$ by the Al(I) centre is not possible because the reaction would be a four-electron process and Al(I) can only give two electrons. However, if either the R_nX or R_mY fragment could act as a two-electron donor to the resulting Al(III) centre, oxidative cleavage of the multiple bond would be a feasible, two-electron process. Efforts were initially focused towards thioureas, $(R_2N)_2C{=}S$, due to the well-established ability of amino groups to stabilize diaminocarbenes[233] and because the strength of the C=S bond (137 kcal mol^{-1}) is the weakest within the family of C=X bonds (X = C, N, O, S).

The investigation started with reaction of **III-1** with the cyclic thiourea S=SIMe, where SIMe is $C(MeNCH_2–)_2$, at room temperature that led to an intractable mixture of products. Addition of the cyclic thiourea at −30 °C to a solution of **III-1** in toluene-d_8 resulted in oxidative cleavage of the carbon–sulfur double bond and clean formation of the carbene-stabilized terminal aluminum sulfide NacNacAl=S(SIMe) (**III-24**) that was subsequently characterized by multinuclear NMR spectroscopy at low temperature (Scheme 123). In particular, the ^{1}H NMR spectrum of **III-24** is consistent with the expected C_s symmetry in solution with two heptets at 3.87 ($^3J_{H–H}$ = 6.8 Hz) and 2.80 ppm ($^3J_{H–H}$ = 6.8 Hz) for the isopropyl methine protons that are coupled to four doublets at 1.85, 1.29, 1.22, and 1.07 ppm ($^3J_{H–H}$ = 6.6, 6.7, 6.8, and 6.7 Hz, respectively) from the isopropyl methyl protons. The C*H* proton from the framework of the NacNac ligand is observed as a singlet at 4.67 ppm while the methyl protons are found at 1.07 ppm as a singlet. The resulting carbene ligand has restricted rotation about the Al–C dative bond due to the N-aromatic groups on the NacNac ligand. This is borne out as two singlets at 4.11 and 3.08 ppm for the N-methyl protons while the methylene units in the backbone appear as broad multiplets at 3.52 and 3.08 (overlapped with the N-methyl singlet) ppm. In the ^{13}C NMR spectrum, the central carbon of the NHC is found at 186.1 ppm, shifted upfield relative to the corresponding signal of the free carbene at 239.8 ppm.[234] While complex **III-24** remains soluble in toluene at low temperatures, warming the solution above 0 °C results in the precipitation of **III-24** as a bright yellow solid. Upon precipitation, **III-24** became insoluble in common organic solvents. However, its constitution is unchanged, confirmed by a satisfactory elemental analysis from the

isolated solid and subsequent reactivity studies. Despite numerous attempts, crystals of **III-24** suitable for X-ray crystallographic analysis were not obtained.

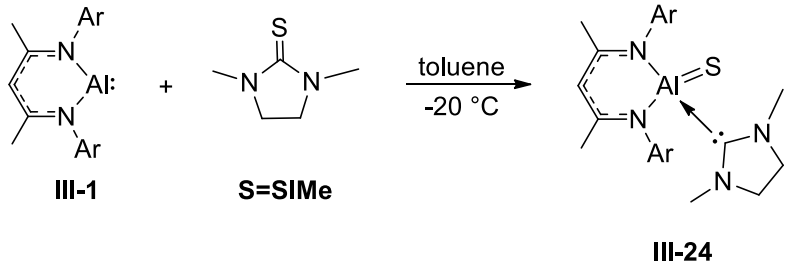

Scheme 123. Preparation of aluminum sulfide **III-24** from the reaction of **III-1** with S=SIMe.

Changing the reagent to the unsaturated cyclic thiourea S=I^{i}Pr, where I^{i}Pr = C(^{i}PrNCH–)$_2$, resulted in a related, but more crystalline complex NacNacAl=S(I^{i}Pr) **III-25** which was cleanly generated in solution at 0 °C and isolated by crystallization from toluene at −30 °C (Scheme 124). Akin to complex **III-24**, crystals of **III-25** are insoluble in most common organic solvents. It is however sparingly soluble in bromobenzene and NMR spectroscopic data were recorded in bromobenzene-d_5. The ^{1}H NMR spectrum of **III-25** revealed two septets at 3.76 ($^{3}J_{H–H}$ = 6.9 Hz) and 2.38 ($^{3}J_{H–H}$ = 6.8 Hz) ppm coupled to four doublets at 1.54, 1.00, 0.86, and 0.44 ppm ($^{3}J_{H–H}$ = 6.6, 7.0, 6.8, and 6.7 Hz, respectively) arising from the inequivalent isopropyl groups on the aromatic rings, a pattern consistent with the expected C_s symmetry in solution. Singlets at 4.92 and 1.40 ppm are assigned to the γ- and methyl protons in the NacNac ligand, respectively. Analogous to the carbene ligand in **III-24**, the unsaturated N-heterocyclic carbene in **III-25** also has restricted rotation about the dative Al–C bond, giving rise to two septets at 8.39 and 4.81 ppm ($^{3}J_{H–H}$ = 6.7 and 6.6 Hz, respectively) coupled to two doublets at 1.09 ($^{3}J_{H–H}$ = 6.5 Hz) and 0.75 ppm ($^{3}J_{H–H}$ = 6.6 Hz). Interestingly, the two methine protons appear at significantly different chemical shifts; the disparity is likely due to the

difference in proximity between the two protons relative to the terminal sulfide ligand. The C*H* protons in the backbone of the imidazole framework give rise to two singlets at 6.57 and 6.42 ppm. Due to the poor solubility of **III-25** in bromobenzene, the signal for the central carbon in the NHC ligand was not observed.

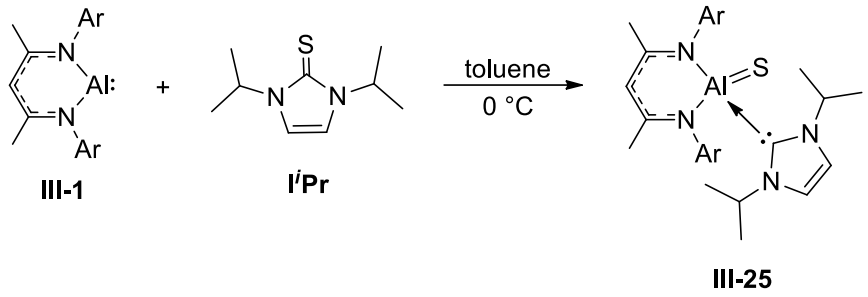

Scheme 124. Preparation of aluminum sulfide **III-25** from the reaction of **III-1** with S=I^{i}Pr.

The molecular structure of **III-25** was determined by X-ray diffraction analysis (Figure 20). The aluminum atom lies in a four-coordinate environment formed by the bidentate NacNac ligand, NHC, and a terminal sulfido ligand. The Al=S bond length of 2.1038(7) Å is noticeably shorter than the average Al–S single bond (2.363 Å, ranging from 2.159–3.277 Å),[b] consistent with the multiple bond character. The closest relative of compound **III-25** is the deprotonated alumothiol [NacNacAl(S)X]$^-$ reported by Roesky *et al.*[235-237] Four derivatives of this anion has been structurally characterized, differing in the identity of the counter-cation and the nature of the X group (X = SH or $OP(OEt)_2$), with the Al–S distances falling in the range of 2.115–2.124 Å. Another closely related compound, also reported by the Roesky group, is the NHC stabilised aluminum hydride complex NacNac'AlH(I^{i}Pr).[138] Akin to the other aluminum complexes described in this chapter, the aluminum atom in **III-25** has a distorted tetrahedral geometry that deviates from the plane defined by the NacNac ligand by 0.458 Å. A similar coordination mode

[b] Based on a search in the Cambridge Crystallographic Data Centre.

was observed by Driess *et al*. in the structurally related silanone NacNac'Si=O(IMe_4), where IMe_4 is C(MeNC(Me)–)$_2$).[238] The Al–C bond length of 2.109(2) Å in **III-25** is longer than the average Al–C distance in four-coordinate NHC complexes of aluminum (2.065 Å).[c] However, this parameter falls within a wide range of distances (2.008–2.162 Å) with only four structures containing longer Al–C distances (ranging from 2.118(2)[239] to 2.162(2) Å[240]). The Al–N distances of 1.927(1) and 1.952(2) Å are elongated compared to the average Al–N bond lengths (1.909 Å) reported in previous sections.

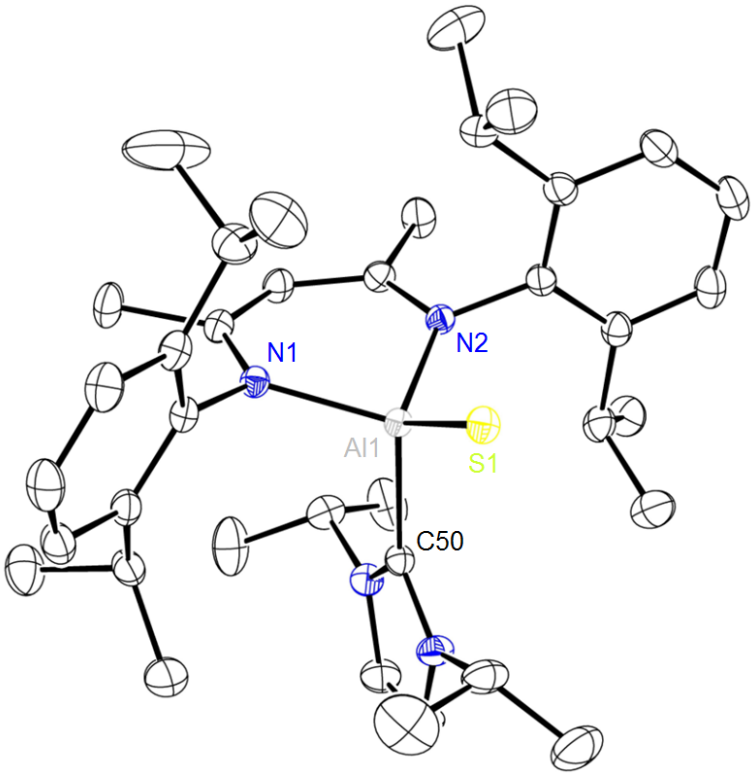

Figure 20. Molecular structure of NacNacAl=S(I^{i}Pr) (**III-25**). Thermal ellipsoids are shown at 30% and the hydrogen atoms are removed for clarity.

Table 10. Selected bond lengths and angles for complex **III-25**.

	Lengths, Å			**Angles, °**	
A1–N1	1.952(2)	Al1–S1	2.1038(7)	N1–A1–N2	94.92(6)
Al1–N2	1.927(1)	Al1–C50	2.109(2)	S1–Al1–C50	114.00(5)

[c] Based on a search in the Cambridge Crystallographic Data Centre.

In order to elucidate the bonding situation in compound **III-25**, density-functional calculations were performed.[d] According to the calculations, the reaction L_2Al + NHC=S → L_2Al=S(NHC) is exothermic, with a calculated ΔE_e = –61.4 kcal mol^{-1} and $\Delta G°_{298}$ = −41.1 kcal mol^{-1}. The energy corresponding to the carbene dissociation process, L_2Al=S(NHC) → L_2Al=S + NHC, is relatively low (47.7 kcal mol^{-1} (ΔE_e) and 28.1 kcal mol^{-1} ($\Delta G°_{298}$)). The optimized metal-ligand bond distances are given in Table 11. A very good agreement between the calculated and experimental distances for **III-25** is observed, with a maximum deviation of 0.017 Å for one of the Al–N bonds. The optimized structure of the monomeric sulfide L_2Al=S exhibits a typical trigonal-planar geometry around the aluminum centre. Coordination of the NHC ligand to this species to give **III-25** results in elongation of all metal-ligand bonds, likely the result of increased steric congestion around the central aluminum atom. Interestingly, the parent Al(I) complex **III-1** also exhibits substantially longer Al–N bonds than L_2Al=S, likely due to the larger size of Al(I) ion.

Table 11. Experimental and calculated aluminum–ligand bond lengths (Å).

Molecule	Al–C^{NHC} exp.	Al–C^{NHC} calcd.	Al–N^{1} exp.	Al–N^{1} calcd.	Al–N^{2} exp.	Al–N^{2} calcd.	Al–S exp.	Al–S calcd.
III-25	2.107(2)	2.094	1.953(1)	1.962	1.927(1)	1.941	2.1035(6)	2.111
$L_2Al(S)$	–	–	–	1.879	–	1.879	–	2.034
III-1[8]	–	–	1.957(2)	2.004	1.957(2)	2.004	–	–

The bonding situation in complex **III-25** was examined by means of the Mayer bond orders[241,242] and Wiberg bond indices[243] (in the natural atomic orbital basis[244]) and the results are summarized in Table 12. The Mayer bond orders clearly demonstrate the multiple-bond character of the Al–S bond in compounds **III-25** and L_2Al=S. In the

[d] DFT calculations were performed by Prof. Sergei F. Vyboishchikov.

trigonal-planar complex $L_2Al{=}S$, the Al–S bond order is the largest, which correlates well with the shortest calculated Al–S bond length. Only a minor decrease of Mayer bond order was observed on going from $L_2Al{=}S$ to **III-25**, suggesting that the transfer of electron density from the carbene ligand to aluminum is rather minor. Further corroborating this conclusion is the observation that the corresponding molecular orbital has primarily carbon lone-pair character, with only minor contribution from aluminum, leading to the conclusion that the Al–C interaction is mainly electrostatic in nature. The two highest occupied molecular orbitals of **III-25** are nearly degenerate at the orbital energy of approximately –4.5 eV (Figure 21). These orbitals mainly correspond to the sulfur lone pairs, but the HOMO also has a significant contribution from an aluminum p_π orbital, providing further evidence of multiple-bond character in the Al–S bond. The lower lying HOMO–2 with the orbital energy of about –5.9 eV is the Al–S σ-bonding orbital. The Wiberg bond indices follow the same trend as the Mayer bond orders but have lower absolute values.

Table 12. Mayer bond orders and Wiberg bond indices for complexes **III-25**, $L_2Al{=}S$, and **III-1**.

	Mayer bond orders				**Wiberg bond indices**		
Molecule	$Al–C^{NHC}$	$Al–N^{L1}$	$Al–N^{L2}$	Al–S	$Al–N^{L1}$	$Al–N^{L2}$	Al–S
III-26	0.48	0.45	0.46	1.49	0.24	0.25	1.20
$L_2Al{=}S$	–	0.64	0.64	1.75	0.30	0.30	1.50
III-1	–	0.51	0.51	–	0.15	0.15	–

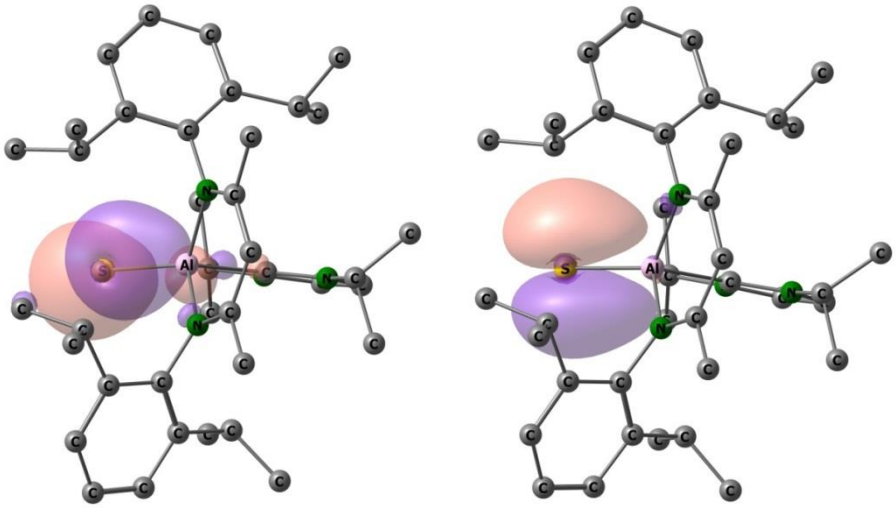

HOMO HOMO–1

Figure 21. Molecular orbital diagrams for $L_2Al{=}S(NHC)$.

To underpin the multiple-bond character in **III-24**, its activity towards cycloaddition with phenyl isothiocyanate has been probed. Thus, reaction of **III-24** with two equivalents of PhN=C=S yielded the cycloaddition product NacNacAl(S_2CNPh) (**III-26**) with concomitant production of zwitterion SIMeC(S)NPh (**III-27**) resulting from the reaction of the liberated carbene with phenyl isothiocyanate (Scheme 125). Similar coupling between carbenes and phenyl isothiocyanate have been reported previously by Cheng and co-workers.[245] The same cycloaddition product was also observed upon reaction of aluminum sulfide **III-25** with phenyl isothiocyanate.

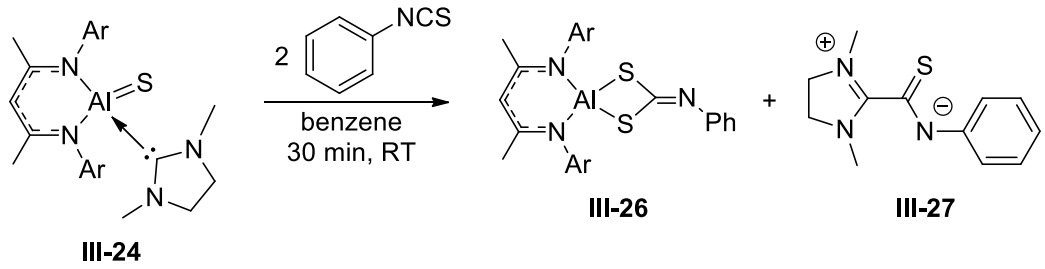

Scheme 125. Cycloaddition of phenyl isothiocyanate with **III-24** to give **III-26** and **III-27**.

The ^{1}H NMR spectrum of **III-26** is consistent with C_s symmetry in solution as evidenced by the pattern of signals observed for the isopropyl moieties, with two multiplets at 2.94 and 2.87 ppm coupling to four doublets at 1.19 ($^{3}J_{H–H}$ = 6.9 Hz), 1.02 ($^{3}J_{H–H}$ = 6.8 Hz), 0.92 ($^{3}J_{H–H}$ = 6.8 Hz), and 0.75 ppm ($^{3}J_{H–H}$ = 6.7 Hz). In comparison with **III-24**, both the C*H* and methyl protons from the framework of the NacNac ligand in **III-26** are observed downfield as singlets at 5.12 and 1.50 ppm, respectively.

For **III-27**, the ^{1}H NMR spectrum revealed a simple pattern of signals with two singlets at 3.85 and 3.20 ppm correlated to the methylene protons in the imidazolidine ring and N-methyl protons, respectively. Signals for the aromatic protons in the phenyl ring are found between 7.40 and 7.00 ppm. In the ^{13}C NMR spectrum, signals for the thioamide and central imidazolidine carbon are found downfield at 167.6 and 164.4 ppm.

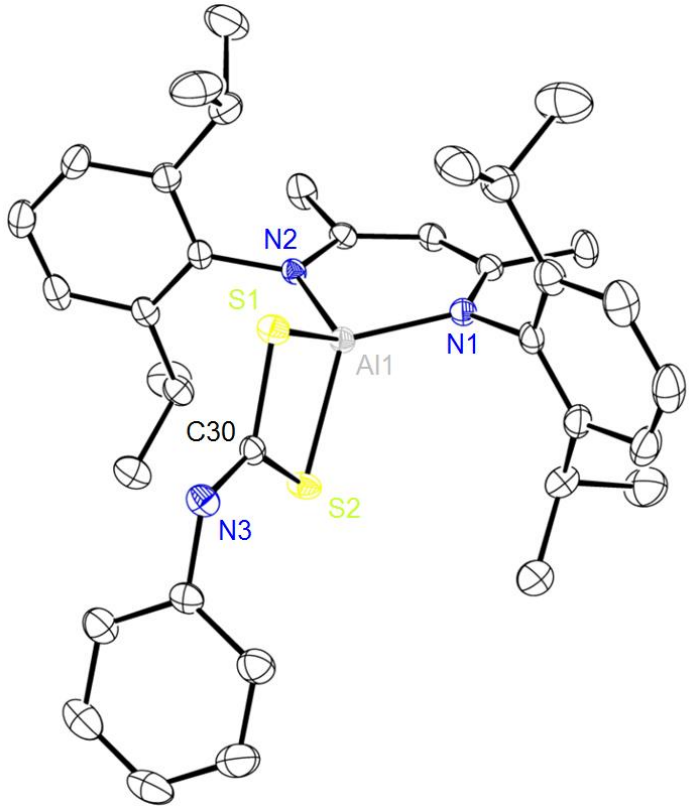

Figure 22. Molecular structure of NacNacAl(S_2CNPh) (**III-26**). Thermal ellipsoids are shown at 30% and the hydrogen atoms are removed for clarity.

Table 13. Selected bond lengths and angles for complex **III-26**.

Lengths, Å		Angles, °	
Al1–N1	1.859(3)	N1–A1–N2	99.5(1)
Al1–N2	1.860(2)	S1–Al1–S2	82.91(4)
Al1–S1	2.226(1)	S1–C30–S2	112.2(2)
Al1–S2	2.227(1)	Al1–S1–C30	82.6(1)
S1–C30	1.764(2)	Al1–S2–C30	82.1(1)
S2–C30	1.787(3)		

The structure of **III-26**, shown in Figure 22, revealed a four-coordinate aluminum centre in a distorted tetrahedral geometry. The Al–S bond lengths are essentially equidistant at 2.226(1) and 2.227(1) Å and fall within the wide range of Al–S single bond distances discussed above. The aluminum atom sits much closer to the N_2C_3 plane, deviating by only 0.228 Å due to the reduced steric bulk around the aluminum centre in **III-26**. The AlS_2C fragment adopts a planar, kite-shaped configuration with the sum of the angles equal to 359.91°. As well, the plane defined by the AlS_2C fragment was found to be nearly perpendicular to the plane defined by the NacNac ligand with an angle of 87.4° between them.

The structure of **III-27**, as seen in Figure 23, was confirmed by X-ray diffraction analysis. In accord with the zwitterionic nature of the compound, the C1–S1 distance of 1.692(2) Å is intermediary between the average distance for a carbon–sulfur single bond, 1.76 Å, and the average distance for a C=S bond of 1.62 Å. Similarly, the C2–N1 and C2–N2 distances of 1.312(3) and 1.313(2), respectively, are nearly identical and intermediate between the average distances for a single and double carbon–nitrogen bond while the C1–N3 distance of 1.283(2) Å is closer to a double bond.

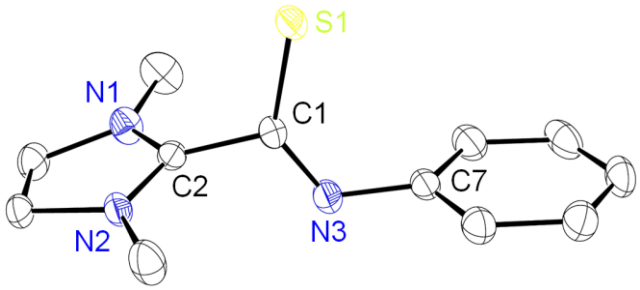

Figure 23. Molecular structure of SIMeC(S)NPh **(III-27)**. Thermal ellipsoids are shown at 30% and the hydrogen atoms are removed for clarity.

Table 14. Selected bond lengths for compound **III-27**.

C2–N1	1.312(3)
C2–N2	1.313(2)
C1–S1	1.692(2)
C1–N3	1.283(2)
N3–C7	1.419(3)

Cycloaddition with alkenes were also examined with **III-24**. One equivalent of 1-hexene was added to a suspension of **III-24** in benzene. No reaction between the two were observed at room temperature, however, upon heating at 50 °C the yellow suspension was gradually consumed and colorless crystals were deposited. In the ^{1}H NMR spectrum of the reaction, the major signals observed were for unreacted olefin and two new singlets confirmed to be the carbene dimerization product, $SIMe_2$, previously reported and characterized by Denk and co-workers.[234] The identity of the crystalline product was then confirmed by X-ray diffraction analysis to be the previously reported sulfide-bridged dimer $[NacNacAl(\mu\text{-}S)]_2$.[227] Therefore, cycloaddition of 1-hexene to **III-24** did not occur and instead at elevated temperatures the carbene ligand dissociates from **III-24** and readily dimerizes to give $SIMe_2$, while the intermediate Lewis-base-free terminal aluminum sulfide couples to give $[NacNacAl(\mu\text{-}S)]_2$. To confirm that the olefin

has no effect on the reaction, heating a suspension of **III-24** in the absence of 1-hexene gives the same result.

Bond activation across the Al=S linkage was also attempted. Phenylsilane was added to a suspension of **III-24** in benzene and no reaction was observed between the two species at room temperature. Unfortunately, heating the mixture did not result in the desired reaction; only the same thermally induced decomposition to the dimeric bis-sulfide aluminum complex and tetraamino olefin was observed.

Wishing to extend this oxidative addition reactivity to other multiple bonds, **III-1** was reacted with the triphenylphosphine sulfide (P=S bond energy = 80 kcal mol^{-1}). Mixing the reagents in a 1:1 ratio did not afford the expected product, NacNacAl=S(PPh_3), but resulted in a mixture of the terminal sulfide NacNacAl=S(S=PPh_3) (**III-28**), unreacted **III-1**, and free triphenylphosphine. The difference in the outcome of the reaction is likely due to the large steric profile of triphenylphosphine, making it incompatible with the bulky 2,6-diisopropylphenyl substituents of the NacNac ligand. Complex **III-28** can be cleanly generated in solution by reacting **III-1** with two equivalents of triphenylphosphine sulfide (Scheme 126).

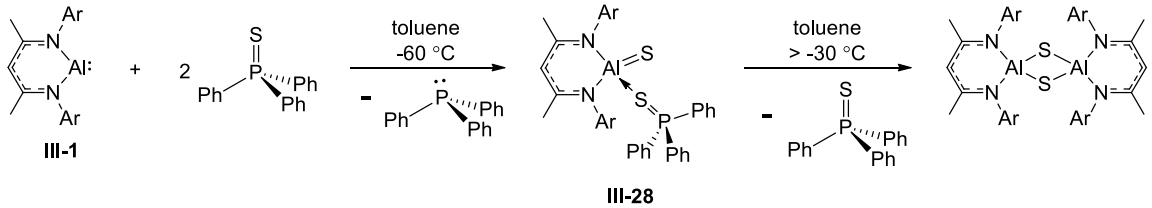

Scheme 126. Generation of **III-28** at low temperature from the reaction between **III-1** and triphenylphosphine sulfide followed by decomposition at elevated temperature.

The ^{1}H NMR spectrum acquired at −60 °C is in accord with the expected C_s symmetry in solution. Two broad singlets were observed at 3.51 and 3.14 ppm, assigned to the isopropyl methine protons, which are coupled to three broad singlets (two signals

have overlapped) at 1.67, 1.11, and 0.70 ppm from the isopropyl methyl protons. Interestingly, upon warming to −30 °C, the signals in the ^{1}H NMR spectrum merged to a more symmetric C_{2v} averaged pattern for the NacNac ligand, suggesting a fast exchange process. Variable-temperature NMR studies in the temperature range of −80 to −30 °C revealed a $\Delta G^{\ddagger}$ value of 10.2 kcal mol^{-1} as the barrier for this exchange process at a coalescence temperature of −50 °C (Figure 24).

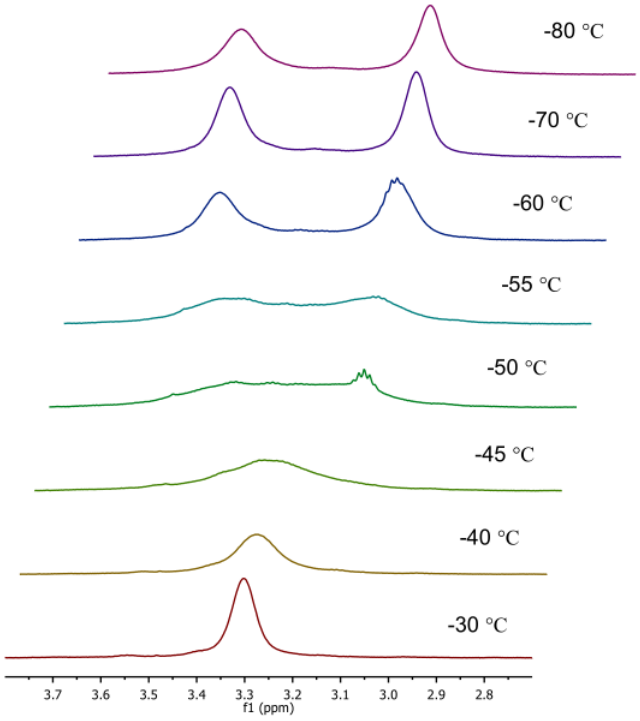

Figure 24. Series of ^{1}H NMR spectrum of **III-28** (600 MHz, toluene-d_8) depicting the coalescence temperature and dynamic behavior of the molecule.

Even at −80 °C, no signal in the ^{31}P NMR spectrum was observed for the coordinated phosphine sulfide. Unlike compounds **III-24** and **III-25**, warming solutions of **III-28** above −30 °C results in the precipitation of a white crystalline material, the identity of which was determined, by carrying out an X-ray diffraction analysis, to be the known sulfide-bridged dimer [NacNacAl(μ-S)]$_2$.[227] Similar to **III-24** and **III-25**, reacting freshly

generated **III-28** with phenyl isothiocyanate also results in the same cycloaddition product **III-26**.

III.6 Activation of C=O and P=O Bonds

After the success in activating C=S and P=S bonds with **III-1**, activation of the corresponding bonds with oxygen were attempted. Initial reaction of **III-1** with the cyclic urea O=SIMe at room temperature resulted in a complex mixture of products as evidenced by the ^{1}H NMR spectrum. As shown in Scheme 127, repeating the reaction at −60 °C in toluene did not produce the expected product of C=O cleavage but cleanly yielded the unexpected aluminum hydride NacNac'AlH(O=SIMe) (**III-29**). In the ^{1}H NMR spectrum of **III-29**, deprotonation of the weakly acidic methyl group in the backbone of the NacNac ligand leads to two singlets integrating to one proton each at 4.03 and 3.27 ppm for the diastereotopic protons of the resulting methylene group and a singlet at 1.77 ppm that integrates to three protons for the remaining methyl moiety. Furthermore, two multiplets resulting from the overlap of four heptets from inequivalent isopropyl methines are observed at 4.18 and 4.01 ppm. The multiplets are found to be coupled to eight doublets ranging from 1.66 to 1.16 ppm corresponding to the isopropyl methyl protons. A multiplet at 1.84 ppm and a singlet at 1.59 ppm is assigned to the methylene and methyl protons of the O=SIMe ligand, shifted upfield with respect to the uncoordinated urea. Unlike the carbene ligand in **III-24** and **III-25**, the urea ligand in **III-29** is free to rotate around the Al–O dative bond based on the observed symmetry in the ^{1}H NMR signals. The aluminum hydride is confirmed by the IR stretch seen at 1810 cm^{-1}.

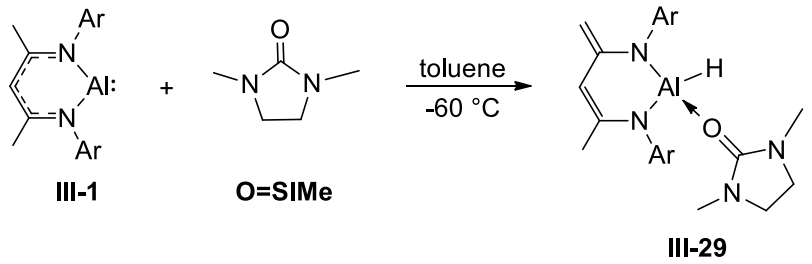

Scheme 127. Preparation of aluminum hydride **III-29** from the reaction of **III-1** with O=SIMe.

The structure of **III-29** was confirmed by X-ray diffraction analysis (Figure 25) and revealed a distorted tetrahedral geometry at the aluminum centre sitting 0.483 Å below the plane defined the NacNac' ligand. The Al–N distances of 1.843(2) and 1.836(2) Å are shorter than the average Al–N distance measured in the structures above but are consistent with the respective bond lengths of 1.844(3) and 1.853(2) Å in the closely related complex NacNac'AlH(I^{i}Pr).[138] The shortened Al–N distance in **III-29** is due to the doubly anionic NacNac' ligand, resulting in tighter binding to the aluminum cation compared to the monoanionic NacNac ligand. The Al1–O1 distance of 1.812(2) Å is longer than the respective distance of 1.769(2) Å found in the adduct between aluminum trichloride and tetramethylurea reported by Nöth and co-workers.[246] The greater distance is unsurprising as the bulky diisopropylphenyl phenyl groups flanking the aluminum centre in **III-29** prevent closer approach of the urea. In the backbone of the NacNac' ligand, the internal C–C lengths, C2–C3: 1.389(3) Å and C3–C4: 1.428(3) Å, are indicative of a double and single bond, respectively, while a more pronounced difference is noted between the terminal C–C (1.461(3) Å) and C=C (1.400(3) Å) bond lengths for the C1–C2 and C4–C5 bond, respectively. The N1–C2 and N2–C4 bond distances of 1.391(3) and 1.397(3) Å, respectively, are nearly identical and intermediate between distances observed for single and double nitrogen–carbon bonds. Currently it is

unknown how **III-29** is formed. Monitoring the reaction by ^{1}H NMR spectroscopy at −70 °C did not result in the observation of any intermediates. One potential pathway involves the urea acting as a proton transfer agent. Alternatively, a σ-adduct (κ^1-O) between **III-1** and O=SIMe could increase the nucleophilicity of the Al(I) centre, facilitating intermolecular deprotonation of the *β*-diketiminate framework to give the final product.

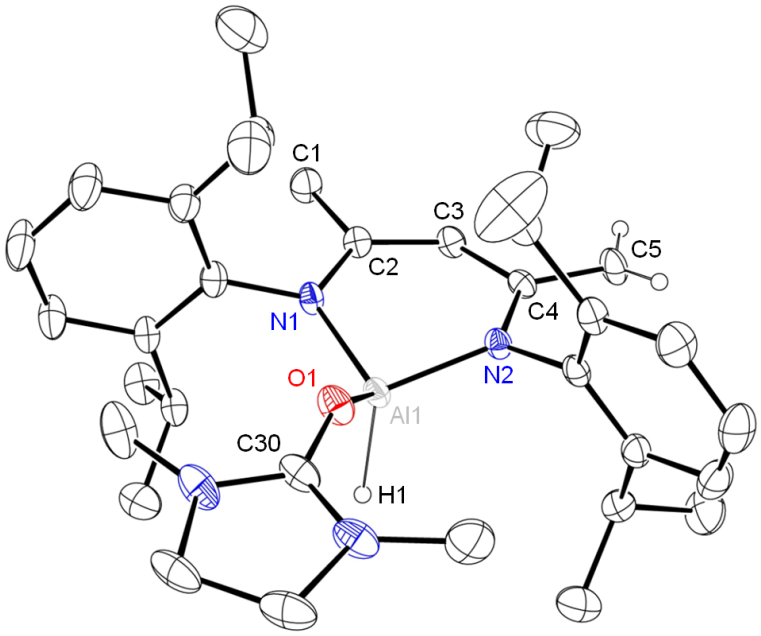

Figure 25. Molecular structure of NacNac'AlH(O=SIMe) (**III-29**). Thermal ellipsoids are shown at 30% for one of two independent molecules and the hydrogen atoms, except the aluminum hydride and methylene protons on C5, are removed for clarity.

Table 15. Selected bond lengths and angles for complex **III-29**.

	Lengths, Å				**Angles, °**
A1–N1	1.843(2)	C2–C3	1.389(3)	N1–A1–N2	101.23(9)
Al1–N2	1.836(2)	C3–C4	1.428(3)	N1–Al1–O1	110.16(9)
Al1–O1	1.812(2)	C4–C5	1.400(3)	N2–Al1–O1	109.02(8)
O1–C30	1.278(3)	N1–C2	1.391(3)	Al1–O1–C30	140.60(2)
C1–C2	1.461(3)	N2–C4	1.397(3)		

Attempts to sequester the coordinated urea with $B(C_6F_5)_3$ resulted in the formation of the zwitterion NacNac$^{B(C_6F_5)_3}$AlH(O=SIMe) (**III-30**), the result of borane

addition to the exocyclic alkene (Scheme 128). The same reactivity has also been demonstrated with related gallium,[28] silicon,[247] and germanium complexes.[86] In the ^{1}H NMR spectrum, a significant downfield shift of the γ-proton to 6.14 ppm was observed relative to the chemical shift of 5.53 ppm for the same proton environment in **III-29**. The methylene protons in the ligand framework are diastereotopic and found as broad doublets at 2.98 (overlapped with a methine heptet) and 2.55 ppm ($^{2}J_{H–H}$ = 19.7 Hz) as a result of germinal coupling, while the methyl protons gave rise to a singlet at 1.51 ppm. As expected, the isopropyl groups in the N-aromatic rings are inequivalent and four heptets are observed at 3.26 ($^{3}J_{H–H}$ = 6.9 Hz), 3.15 ($^{3}J_{H–H}$ = 6.9 Hz), 2.98, and 2.68 ppm ($^{3}J_{H–H}$ = 6.8 Hz). The methine protons are coupled to eight well-separated doublets at 1.71, 1.57, 1.29, 1.14, 1.02, 0.97, 0.82, and 0.73 ppm ($^{3}J_{H–H}$ = 6.7, 6.7, 6.7, 6.8, 6.8, 6.8, 6.7, and 6.9 Hz, respectively). The cyclic urea remains coordinated to the aluminum centre, with the signals for the methylene and methyl protons observed as singlets at 2.09 and 1.80 ppm, respectively. The ^{11}B NMR spectrum shows a singlet resonance at −14.3 ppm and the ^{19}F NMR spectrum display three resonances (−130.8, −162.2, and −166.4 ppm) for the *ortho*, *para*, and *meta* fluorine atoms, respectively, for the $B(C_6F_5)_3$ fragment.

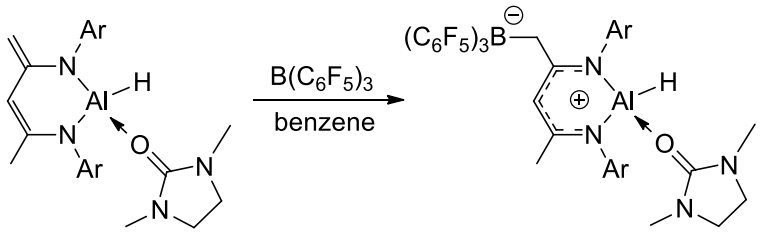

III-29 **III-30**

Scheme 128. Preparation of zwitterion **III-30** from the reaction of **III-29** with $B(C_6F_5)_3$.

While C=O bond (179 kcal mol^{-1}) activation by **III-1** was unsuccessful, addition of the weaker P=O bond (110 kcal mol⁻1) across the Al(I) centre should be more feasible and the reaction between triphenylphosphine oxide and **III-1** was investigated. Unexpectedly, addition of one equivalent of the phosphine oxide to **III-1** gave a mixture of NacNacAl'OH(O=PPh_3) (**III-31**) and unreacted **III-1**. Cleavage of the P=O bond was evinced by the production of triphenylphosphine in solution, confirmed by ^{1}H and ^{31}P NMR spectroscopy, which was believed to give an intermediate terminal aluminum oxide that then proceeds to rapidly deprotonate one of the methyl groups in the NacNac framework to furnish the final aluminum hydroxide compound. The reaction therefore requires two equivalents of triphenylphosphine oxide to fully react with **III-1** and give **III-31** (Scheme 129).

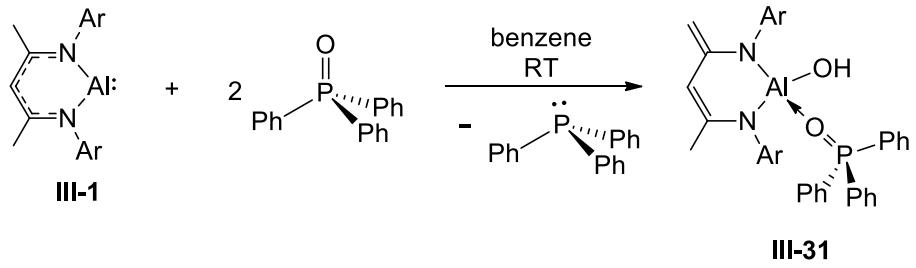

Scheme 129. Reaction of **III-1** with two equivalents of triphenylphosphine oxide to prepare NacNac'AlOH(O=PPh_3) (**III-31**).

In the ^{1}H NMR spectrum, the diastereotopic methylene protons in the NacNac' ligand give rise to singlets at 4.01 and 3.16 ppm while the methyl protons are found as a singlet at 1.78 ppm. The methine protons in the four inequivalent isopropyl groups are found as a multiplet, from three overlapping heptets at 4.09 ppm and a heptet at 3.94 ($^{3}J_{H-H}$ = 6.8 Hz) ppm that are coupled to the isopropyl methyl protons, appearing as a series of doublets spanning the region from 1.70 to 0.90 ppm. Finally, the hydroxyl proton is assigned to the singlet found at 0.58 ppm. In the ^{31}P NMR spectrum, the coordinated

triphenylphosphine oxide is observed at 44.8 ppm, shifted downfield with respect to free triphenylphosphine oxide (24.8 ppm). Complex **III-31** was isolated as a yellow oil and resisted all attempts at recrystallization.

With the intention of producing a more crystalline analogue of **III-31**, two equivalents of triethylphosphine oxide were reacted with **III-1** to prepare NacNac'AlOH(O=PEt$_3$) (**III-32**), as seen in Scheme 130. The ^{1}H NMR spectrum of **III-32** is similar to **III-31** with two singlets at 4.00 and 3.17 ppm for the diastereotopic methylene protons and a singlet at 1.77 ppm for the methyl protons in the NacNac' framework. Three of the four isopropyl methine protons have overlapped to give a multiplet at 3.98 ppm while the final methine proton is observed as a hepet at 3.85 ppm ($^3J_{H–H}$ = 6.9 Hz). Coupled to the methine protons are the isopropyl methyl protons found as overlapping doublets between 1.70 and 1.30 ppm. The ethyl groups of the coordinated triethylphosphine oxide give rise to a doublet of quartets at 1.02 ppm ($^3J_{H–H}$ = 7.8 Hz, $^2J_{P–H}$ = 13.3 Hz) coupled to a doublet of triplets at −0.06 ppm ($^3J_{H–H}$ = 7.8 Hz, $^3J_{P–H}$ = 18.3 Hz) while the hydroxyl proton is assigned to the singlet at 0.43 ppm. A singlet is present at 77.0 ppm in the ^{31}P NMR spectrum due to the coordinated triethylphosphine oxide moiety, shifted downfield relative to the free phosphine oxide at 45.4 ppm.

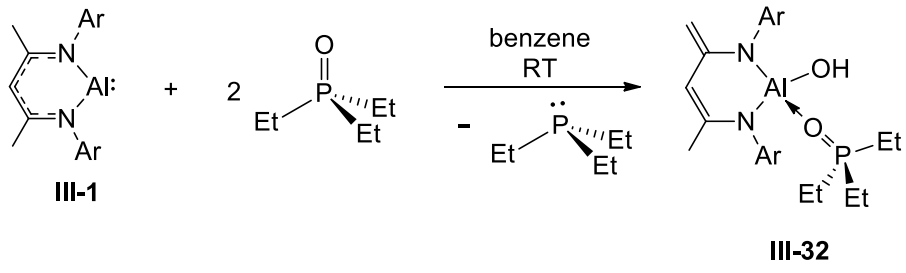

Scheme 130. Reaction of **III-1** with two equivalents of triethylphosphine oxide to prepare NacNac'AlOH(O=PEt$_3$) (**III-32**).

As hoped, **III-32** is isolated as a solid and crystals suitable for X-ray diffraction analysis were obtained by slow evaporation of a THF solution. The crystal structure of **III-32** revealed a four-coordinate aluminum centre in a distorted tetrahedral geometry with a mirror plane running through Al1 and C3 (Figure 26). The aluminum atom sits 0.396 Å below the plane defined by the N_2C_3 framework of the NacNac' ligand, while the Al1–N1 distance was found to be 1.833(1) Å, comparable to the respective distance in **III-29**. Due to the crystallographically imposed mirror plane, the C1–C2 distance of 1.433(2) Å and C2–C3 distance of 1.411(2) Å are intermediate between the distances for single and double carbon–carbon bonds (*cf*. 1.461(3) Å for a C–C bond and 1.389(3) Å for a C=C bond in the backbone of the NacNac' ligand in **III-29**). As well, the C1 atom is disordered and modelled as a CH_3 or CH_2 group with equal probability between the two.

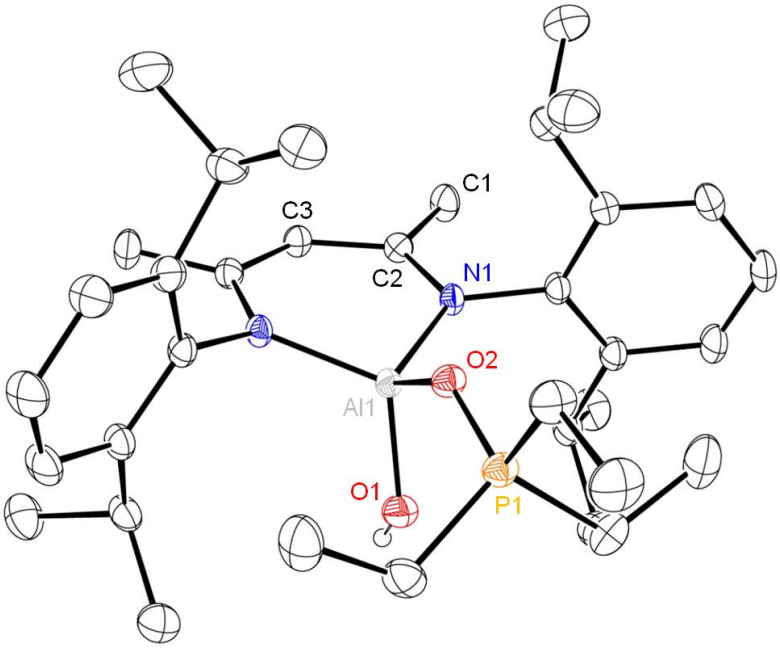

Figure 26. Molecular structure of NacNac'AlOH(O=PEt_3) (**III-32**). Thermal ellipsoids are shown at 30% and the hydrogen atoms, except the hydroxyl proton, are removed for clarity. A mirror plane runs through Al1 and C3, thus the left side of the molecule is a reflection of the right side.

Table 16. Selected bond lengths and angles for complex **III-32**.

Lengths, Å				Angles, °	
A1–N1	1.833(1)	C1–C2	1.433(2)	N1–A1–N1a	102.47(8)
Al1–O1	1.731(2)	C2–C3	1.411(2)	N1–Al1–O1	116.77(6)
Al1–O2	1.804(2)	N1–C2	1.396(2)	N1–Al1–O2	111.40(5)
O2–P1	1.533(2)			Al1–O2–P1	133.84(1)

The Al1–O1 distance of 1.731(2) Å is comparable to the average terminal Al–OH bond in related NacNac complexes (1.724 Å)[e] while the Al1–O2 distance of 1.804(2) Å is similar to the respective bond length of 1.781(1) Å found in the cationic complex $[NacNacAlMe(O{=}PEt_3)][B(C_6F_5)_4]$.[248]

[e] Based on a search in the Cambridge Crystallographic Data Centre.

IV. Low-Valent Germanium and Zinc Complexes Stabilized by a Redox Active Bis(imino)pyridine Ligand

IV.1 Introduction

Redox-active ligands have attracted increasing attention recently, particularly in catalytic applications, due to their ability to imbue novel reactivity to first-row transition metals by moderating the loss or gain of protons and electrons.[249-251] Of particular note is the family of bis(imino)pyridine ligands which show excellent ability to stabilize formally low-valent metal centres as a result of their good σ-donor and strong π-acceptor properties,[252] along with their exceptional capacity to accommodate excess negative charge.[253] In an exemplary example of these features, Chirik and co-workers have reported a series of bis(imino)pyridine complexes of iron in the formally zero-valent oxidation state,[254,255] as well as reduced bis(imino)pyridine complexes of cobalt.[256,257] These complexes have been demonstrated to be active catalysts for alkene hydrogenation,[258-261] alkene hydrosilylation,[262-264] as well as alkene and alkyne hydroboration.[265-267] The unique properties of these ligands make them promising for the stabilization of main-group element centres in unusually low oxidation states. Recently, Ragogna *et al*. have reported cationic phosphorus(I) complexes stabilized by bis(imino)pyridine ligands,[268,269] while Fischer and Flock have prepared a zero-valent tin complex utilizing the same ligand framework.[270] The bis(imino)pyridine platform has also been used for the preparation of unique square planar aluminum complexes as reported by Berben and co-workers,[271,272] followed recently by the report of their use in the electrocatalytic generation of H_2.[273]

The objective of this project is to utilize the bis(imino)pyridine ligand to stabilize and isolate unusually low oxidation state complexes of germanium and zinc. As mentioned earlier in Chapter II, recent reports have established the synthesis and isolation of zero valent complexes of silicon and germanium. In every instance so far, carbenoid-based ligands were utilized due to their strong σ-donating and π-accepting properties. The extension of this chemistry to different ligand environments, particularly those based on hard donors, could lead to new structural and reactivity patterns. The first half of this chapter will delineate the synthesis, characterization, and reactivity of a Ge(0) complex stabilized by the bis(imino)pyridine ligand. On the other hand, there is great interest in utilizing zinc complexes for bond activation and catalysis due to the bio-compatibility of zinc[274] and its abundance in the Earth's crust. Zinc compounds almost exclusively have the metal in the +2 oxidation state and access to lower oxidation states is unfavourable. However, since the turn of the century, many dimeric Zn(I) complexes have been reported in the literature with a sigma bond between the two zinc centres.[275] Even rarer is the zero valent oxidation state of zinc, with only a few reports in the literature.[276-278] The second half of this chapter will detail the synthesis and characterization of rare, monomeric formally Zn(I) and Zn(0) bis(imino)pyridine complexes.

IV.2 Preparation of Bis(imino)pyridine Complexes of Germanium

Reaction of two equivalents of $GeCl_2$·dioxane with the bulky bis(imino)pyridine ligand 2,6-$(ArN{=}CMe)_2C_5H_3N$ ($^{Me}I_2P$, Ar = 2,6-$^{i}Pr_2C_6H_3$) resulted in formation of the Ge(II) cation $[^{Me}I_2PGeCl][GeCl_4]$ (**IV-1**). The same cation can also be generated by reacting $^{Me}I_2P$ with one equivalent of $GeCl_2$·dioxane in the presence of one equivalent of BCl_3 or $BF_3{\cdot}Et_2O$ to give the ionic compounds $[^{Me}I_2PGeCl][BCl_4]$ (**IV-2**) and

[$^{Me}I_2PGeCl$][BF_3Cl] (**IV-3**), respectively (Scheme 131). In the ^1H NMR spectrum, all three complexes display a similar pattern of signals, including a triplet (~ 9.1 ppm) and doublet (~ 8.8 ppm) corresponding to the *para* and *meta* protons on the pyridine ring, respectively. As well, the isopropyl groups of the ligand are equivalent and give rise to two doublets (~ 1.2 and 1.1 ppm) for the isopropyl methyl protons that are both coupled to a heptet (~ 2.8 ppm) for the isopropyl methine protons. The imino-methyl moiety is observed as a singlet at ~ 2.7 ppm. In the ^{11}B NMR spectrum, a singlet at 6.8 and −1.1 ppm is observed for **IV-2** and **IV-3**, respectively, while a singlet at −152.3 ppm is seen in the ^{19}F NMR spectrum for **IV-3**. In the IR spectrum, the imine linkage gives rise to a band at approximately 1660 cm^{-1}, blue shifted in comparison to the free ligand (1642 cm^{-1}).[279] Concurrently, the synthesis and characterization of **IV-1** was also reported independently by Roesky and co-workers.[280]

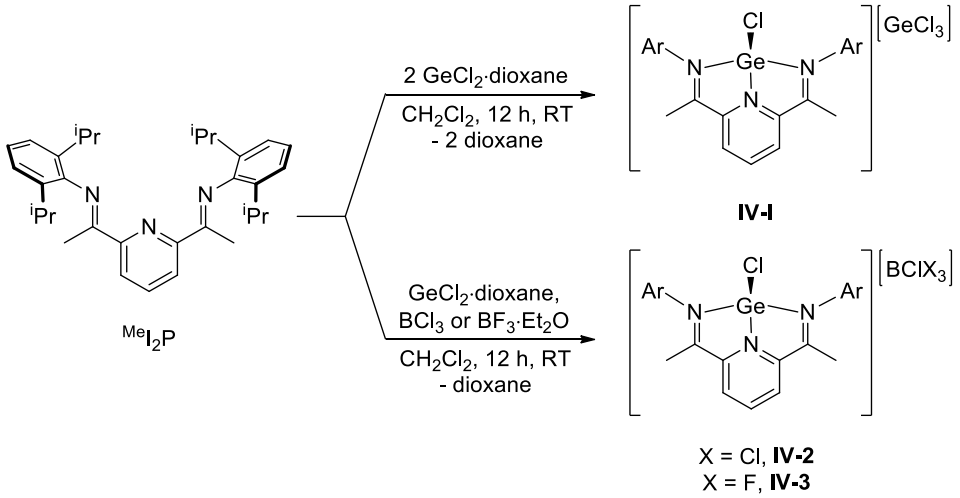

Scheme 131. Preparation of [$^{Me}I_2PGeCl$][X] (**IV-1** – **IV-3**).

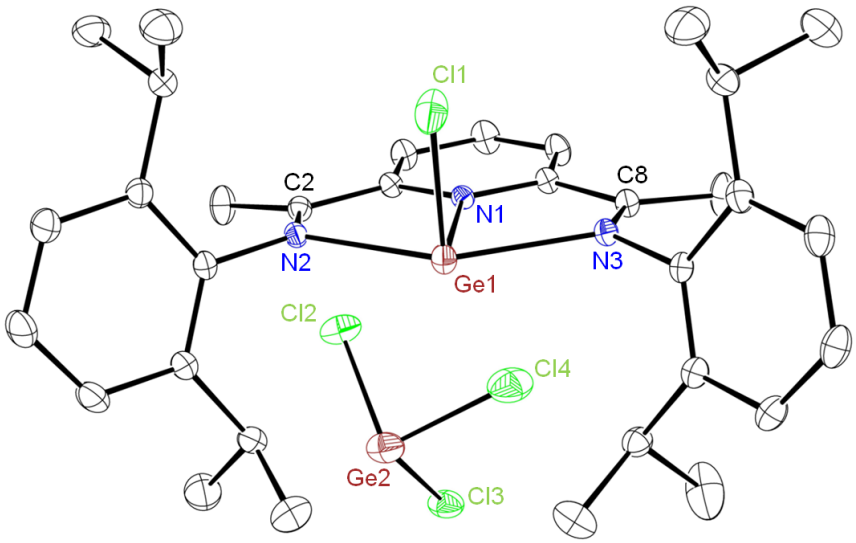

Figure 27. Molecular structure of [$^{Me}I_2$PGeCl][$GeCl_3$] (**IV-1**). Thermal ellipsoids are shown at 30% and the hydrogen atoms are removed for clarity.

Table 17. Selected bond lengths and angles for complex **IV-1**.

Lengths, Å		**Angles, °**	
Ge1–N1	2.074(2)	Cl1–Ge1–N1	94.69(6)
Ge1–N2	2.276(2)	Cl1–Ge1–N2	89.71(5)
Ge1–N3	2.262(2)	Cl1–Ge1–N3	88.92(5)
Ge1–Cl1	2.2258(9)	N1–Ge1–N2	73.36(7)
Ge2–Cl2	2.330(1)	N1–Ge1–N3	73.41(7)
Ge2–Cl3	2.2801(9)	N2–Ge1–N3	146.50(7)
Ge2–Cl4	2.332(1)	Cl2–Ge2–Cl3	95.81(4)
N2–C2	1.278(3)	Cl2–Ge2–Cl4	95.75(4)
N3–C8	1.274(8)	Cl3–Ge2–Cl4	96.62(4)

Additionally, the crystal structure of **IV-1** has been determined by X-ray crystallography, shown in Figure 27. In the cationic portion of the structure, the germanium atom is connected to the three nitrogen atoms of the bis(imino)pyridine ligand and one chlorine atom and adopts a distorted square pyramidal geometry if the lone pair on germanium is considered as the forth vertex of the square plane. The chlorine atom, with a Ge1–Cl1 bond distance of 2.2258(9) Å, sits nearly perpendicular to the

square plane constituting the three nitrogen atoms with an average N–Ge–Cl1 bond angle of 91.11°. The bond distances in the bis(imino)pyridine framework of **IV-1** are nearly identical to the distances found in the free $^{Me}I_2P$ ligand.[279] In the counterion, the Ge(II) centre is bonded to three chlorine atoms, resulting in the distorted trigonal pyramidal shape of the anion. The three Ge2–Cl bond lengths are nearly equidistant with an average value of 2.314 Å. Similarly, the Cl–Ge2–Cl bond angles are nearly equivalent, yielding an average bond angle of 96.06°.

The reduction of **IV-1** with two equivalents of KC_8 affords the air and moisture sensitive dark green compound $^{Me}I_2PGe$ (**IV-4**) which can be classified as a complex of Ge(0) ligated by the $^{Me}I_2P$ ligand (Scheme 132). Utilization of **IV-1** was crucial as the reduction of **IV-2** and **IV-3** with KC_8 led to an intractable mixture of products.

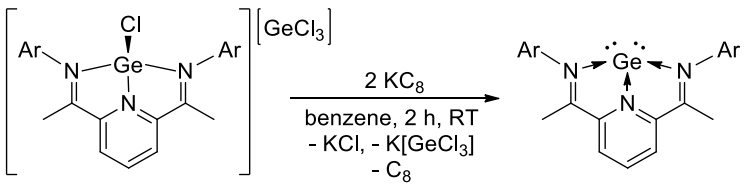

IV-1 **IV-4**

Scheme 132. Reduction of **IV-1** with 2 equivalents of KC_8 to give $^{Me}I_2PGe$ (**IV-4**).

Solution NMR spectra of **IV-4** in deuterated benzene are consistent with an NMR-averaged C_{2v} geometry. In particular, the equivalent isopropyl groups of the ligand give rise to two doublets, each integrating to six protons at 1.08 ($^3J_{H–H}$ = 6.8 Hz) and 1.16 ($^3J_{H–H}$ = 7.0 Hz) ppm, that are both coupled to a heptet at 2.66 ppm ($^3J_{H–H}$ = 6.9 Hz) integrated as four protons. The iminoacyl signal was observed as a singlet at 2.04 ppm integrated as six protons. The NMR-averaged C_{2v} symmetry of **IV-4** persists over a temperature range of −70 °C to 25 °C in a toluene-d_8 solution. A peculiar feature of the ^{1}H NMR spectrum of **IV-4** is the upfield shift of the *para*-CH resonance of the pyridine

ligand upon formation of the complex (6.35 ppm, t, $^{3}J_{H–H}$ = 7.6 Hz) in **IV-4** versus 7.29 ppm in the free ligand). A similar upfield shift is observed for the related zero-valent tin complex, which shows increased shielding of the respective signal at 6.23 ppm[270] and the isoelectronic bis(imino)pyridine complex of phosphorus(I), $[^{Fc}I_2PP]^+$, where $^{Fc}I_2P$ is 2,6-$(FcN{=}CH)_2C_5H_3N$ (Fc = ferrocenyl). In the phosphorus complex, the *para*-CH signal is observed at 7.12 ppm versus 7.84 ppm in the free ligand.[269] An initial interpretation of this unusual shift was that it was due to the partial population of a low-lying triplet state with increased hyperfine coupling to the *para*-CH proton. In accord with this hypothesis, EPR spectra of the crude reaction mixture and the recrystallized complex displayed a weak signal, the simulation of which was consistent with significant spin localization in the *para* position of the pyridine ring.[f] However, multiple recrystallizations of **IV-4** resulted in a marked decrease in the intensity of the EPR signal. As well, DFT calculations (*vide infra*) showed that the lowest triplet state of **IV-4** lies 17.7 kcal mol^{-1} above the singlet ground state. Moreover, variable temperature ^{1}H NMR spectra did not reveal any significant temperature dependence, inconsistent with the presence of a temperature accessible excitation to the triplet state, which allows one to rule out its impact on the ^{1}H NMR data. Finally, mixing a sample of purified **IV-4** with the starting complex **IV-1** results in the appearance of the same EPR signal but with a roughly 20-fold increase in intensity (Figure 28). Therefore, the EPR-active species is tentatively assigned as a radical formed by the reduction of **IV-1** by **IV-4**. Heavier group 14 radicals are well-established, with the first group-14 metal radical reported almost 40 years ago by Lappert and co-workers[281] and recently reviewed.[282] More recent is the isolation of a stable and neutral Ge(I) radical reported by the Jones group.[283] In the IR spectrum of **IV-**

[f] EPR spectra acquisition and simulation were performed by Prof. Art van der Est.

4, the N=C_{imine} stretch at 1575 cm^{-1} is red shifted with respect to the free ligand (1642 cm^{-1}) and the cation **IV-1** (1655 cm^{-1}), suggestive of a decreased N=C bond order.

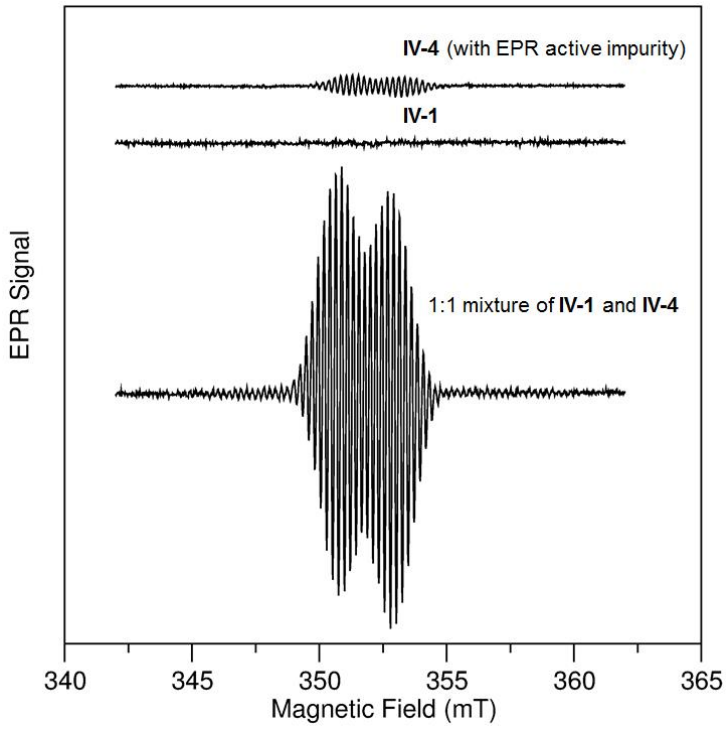

Figure 28. EPR spectra of **IV-1**, **IV-4**, and 1:1 mixture of **IV-1** and **IV-4** resulting in a significant increase in the intensity of the EPR signal.

The molecular structure of **IV-4**, determined by X-ray diffraction analysis, is shown in Figure 29. The molecule is bisected by a crystallographically imposed mirror plane such that the left side of the molecule is a reflection of the right side. The coordination sphere of germanium in **IV-4** is comprised of three nitrogen atoms, one from the central pyridine ring and two from the imino groups, N2 and N2a. Refinement of the germanium atom in the special position results in significant elongation of its thermal ellipsoid parallel with the N2–N2a vector, suggesting disorder within the structure. The disorder was successfully modeled by shifting the germanium atom in the plane of the pyridine fragment towards one of the imino nitrogen atoms. As a result, the Ge1–N2 bond distance of 2.047(8) Å is noticeably shorter than the Ge1–N2a distance of

2.306(8) Å. However, the latter value is still comparable to the Ge–N_{imine} bond lengths observed in **IV-1** (2.276(2) and 2.262(2) Å). A shorter distance in the Ge1–N1 bond is noted compared to the corresponding bond in **IV-1** (1.8988(18) Å versus 2.074(2) Å). The N2–Ge1–N2a bond angle is more obtuse in **IV-4** (152.76(8)°) compared to **IV-1** (146.50(7)°), reflecting the closer binding of the germanium atom to the pyridine ring in the former. An elongation of the N2–C4 bond of the imino fragment in **IV-4** to 1.320(2) Å was observed, indicative of a decrease in bond order upon reduction, compared to the cation **IV-1** (1.278(3) and 1.274(8) Å). A similar effect was also seen in the related tin(0) bis(imino)pyridine complex with the N–C bond length increasing from 1.308(3) Å to 1.321(3) Å.[270]

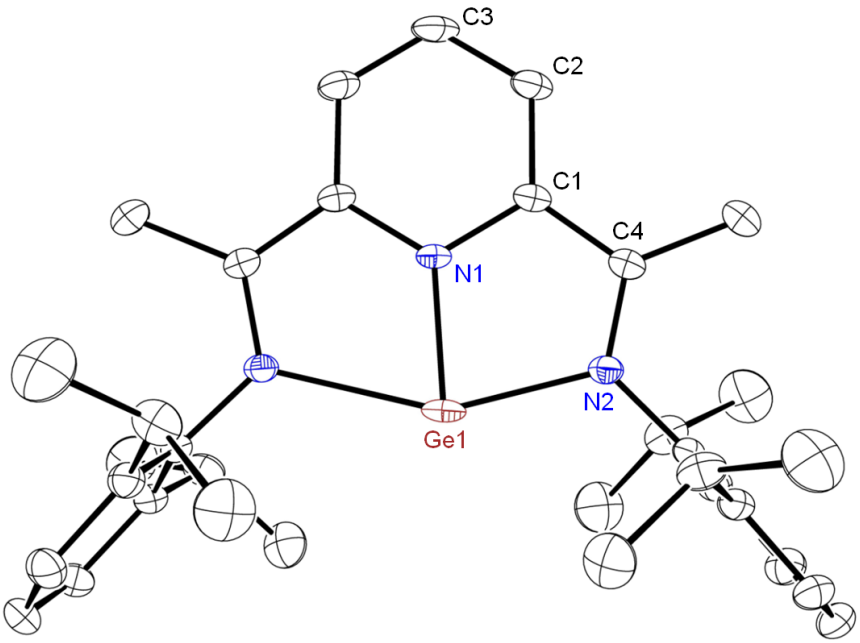

Figure 29. Molecular structure of $^{Me}I_2PGe$ (**IV-4**). Thermal ellipsoids are shown at 30% and the hydrogen atoms are removed for clarity. A mirror plane runs through C3 and N1, thus the left side of the molecule is a reflection of the right side. The Ge1 atom is disordered but only one position is shown for clarity.

Table 18. Selected bond lengths and angles for complex **IV-4**.

Lengths, Å				Angles, °	
Ge1–N1	1.8988(18)	C1–C2	1.389(2)	N1–Ge1–N2	79.61(17)
Ge1–N2	2.047(8)	C1–C4	1.418(2)	N1–Ge1–N2a	73.19(18)
Ge1–N2a	2.306(8)	C2–C3	1.378(2)	N2–Ge1–N2a	152.76(8)
N1–C1	1.4051(19)	N2–C4	1.320(2)		

Within the pyridine ring, a similar phenomenon was seen in the nitrogen–carbon bond. The N1–C1 distance of 1.4051(19) Å is elongated compared to the corresponding distances of 1.343(3) and 1.345(3) Å in **IV-1**, however the C–C distances of 1.389(2) and 1.378(2) Å in **IV-4** remain similar to the corresponding distances in **IV-1** (1.377(4)–1.393(3) Å). The metrical data is suggestive of partial charge transfer to the imino groups and pyridine ring upon reduction of **IV-1** to give **IV-4**.

Qualitatively, the spectral and X-ray crystallographic data for **IV-4** suggests that its singlet ground state can be represented as a resonance of the canonical forms **A** and **B** (Scheme 133). Form **B** is a singlet biradical with unpaired electron density localized on the imino carbon atoms as a result of charge transfer from the Ge(0) centre to the antibonding π* N=C orbital, which is primarily localized on the carbon atoms. The contribution of **B** accounts for the elongation of the $N=C_{imine}$ bond in **IV-4** and the red shift of the N=C stretch in the IR spectrum of **IV-4** in comparison with that of the free ligand.

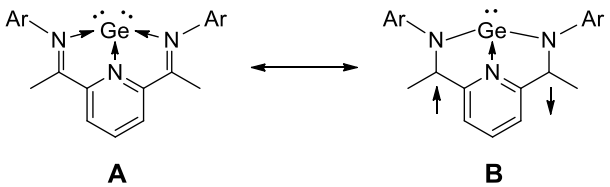

Scheme 133. Two canonical representations, **A** and **B**, for **IV-4**.

To gain additional insight into the electronic structure of **IV-4**, DFT calculations at the [wB97XD/6-311G(d,p)] level were performed.[g] The optimized singlet ground-state structure of **IV-4** is shown in Figure 30. The calculated N1–Ge distance of 1.92 Å is close to the value determined by X-ray crystallography (1.8988(18) Å). Gratifyingly, the DFT calculations confirm the C_s symmetry of **IV-4** by showing two different Ge–N_{imine} bond lengths of 1.93 Å and 2.55 Å, respectively, which are in good agreement with the values of 2.047(8) Å and 2.306(8) Å determined by X-ray crystallography. This difference represents an approximate 14% displacement of the germanium atom from the central position. The asymmetry is symptomatic of a short-lived stationary point on a shallow double-well potential energy surface (derived from a fluxional exchange of the germanium atom between the two imino nitrogen atoms), and indeed the variable temperature NMR data discussed above suggests that exchange between the two degenerate sites occurs readily in solution even at very low temperature. Associated with the asymmetric nature of **IV-4** is a slight yet measurable (1.28 Å vs. 1.36 Å) difference between the two N=C imine bond lengths, both of which are elongated when compared with those computed for the free ligand (1.27 Å). Consistent with the experimental observations, both N=C_{imine} stretches in **IV-4** (1726 cm^{-1} and 1401 cm^{-1}) were calculated to be of lower frequency than those of the free ligand (1772 cm^{-1} and 1777 cm^{-1}). Also consistent is an upfield shift of the *para*-CH resonance of the pyridine ligand in the computed ^{1}H NMR spectrum of **IV-4** (6.75 ppm) relative to the free ligand (7.96 ppm).

For comparison, the computed triplet state of **IV-4** (Figure 30) is symmetric and 17.7 kcal mol^{-1} higher in energy than the singlet state. Analysis of the spin density revealed that the largest component of the spin resides on the germanium atom with

[g] DFT calculations were performed by Lee Belding and Prof. Travis Dudding.

significant spin density on the pyridine backbone. Structurally, the two imine bonds are equivalent in length (1.34 Å) and both Ge–N_{imine} bond lengths are equal at 2.07 Å. Additional features of the triplet state include distortion of the germanium atom from the plane of the ligand, an elongated Ge–N1 distance (1.96 Å), and slight twisting of the N-aryl ring systems with respect to the pyridine backbone, as opposed to the perpendicular relationship observed in the singlet state.

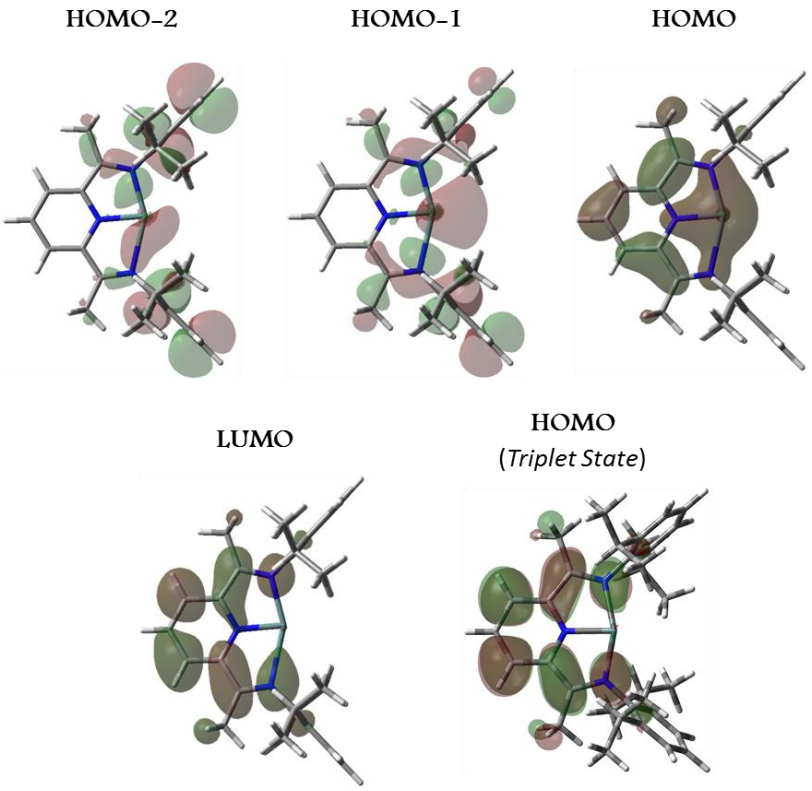

Figure 30. Calculated structure and orbital compositions of key frontier orbitals of the singlet state of **IV-4** and the HOMO of the triplet state.

Molecular orbital analysis provided further insight into the structure of **IV-4**. The HOMO of the singlet form corresponds to a diffuse π-type orbital centreed around the Ge(0) atom. This orbital spans across the two bridging imino nitrogen atoms and includes what appears to be a back-bonding interaction between a Ge(0) 4p orbital and a 2p orbital from the pyridine nitrogen. Another striking feature of the HOMO is the presence of an

antibonding interaction across the $N{=}C_{imine}$ bond which accounts for the elongation of the bond observed in the X-ray crystallographic structure and the red shift of the imine band in the IR spectrum. In all, the HOMO of **IV-4** is the result of delocalization of a germanium-centreed lone pair over the π-system of the ligand, comprised of the imino and pyridyl nitrogen atoms. Therefore, it can be surmised that there is partial multiple-bond character in the $Ge–N_{imine}$ bonds, consistent with the shorter bond lengths observed in **IV-4** compared to **IV-1**. On the other hand, the HOMO−1 corresponds to a Ge(0)-centreed σ-type lone pair, while the HOMO−2 is a bonding component of the 3c-4e interaction between an in-plane germanium 4p orbital and the two lone pairs on the imino nitrogen atoms. The LUMO of **IV-4** lies 0.21 eV above the HOMO and is entirely ligand-based as there is no apparent orbital density at the germanium centre. In the triplet state, the HOMO closely resembles the LUMO of the singlet state in accord with the Frank-Condon principle. The large energy difference between the singlet and triplet state renders the triplet state thermally inaccessible and is reflected in the experimental data.

Interestingly, NBO analysis revealed the non-intuitive presence of four germanium-centreed lone pairs. One lone pair sits in a σ orbital with an occupancy of 1.77e which can be seen in the HOMO−1 and corresponds to a classic Lewis representation of a lone pair. The second lone pair, corresponding to the HOMO−2, has a low occupancy (0.27e) as a result of delocalization into the π-system of the ligand. The third and fourth lone pairs, also with small occupancies of 0.55e and 0.50e, respectively, are perhaps an artifact of the 3c-4e bond (i.e., a non-classical Lewis representation). This notion is supported by strong donation of the lone pairs on the imino nitrogen atoms into the orbitals assigned by NBO analysis as the third and fourth lone pair of Ge(0) ($N(2a)_{LP}$

→ $Ge_{LP(3)}$ = 0.11 kcal mol^{-1}, $N(2)_{LP}$ → $Ge_{LP(3)}$ = 42.3 kcal mol^{-1}, $N(2a)_{LP}$ → $Ge_{LP(4)}$ =15.2 kcal mol^{-1}, $N(2)_{LP}$ → $Ge_{LP(4)}$ = 31.7 kcal mol^{-1}). This ultimately results in the measured excess of electron density assigned as the third and fourth lone pairs on the Ge(0) centre.

IV.2 Reactivity of $^{Me}I_2PGe$ (IV-4)

With complex **IV-4** in hand, its reactivity towards the activation of robust sigma bonds was probed. In an attempt to observe Si–H bond activation across the low-valent germanium centre in **IV-4**, one equivalent of phenyl silane was added to a solution of **IV-4** in benzene. No reaction was observed even at elevated temperatures. Prolonged heating of the mixture at 100 °C resulted in deposition of a germanium mirror in the NMR tube, along with consumption of **IV-4** and liberation of free ligand. A similar result was obtained upon repeating the reaction with pinacolborane. Complex **IV-4** is even resistant towards reaction with methyl iodide, showing no evidence for C–I bond cleavage even upon heating. The dearth of reactivity seen in complex **IV-4** is likely due to the lack of orbital density at the germanium atom in the LUMO. Previously, bond activation by singlet carbenes, silylenes, and germylenes have been rationalized by the availability of a donor (lone pair in a non-bonding orbital) and acceptor (vacant orbital) frontier orbital in modestly separated energy levels, similar to the situation found in transition-metal complexes. Bond cleavage proceeds via interaction of the lone pair with an antibonding orbital on the substrate followed by attack of the hydride-like hydrogen on the positively polarized group 14 element centre.[51] Without the appropriate accepting orbital at the germanium centre in **IV-4**, the proposed pathway is inaccessible and no bond activation

is observed, while the thermal decomposition of **IV-4** to germanium metal and free ligand is reminiscent of the chemical vapour deposition technique to prepare thin metal films.

On the other hand, addition of one equivalent of water to **IV-4** results in the immediate disappearance of the characteristic dark blue-green color of the complex along with precipitation of a brown solid (Scheme 134).

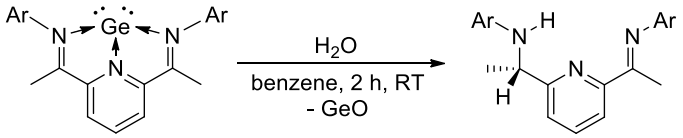

IV-4 **IV-5**

Scheme 134. Addition of H_2O to **IV-4** to give **IV-5**.

The product of the reaction was determined to be the partially hydrogenated ligand $^{Me}I_2PH_2$ (**IV-5**) in which one of the imine arms has been hydrogenated to an amine linkage, while the brown precipitate is presumably germanium oxide formed as a by-product of the reaction. The ^{1}H NMR spectrum revealed an asymmetrically substituted pyridine ring with two doublets observed for the *meta* protons at 8.35 and 6.60 ppm. The imino-methyl group on the imine arm gives rise to a singlet integrating to three protons at 2.30 ppm. The N–H proton on the amine linkage manifests as a singlet at 4.41 ppm, while the methine proton is found as a quartet at 4.31 ppm that is coupled to a doublet from the amino-methyl group at 1.53 ppm. The inequivalent isopropyl groups give rise to a heptet at 3.45 ppm that integrates to two protons and two partially overlapped heptets integrating to two protons localized at 2.92 ppm for the methine protons. The isopropyl methyl groups are observed as an overlapping collection of doublets at 1.18 ppm that integrates to twenty four protons in total. Conclusive evidence for the structure of **IV-5** was provided by the X-ray crystal structure as seen in Figure 31. The N2–C8 bond

distance of 1.274(3) Å is consistent with a double bond, while the longer bond length of 1.481(3) Å between N3–C2 is in accord with a single bond between the two atoms.

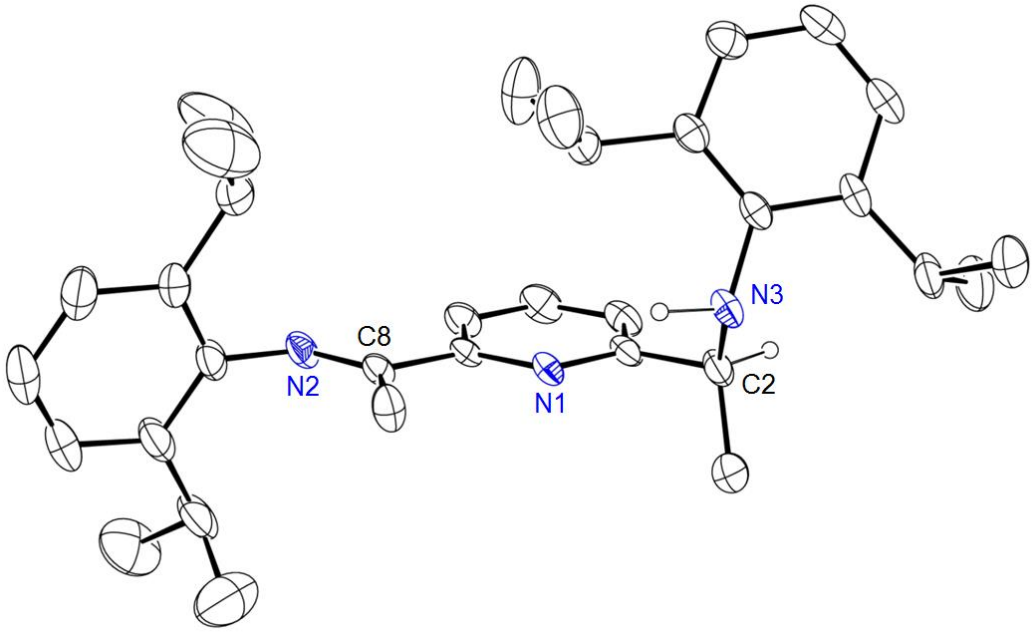

Figure 31. Molecular structure of MeI_2PH_2 (**IV-5**). Thermal ellipsoids are shown at 30% and the hydrogen atoms, except the ones on C2 and N3, are removed for clarity.

Interestingly, it was observed that the amino and methine proton in the hydrogenated arm undergo intramolecular exchange with each other via the 1D ^{1}H EXSY NMR experiment. In order to elucidate the mechanism of the exchange, a series of kinetic measurements in the temperature range of 279.4–310.1 K were performed. From the data recorded, an Eyring plot was constructed and the unusual activation parameters of $\Delta H^{\ddagger}$ = −2.94(3) kcal mol^{-1} and $\Delta S^{\ddagger}$ = −69.4(2) cal K^{-1}·mol^{-1} were extracted (Figure 32). Though a negative enthalpy of activation is surprising for solution reactions, there are several precedents in the literature.[284-287] In previous examples, the negative enthalpy of activation is attributed to the presence of a low-concentration intermediate ($\Delta G° > 0$) that is enthalpically favoured ($\Delta H° < 0$). In this particular case, it is proposed that an intermediate π-stacked dimer is formed between two molecules of **IV-5**. Exchange of

protons then occurs intermolecularly within the dimer followed by dissociation to affect an overall intramolecular exchange between the amino and methine protons.

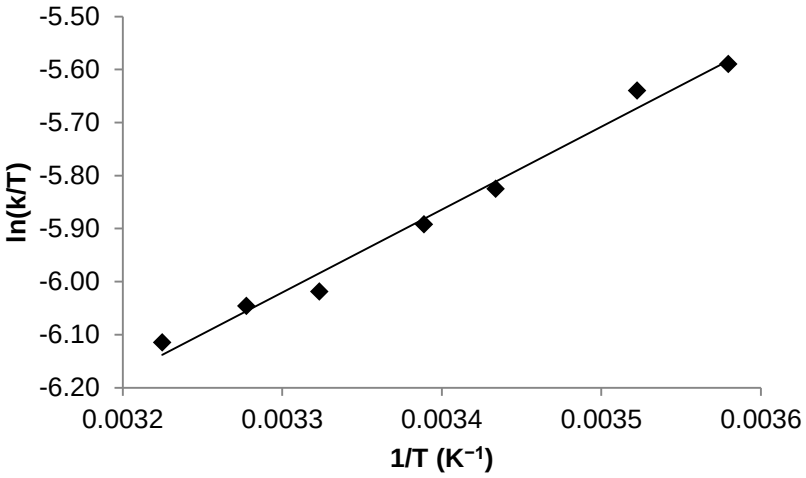

Figure 32. Eyring plot for the intramolecular proton exchange in **IV-5** (R^2 = 0.987).

IV.3 Preparation of Bis(imino)pyridine Complexes of Zinc

Due to the lack of reactivity demonstrated by **IV-4**, it was supposed that the isoelectronic zinc analogue would be more reactive and participate in a greater variety of reactions. Therefore, following the synthetic strategy used to prepare **IV-4**, initial attempts to reduce the known divalent zinc complex $^{Me}I_2PZnCl_2$[288] with two equivalents of KC_8 in benzene were attempted. Unfortunately, the only isolable products in these reactions was the free bis(imino)pyridine ligand.

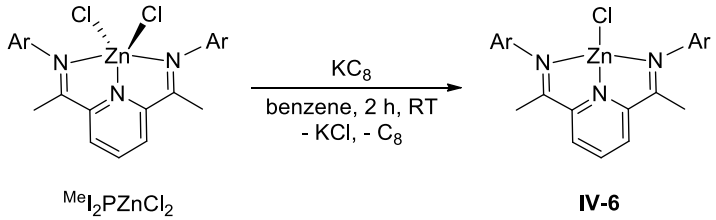

Scheme 135. Mono-reduction of $^{Me}I_2PZnCl_2$ to prepare $^{Me}I_2PZnCl$ (**IV-6**).

On the other hand, mono-reduction of $^{Me}I_2PZnCl_2$ with one equivalent of KC_8 in benzene yielded the neutral complex $^{Me}I_2PZnCl$ (**IV-6**) with zinc in the formal +1

oxidation state (Scheme 135). During the course of this thesis, Berben and co-workers disclosed a report on the closely related zinc complex $^{Ph}I_2PZnCl$, where $^{Ph}I_2P$ is 2,6-$(ArN{=}CPh)_2C_5H_3N$.[289] Compound **IV-6** is NMR silent but its EPR spectrum is consistent with the presence of a single unpaired electron delocalized over the bis(imino)pyridine ligand (Figure 33).[h] The hyperfine couplings obtained by simulating the EPR spectrum show significant interaction between the unpaired electron and the nuclei on the bis(imino)pyridine ligand. The largest couplings are found for the protons of the imine methyl groups and the *para* proton of the pyridine ring, indicative of high spin density at these positions (Table 19).

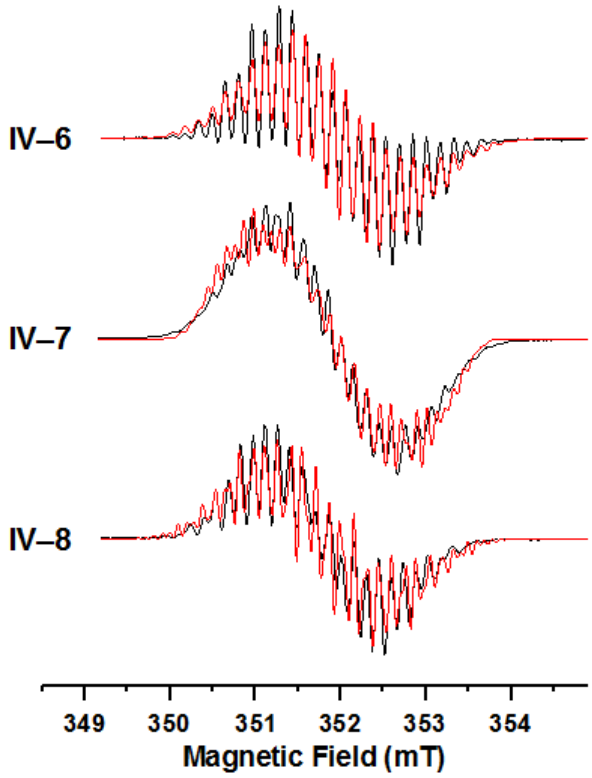

Figure 33. EPR spectra of compounds **IV-6**, **IV-7**, and **IV-8**. The experimental spectra are in black and simulations using the hyperfine couplings given in Table 19 are in red.

[h] EPR spectra acquisition and simulation were performed by Dr. Prashanth K. Poddutoori and Prof. Art van der Est.

Table 19. Isotropic hyperfine coupling constants in MHz of compounds **IV-6**, **IV-7**, and **IV-8**.

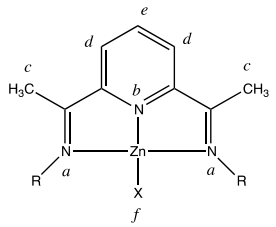

	Experiment			DFT Calculation	
Nucleus	**IV-8** (X = CH_3)	**IV-6** (X = Cl)	**IV-7** (X=Cl, DMAP)	**IV-6** (X = Cl)	**IV-7** (X=Cl, DMAP)
A	4.45	4.60	5.86	4.74	5.74
B	12.12	12.34	15.57	12.35	15.60
C	8.08	7.59	3.43	5.69	4.61
D	5.19	5.23	5.29	5.36	5.52
E	–17.49	–16.79	–16.94	–16.74	–17.32
F	2.64	0.64	1.00	0.66	0.61

The molecular structure of **IV-6** (Figure 34), determined by X-ray diffraction analysis, displays a nearly planar coordination environment around the zinc centre. Four-coordinate zinc centres typically adopt a tetrahedral geometry, with examples for a square planar geometry found only in zinc porphyrinoids where the geometry is imposed by the rigidity of the tetrapyrrole ring. Using the τ_4 parameter as described by Houser (Eqn 1) where α and β are the two largest bond angles in a four-coordinate complex, the deviation from ideal tetrahedron ($\tau_4 = 1$) or square planar ($\tau_4 = 0$) geometry can be quantified.[290]

$$\tau_4 = \frac{360° - (\alpha + \beta)}{141°} \qquad (1)$$

Complex **IV-6** has a τ_4 value of 0.26, supporting its description as a distorted square plane. Unlike complex **IV-4**, the zinc atom in **IV-6** is only slightly shifted from the central position such that the $Zn–N_{imine}$ distances are nearly equivalent at 2.153(2) and 2.220(2) Å. These distances are comparable to the respective distances in $^{Ph}I_2PZnCl$ (2.117(1) and 2.237(1) Å)[289] but are significantly shorter than those in the parent

dichloride $^{Me}I_2PZnCl_2$ (2.297(2) and 2.314(2) Å),[288] suggestive of multiple Zn–N bond character in **IV-6**. The N=C bonds in the imine moiety are marginally different at 1.295(2) and 1.307(2) Å and are slightly elongated compared to the respective distances in $^{Me}I_2PZnCl_2$ (1.272(4) and 1.278(4) Å),[288] as a result of the partial electron density transfer from the over-reduced zinc centre. A similar effect is also observed in $^{Ph}I_2PZnCl$ (1.306(2) and 1.323(2) Å), as reported by Berben *et al*.[289] The N–C bonds of the pyridine ring of **IV-6** are also slightly elongated to 1.361(3) and 1.371(2) Å versus 1.326(4) and 1.338(3) Å[288] in $^{Me}I_2PZnCl_2$. The chloride group lies trans to the N_{py} atom, displaying a nearly linear Cl1–Zn1–N1 angle of 172.05(5)°, suggestive of sp-hybridization at the zinc centre. The bonding between the zinc atom and the imine groups is mainly due to the donation of the nitrogen lone pairs into an empty 4p orbital of zinc lying in the ZnN_3Cl plane, resulting in a 3c-4e bond between the three atoms.

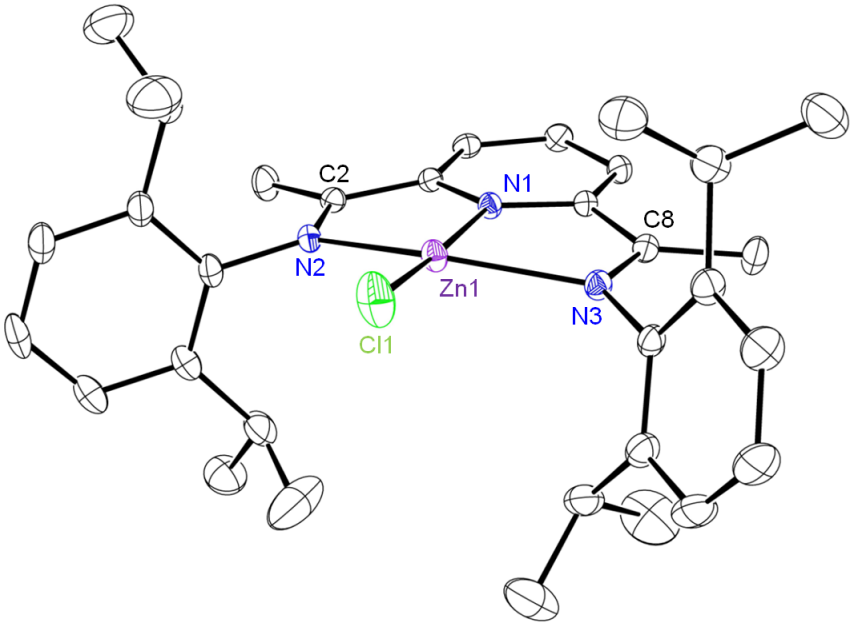

Figure 34. Molecular structure of $^{Me}I_2PZnCl$ (**IV-6**). Thermal ellipsoids are shown at 30% and the hydrogen atoms are removed for clarity.

Table 20. Selected bond lengths and angles for complex **IV-6**.

Lengths, Å		Angles, °	
Zn1–N1	1.940(2)	Cl1–Zn1–N1	172.05(5)
Zn1–N2	2.153(2)	Cl1–Zn1–N2	106.42(5)
Zn1–N3	2.220(2)	Cl1–Zn1–N3	100.63(5)
Zn1–Cl1	2.1565(8)	N1–Zn1–N2	77.94(7)
N2–C2	1.307(2)	N1–Zn1–N3	76.60(6)
N3–C8	1.295(2)	N2–Zn1–N3	150.79(6)

Further support of this bonding mode is provided by the π conjugation between the orthogonal 4p orbital of zinc and the N=C π bond, as revealed by DFT calculations (*vide infra*).

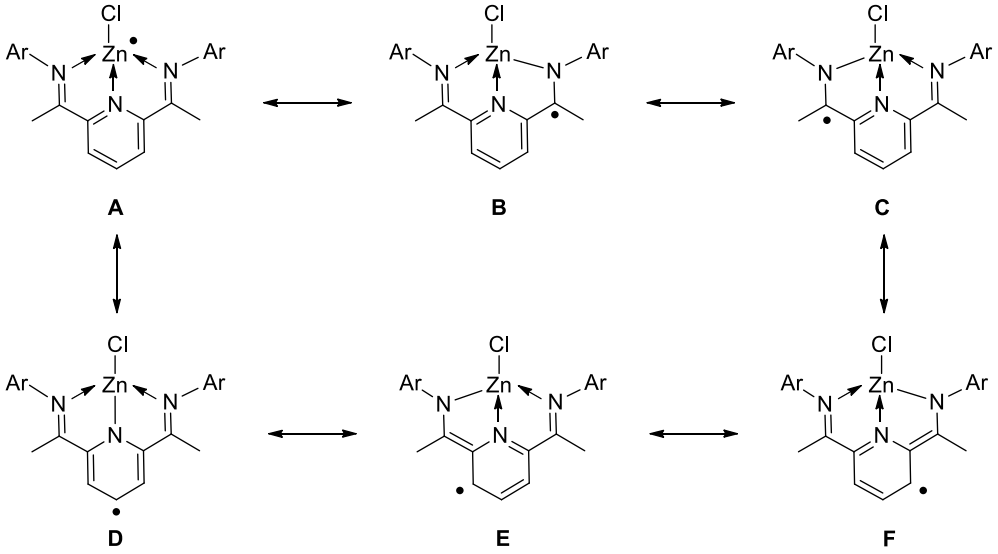

Scheme 136. Canonical representations of **IV-6**.

Due to the redox-active nature of the bis(imino)pyridine ligands, the oxidation state of zinc in **IV-6** is ambiguous. Complex **IV-6** can be considered as a monovalent zinc species ligated by a neutral ligand (**A** in Scheme 136). However, structural and EPR data of **IV-6** points to significant charge delocalization onto the ligand allowing for the description of **IV-6** as a divalent zinc molecule stabilized by a radical-anionic ligand

(structures **B**–**F** in Scheme 136). Based on the metrical parameters, forms **B**, **C**, **E**, and **F** have a lower contribution compared to the canonical form **D**.

As seen in Scheme 137, addition of one equivalent of DMAP to **IV-6** furnishes the complex $^{Me}I_2PZnCl(DMAP)$ (**IV-7**). Similar to **IV-6**, **IV-7** is NMR silent and the EPR spectrum is consistent with the presence of a single unpaired electron delocalized over the ligand framework (Figure 33). The pattern of couplings in the EPR signal does not change significantly with addition of the DMAP molecule and only an increase of the inhomogeneous linewidth is observed due to unresolved coupling to the nuclei of the DMAP ligand (Table 19). In the same article referenced earlier, Berben *et al.* also prepared the pyridine adduct of $^{Ph}I_2PZnCl$, $^{Ph}I_2PZnCl(py)$,[289] a compound closely related to **IV-7**.

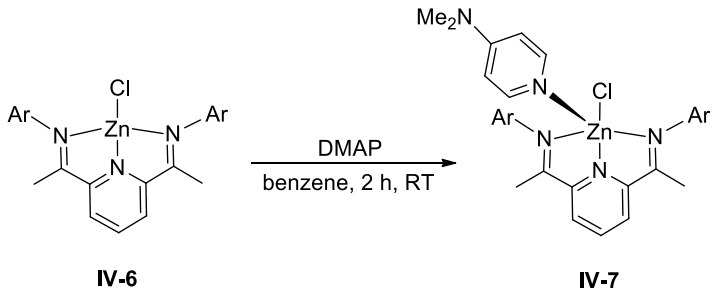

IV-6 **IV-7**

Scheme 137. Addition of DMAP to **IV-6** to give $^{Me}I_2PZnCl(DMAP)$ (**IV-7**).

The X-ray crystal structure of **IV-7** (Figure 35) revealed a five-coordinate zinc atom in an approximate square pyramidal geometry with elongated metal ligand bonds. The τ_5 parameter, on which the τ_4 parameter is based, introduced by Addison and Reedjik, is a simple metric to assess the molecular shape of five-coordinate metal complexes. The parameter is calculated simply by using the two largest bond angles in the complex (Eqn 2) to give a value ranging from 1 (ideal trigonal bipyramidal) to 0 (ideal square pyramidal).[291]

$$\tau_5 = \frac{\beta - \alpha}{60} \qquad (2)$$

A τ_5 value of 0.14 is calculated for **IV-7**, consistent with its description as a near square pyramidal geometry. The Zn1–N1 distance to the central pyridine ring is elongated from 1.940(2) Å in **IV-6** to 1.996(2) in **IV-7**, while the Zn1–Cl1 distance is elongated from 2.1565(8) to 2.2264(9), respectively. Similar elongation for the Zn–N_{py} bond (1.949(1) Å for $^{Ph}I_2PZnCl$ and 1.984(2) Å for $^{Ph}I_2PZnCl(py)$) and the Zn–Cl bond (2.1627(6) and 2.2147(7) Å for $^{Ph}I_2PZnCl$ and $^{Ph}I_2PZnCl(py)$, respectively) was also observed upon coordination of pyridine to $^{Ph}I_2PZnCl$.[289] The Zn–N_{imine} distances of 2.242(2) and 2.237(2) Å are also noticeably longer than the corresponding bonds in **IV-6** and comparable to the distances in $^{Ph}I_2PZnCl(py)$ (2.239(2) and 2.418(2) Å).[289] The DMAP ligand sits at a distance of 2.077(3) Å away from the zinc atom in the apical position, nearly orthogonal to the ZnN_3Cl base but tilted slightly towards the imino nitrogen N3, such that the N2–Zn1–N4 and Cl1–Zn1–N4 angle is 107.61(9)° and 102.19(7)°, respectively, while the N3–Zn1–N4 bond angle is 97.57(9)°. Further room to accommodate the DMAP ligand is created by a decrease in the Cl1–Zn1–N1 bond angle to 153.00(7)° (*cf.* 172.05(5) Å). These structural features suggest that coordination of DMAP to the out-of-plane 4p orbital of zinc occurs, which results in the loss of any potential π conjugation between the zinc centre and the imino nitrogens. However, contrary to that notion, the imino N=C distances remain virtually unchanged at 1.297(4) and 1.308(4) Å.

The zinc chloride moiety in **IV-6** can be easily substituted by the addition of one equivalent of methyl lithium to furnish the zinc alkyl complex $^{Me}I_2PZnMe$ (**IV-8**). Complex **IV-8** is similarly NMR silent but the EPR spectrum is comparable to the EPR

spectrum of **IV-6**, consistent with a single unpaired electron delocalized over the bis(imino)pyridine ligand (Figure 33). The molecular structure of **IV-8**, as determined by X-ray crystallography, revealed a four-coordinate, nearly square planar geometry around the zinc centre, reminiscent of the structure for **IV-6** (Figure 36). A value of 0.30 was found for the τ_4 parameter with a nearly linear C34–Zn1–N1 angle of 173.0(3)°.

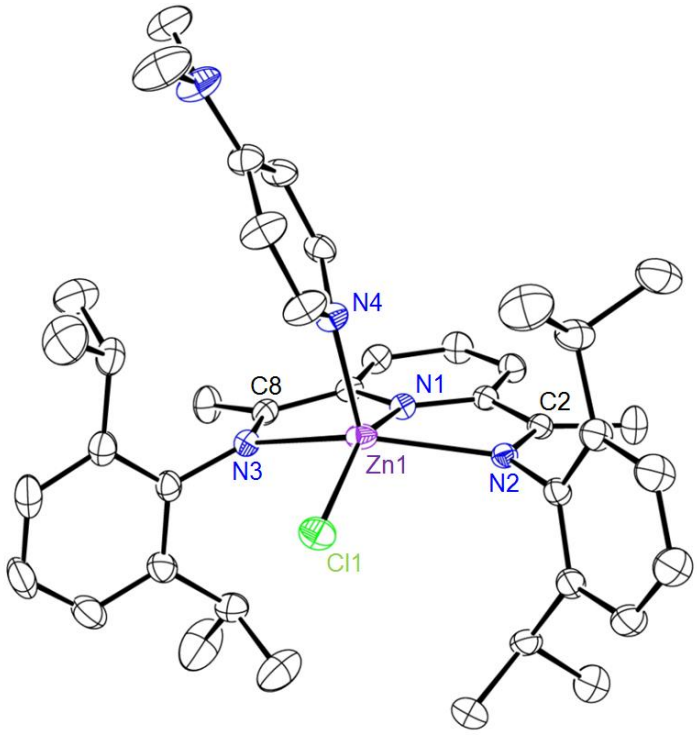

Figure 35. Molecular structure of $^{Me}I_2PZnCl(DMAP)$ (**IV-7**). Thermal ellipsoids are shown at 30% and the hydrogen atoms are removed for clarity.

Table 21. Selected bond lengths and angles for complex **IV-7**.

Lengths, Å		**Angles, °**			
Zn1–N1	1.996(2)	Cl1–Zn1–N1	153.00(7)	N1–Zn1–N3	73.71(9)
Zn1–N2	2.242(2)	Cl1–Zn1–N2	99.43(6)	N1–Zn1–N4	104.5(1)
Zn1–N3	2.327(2)	Cl1–Zn1–N3	99.13(6)	N2–Zn1–N3	144.55(9)
Zn1–N4	2.077(3)	Cl1–Zn1–N4	102.19(7)	N2–Zn1–N4	107.61(9)
Zn1–Cl1	2.2264(9)	N1–Zn1–N2	76.05(9)	N3–Zn1–N4	97.57(9)
N2–C2	1.308(4)				
N3–C8	1.297(4)				

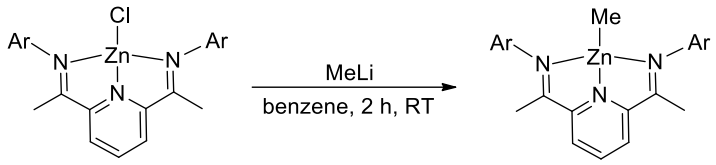

IV-6 **IV-8**

Scheme 138. Synthesis of $^{Me}I_2PZnMe$ (**IV-8**) from the addition of MeLi to **IV-6**.

The Zn1–N1 (1.967(4) Å), Zn1–N2 (2.298(4) Å), and Zn1–N3 (2.263(4) Å) distances are slightly longer compared to the respective bond lengths in **IV-6**, while the Zn1–C34 distance of 1.958(8) Å is comparable to the average Zn–Me distance on a four-coordinate zinc centre (1.975 Å).[i] Due to the partial electron density transfer to the bis(imino)pyridine ligand, the N=C bonds in the imine linkage are slightly elongated (1.291(7) and 1.297(7) Å) compared to the equivalent distances in $^{Me}I_2PZnCl_2$.

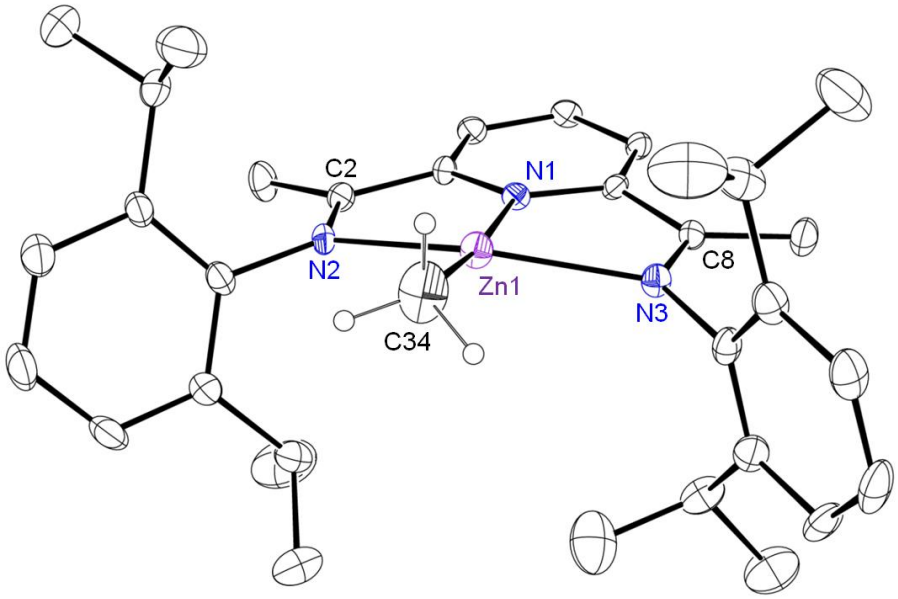

Figure 36. Molecular structure of $^{Me}I_2PZnMe$ (**IV-8**). Thermal ellipsoids are shown at 30% and the hydrogen atoms, except the ones on C34, are removed for clarity.

[i] Based on a search in the Cambridge Crystallographic Data Centre.

Table 22. Selected bond lengths and angles for complex **IV-8**.

Lengths, Å		Angles, °	
Zn1–N1	1.967(4)	C34–Zn1–N1	173.0(3)
Zn1–N2	2.298(4)	C34–Zn1–N2	102.5(2)
Zn1–N3	2.263(4)	C34–Zn1–N3	108.7(2)
Zn1–C34	1.958(8)	N1–Zn1–N2	75.1(2)
N2–C2	1.291(7)	N1–Zn1–N3	75.5(2)
N3–C8	1.297(7)	N2–Zn1–N3	145.3(2)

Further reduction of **IV-7** with KC_8 in the presence of another equivalent of DMAP yields the extremely air and moisture sensitive, formally Zn(0), complex $^{Me}IP_2Zn(DMAP)_2$ (**IV-9**) (Scheme 139). At room temperature, the ^1H NMR spectrum of **IV-9** in deuterated benzene is consistent with an average C_{2v} symmetry, displaying two broad doublets at 1.21 and 0.97 ppm from the isopropyl groups on the aromatic rings that are both coupled to a broad heptet at 3.32 ppm. The imino-methyl protons and the methyl groups from the DMAP ligands overlap and give rise to a broad singlet at 2.06 ppm. The broad signals coupled with the symmetric pattern observed in the ^1H NMR spectrum is indicative of a highly fluxional molecule in solution, likely from the two DMAP ligands in rapid exchange with each other. In an attempt to freeze out the dynamic process, ^1H NMR spectra of **IV-9** were recorded at low temperatures in toluene-d_8. Cooling the solution down to −80 °C resulted in further broadening of the signals, suggesting that the coalescence point was approached if not reached; however, the signals could not be resolved due to the encroaching freezing point of the solvent. EPR experiments revealed that compound **IV-9** is not EPR active between 100 and 300 K.

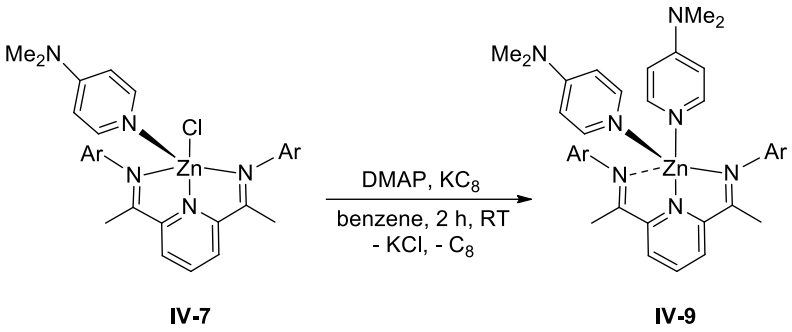

IV-7 **IV-9**

Scheme 139. Reduction of **IV-7** to give $^{Me}I_2PZn(DMAP)_2$ (**IV-9**).

The crystal structure of **IV-9** was obtained by X-ray diffraction analysis and displayed in Figure 37. The two DMAP ligands were found to be coordinated to the zinc centre, one *trans* to the central pyridine ring and the other approximately orthogonal to the plane of the ligand framework. In contrast to compounds **IV-6** and **IV-7**, the zinc atom occupies a very asymmetric position between the two imino nitrogens, with one $Zn–N_{imine}$ distance significantly shorter than the other (2.024(3) Å vs. 2.587(3) Å), such that the zinc atom adopts an unprecedented see-saw geometry. The value of τ_4 for **IV-9** was calculated to be 0.67, comparable to τ_4 values of ~0.70 found for other structures described previously as see-saw.[290] The Zn1–N1 distance of 1.976(2) Å is similar to the equivalent distances in **IV-6** and **IV-7**, whereas the $Zn–N_{DMAP}$ bonds are longer. The DMAP lying *trans* to N1, with a N1–Zn1–N5 bond angle of 155.1(1)°, has a Zn1–N5 distance of 2.071(2) Å, while the orthogonal DMAP has an even longer bond distance of 2.135(3) Å between Zn1 and N4. The asymmetric coordination of zinc results in a more pronounced difference between the two imine fragments. The imine moiety loosely bound to zinc has a N–C distance of 1.301(4) Å, consistent with a double bond between them, while the tightly coordinated arm shows a much longer N–C distance of 1.407(4) Å due to a nearly complete reduction of the imino double bond. Another noticeable feature in the crystal structure **IV-9** is the significant variation in the bond lengths of the central

pyridine ring. Most significant is the shortening of the N1–C3 bond versus the N1–C7 bond (1.347(5) and 1.412(4) Å, respectively) and the noticeable contraction of the bond between the C_{imine} and C_{ipso} carbons. Thus, reduction of the imine group confers an essentially double bond character to the C7–C8 bond (1.380(4) Å), which is much shorter than the corresponding C2–C3 bond of 1.477(5) Å on the opposite side.

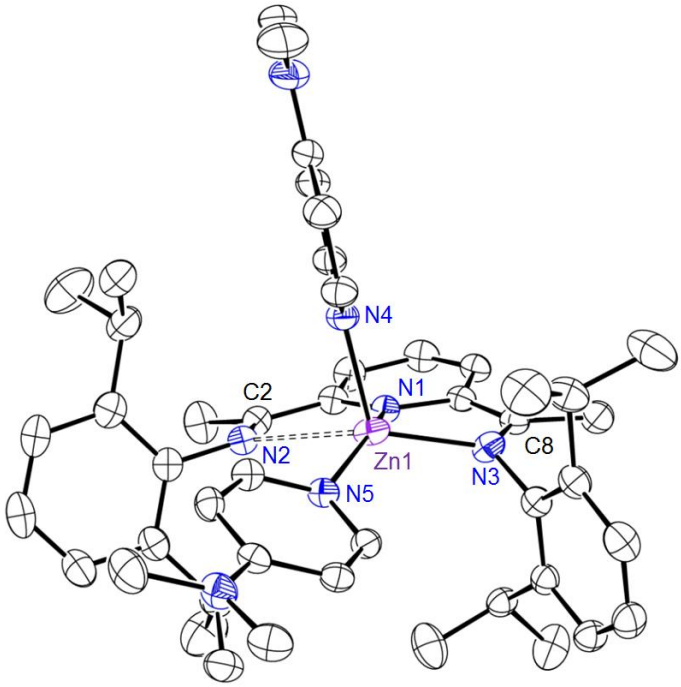

Figure 37. Molecular structure of $^{Me}I_2PZn(DMAP)_2$ (**IV-9**). Thermal ellipsoids are shown at 30% for one of two independent molecules and the hydrogen atoms are removed for clarity.

Table 23. Selected bond lengths and angles for complex **IV-9**.

Lengths, Å		**Angles, °**	
Zn1–N1	1.976(2)	N1–Zn1–N3	82.6(1)
Zn1–N2	2.587(3)	N1–Zn1–N4	101.4(1)
Zn1–N3	2.024(3)	N1–Zn1–N5	155.1(1)
Zn1–N4	2.135(3)	N3–Zn1–N4	110.9(1)
Zn1–N5	2.071(2)	N3–Zn1–N5	109.9(1)
N2–C2	1.301(4)	N4–Zn1–N5	94.2(1)
N3–C8	1.394(4)		

Analysis of the metrical parameters is suggestive for an alternative description of **IV-9** as a Zn(II) species stabilized by a dearomatized diamide ligand (Figure 38).

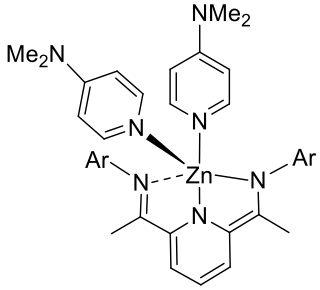

Figure 38. Alternative bonding description for **IV-9**.

The electronic structures of **IV-6**, **IV-7**, and **IV-9** were analyzed further using DFT calculations performed at the uwB97XD 6-31+G(d,p) level of theory, using the geometries obtained from the crystal structures.[j] The hybrid meta-GGA functional wB97XD was chosen for its dispersion and long-range correction terms,[292] its previous success with transition metal complexes,[293] and to remain consistent with calculations performed on the germanium complex **IV-4**. NBO analysis of **IV-7** and **IV-8** revealed that binding of DMAP is associated with a measurable increase of electron charge density at the zinc centre from +1.136 to +1.071. Furthermore, elongation of the Zn–N bond distances to the bis(imino)pyridine ligand upon ligation of DMAP was correlated with decreased NBO interactions between the imino nitrogen atoms and zinc (ΔE_{NBO} = 3.79, 3.55, and 4.33 kcal mol^{-1}), confirming that there was a significant reduction in ligand-metal binding. In agreement with the EPR spectra, the computed spin density of the system shows only a small perturbation upon DMAP coordination. Apparent from the HOMO (SOMO) and the computed spin density, the unpaired electron in **IV-6** sits in a highly delocalized π-system spread over the zinc centre, imine ligands, and the pyridine

[j] DFT calculations were performed by Lee Belding and Prof. Travis Dudding.

ring (Figure 39). The topology of this orbital strongly resembles that of **IV-4** and can be ascribed to delocalization of an electron from the zinc 4p orbital onto the bis(imino)pyridine ligand. Upon coordination of DMAP, this π-system is perturbed in such a way that the SOMO is no longer delocalized across the Zn atom in **IV-7**.

$^{Me}I_2PZnCl$ (**IV-6**)

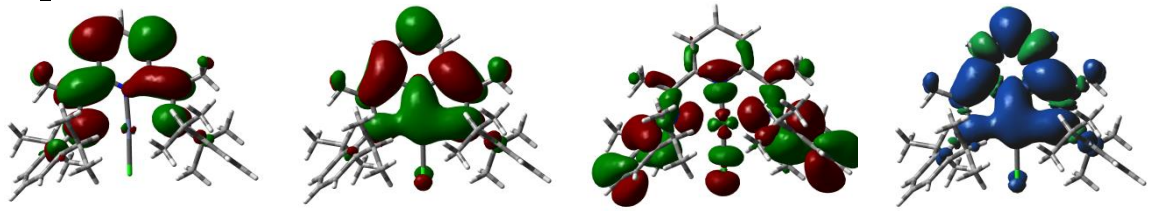

LUMO **HOMO** **HOMO−1** **Spin Density**

$^{Me}I_2PZnCl(DMAP)$ (**IV-7**)

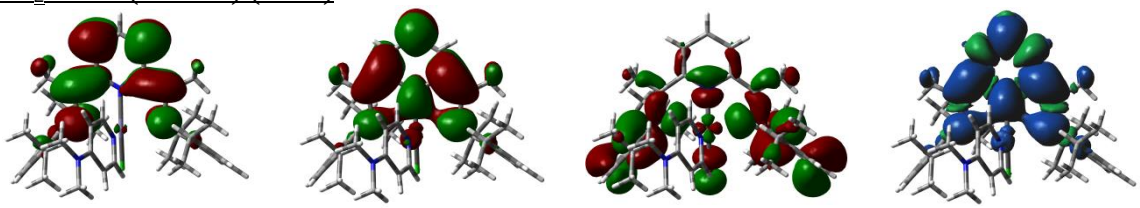

LUMO **HOMO** **HOMO−1** **Spin Density**

Figure 39. Frontier molecular orbitals of complexes **IV-6** and **IV-7**.

The difference in the imino bond lengths observed in the X-ray structure of **IV-9** was well reflected by NBO analysis which revealed a marked difference in donation from N2 and N3 of the bis(imino)pyridine ligand to the zinc centre ($N3_{E_{NBO}}$ = 25.6 kcal mol^{-1} and $N2_{E_{NBO}}$ = 7.4 kcal mol^{-1}). The low NBO donation from N2, combined with an elongated Zn–N bond length, is indicative of significant dissociation of N2 from the zinc centre. In fact, considering the shorter Zn–N4 bond distance (relative to the Zn–N2 bond distance), as well as the larger NBO donation from N4 to the Zn centre ($N4_{E_{NBO}}$ = 18.0 kcal mol^{-1}), it is more accurate to consider N4 rather than N2 as the fourth ligated nitrogen atom. As such, the geometry around the zinc atom in **IV-9** is more accurately described as a see-saw. Associated with **IV-9** is a degree of back-donation from the zinc

centre to the bis(imino)pyridine ligand (E_{NBO} = 0.84, 0.45, and 0.55 kcal mol^{-1}) and the two coordinating DMAP ligands (E_{NBO} = 0.15 and 0.27 kcal mol^{-1}). Consistent with the results of NMR and EPR spectroscopic studies of **IV-9**, the computed singlet-triplet gap is 6.7 kcal mol^{-1}, suggesting that **IV-9** exists in a singlet ground state at room temperature. Akin to **IV-7**, the LUMO of **IV-9** is entirely ligand based, while the HOMO and HOMO−1 have only minimal contribution from the zinc centre (Figure 40).

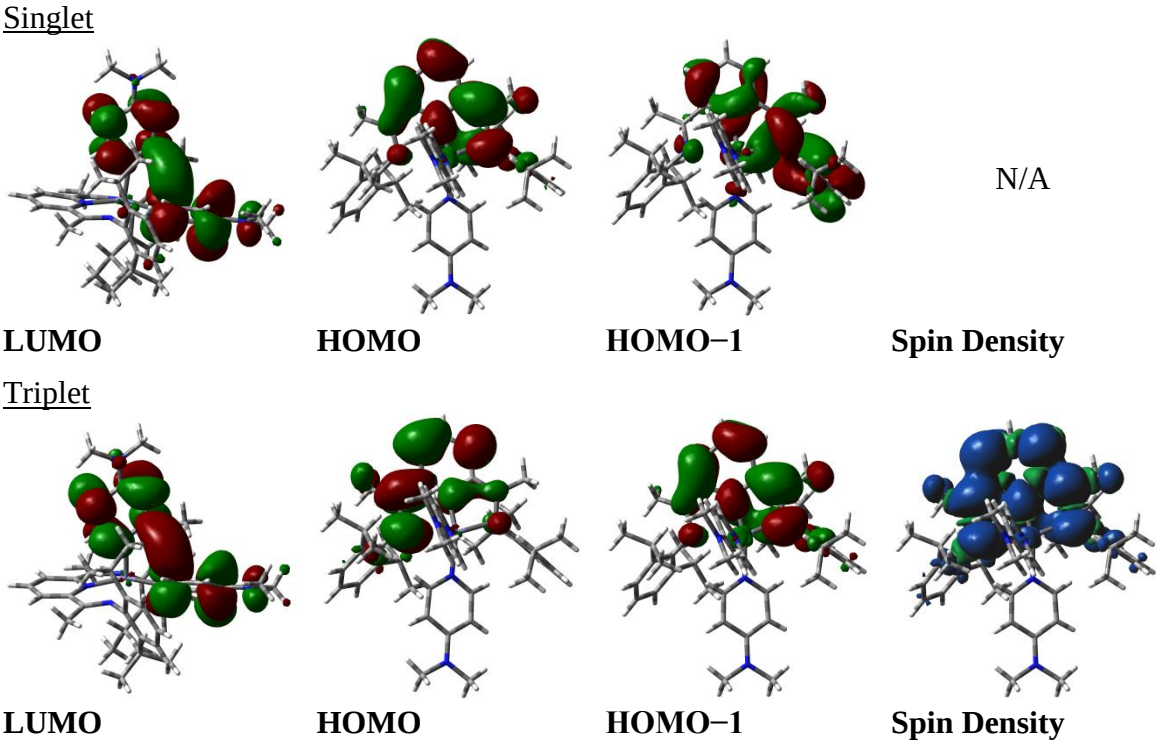

Figure 40. Comparison of the molecular orbitals for the singlet and triplet states of **IV-9**.

V. Conclusions and Future Work

In an effort to expand the reactivity of the aluminum(I) complex **III-1** towards activation of σ-bonds, a variety of substrates were reacted with **III-1**. It was found that **III-1** can activate a wide array of H–X bonds to give an assortment of substituted hydrido aluminum compounds, including the first example of an aluminum hydrido boryl complex and rare examples of silyl hydride derivatives of aluminum. Interestingly, reaction of **III-2** with **III-1** resulted in an equilibrium mixture of the starting compounds and the oxidative addition product. The reaction is reversible upon heating, shifting the equilibrium to the left resulting in a mixture of **III-1** and **III-2**, a proof of principle for the possibility of reductive elimination from a main group centre. Complex **III-1** can also oxidatively add aryl and alkyl C–F bonds, the latter being notoriously difficult to activate with limited examples in the literature. Mechanistic studies revealed that a bimolecular, concerted oxidative addition mechanism was operative in these reactions. Activation of $C(sp^3)$–O and $C(sp^3)$–S bonds were also observed upon reaction with **III-1**. Finally, oxidative addition of disulphides and diphosphides were shown with **III-1**.

The reaction of **III-1** with a cyclic thiourea resulted in oxidative cleavage of the C=S bond to yield the first example of a monomeric, terminal aluminum sulfide that was stabilized by the resulting carbene fragment. The terminal sulfide was characterized by spectroscopic methods and the structure was confirmed by X-ray diffraction analysis. DFT calculations were performed to probe the nature of the aluminum–sulfur bond and the results support its description as an Al=S double bond. Furthermore, the Al=S bond is reactive towards cycloaddition with phenyl isothiocyanate to give a novel alumocycle. Related reaction of **III-1** with triphenylphosphine sulfide resulted in similar cleavage of

the P=S, bond however the resulting aluminum sulfide is only stable at low temperature, decomposing to give a dimeric sulfide-bridged dimer upon warming. Unexpectedly, reaction of **III-1** with a cyclic urea did not give the desired aluminum oxo species but instead a novel hydride was formed as a result of intramolecular proton transfer. No evidence of C=O bond cleavage was observed even upon monitoring the reaction at low temperature. However, reaction of **III-1** with phosphine oxides resulted in P=O bond cleavage, supported by the production of the resulting phosphine, but the final product obtained was an aluminum hydroxo species due to the highly basic oxo moiety deprotonating a mildly acidic methyl proton in the ligand framework. These results demonstrate the highly reactive nature of the aluminum(I) centre and present a new route for the preparation of aluminum complexes with multiple bonds.

An obvious extension of the aluminum chemistry presented is the preparation of aluminum imides and phosphides using the same strategy. As outlined in Scheme 140, reaction of accessible guanidines and carbene phosphinidenes with **III-1** should afford the desired carbene stabilized aluminum imide and phosphide.

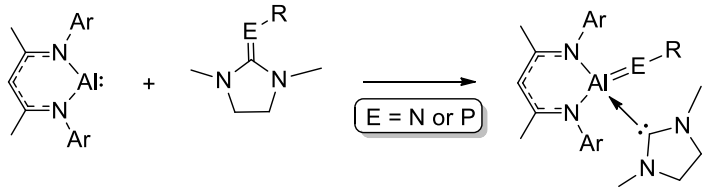

Scheme 140. Proposed pathway to terminal aluminum imides and phosphides.

While tetraamino-substituted olefins are available, preliminary results showed no reaction with **III-1**, necessitating a different synthetic route to an aluminum alkylidene complex. As shown in Scheme 141, reaction of **III-1** with a dihalomethane, a reaction that should be feasible considering that **III-1** can oxidatively add C–F bonds. Reduction of the resulting halo alkyl aluminum derivative in the presence of an appropriate Lewis

base will generate, hopefully, the desired aluminum alkylidene. The synthetic strategy outlined should also be applicable for the preparation of a terminal aluminum silylene complex.

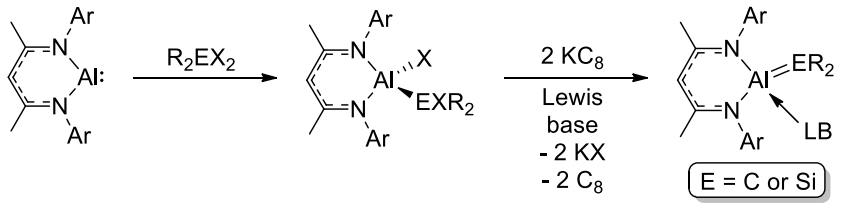

Scheme 141. Proposed synthesis of terminal aluminum alkylidenes and silylenes.

With regards to the isolation of an aluminum oxo species, modification of the *β*-diketiminate ligand should obviate the proton abstraction by the oxo ligand to generate a hydroxo compound. The NacNac ligands shown in Scheme 142 lack an acidic C–H bond in the backbone and should allow for the isolation of a terminal aluminum oxo bond upon reaction of the corresponding Al(I) compound with a cyclic urea or phosphine oxide.

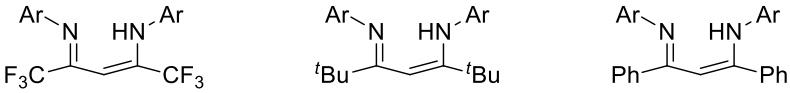

Scheme 142. Alternative NacNac ligands for the isolation of a terminal aluminum oxo.

The second major objective of this thesis was the synthesis and characterization of low valent germanium and zinc compounds stabilized by the bis(imino)pyridine ligand. Reduction of the cationic chloro germylene **IV-1** gave the desired Ge(0) compound **IV-4** which was characterized by spectroscopic methods, X-ray diffraction analysis, and DFT calculations. The data obtained were consistent with a Ge(0) centre with the unpaired electron density partially delocalized into the bis(imino)pyridine framework. Unfortunately **IV-4** has a large singlet-triplet energy gap and thus turned out to be unreactive towards bond activation with silanes or boranes but the hydrolysis of **IV-4** resulted in oxidation of the germanium atom into an oxide and partial hydrogenation of

the ligand. Mono reduction of the divalent zinc chloride bis(imino)pyridine complex gave complex **IV-6** with zinc in the formal +1 oxidation state. The zinc atom adopts an unusual square-planar geometry with a single unpaired electron delocalized over the ligand framework. Subsequent reduction of **IV-6** in the presence of DMAP gave the desired formally zero valent zinc complex **IV-9**. A highly asymmetric coordination of the imino arms of the ligand allowed for the description of the zinc atom in **IV-9** as being a four-coordinate atom in an approximate see-saw geometry. With compound **IV-9** in hand, future work should be focused on exploring its reactivity with different substrates. Bond activation should be feasible with the reduced zinc centre and substrates with H–X bonds are an obvious place to start. Furthermore, reaction of **IV-9** with azides could furnish unknown zinc imides, while reaction with N_2O or pyridine N-oxide may result in the production of novel zinc oxides.

VI. Experimental

VI.1 General Methods and Solvents

Unless stated otherwise, all manipulations were performed using standard inert atmosphere (N_2 gas) glovebox and Schlenk techniques. All glassware was rinsed with organic solvents and stored in a 190 °C oven for a minimum of 2 hours before immediate transfer to the glovebox or assembly and evacuation on the vacuum line. Liquid nitrogen (−196 °C), dry ice/acetone (−78 °C), brine/ice (−10 °C), and water/ice (0 °C) baths were used to maintain low temperature conditions during reactions, when required. Benzene, toluene, hexanes, diethyl ether, tetrahydrofuran, and dichloromethane were dried and purified using a Grubbs-type solvent purification system. Benzene-d_6 and toluene-d_8 were dried and distilled from K/Na alloy and stored in a glass vessel in the glovebox. Chloroform-d_1, dichloromethane-d_2, and bromobenzene-d_5 were dried and distilled from CaH_2 and stored in a glass vessel in the glovebox.

VI.2 Instrumentation and Analysis

NMR spectra were obtained with a Bruker DPX-300, AVANCE III HD 400 MHz, and DPX-600 spectrometers (^{1}H, 300, 400, and 600 MHz; ^{13}C, 75, 101, and 151 MHz; ^{11}B, 96, 128, and 193 MHz; ^{19}F, 282, 377, and 565 MHz; ^{29}Si, 60, 80, and 119 MHz; ^{31}P, 121, 162, and 243 MHz) at room temperature, unless stated otherwise, then processed and analyzed with MestReNova software (v10.0.2-15465). EPR spectra were collected on a Bruker Elexys E580 instrument operating in continuous wave mode. The simulation of the EPR spectra was carried out using the Easyspin software.[294] IR spectra were measured on a Perkin-Elmer 1600 FT-IR spectrometer. Elemental analyses were performed by the ANALEST laboratory at the University of Toronto, the analytical

laboratory of McMaster University, the analytical laboratory of the London Metropolitan University, or the Elemental Analysis Service at the Université de Montréal. Analyses were done in quadruplicate but several aluminum compounds were found to be low in carbon, regardless if a single crystal or a well ground powder was submitted.

X-ray crystallographic analyses were performed on suitable crystals coated in perfluoropolyether oil and mounted on a glass fiber. Measurements were collected on a Bruker AXS SMART single crystal diffractometer equipped with a sealed Mo tube source and an APEX II CCD detector. Full details can be found in individual tables for each crystal structure (Appendix).

VI.3 Starting Materials

Methylphenylsilane, pinacolborane, *tert*-butylamine, aniline, isopropanol, hexafluorobenzene, pentafluorobenzene, 1,2,3,4-tetrafluorobenzene, 1,2,3-trifluorobenzene, 1,3,5-trifluorobenzene, 1-fluoropentane, diethyl sulfide, diphenyl disulfide, phenyl isothiocyanate, 1,3-dimethyl-2-imidazolidinone (O=SIMe), triphenylphosphine oxide, triethylphosphine oxide, boron trichloride (1.0 M in hexane), boron trifluoride diethyl etherate, 4-dimethylaminopyridine, and methyllithium (1.6 M in diethyl ether) were purchased from Sigma-Aldrich. 1,2,4,5-Tetrafluorobenzene and fluorocyclohexane were purchased from Alfa Aesar. Pentamethylcyclopentadiene and tris(pentafluorophenyl)borane were purchased from Strem Chemicals. Germanium dichloride-dioxane complex ($GeCl_2$·dioxane) was purchased from Gelest. Phenylsilane and diphenylphosphine were prepared by the reduction of trichlorophenylsilane and chlorodiphenylphosphine with lithium aluminum hydride, respectively. Tetraphenyl diphosphine was prepared by reaction of chlorodiphenylphosphine with one equivalent of

lithium metal.[295] S=SIMe,[296] S=I^{i}Pr,[297] triphenylphosphine sulfide,[298] MeI_2P,[299] and potassium graphite[300] (KC_8) were prepared according to literature procedures. Complexes **III-1**,[8] **III-2**,[301] and MeI_2PZnCl_2[288] were prepared according to literature procedures. All deuterated solvents for NMR experiments were purchased from Cambridge Isotope Laboratories.

VI.4 Experimental Procedures Pertaining to Chapter III

Generation of NacNacAlH$_2$ (III-2)

An NMR tube was charged with **III-1** (0.007 g, 0.016 mmol) dissolved in 0.6 mL of benzene-d_6. Hydrogen gas (4 atm) was introduced into the sample and heated at 70 °C overnight to cleanly furnish **III-2**. The spectroscopic data are consistent with previously published data.[177]

Preparation of NacNacAlH(SiH$_2$Ph) (III-3)

A solution of **III-1** (0.118 g, 0.265 mmol) in benzene (6 mL) was added to a flask followed by the addition of phenylsilane (0.033 mL, 0.265 mmol). The reaction was stirred overnight at room temperature to yield a dark yellow solution. Volatiles were removed under vacuo and taken up in hexanes. Colourless crystals of **III-3** were obtained upon cooling to −30 °C (0.092 g, 0.166 mmol, 63%).

^{1}H NMR (600 MHz, benzene-d_6): δ 7.13 (m, 2H, C_6H_5), 7.08 (m, 2H, C_6H_5), 6.96 (m, 7H, C_6H_3 and C_6H_5), 4.93 (s, 1H, C*H*), 3.87 (d, 2H, SiH_2Ph, $^3J_{H–H}$ = 2.8 Hz), 3.42 (hept, 2H, C*H*(CH$_3$)$_2$, $^3J_{H–H}$ = 6.9 Hz), 3.35 (hept, 2H, C*H*(CH$_3$)$_2$, $^3J_{H–H}$ = 6.9 Hz), 1.54 (s, 6H, NCCH_3), 1.43 (d, 6H, CH(CH_3)$_2$, $^3J_{H–H}$ = 6.8 Hz), 1.17 (d, 6H, CH(CH_3)$_2$, $^3J_{H–H}$ = 6.7 Hz), 1.13 (d, 6H, CH(CH_3)$_2$, $^3J_{H–H}$ = 6.9 Hz), 1.11 (d, 6H, CH(CH_3)$_2$, $^3J_{H–H}$ = 6.8 Hz). **^{13}C{^{1}H} NMR** (151 MHz, benzene-d_6): δ 171.0 (N*C*CH$_3$), 145.6, 143.0, 134.7, 128.3,

127.7, 127.5, 127.4, 125.2, 124.4 (C_6H_3 and C_6H_5), 140.5 (C_{ipso}), 136.3 (*o-C* Ph), 97.8 (*C*H), 29.4, 28.2 ($CH(CH_3)_2$), 26.2, 24.8, 24.3, 24.2 ($CH(CH_3)_2$), 23.0 ($NCCH_3$). **^{29}Si INEPT+ NMR** (119 MHz, benzene-d_6, J = 200 Hz): δ −74.3 (m, *Si*H_2Ph). **IR** (nujol): ν = 2065 cm^{-1} (Si–H), 1785 cm^{-1} (Al–H). **Elem. Anal.** (%): Calculated for $C_{35}H_{49}AlN_2Si$: C, 76.04; H, 8.93; N, 5.07. Found: C, 74.71; H, 9.10; N, 5.01.

Preparation of NacNacAlH(SiHMePh) (III-4)

A flask containing **III-1** (0.120 g, 0.270 mmol) in benzene (8 mL) was charged with methylphenylsilane (0.037 mL, 0.270 mmol) and heated with stirring for 16 hours at 70 °C. Solvent was removed from the resulting yellow solution and the residue was dissolved in a 1:2 mixture of toluene and hexanes. Cooling the solution to −30 °C afforded colourless crystals of **III-4** (0.107 g, 0.189 mmol, 70%).

^{1}H NMR (300 MHz, benzene-d_6): 7.05 (m, 9H, C_6H_3, *m-H* Ph and *p-H* Ph), 6.90 (m, 2H, *o-H* Ph), 4.93 (s, 1H, C*H*), 4.20 (dq, 1H, Si*H*(CH_3)Ph, $^3J_{H(Si)–H(C)}$ = 5.1 Hz, $^3J_{H(Si)–H(Al)}$ = 6.6 Hz), 3.46 (m, 3H, C*H*(CH_3)$_2$,), 3.23 (hept, 1H, C*H*(CH_3)$_2$, $^3J_{H–H}$ = 6.9 Hz), 1.56 (s, 3H, NCC*H*$_3$), 1.53 (s, 3H, NCC*H*$_3$), 1.52 (d, 3H, CH(C*H*$_3$)$_2$, $^3J_{H–H}$ = 6.8 Hz), 1.44 (d, 3H, CH(C*H*$_3$)$_2$, $^3J_{H–H}$ = 6.8 Hz), 1.39 (d, 3H, CH(C*H*$_3$)$_2$, $^3J_{H–H}$ = 6.7 Hz), 1.16 (d, 3H, CH(C*H*$_3$)$_2$, $^3J_{H–H}$ = 6.9 Hz), 1.13 (d, 6H, CH(C*H*$_3$)$_2$, $^3J_{H–H}$ = 6.8 Hz), 1.09 (d, 3H, CH(C*H*$_3$)$_2$, $^3J_{H–H}$ = 6.9 Hz), 0.82 (d, 3H, CH(C*H*$_3$)$_2$, $^3J_{H–H}$ = 6.7 Hz), −0.14 (d, 3H, SiH(C*H*$_3$)Ph, $^3J_{H–H}$ = 5.1 Hz). **^{13}C{^{1}H} NMR** (75 MHz, benzene-d_6): δ 170.9, 170.6 (N*C*CH_3), 145.6, 143.1, 142.8, 127.6, 127.5, 127.3, 127.1, 125.4, 125.2, 124.4 (C_6H_3 and C_6H_5), 140.9, 140.9 (C_{ipso}), 140.1 (C_{ipso} Ph), 134.9 (*o-C* Ph), 97.6 (*C*H), 29.5, 29.3, 28.2, 28.0 (*C*H(CH_3)$_2$), 26.4, 25.5, 24.8, 24.8, 24.4, 24.2, 24.1 (CH(*C*H$_3$)$_2$), 23.1, 22.9 (NC*C*H$_3$), −7.3 (SiH(*C*H$_3$)Ph). **^{29}Si INEPT+ NMR** (119 MHz, benzene-d_6, J = 200 Hz):

δ −47.2 (m, *Si*H(CH$_3$)Ph). **IR** (nujol): ν = 2065 cm^{-1} (Si–H), 1785 cm^{-1} (Al–H). **Elem. Anal.** (%): Calculated for $C_{36}H_{51}AlN_2Si$: C, 76.28; H, 9.07; N, 4.94. Found: C, 75.64; H, 9.31; N, 4.84.

Preparation of NacNacAlH(BPin) (III-5)

To a dark red solution of **III-1** (0.119 g, 0.268 mmol) in benzene (5 mL) was added pinacolborane (0.039 mL, 0.268 mmol) at room temperature. The mixture was stirred for 3 hours to afford a yellow solution. Solvent was removed to give a pale yellow solid. Colourless crystals of **III-5** were obtained upon cooling a hexanes solution to −30 °C (0.080 g, 0.152 mmol, 57%).

^{1}H NMR (300 MHz, benzene-d_6): δ 7.13 (m, 6H, C$_6$*H*$_3$), 5.00 (s, 1H, C*H*), 3.50 (m, 4H, C*H*(CH$_3$)$_2$), 1.59 (s, 6H, NCC*H*$_3$), 1.53 (d, 6H, CH(C*H*$_3$)$_2$, $^3J_{H–H}$ = 6.8 Hz), 1.43 (d, 6H, CH(C*H*$_3$)$_2$, $^3J_{H–H}$ = 6.7 Hz), 1.19 (d, 12H, CH(C*H*$_3$)$_2$, $^3J_{H–H}$ = 6.7 Hz), 0.73 (s, 12H, OC(C*H*$_3$)$_2$). **^{13}C{^{1}H} NMR** (75 MHz, benzene-d_6): δ 170.3 (N*C*CH$_3$), 145.7, 143.5, 126.8, 124.5, 123.9 (*C*$_6$H$_3$), 141.4 (*C*$_{ipso}$), 97.7 (*C*H), 81.2 (O*C*(CH$_3$)$_2$), 29.1, 28.2 (*C*H(CH$_3$)$_2$), 26.7, 24.8, 24.4, 24.2 (CH(*C*H$_3$)$_2$), 25.1 (OC(*C*H$_3$)$_2$), 23.1 (NC*C*H$_3$). **^{11}B NMR** (96 MHz, benzene-d_6): δ 34.9 (br s, *B*–Pin). **IR** (nujol): ν = 1795 cm^{-1} (Al–H). **Elem. Anal.** (%): Calculated for $C_{35}H_{54}AlBN_2O_2$: C, 73.41; H, 9.51; N, 4.89. Found: C, 72.70; H, 9.77; N, 4.88.

Generation of (NacNacAlH–)$_2$ (III-6)

A solution of **III-1** (0.012 g, 0.027 mmol) in benzene-d_6 (0.6 ml) was added to **III-2** (0.012 g, 0.027 mmol) and the mixture charged into an NMR tube. The tube was allowed to stand for 4 hours at room temperature and the resulting solution contained a mixture of **III-1**, **III-2**, and **III-6**.

^{1}H NMR (600 MHz, benzene-d_6): 7.17 (m, 8H, C_6H_3) 7.01 (t, 2H, *m-H* Ar, $^{3}J_{H–H}$ = 7.6 Hz), 6.85 (d, 2H, *p-H* Ar, $^{3}J_{H–H}$ = 7.7 Hz), 4.69 (s, 2H, C*H*), 3.77 (hept, 2H, C*H*$(CH_3)_2$, $^{3}J_{H–H}$ = 6.1 Hz), 3.67 (hept, 2H, C*H*$(CH_3)_2$, $^{3}J_{H–H}$ = 6.9 Hz), 3.53 (hept, 2H, C*H*$(CH_3)_2$, $^{3}J_{H–H}$ = 6.9 Hz), 2.95 (sp, 2H, C*H*$(CH_3)_2$, $^{3}J_{H–H}$ = 6.6 Hz), 1.74 (d, 6H, CH(C*H*$_3)_2$, $^{3}J_{H–H}$ = 6.8 Hz), 1.50 (m, 12H, NCC*H*$_3$ and CH(C*H*$_3)_2$), 1.31 (s, 6H, NCC*H*$_3$), 1.21 (d, 6H, CH(C*H*$_3)_2$, $^{3}J_{H–H}$ = 6.9 Hz), 1.12 (d, 6H, CH(C*H*$_3)_2$, $^{3}J_{H–H}$ = 6.8 Hz), 1.09 (d, 6H, CH(C*H*$_3)_2$, $^{3}J_{H–H}$ = 7.0 Hz), 0.90 (d, 6H, CH(C*H*$_3)_2$, $^{3}J_{H–H}$ = 6.6 Hz), 0.84 (d, 6H, CH(C*H*$_3)_2$, $^{3}J_{H–H}$ = 6.6 Hz). **^{13}C{^{1}H} NMR** (151 MHz, benzene-d_6): δ 169.8, 168.4 (N*C*CH_3), 145.8, 145.6, 144.5, 143.8, 143.0, 142.1, 127.7, 127.4, 127.0, 126.9, 125.5, 125.1, 124.4, 124.0 (*C*$_6H_3$), 98.1 (*C*H), 29.9, 28.4, 28.1, 27.7 (*C*H$(CH_3)_2$), 28.8, 26.0, 25.6, 25.3, 25.1, 25.1, 24.9 (CH(*C*$H_3)_2$), 24.4, 23.4 (NC*C*H_3). **IR** (nujol): ν = 1778, 1772 cm^{-1} (Al–H).

Preparation of NacNacAlH(Cp*) (III-7)

Pentamethylcyclopentadiene (0.043 mL, 0.277 mmol) was added to a flask containing **III-1** (0.123 g, 0.277 mmol) in benzene (8 mL). The mixture was heated with stirring at 70 °C for 3 days to give a pale orange solution. Removal of the solvent in vacuo yielded a yellow solid. The product was recrystallized in a 1:2 mixture of toluene and hexanes at −30 °C to give yellow crystals of **III-7** (0.099 g, 0.170 mmol, 61%).

^{1}H NMR (300 MHz, benzene-d_6): δ 7.15 (m, 6H, C_6H_3), 4.90 (s, 1H, C*H*), 3.57 (hept, 2H, C*H*$(CH_3)_2$, $^{3}J_{H–H}$ = 6.8 Hz), 3.16 (hept, 2H, C*H*$(CH_3)_2$, $^{3}J_{H–H}$ = 6.9 Hz), 1.48 (s, 15H, C_5(C*H*$_3)_5$), 1.44 (m, 18H, NCC*H*$_3$ and CH(C*H*$_3)_2$), 1.15 (d, 6H, CH(C*H*$_3)_2$, $^{3}J_{H–H}$ = 6.8 Hz), 1.03 (d, 12H, CH(C*H*$_3)_2$, $^{3}J_{H–H}$ = 6.7 Hz). **^{13}C{^{1}H} NMR** (75 MHz, benzene-d_6): δ 170.3 (N*C*CH_3), 145.7, 142.8, 127.5, 125.7, 123.9 (*C*$_6H_3$), 144.0 (*C*$_{ipso}$), 121.5

($C_5(CH_3)_5$), 98.0 (CH), 29.9, 28.3 ($CH(CH_3)_2$), 25.4, 24.9, 24.5, 24.3 ($CH(CH_3)_2$), 23.5 ($NCCH_3$), 12.3 ($C_5(CH_3)_5$). **IR** (nujol): ν = 1802 cm^{-1} (Al–H). **Elem. Anal.** (%): Calculated for $C_{39}H_{57}AlN_2$: C, 80.64; H, 9.89; N, 4.82. Found: C, 82.39; H, 10.33; N, 4.93.

Preparation of NacNacAlH(NH^{t}Bu) (III-8)

To a dark red solution of **III-1** (0.120 g, 0.270 mmol) in benzene (6 mL) was added *tert*-butylamine (0.028 mL, 0.270 mmol) at room temperature. The mixture was stirred for 3 days to afford a dark yellow solution. Solvent was removed and the solid was dissolved in hexanes which afforded colourless crystals of **III-8** upon cooling to −30 °C (0.070 g, 0.135 mmol, 50%).

^{1}H NMR (300 MHz, benzene-d_6): δ 7.12 (m, 6H, C_6H_3), 4.86 (s, 1H, CH), 3.46 (hept, 2H, $CH(CH_3)_2$, $^3J_{H–H}$ = 6.8 Hz), 3.31 (hept, 2H, $CH(CH_3)_2$, $^3J_{H–H}$ = 6.9 Hz), 1.57 (s, 6H, $NCCH_3$), 1.45 (m, 12H, $CH(CH_3)_2$), 1.15 (d, 6H, $CH(CH_3)_2$, $^3J_{H–H}$ = 6.9 Hz), 1.11 (d, 6H, $CH(CH_3)_2$, $^3J_{H–H}$ = 6.8 Hz), 0.90 (s, 9H, $NC(CH_3)_3$), −0.03 (s, 1H, NH). **^{13}C{^{1}H} NMR** (75 MHz, benzene-d_6): δ 169.7 ($NCCH_3$), 144.9, 143.6, 127.1, 124.8, 123.9 (C_6H_3), 140.8 (C_{ipso}), 96.3 (CH), 48.6 ($NC(CH_3)_3$), 35.5 ($NC(CH_3)_3$), 28.9, 28.3 ($CH(CH_3)_2$), 25.8, 24.9, 24.8, 24.3 ($CH(CH_3)_2$), 23.3 ($NCCH_3$). **IR** (nujol): ν = 1812 cm^{-1} (Al–H). **Elem. Anal.** (%): Calculated for $C_{33}H_{52}AlN_3$: C, 76.55; H, 10.12; N, 8.12. Found: C, 71.94; H, 9.87; N, 8.54.

Preparation of NacNacAlH(NHPh) (III-9)

Aniline (0.025 mL, 0.270 mmol) was added to a flask containing **III-1** (0.120 g, 0.270 mmol) in benzene (6 ml). The mixture was stirred for 16 hours at room temperature to give a yellow solution. Removal of the solvent in vacuo yielded a pale yellow solid. The

product was recrystallized in hexanes at −30 °C to give colourless crystals of **III-9** (0.095 g, 0.177 mmol, 66%).

^{1}H NMR (300 MHz, benzene-d_6): δ 7.12 (m, 8H, C_6H_3 and *o*-*H* Ph), 6.68 (t, 1H, *p*-*H* Ph, $^3J_{H–H}$ = 7.3 Hz), 6.38 (br d, 2H, *m*-*H* Ph, $^3J_{H–H}$ = 7.0 Hz) 5.07 (s, 1H, C*H*), 3.36 (hept, 2H, C*H*$(CH_3)_2$, $^3J_{H–H}$ = 6.9 Hz), 3.27 (s, 1H, N*H*), 3.17 (hept, 2H, C*H*$(CH_3)_2$, $^3J_{H–H}$ = 6.7 Hz), 1.56 (s, 6H, NCC*H*$_3$), 1.44 (d, 6H, CH(C*H*$_3)_2$, $^3J_{H–H}$ = 6.8 Hz), 1.14 (d, 6H, CH(C*H*$_3)_2$, $^3J_{H–H}$ = 6.8 Hz), 1.03 (d, 6H, CH(C*H*$_3)_2$, $^3J_{H–H}$ = 6.8 Hz), 0.96 (d, 6H, CH(C*H*$_3)_2$, $^3J_{H–H}$ = 6.6 Hz). **^{13}C{^{1}H} NMR** (75 MHz, benzene-d_6): δ 170.5 (N*C*CH$_3$), 152.1, 146.4, 143.7, 125.0, 124.4 (*C*$_6$H$_3$), 140.0 (*C*$_{ipso}$), 128.8 (*o*-*C* Ph), 117.8 (*m*-*C* Ph), 115.4 (*p*-*C* Ph), 97.5 (*C*H), 29.1, 27.8 (*C*H$(CH_3)_2$), 25.1, 24.9, 24.8, 24.4 (CH(*C*H$_3)_2$), 23.4 (NC*C*H$_3$). **IR** (nujol): ν = 1854 cm^{-1} (Al–H). **Elem. Anal.** (%): Calculated for $C_{35}H_{48}AlN_3$: C, 78.17; H, 9.00; N, 7.81. Found: C, 77.74; H, 8.72; N, 7.63.

Prepartion of NacNacAlH(PPh$_2$) (III-10)

A solution of **III-1** (0.120 g, 0.270 mmol) in benzene (6 mL) was added to a flask followed by the addition of diphenylphosphine (0.047 mL, 0.270 mmol). The reaction was stirred for 24 hours at room temperature to yield a yellow solution. Volatiles were removed under vacuo to afford a yellow solid. Yellow crystals of **III-10** were obtained upon cooling a toluene solution layered with hexanes to −30 °C (0.133 g, 0.211 mmol, 78%).

^{1}H NMR (300 MHz, benzene-d_6): δ 6.91 (m, 16H, C_6H_3 and C_6H_5), 4.92 (s, 1H, C*H*), 3.69 (hept, 2H, C*H*$(CH_3)_2$, $^3J_{H–H}$ = 6.9 Hz), 3.21 (hept, 2H, C*H*$(CH_3)_2$, $^3J_{H–H}$ = 6.8 Hz), 1.64 (d, 6H, CH(C*H*$_3)_2$, $^3J_{H–H}$ = 6.8 Hz), 1.51 (s, 6H, NCC*H*$_3$), 1.12 (d, 6H, CH(C*H*$_3)_2$, $^3J_{H–H}$ = 6.9 Hz), 1.08 (d, 6H, CH(C*H*$_3)_2$, $^3J_{H–H}$ = 6.8 Hz), 1.00 (d, 6H, CH(C*H*$_3)_2$, $^3J_{H–H}$ =

6.7 Hz). **^{13}C{^{1}H} NMR** (75 MHz, benzene-d_6): δ 171.0 (N*C*CH$_3$), 144.9, 143.5, 139.5, 139.2, 136.0, 135.7, 127.9, 127.8, 125.6, 125.4, 124.6 (*C*$_6$H$_3$ and *C*$_6$H$_5$), 140.8 (*C*$_{ipso}$), 97.6 (*C*H), 29.6, 28.2 (CH(*C*H$_3$)$_2$), 25.0, 24.7, 24.2, 24.1 (CH(*C*H$_3$)$_2$), 23.3 (NC*C*H$_3$). **^{31}P{^{1}H} NMR** (121 MHz, benzene-d_6): δ −67.85 (s, *P*Ph$_2$). **IR** (nujol): ν = 1778 cm^{-1} (Al–H). **Elem. Anal.** (%): Calculated for $C_{41}H_{52}AlN_2P$: C, 78.06; H, 8.31; N, 4.44. Found: C, 77.38; H, 8.42; N, 4.42.

Preparation of NacNacAlH(O^{i}Pr) (III-11)

A flask containing **III-1** (0.120 g, 0.270 mmol) in benzene (6 mL) was charged with isopropanol (0.020 mL, 0.270 mmol) and stirred for 16 hours at room temperature. Solvent was removed from the resulting yellow solution and the residue was dissolved hexanes. Cooling the solution to −30 °C afforded colourless crystals of **III-11** (0.070 g, 0.139 mmol, 51%).

^{1}H NMR (300 MHz, benzene-d_6): δ 7.11 (m, 6H, C$_6$*H*$_3$), 4.87 (s, 1H, C*H*), 3.90 (hept, 1H, OC*H*(CH$_3$)$_2$, $^{3}J_{H–H}$ = 6.1 Hz), 3.40 (m, 4H, C*H*(CH$_3$)$_2$), 1.57 (s, 6H, NCC*H*$_3$), 1.52 (d, 6H, CH(C*H*$_3$)$_2$, $^{3}J_{H–H}$ = 6.8 Hz), 1.41 (d, 6H, CH(C*H*$_3$)$_2$, $^{3}J_{H–H}$ = 6.7 Hz), 1.15 (m, 12H, CH(C*H*$_3$)$_2$), 0.72 (d, 6H, OCH(C*H*$_3$)$_2$, $^{3}J_{H–H}$ = 6.0 Hz). **^{13}C{^{1}H} NMR** (75 MHz, C$_6$D$_6$): δ 170.0 (N*C*CH$_3$), 144.8, 144.4, 127.3, 124.5, 124.3 (*C*$_6$H$_3$), 139.6 (*C*$_{ipso}$), 96.2 (*C*H), 64.0 (O*C*H(CH$_3$)$_2$), 28.8, 28.3 (*C*H(CH$_3$)$_2$), 27.6 (OCH(*C*H$_3$)$_2$) 26.0, 24.7, 24.7, 24.5 (CH(*C*H$_3$)$_2$), 23.0 (NC*C*H$_3$). **IR** (nujol): ν = 1824 cm^{-1} (Al–H). **Elem. Anal.** (%): Calculated for $C_{32}H_{49}AlN_2O$: C, 76.15; H, 9.79; N, 5.55. Found: C, 76.37; H, 10.18; N, 5.60.

Preparation of NacNacAlF(C_6F_5) (III-12)

A solution of **III-1** (0.104 g, 0.234 mmol) in benzene (7 mL) was added to a vial followed by the addition of hexafluorobenzene (0.027 mL, 0.234 mmol). The reaction was stirred for 30 minutes at room temperature to yield a yellow solution. Volatiles were removed under vacuo and taken up in a 1:1 mixture of toluene and hexanes. Colourless crystals of **III-12** were obtained upon cooling to −30 °C (0.105 g, 0.166 mmol, 71%).

^{1}H NMR (400 MHz, benzene-d_6): δ 7.09 (m, 4H, C_6H_3), 6.89 (m, 2H, C_6H_3), 5.00 (s, 1H, C*H*), 3.40 (hept, 2H, C*H*$(CH_3)_2$, $^3J_{H–H}$ = 6.9 Hz), 2.91 (hept, 2H, C*H*$(CH_3)_2$, $^3J_{H–H}$ = 6.9 Hz), 1.50 (s, 6H, NCCH_3), 1.48 (d, 6H, CH(CH_3)$_2$, $^3J_{H–H}$ = 6.9 Hz), 1.10 (d, 6H, CH(CH_3)$_2$, $^3J_{H–H}$ = 6.9 Hz), 1.00 (d, 6H, CH(CH_3)$_2$, $^3J_{H–H}$ = 6.7 Hz), 0.46 (d, 6H, CH(CH_3)$_2$, $^3J_{H–H}$ = 6.8 Hz). **^{13}C{^{1}H} NMR** (101 MHz, benzene-d_6): δ 172.0 (N*C*CH_3), 145.0, 144.3, 125.0, 124.8 (C_6H_3), 138.0 (C_{ipso}), 98.8 (*C*H), 29.1, 27.9 (*C*H$(CH_3)_2$), 25.0, 24.6, 24.6, 24.3 (CH(*C*H_3)$_2$), 23.3 (NC*C*H_3). **^{13}C{^{19}F} NMR** (101 MHz, benzene-d_6): δ 151.4 (s, *o*-*C*–F), 142.3 (s, *p*-*C*–F), 137.5 (s, *m*-*C*–F). **^{19}F NMR** (377 MHz, benzene-d_6): δ −118.7 (*o*-F), −153.4 (*p*-F), −162.2 (*m*-F), −168.2 (Al–*F*). **Elem. Anal.** (%): Calculated for $C_{35}H_{41}AlF_6N_2$: C, 66.65; H, 6.55; N, 4.44. Found: C, 66.52; H, 6.64; N, 4.50.

Preparation of NacNacAlF(3-C_6HF_4-1,2,4,5) (III-13)

To a dark red solution of **III-1** (0.099 g, 0.223 mmol) in benzene (8 mL) was added pentafluorobenzene (0.025 mL, 0.223 mmol) at room temperature. The mixture was stirred for 30 minutes to afford a yellow solution. Solvent was removed and the solid was dissolved in a 1:2 mixture of toluene and hexanes which afforded colourless crystals of **III-13** upon cooling to −30 °C (0.075 g, 0.122 mmol, 55%).

^{1}H NMR (400 MHz, benzene-d_6): δ 7.09 (m, 4H, C_6H_3), 6.92 (m, 2H, C_6H_3), 6.46 (m, 1H, C_6F_4H), 5.03 (s, 1H, C*H*), 3.44 (hept, 2H, C*H*$(CH_3)_2$, $^{3}J_{H–H}$ = 6.9 Hz), 3.01 (hept, 2H, C*H*$(CH_3)_2$, $^{3}J_{H–H}$ = 6.8 Hz), 1.52 (s, 6H, NCC*H*$_3$), 1.49 (d, 6H, CH(C*H*$_3$)$_2$, $^{3}J_{H–H}$ = 6.9 Hz), 1.12 (d, 6H, CH(C*H*$_3$)$_2$, $^{3}J_{H–H}$ = 6.9 Hz), 1.04 (d, 6H, CH(C*H*$_3$)$_2$, $^{3}J_{H–H}$ = 6.7 Hz), 0.50 (d, 6H, CH(C*H*$_3$)$_2$, $^{3}J_{H–H}$ = 6.8 Hz). **^{13}C{^{1}H} NMR** (101 MHz, benzene-d_6): δ 171.9 (N*C*CH$_3$), 145.0, 144.4, 125.0, 124.8 (*C*$_6$H$_3$), 138.1 (*C*$_{ipso}$), 107.3 (*p*-*C* C_6F_4H), 98.8 (*C*H), 29.1, 27.8 (*C*H$(CH_3)_2$), 25.1, 24.7, 24.6, 24.3 (CH(*C*H$_3$)$_2$), 23.3 (NC*C*H$_3$). **^{13}C{^{19}F} NMR** (101 MHz, benzene-d_6): δ 151.5 (d, *o*-*C*–F), 146.1 (d, *m*-*C*–F). **^{19}F NMR** (377 MHz, benzene-d_6): δ −120.5 (*o*-F), −139.8 (*m*-F), −168.5 (Al–*F*). **Elem. Anal.** (%): Calculated for $C_{35}H_{42}AlF_5N_2$: C, 68.61; H, 6.91; N, 4.57. Found: C, 68.50; H, 7.06; N, 4.61.

Preparation of NacNacAlF(2-$C_6H_2F_3$-1,3,4) (III-14)

1,2,3,4-Tetrafluorobenzene (0.024 mL, 0.223 mmol) was added to a vial containing **III-1** (0.099 g, 0.223 mmol) in benzene (8 ml). The mixture was stirred for 16 hours at room temperature to afford a pale yellow solution. Removal of the solvent in vacuo yielded a pale yellow solid. The product was recrystallized in a 1:2 mixture of toluene and hexanes at −30 °C to give colourless crystals of **III-14** (0.090 g, 0.151 mmol, 68%).

^{1}H NMR (400 MHz, benzene-d_6): δ 7.10 (m, 4H, C_6H_3), 6.94 (m, 2H, C_6H_3), 6.56 (m, 1H, *p*-*H* $C_6F_3H_2$), 6.24 (m, 1H, *m*-*H* $C_6F_3H_2$), 5.05 (s, 1H, C*H*), 3.49 (hept, 2H, C*H*$(CH_3)_2$, $^{3}J_{H–H}$ = 6.8 Hz), 3.08 (hept, 2H, C*H*$(CH_3)_2$, $^{3}J_{H–H}$ = 6.8 Hz), 1.55 (s, 6H, NCC*H*$_3$), 1.50 (d, 6H, CH(C*H*$_3$)$_2$, $^{3}J_{H–H}$ = 6.8 Hz), 1.13 (d, 6H, CH(C*H*$_3$)$_2$, $^{3}J_{H–H}$ = 6.9 Hz), 1.07 (d, 6H, CH(C*H*$_3$)$_2$, $^{3}J_{H–H}$ = 6.7 Hz), 0.51 (d, 6H, CH(C*H*$_3$)$_2$, $^{3}J_{H–H}$ = 6.7 Hz). **^{13}C{^{1}H} NMR** (101 MHz, benzene-d_6): δ 171.6 (N*C*CH$_3$), 145.1, 144.6, 124.9, 124.7

(C_6H_3), 138.5 (C_{ipso}), 118.6 (*p*-*C* $C_6F_3H_2$), 110.8 (*m*-*C* $C_6F_3H_2$), 98.7 (*C*H), 29.1, 27.9 (*C*H(CH_3)$_2$), 25.1, 24.7, 24.6, 24.3 (CH(*C*H$_3$)$_2$), 23.3 (NC*C*H$_3$). **^{13}C{^{19}F} NMR** (101 MHz, benzene-d_6): δ 165.0 (dd, *o*-*C*–F), 156.7 (d, *o*-*C*–F), 147.6 (s, *m*-*C*–F). **^{19}F NMR** (377 MHz, benzene-d_6): δ −95.4, −114.6 (*o*-F), −145.1 (*m*-F), −168.6 (Al–*F*). **Elem. Anal.** (%): Calculated for $C_{35}H_{43}AlF_4N_2$: C, 70.69; H, 7.29; N, 4.71. Found: C, 70.57; H, 7.36; N, 4.89.

Preparation of NacNacAlF(2-$C_6H_2F_3$-1,4,5) (III-15)

A flask containing **III-1** (0.092 g, 0.207 mmol) in benzene (7 mL) was charged with 1,2,4,5-tetrafluorobenzene (0.023 mL, 0.207 mmol) and heated with stirring for 2 days at 70 °C. Solvent was removed from the resulting yellow solution and the residue was dissolved in a 1:1 mixture of toluene and hexanes. Cooling the solution to −30 °C afforded colourless crystals of **III-15** (0.080 g, 0.135 mmol, 65%).

^{1}H NMR (400 MHz, benzene-d_6): δ 7.13 (m, 4H, C_6H_3), 6.96 (m, 2H, C_6H_3), 6.90 (m, 1H, *m*-*H* $C_6F_3H_2$), 6.45 (m, 1H, *o*-*H* $C_6F_3H_2$), 4.98 (s, 1H, C*H*), 3.50 (hept, 2H, C*H*(CH_3)$_2$, $^3J_{H–H}$ = 7.0 Hz), 3.05 (hept, 2H, C*H*(CH_3)$_2$, $^3J_{H–H}$ = 6.9 Hz), 1.55 (s, 6H, NCC*H*$_3$), 1.51 (d, 6H, CH(C*H*$_3$)$_2$, $^3J_{H–H}$ = 6.8 Hz), 1.15 (d, 6H, CH(C*H*$_3$)$_2$, $^3J_{H–H}$ = 6.9 Hz), 1.07 (d, 6H, CH(C*H*$_3$)$_2$, $^3J_{H–H}$ = 6.8 Hz), 0.54 (d, 6H, CH(C*H*$_3$)$_2$, $^3J_{H–H}$ = 6.8 Hz). **^{13}C{^{1}H} NMR** (101 MHz, benzene-d_6): δ 171.5 (N*C*CH$_3$), 145.1, 144.3, 125.0, 124.7 (C_6H_3), 138.8 (C_{ipso}), 126.6 (*m*-*C* $C_6F_3H_2$), 104.2 (*o*-*C* $C_6F_3H_2$), 98.4 (*C*H), 28.8, 28.1 (*C*H(CH_3)$_2$), 24.9, 24.8, 24.8, 24.0 (CH(*C*H$_3$)$_2$), 23.3 (NC*C*H$_3$). **^{13}C{^{19}F} NMR** (101 MHz, benzene-d_6): δ 165.5 (dd, *o*-*C*–F), 151.4 (t, *p*-*C*–F), 147.5 (t, *m*-*C*–F). **^{19}F NMR** (377 MHz, benzene-d_6): δ −94.8 (*o*-F), −133.7 (*p*-F), −145.6 (*m*-F), −170.1 (Al–*F*).

Elem. Anal. (%): Calculated for $C_{35}H_{43}AlF_4N_2$: C, 70.69; H, 7.29; N, 4.71. Found: C, 70.54; H, 7.42; N, 4.80.

Preparation of NacNacAlF(2-$C_6H_3F_2$-1,3) (III-16-1) and NacNacAlF(1-$C_6H_3F_2$-2,3) (III-16-2)

1,2,3-Trifluorobenzene (0.023 mL, 0.223 mmol) was added to a flask containing **III-1** (0.099 g, 0.223 mmol) in benzene (8 ml). The mixture was heated with stirring at 80 °C for 4 days to give a pale yellow solution. Removal of the solvent in vacuo yielded a yellow solid. The product was recrystallized in a 1:2 mixture of toluene and hexanes at −30 °C to give colourless crystals of **III-16** (0.081 g, 0.140 mmol, 63%).

III-16-1: **^{1}H NMR** (75%) (400 MHz, benzene-d_6): δ 7.11 (m, 4H, C_6H_3), 6.96 (m, 2H, C_6H_3), 6.77 (m, 1H, *p-H* $C_6F_2H_3$), 6.50 (m, 2H, *m-H* $C_6F_2H_3$), 5.07 (s, 1H, C*H*), 3.53 (hept, 2H, C*H*$(CH_3)_2$, $^3J_{H–H}$ = 6.7 Hz), 3.15 (hept, 2H, C*H*$(CH_3)_2$, $^3J_{H–H}$ = 7.1 Hz), 1.57 (s, 6H, NCC*H*$_3$), 1.52 (d, 6H, CH(C*H*$_3$)$_2$, $^3J_{H–H}$ = 7.0 Hz), 1.15 (d, 6H, CH(C*H*$_3$)$_2$, $^3J_{H–H}$ = 6.9 Hz), 1.11 (d, 6H, CH(C*H*$_3$)$_2$, $^3J_{H–H}$ = 6.8 Hz), 0.51 (d, 6H, CH(C*H*$_3$)$_2$, $^3J_{H–H}$ = 6.8 Hz). **^{13}C{^{1}H} NMR** (75%) (101 MHz, benzene-d_6): δ 171.3 (NC*C*H$_3$), 145.1, 144.7, 124.9, 124.7 (*C*$_6$H$_3$), 138.8 (*C*$_{ipso}$), 132.2 (*p-C* $C_6F_3H_2$), 110.5 (*m-C* $C_6F_3H_2$), 98.6 (*C*H), 29.1, 27.9 (*C*H$(CH_3)_2$), 25.1, 24.8, 24.7, 24.3 (CH(*C*H$_3$)$_2$), 23.3 (NC*C*H$_3$). **^{13}C{^{19}F}** (75%) (101 MHz, benzene-d_6): δ 171.3 (*o-C*–F). **^{19}F NMR** (75%) (377 MHz, benzene-d_6): δ −89.2 (*o*-F), −168.4 (Al–*F*).

III-16-2: **^{1}H NMR** (25%) (400 MHz, benzene-d_6): δ 7.11 (m, 4H, C_6H_3), 7.01 (m, 1H, $C_6F_2H_3$), 6.96 (m, 2H, C_6H_3), 6.71 (m, 1H, $C_6F_2H_3$), 6.41 (m, 1H, $C_6F_2H_3$), 5.03 (s, 1H, C*H*), 3.53 (hept, 2H, C*H*$(CH_3)_2$, $^3J_{H–H}$ = 6.7 Hz), 3.15 (hept, 2H, C*H*$(CH_3)_2$, $^3J_{H–H}$ = 7.1 Hz), 1.55 (s, 6H, NCC*H*$_3$), 1.52 (d, 6H, CH(C*H*$_3$)$_2$, $^3J_{H–H}$ = 7.0 Hz), 1.15 (d, 6H, CH(C*H*$_3$)$_2$, $^3J_{H–H}$ = 6.9 Hz), 1.08 (d, 6H, CH(C*H*$_3$)$_2$, $^3J_{H–H}$ = 6.8 Hz), 0.51 (d, 6H,

CH(CH_3)$_2$, $^3J_{H–H}$ = 6.8 Hz). **^{13}C{^{1}H} NMR** (25%) (101 MHz, benzene-d_6): δ 171.4 (N*C*CH$_3$), 145.0, 144.7, 124.8, 124.7 (*C*$_6$H$_3$), 138.7 (*C*$_{ipso}$), 134.5, 117.8 (C$_6$F$_3$H$_2$), 98.2 (*C*H), 29.0, 28.0 (*C*H(CH$_3$)$_2$), 25.1, 24.9, 24.8, 24.0 (CH(*C*H$_3$)$_2$), 23.3 (NC*C*H$_3$). **^{13}C{^{19}F} NMR** (25%) (101 MHz, benzene-d_6): δ 158.0 (*o*-*C*–F), 150.9 (*m*-*C*–F). **^{19}F NMR** (25%) (377 MHz, benzene-d_6): δ −119.2 (*o*-F), −140.9 (*m*-F), −172.7 (Al–*F*). **Elem. Anal.** (%): Calculated for C$_{35}$H$_{44}$AlF$_3$N$_2$: C, 72.89; H, 7.69; N, 4.86. Found: C, 72.87; H, 7.73; N, 4.88.

Generation of NacNacAlF(1-C$_6$H$_3$F$_2$-3,5) (III-17)

An NMR tube was charged with **III-1** (0.015 g, 0.034 mmol) and dissolved in 0.6 mL of benzene-d_6. 1,3,5-trifluorobenzene (0.004 mL, 0.034 mmol) was introduced and the sample was heated at 100 °C for 4 days to furnish **III-17** along with an unidentified by-product.

^{19}F NMR (377 MHz, benzene-d_6): δ −112.3 (*m*-F), −159.3 (Al–*F*).

Preparation of NacNacAlF(C$_5$H$_{11}$) (III-18)

To a dark red solution of **III-1** (0.095 g, 0.214 mmol) in benzene (7 mL) was added 1-fluoropentane (0.024 mL, 0.214 mmol) at room temperature. The mixture was stirred for 30 minutes to afford a yellow solution. Solvent was removed to give a yellow solid. Colourless crystals of **III-18** were obtained upon cooling a hexanes solution to −30 °C (0.065 g, 0.122 mmol, 57%).

^{1}H NMR (400 MHz, benzene-d_6): δ 7.17 (m, 4H, C$_6$*H*$_3$), 7.10 (m, 2H, C$_6$*H*$_3$), 5.00 (s, 1H, C*H*), 3.65 (hept, 2H, C*H*(CH$_3$)$_2$, $^3J_{H–H}$ = 6.8 Hz), 3.20 (hept, 2H, C*H*(CH$_3$)$_2$, $^3J_{H–H}$ = 6.8 Hz), 1.60 (s, 6H, NCC*H*$_3$), 1.49 (d, 6H, CH(C*H*$_3$)$_2$, $^3J_{H–H}$ = 6.8 Hz), 1.37 (d, 6H, CH(C*H*$_3$)$_2$, $^3J_{H–H}$ = 6.8 Hz), 1.20 (d, 6H, CH(C*H*$_3$)$_2$, $^3J_{H–H}$ = 6.9 Hz), 1.09 (d, 10H,

$CH(CH_3)_2$, $AlCH_2CH_2CH_2$, and CH_2CH_3, $^3J_{H–H}$ = 6.8 Hz), 1.02 (m, 2H, $AlCH_2CH_2CH_2$), 0.72 (t, 3H, CH_2CH_3, $^3J_{H–H}$ = 7.1 Hz), −0.12 (m, 2H, $AlCH_2$). **$^{13}C\{^1H\}$ NMR** (101 MHz, benzene-d_6): δ 170.2 ($NCCH_3$), 145.5, 143.2, 125.1, 124.0 (C_6H_3), 140.2 (C_{ipso}), 97.7 (*C*H), 38.0 ($AlCH_2CH_2CH_2$), 29.0, 28.0 ($CH(CH_3)_2$), 27.9 ($AlCH_2CH_2CH_2$), 25.8, 24.9, 24.4, 24.1 ($CH(CH_3)_2$), 23.1 ($NCCH_3$), 22.7 (CH_2CH_3) 14.2 (CH_2CH_3), 5.7 ($AlCH_2$). **^{19}F NMR** (377 MHz, benzene-d_6): δ −157.6 (Al–*F*). **Elem. Anal.** (%): Calculated for $C_{34}H_{52}AlFN_2$: C, 76.36; H, 9.80; N, 5.24. Found: C, 76.23; H, 9.90; N, 5.24.

Preparation of NacNacAlF(C_6H_{11}) (III-19)

Fluorocyclohexane (0.025 mL, 0.225 mmol) was added to a vial containing **III-1** (0.100 g, 0.225 mmol) in benzene (8 ml). Stirring the mixture for 30 minutes at room temperature afforded a pale yellow solution. Removal of the solvent in vacuo yielded an off-white solid. The product was recrystallized in a 1:1 mixture of toluene and hexanes at −30 °C to give colourless crystals of **III-19** (0.081 g, 0.148 mmol, 66%).

^1H NMR (400 MHz, benzene-d_6): δ 7.14 (m, 4H, C_6H_3), 7.08 (m, 2H, C_6H_3), 4.97 (s, 1H, C*H*), 3.58 (hept, 2H, $CH(CH_3)_2$, $^3J_{H–H}$ = 6.8 Hz), 3.24 (hept, 2H, $CH(CH_3)_2$, $^3J_{H–H}$ = 6.9 Hz), 1.57 (s, 7H, $NCCH_3$ and $AlCH(CH_2)_2CH_2$), 1.49 (d, 8H, $CH(CH_3)_2$ and $AlCH(CH_2)_2CH_2$, $^3J_{H–H}$ = 6.5 Hz), 1.40 (d, 6H, $CH(CH_3)_2$, $^3J_{H–H}$ = 6.8 Hz), 1.27 (m, 3H, $AlCH(CH_2)_2CH_2$), 1.16 (d, 6H, $CH(CH_3)_2$, $^3J_{H–H}$ = 6.9 Hz), 1.08 (d, 6H, $CH(CH_3)_2$, $^3J_{H–H}$ = 6.8 Hz), 1.02 (m, 2H, $AlCH(CH_2)_2CH_2$), 0.76 (m, 2H, $AlCH(CH_2)_2CH_2$), 0.26 (m, 1H, $AlCH(CH_2)_2CH_2$). **$^{13}C\{^1H\}$ NMR** (101 MHz, benzene-d_6): δ 170.2 ($NCCH_3$), 145.5, 143.3, 125.2, 123.9 (C_6H_3), 140.7 (C_{ipso}), 97.7 (*C*H), 30.0 ($AlCH(CH_2)_2CH_2$), 29.5 ($AlCH(CH_2)_2CH_2$), 29.1, 27.9 ($CH(CH_3)_2$), 28.1 ($AlCH(CH_2)_2CH_2$), 25.6, 24.9, 24.6, 24.0 ($CH(CH_3)_2$), 23.1 ($NCCH_3$), 21.2 ($AlCH(CH_2)_2CH_2$). **^{19}F NMR** (377 MHz, benzene-

d_6): δ −161.8 (Al–*F*). **Elem. Anal.** (%): Calculated for $C_{35}H_{52}AlFN_2$: C, 76.88; H, 9.59; N, 5.12. Found: C, 76.81; H, 9.65; N, 5.24.

Preparation of NacNacAl(–$OCH_2CH_2CH_2CH_2$–) (III-20)

To a dark red solution of **III-1** (0.095 g, 0.214 mmol) in benzene (7 mL) was added THF (0.017 mL, 0.214 mmol) at room temperature. The mixture was stirred overnight to afford a yellow solution. Solvent was removed to give a pale yellow solid. Colourless crystals of **III-20** were obtained upon cooling a 1:4 solution of toluene and diethyl ether to −30 °C (0.057 g, 0.110 mmol, 52%).

^{1}H NMR (400 MHz, benzene-d_6): δ 7.18 (m, 3H, C_6H_3), 7.14 (m, 1H, C_6H_3), 7.09 (m, 2H, C_6H_3), 4.92 (s, 1H, C*H*), 4.16 (t, 2H, OCH_2, $^3J_{H–H}$ = 5.4 Hz) 3.80 (hept, 2H, $CH(CH_3)_2$, $^3J_{H–H}$ = 6.8 Hz), 3.15 (hept, 2H, $CH(CH_3)_2$, $^3J_{H–H}$ = 6.9 Hz), 1.56 (s, 8H, $NCCH_3$ and $AlCH_2CH_2$), 1.47 (d, 6H, $CH(CH_3)_2$, $^3J_{H–H}$ = 6.6 Hz), 1.32 (m, 8H, $CH(CH_3)_2$ and OCH_2CH_2), 1.14 (d, 6H, $CH(CH_3)_2$, $^3J_{H–H}$ = 6.8 Hz), 1.04 (d, 6H, $CH(CH_3)_2$, $^3J_{H–H}$ = 6.8 Hz), 0.05 (t, 2H, $AlCH_2$, $^3J_{H–H}$ = 6.9 Hz). **^{13}C{^{1}H} NMR** (101 MHz, benzene-d_6): δ 169.8 ($NCCH_3$), 145.8, 143.6, 127.5, 124.9, 124.1 (C_6H_3), 140.8 (C_{ipso}), 97.3 (*C*H), 67.2 (OCH_2), 36.0 (OCH_2CH_2), 29.0, 28.2 ($CH(CH_3)_2$), 25.7 ($CH(CH_3)_2$ and $AlCH_2CH_2$), 25.0, 25.0, 24.1 ($CH(CH_3)_2$), 23.5 ($NCCH_3$), 7.1 ($AlCH_2$). **Elem. Anal.** (%): Calculated for $C_{33}H_{49}AlN_2O$: C, 76.70; H, 9.56; N, 5.42. Found: C, 76.48; H, 9.76; N, 5.27.

Preparation of NacNacAlEt(SEt) (III-21)

Diethyl sulfide (0.022 mL, 0.202 mmol) was added to a flask containing **III-1** (0.090 g, 0.202 mmol) in benzene (7 mL). The mixture was heated with stirring at 50 °C overnight to give a yellow solution. Removal of the solvent in vacuo yielded a yellow solid. The

product was recrystallized from hexanes at −30 °C to give yellow crystals of **III-21** (0.044 g, 0.082 mmol, 41%).

^{1}H NMR (400 MHz, benzene-d_6): δ 7.18 (m, 4H, C_6H_3), 7.09 (m, 2H, C_6H_3), 4.80 (s, 1H, C*H*), 3.79 (hept, 2H, C*H*$(CH_3)_2$, $^{3}J_{H–H}$ = 6.8 Hz), 3.31 (hept, 2H, C*H*$(CH_3)_2$, $^{3}J_{H–H}$ = 6.8 Hz), 2.68 (q, 2H, S–CH_2, $^{3}J_{H–H}$ = 7.4 Hz), 1.60 (d, 6H, CH(CH_3)$_2$, $^{3}J_{H–H}$ = 6.6 Hz), 1.54 (s, 6H, NCCH_3), 1.35 (m, 9H, CH(CH_3)$_2$ and SCH_2CH_3), 1.25 (d, 6H, CH(CH_3)$_2$, $^{3}J_{H–H}$ = 6.9 Hz), 1.08 (d, 6H, CH(CH_3)$_2$, $^{3}J_{H–H}$ = 6.8 Hz), 0.94 (t, 3H, $AlCH_2CH_3$, $^{3}J_{H–H}$ = 8.1 Hz), 0.06 (q, 2H, AlCH_2, $^{3}J_{H-H}$ = 8.1 Hz). **^{13}C{^{1}H} NMR** (101 MHz, benzene-d_6): δ 170.7 (N*C*CH_3), 145.8, 143.8, 127.6, 125.3, 124.2 (C_6H_3), 140.6 (C_{ipso}), 98.6 (*C*H), 28.8, 28.3 (*C*H$(CH_3)_2$), 26.9, 25.0, 25.0, 24.6 (CH(*C*H_3)$_2$), 23.5 (NC*C*H_3), 20.9 (S*C*H_2), 20.1 (SCH_2CH_3), 9.3 ($AlCH_2CH_3$), −0.3 (Al*C*H_2). **Elem. Anal.** (%): Calculated for $C_{33}H_{51}AlN_2S$: C, 74.11; H, 9.61; N, 5.24. Found: C, 73.93; H, 9.73; N, 5.33.

Preparation of NacNacAl(SPh$_2$) (III-22)

A solution of **III-1** (0.099 g, 0.223 mmol) in benzene (4 mL) was added to a vial followed by the addition of diphenyl disulfide (0.049 g, 0.223 mmol) dissolved in 3 mL of benzene. The reaction was stirred for 3 hours at room temperature to yield a yellow solution. Volatiles were removed under vacuo and taken up in diethyl ether. Colourless crystals of **III-22** were obtained upon cooling to −30 °C (0.073 g, 0.110 mmol, 49%).

^{1}H NMR (400 MHz, benzene-d_6): δ 7.19 (m, 4H, C_6H_3 and C_6H_5), 7.14 (m, 2H, C_6H_3 and C_6H_5), 7.06 (m, 4H, C_6H_3 and C_6H_5), 6.89 (m, 6H, C_6H_3 and C_6H_5), 5.15 (s, 1H, C*H*), 3.33 (hept, 4H, C*H*$(CH_3)_2$, $^{3}J_{H–H}$ = 6.7 Hz), 1.53 (s, 6H, NCCH_3), 1.44 (d, 12H, CH(CH_3)$_2$, $^{3}J_{H–H}$ = 6.6 Hz), 1.02 (d, 12H, CH(CH_3)$_2$, $^{3}J_{H–H}$ = 6.8 Hz). **^{13}C{^{1}H} NMR** (101 MHz, benzene-d_6): δ 172.2 (N*C*CH_3), 145.2, 125.1 (C_6H_3), 139.8 (C_{ipso} in C_6H_3),

136.7, 134.1, 129.3, 127.3, 124.4 (C_6H_3 and C_6H_5), 99.4 (*C*H), 28.9 (*C*H(CH_3)$_2$), 25.2, 25.0 (CH(*C*H_3)$_2$), 24.0 (NC*C*H_3). **Elem. Anal.** (%): Calculated for $C_{41}H_{51}AlN_2S_2$: C, 74.28; H, 7.75; N, 4.23. Found: C, 74.61; H, 7.52; N, 4.27.

Preparation of NacNacAl(PPh$_2$)$_2$ (III-23)

A flask containing **III-1** (0.101 g, 0.227 mmol) in benzene (7 mL) was charged with tetraphenyl diphosphine (0.084 g, 0.227 mmol) dissolved in benzene (2 mL) and heated with stirring for 3 days at 70 °C. Solvent was removed from the resulting orange solution and the residue was dissolved in hexanes. Cooling the solution to −30 °C afforded orange crystals of **III-23** (0.107 g, 0.131 mmol, 58%).

^{1}H NMR (400 MHz, benzene-d_6): δ 7.57 (d, 4H, *p*-*H* C_6H_5, $^3J_{H–H}$ = 7.4 Hz), 7.04 (m, 12H, C_6H_3 and C_6H_5), 6.77 (m, 10H, C_6H_3 and C_6H_5), 4.99 (s, 1H, C*H*), 3.79 (hept, 2H, C*H*(CH_3)$_2$, $^3J_{H–H}$ = 6.5 Hz), 3.65 (hept, 2H, C*H*(CH_3)$_2$, $^3J_{H–H}$ = 6.6 Hz), 1.61 (d, 6H, CH(C*H*$_3$)$_2$, $^3J_{H–H}$ = 6.7 Hz), 1.53 (s, 6H, NCC*H*$_3$), 1.09 (d, 6H, CH(C*H*$_3$)$_2$, $^3J_{H–H}$ = 6.8 Hz), 1.03 (d, 6H, CH(C*H*$_3$)$_2$, $^3J_{H–H}$ = 6.5 Hz), 0.98 (d, 6H, CH(C*H*$_3$)$_2$, $^3J_{H–H}$ = 6.6 Hz). **^{13}C{^{1}H} NMR** (101 MHz, benzene-d_6): δ 171.7 (N*C*CH$_3$), 146.0, 144.3, 125.9, 125.0 (*C*$_6$H$_3$), 141.6 (*C*$_{ipso}$ in C_6H_3), 137.9, 135.4, 125.8, 125.6, (*C*$_6$H$_5$), 135.1 (*p*-*C* C_6H_5), 101.0 (*C*H), 29.5, 28.7 (*C*H(CH_3)$_2$), 25.6, 25.6, 25.3, 25.0 (CH(*C*H_3)$_2$), 24.6 (NC*C*H$_3$). **^{31}P{^{1}H} NMR** (162 MHz, C_6D_6): δ −36.8 (s, *P*Ph$_2$), −50.0 (s, *P*Ph$_2$). **Elem. Anal.** (%): Calculated for $C_{53}H_{61}AlN_2P_2$: C, 78.11; H, 7.54; N, 3.44. Found: C, 78.10; H, 7.65; N, 3.51.

Preparation of NacNacAl=S(SIMe) (III-24)

A solution of **III-1** (0.058 g, 0.135 mmol) in toluene (7 mL) was added to a Schlenk flask and cooled down to −50 °C with an acetone/dry ice bath. A solution of S=SIMe (0.017 g, 0.135 mmol) in toluene (3 mL) was added dropwise over a couple of minutes. The

reaction was stirred for 5 minutes then left to stand as the reaction slowly warmed up. After warming to room temperature overnight, yellow solid was obtained and collected via filtration. The product was washed with benzene (5 mL) and the volatiles were removed under vacuo to yield **III-24** as a bright yellow solid (0.060 g, 0.104 mmol, 80%). NMR spectroscopic data was obtained from a sample of **III-24** generated in-situ at low temperature.

^{1}H NMR (600 MHz, toluene-d_8, −20 °C): δ 7.17 (m, 6H, C_6H_3), 4.67 (s, 1H, C*H*), 4.11 (s, 3H, NCH_3), 3.87 (hept, 2H, C*H*$(CH_3)_2$, $^{3}J_{H–H}$ = 6.8 Hz), 3.52 (m, 2H, NCH_2), 3.08 (br s, 5H, NCH_3 and NCH_2), 2.80 (hept, 2H, C*H*$(CH_3)_2$, $^{3}J_{H–H}$ = 6.8 Hz), 1.85 (d, 6H, CH(C$H_3)_2$, $^{3}J_{H–H}$ = 6.6 Hz), 1.32 (s, 6H, NCCH_3), 1.29 (d, 6H, CH(C$H_3)_2$, $^{3}J_{H–H}$ = 6.7 Hz), 1.22 (d, 6H, CH(C$H_3)_2$, $^{3}J_{H–H}$ = 6.8 Hz), 1.07 (d, 6H, CH(C$H_3)_2$, $^{3}J_{H–H}$ = 6.7 Hz). **^{13}C{^{1}H} NMR** (151 MHz, toluene-d_8, −20 °C): δ 186.1 (N*C*N), 170.3 (N*C*CH_3), 146.2, 143.8, 142.9, 127.2, 125.2, 123.9 (*C*$_6H_3$), 99.2 (*C*H), 54.9, 51.1 (N*C*H_2), 38.5, 37.3 (N*C*H_3), 29.9, 28.2 (*C*H$(CH_3)_2$), 26.5, 25.6, 25.3, 25.3 (CH(*C*$H_3)_2$), 24.7 (NC*C*H_3). **Elem. Anal.** (%): Calculated for $C_{34}H_{51}AlN_4S$: C, 71.04; H, 8.94; N, 9.75; S, 5.58. Found: C, 69.28; H, 9.01; N, 9.55;S, 5.52.

Preparation of NacNacAl=S(I^{i}Pr) (III-25)

A solution of **III-1** (0.057 g, 0.128 mmol) in toluene (3 mL) was added to a vial then cooled down to 0 °C. A toluene solution of S=I^{i}Pr (0.024 g, 0.128 mmol, 2 mL) was added and the reaction was left to stir for 5 minutes. The vial was then placed in a −30 °C freezer after which yellow crystals were obtained after a week (0.015 g, 0.024 mmol, 19%). Due to the very poor solubility of **III-25** in bromobenzene, only ^{1}H NMR spectroscopic data is presented.

^{1}H NMR (600 MHz, bromobenzene-d_5): δ 8.39 (hept, 1H, NC*H*$(CH_3)_2$, $^3J_{H–H}$ = 6.7 Hz), δ 6.98 (m, 6H, C_6H_3), δ 6.57 (s, 1H, NC*H*), δ 6.42 (s, 1H, NC*H*), 4.92 (s, 1H, C*H*), δ 4.81 (hept, 1H, NC*H*$(CH_3)_2$, $^3J_{H–H}$ = 6.6 Hz), 3.76 (hept, 2H, C*H*$(CH_3)_2$, $^3J_{H–H}$ = 6.9 Hz), 2.38 (hept, 2H, C*H*$(CH_3)_2$, $^3J_{H–H}$ = 6.8 Hz), 1.54 (d, 6H, CH(C*H*$_3)_2$, $^3J_{H–H}$ = 6.6 Hz), 1.40 (s, 6H, NCC*H*$_3$), 1.09 (d, 6H, NCH(C*H*$_3)_2$, $^3J_{H–H}$ = 6.5 Hz), 1.00 (d, 6H, CH(C*H*$_3)_2$, $^3J_{H–H}$ = 7.0 Hz), 0.86 (d, 6H, CH(C*H*$_3)_2$, $^3J_{H–H}$ = 6.8 Hz), 0.75 (d, 6H, NCH(C*H*$_3)_2$, $^3J_{H–H}$ = 6.6 Hz), 0.44 (d, 6H, CH(C*H*$_3)_2$, $^3J_{H–H}$ = 6.7 Hz). **Elem. Anal.** (%): Calculated for $C_{38}H_{57}AlN_4S·C_7H_8$: C, 74.96; H, 9.09; N, 7.77; S, 4.45. Found: C, 74.06; H, 9.39; N, 7.91; S, 4.29.

Preparation of NacNacAl(S_2CNPh) (III-26) and SIMeC(S)NPh (III-27)

To a suspension of **III-24** (0.051 g, 0.089 mmol) in benzene (5 mL) was added phenyl isothiocyanate (0.021 mL, 0.177 mmol). The reaction was stirred for 30 minutes at room temperature to yield a pale yellow solution. Volatiles were removed under vacuo and taken up in a 3:1 mixture of THF and hexanes and filtered. White precipitate of **III-26** (0.024 g, 0.039 mmol, 45 %) and colourless crystals of **III-27** (0.010 g, 0.043 mmol, 50 %) were obtained upon cooling to −30 °C and separated manually. X-ray quality crystals of **III-26** were grown from a toluene solution at −30 °C.

^{1}H NMR for NacNacAl(S_2CNPh) (400 MHz, toluene-d_8): δ 7.19 (m, 2H, C_6H_3 and C_6H_5), 7.08 (m, 3H, C_6H_3 and C_6H_5), 6.99 (m, 3H, C_6H_3 and C_6H_5), 6.93 (m, 3H, C_6H_3 and C_6H_5), 5.12 (s, 1H, C*H*), 2.90 (m, 4H, C*H*$(CH_3)_2$), 1.50 (s, 6H, NCC*H*$_3$), 1.19 (d, 6H, CH(C*H*$_3)_2$, $^3J_{H–H}$ = 6.9 Hz), 1.02 (d, 6H, CH(C*H*$_3)_2$, $^3J_{H–H}$ = 6.8 Hz), 0.92 (d, 6H, CH(C*H*$_3)_2$, $^3J_{H–H}$ = 6.8 Hz), 0.75 (d, 6H, CH(C*H*$_3)_2$, $^3J_{H–H}$ = 6.7 Hz). **^{13}C{^{1}H} NMR for NacNacAl(S_2CNPh)** (101 MHz, toluene-d_8): δ 170.3 (N*C*CH_3), 146.2, 145.5, 143.3,

138.0, 124.9, 124.0, 123.8, 121.1 (C_6H_3), 100.0 (*C*H), 30.2, 28.9 (*C*H(CH_3)$_2$), 25.4, 24.9, 24.5 (CH(*C*H_3)$_2$), 24.0 (NC*C*H_3). **Elem. Anal.** (%): Calculated for $C_{36}H_{46}AlN_3S_2$: C, 70.66; H, 7.58; N, 6.87; S, 10.48. Found: C, 69.84; H, 7.75; N, 6.92; S, 10.32.

^{1}H NMR for SIMeC(S)NPh (400 MHz, dichloromethane-d_2): δ 7.31 (dd, 2H, *m*-H C_6H_5, $^3J_{H–H}$ = 8.3 and 7.2 Hz), 7.22 (m, 2H, *o*-H C_6H_5), 7.02 (tt, 1H, *p*-H C_6H_5, $^3J_{H–H}$ = 7.3 Hz and $^4J_{H–H}$ = 1.3 Hz), 3.85 (s, 4H, NCH_2), 3.20 (s, 6H, NCH_3). **^{13}C{^{1}H} NMR for SIMeC(S)NPh** (101 MHz, dichloromethane-d_2): δ 167.6 (S*C*N), 164.4 (N*C*N), 151.6 (C_{ipso}), 128.9 (*m*-C C_6H_5), 123.6 (*p*-C C_6H_5), 122.7 (*o*-C C_6H_5), 50.1 (N*C*H_2), 34.1 (N*C*H_3). **Elem. Anal.** (%): Calculated for $C_{12}H_{15}N_3S$: C, 61.77; H, 6.48; N, 18.01; S, 13.74. Found: C, 61.83; H, 6.50; N, 18.20; S, 13.85.

Generation of NacNacAl=S(S=PPh$_3$) (III-28)

An NMR tube was charged with **III-1** (0.012 g, 0.027 mmol) and dissolved in 0.5 mL of toluene-d_8 then cooled to −78 °C with a dry ice/acetone bath. Triphenylphosphine sulfide (0.016 g, 0.054 mmol) was dissolved in 0.8 mL of toluene-d_8 then added to the NMR tube. The sample was mixed briefly before insertion into the NMR instrument precooled to −60 °C.

^{1}H NMR (600 MHz, toluene-d_8, −60 °C): δ 7.22 (m, 2H, C_6H_3), 4.74 (s, 1H, C*H*), 3.51 (br s, 2H, C*H*(CH_3)$_2$), 3.14 (br s, 2H, C*H*(CH_3)$_2$), 1.67 (br s, 6H, CH(CH_3)$_2$), 1.17 (s, 6H, NCCH_3), 1.11 (br s, 12H, CH(CH_3)$_2$), 0.70 (br s, 6H, CH(CH_3)$_2$). **^{13}C{^{1}H} NMR** (151 MHz, toluene-d_8, −60 °C): δ 171.3 (N*C*CH_3), 142.9, 131.8 (C_6H_3), 99.7 (*C*H), 25.5 (CH(*C*H_3)$_2$ and NC*C*H_3).

Preparation of NacNac'AlH(O=SIMe) (III-29)

A dark red solution of **III-1** (0.081 g, 0.182 mmol) in toluene (5 mL) was transferred to a flask and cooled down to −70 °C with an acetone/dry ice bath then O=SIMe (0.020 mL, 0.182 mmol) was added. Within minutes the solution color changed to yellow and left to stir as the reaction slowly warmed up overnight. The yellow solution was then concentrated to approximately 1 mL, layered with diethyl ether (2 mL) and left in the −30 °C freezer overnight to yield **2** as yellow crystals (0.045 g, 0.081 mmol, 44%).

^{1}H NMR (400 MHz, benzene-d_6): δ 7.28 (m, 3H, C_6H_3), 7.13 (s, 3H, C_6H_3), 5.53 (s, 1H, C*H*), 4.18 (m, 2H, C*H*$(CH_3)_2$), 4.01 (m, 3H, C*H*$(CH_3)_2$ and NCC*H*$_2$), 3.26 (s, 1H, NCC*H*$_2$), 1.84 (m, 4H, NC*H*$_2$), 1.77 (s, 3H, NCC*H*$_3$), 1.64 (d, 3H, CH(C*H*$_3$)$_2$, $^{3}J_{H–H}$ = 6.8 Hz), 1.58 (m, 9H, NC*H*$_3$ and CH(C*H*$_3$)$_2$), 1.51 (d, 3H, CH(C*H*$_3$)$_2$, $^{3}J_{H–H}$ = 6.9 Hz), 1.37 (t, 6H, CH(C*H*$_3$)$_2$, $^{3}J_{H–H}$ = 6.8 Hz), 1.32 (d, 3H, CH(C*H*$_3$)$_2$, $^{3}J_{H–H}$ = 6.9 Hz), 1.24 (d, 3H, CH(C*H*$_3$)$_2$, $^{3}J_{H–H}$ = 7.0 Hz), 1.18 (d, 3H, CH(C*H*$_3$)$_2$, $^{3}J_{H–H}$ = 7.0 Hz). **^{13}C{^{1}H} NMR** (101 MHz, benzene-d_6): δ 160.0 (*C*=O), 155.6 (N*C*CH$_2$), 148.8, 148.5, 148.2, 148.2, 144.2, 143.9, 125.4, 125.1, 124.6, 124.0, 123.8, 123.5 (*C*$_6$H$_3$), 144.8 (N*C*CH$_3$), 102.4 (*C*H), 80.0 (NC*C*H$_2$), 44.6 (N*C*H$_2$), 30.0 (N*C*H$_3$), 28.4, 28.0, 27.9, 27.8 (*C*H$(CH_3)_2$), 26.7, 26.4, 26.0, 25.4, 25.4, 24.9, 24.7, 24.3 (CH(*C*H$_3$)$_2$), 23.6 (NC*C*H$_3$). **IR** (nujol): ν = 1810 cm^{-1} (Al–H). **Elem. Anal.** (%): Calculated for $C_{34}H_{51}AlN_4O·0.5C_4H_{10}O$: C, 72.57; H, 9.47; N, 9.40. Found: C, 71.67; H, 9.22; N, 9.07.

Generation of NacNac$^{B(C_6F_5)_3}$AlH(O=SIMe) (III-30)

Tris(pentafluorophenyl)borane (0.015 g, 0.029 mmol) was added to a solution of **III-29** (0.016 g, 0.029 mmol) dissolved in 0.5 mL of benzene-d_6 and transferred into an NMR

tube. The tube was mixed and allowed to stand for 30 minutes at room temperature. NMR analysis showed quantitative production of **III-30**.

^{1}H NMR (400 MHz, benzene-d_6): δ 7.09 (m, 4H, C_6H_3), 6.96 (m, 2H, C_6H_3), 6.14 (s, 1H, C*H*), 3.25 (hept, 1H, C*H*$(CH_3)_2$, $^{3}J_{H–H}$ = 6.9 Hz), 3.15 (hept, 1H, C*H*$(CH_3)_2$, $^{3}J_{H–H}$ = 6.9 Hz), 2.98 (m, 2H, C*H*$(CH_3)_2$ and NCC*H*$_2$), 2.68 (hept, 1H, C*H*$(CH_3)_2$, $^{3}J_{H–H}$ = 6.8 Hz), 2.55 (d, 1H, NCC*H*$_2$, $^{2}J_{H–H}$ = 19.7 Hz), 2.09 (br s, 4H, NC*H*$_2$), 1.80 (s, 6H, NC*H*$_3$), 1.71 (d, 3H, CH(C*H*$_3)_2$, $^{3}J_{H–H}$ = 6.7 Hz), 1.57 (d, 3H, CH(C*H*$_3)_2$, $^{3}J_{H–H}$ = 6.7 Hz), 1.51 (s, 3H, NCC*H*$_3$), 1.29 (d, 3H, CH(C*H*$_3)_2$, $^{3}J_{H–H}$ = 6.7 Hz), 1.14 (d, 3H, CH(C*H*$_3)_2$, $^{3}J_{H–H}$ = 6.8 Hz), 1.02 (d, 3H, CH(C*H*$_3)_2$, $^{3}J_{H–H}$ = 6.8 Hz), 0.97 (d, 3H, CH(C*H*$_3)_2$, $^{3}J_{H–H}$ = 6.8 Hz), 0.82 (d, 3H, CH(C*H*$_3)_2$, $^{3}J_{H–H}$ = 6.7 Hz), 0.73 (d, 3H, CH(C*H*$_3)_2$, $^{3}J_{H–H}$ = 6.9 Hz). **^{13}C{^{1}H} NMR** (101 MHz, benzene-d_6): δ 185.9 (N*C*CH$_2$), 169.5 (N*C*CH$_3$), 158.0 (*C*=O), 144.9, 144.8, 144.7, 144.2, 138.8, 137.8, 125.6, 125.2, 124.8, 124.4 (C_6H_3), 100.9 (*C*H), 44.6 (N*C*H$_2$), 30.2 (N*C*H$_3$), 29.0, 28.9, 28.1, 27.9 (*C*H$(CH_3)_2$), 26.2, 26.1, 24.9, 24.8, 24.1, 24.0, 23.8, 23.7 (CH(*C*H$_3)_2$), 22.8 (NC*C*H$_3$). **^{11}B{^{1}H} NMR** (128 MHz, benzene-d_6): δ −14.3 (*B*$(C_6F_5)_3$). **^{19}F{^{1}H} NMR** (377 MHz benzene-d_6): δ −130.8 (*o*-F), −162.2 (*p*-F), −166.4 (*m*-F).

Preparation of NacNac'AlOH(O=PPh$_3$) (III-31)

To a dark red solution of **III-1** (0.073 g, 0.164 mmol) in benzene (4 mL) was added triphenylphosphine oxide (0.091 mL, 0.328 mmol) dissolved in 2 mL of benzene. The color of the solution quickly changes to yellow and the reaction was stirred for 1 hour at room temperature. Volatiles were removed under and the tacky yellow oil obtained was washed with hexanes (2 x 1 mL) and diethyl ether (2 x 1 mL) to give **III-31** (0.067 g, 0.091 mmol, 55%).

^{1}H NMR (400 MHz, benzene-d_6): δ 7.26 (m, 3H, C_6H_3), 7.14 (m, 4H, C_6H_3), 6.97 (m, 7H, C_6H_3), 6.83 (m, 7H, C_6H_3), 5.48 (s, 1H, C*H*), 4.09 (m, 3H, C*H*$(CH_3)_2$), 4.01 (s, 1H, NCCH_2), 3.94 (hept, 1H, C*H*$(CH_3)_2$, $^{3}J_{H–H}$ = 6.8 Hz), 3.16 (s, 1H, NCCH_2), 1.78 (s, 3H, NCCH_3), 1.65 (d, 3H, CH(CH_3)$_2$, $^{3}J_{H–H}$ = 6.7 Hz), 1.57 (d, 3H, CH(CH_3)$_2$, $^{3}J_{H–H}$ = 6.7 Hz), 1.40 (d, 3H, CH(CH_3)$_2$, $^{3}J_{H–H}$ = 6.7 Hz), 1.31 (d, 3H, CH(CH_3)$_2$, $^{3}J_{H–H}$ = 6.8 Hz), 1.16 (d, 3H, CH(CH_3)$_2$, $^{3}J_{H–H}$ = 6.9 Hz), 0.97 (m, 9H, CH(CH_3)$_2$), 0.57 (s, 1H, O*H*). **^{13}C{^{1}H} NMR** (101 MHz, benzene-d_6): δ 156.8 (N*C*CH_2), 149.0, 148.3, 148.0, 144.8, 144.6, 134.3, 134.1, 133.2, 133.1, 127.0, 125.9, 125.1, 125.1, 124.5, 124.1, 123.9, 123.5 (*C*$_6H_3$), 145.7 (N*C*CH_3), 101.4 (*C*H), 79.8 (NC*C*H_2), 28.5, 28.4, 28.2, 27.9 (*C*H$(CH_3)_2$), 26.9, 26.6, 25.2, 25.1, 24.9, 24.8 (CH(*C*H_3)$_2$), 23.8 (NC*C*H_3). **^{31}P{^{1}H} NMR** (162 MHz, benzene-d_6): δ 44.8 (s, O=*P*Ph_3).

Preparation of NacNac'AlOH(O=PEt$_3$) (III-32)

III-1 (0.073 g, 0.164 mmol) was added to a vial and dissolved in benzene (3 mL). To this a solution of triethylphosphine oxide (0.044 g, 0.328 mmol) dissolved in 2 mL of benzene was added. Immediately the red color of the solution disappeared and the reaction was left to stir for 1 hour at room temperature. Volatiles were then removed to give a white solid. Colorless crystals of **III-32** were obtained from the slow evaporation of a THF solution of the crude product (0.064 g, 0.108 mmol, 65%).

^{1}H NMR (400 MHz, benzene-d_6): δ 7.26 (m, 3H, C_6H_3), 7.15 (s, 3H, C_6H_3), 5.42 (s, 1H, C*H*), 3.99 (m, 4H, C*H*$(CH_3)_2$ and NCCH_2), 3.85 (hept, 1H, C*H*$(CH_3)_2$, $^{3}J_{H–H}$ = 6.9 Hz), 3.17 (s, 1H, NCCH_2), 1.77 (s, 3H, NCCH_3), 1.67 (d, 3H, CH(CH_3)$_2$, $^{3}J_{H–H}$ = 6.8 Hz), 1.59 (d, 3H, CH(CH_3)$_2$, $^{3}J_{H–H}$ = 6.8 Hz), 1.36 (m, 18H, CH(CH_3)$_2$), 1.02 (dq, 6H, PC$H_2$$CH_3$, $^{2}J_{P–H}$ = 13.3 Hz, $^{3}J_{H–H}$ = 7.8 Hz), 0.43 (s, 1H, O*H*), −0.06 (dt, 9H, PCH_2CH_3, $^{3}J_{P–H}$ = 18.3

Hz, $^{3}J_{H–H}$ = 7.8 Hz). **$^{13}C\{^{1}H\}$ NMR** (101 MHz, benzene-d_6): δ 156.5 (N*C*CH_2), 148.9, 148.2, 148.1, 144.1, 144.1, 125.1, 125.1, 124.2, 124.0, 123.7, 123.3 (C_6H_3), 145.3 (N*C*CH_3), 100.8 (*C*H), 79.1 (NC*C*H_2), 28.4, 28.2, 28.1, 27.7 (*C*H$(CH_3)_2$), 27.1, 26.6, 25.4, 25.3, 25.2, 25.1, 25.0, 24.7 (CH(*C*$H_3)_2$), 23.5 (NC*C*H_3), 16.8 (d, P*C*H_2CH_3, $^{1}J_{P–C}$ = 65.8 Hz), 4.0 (d, PCH_2*C*H_3, $^{2}J_{P–C}$ = 4.0 Hz). **$^{31}P\{^{1}H\}$ NMR** (162 MHz, benzene-d_6): δ 77.0 (s, O=*P*Et_3). **Elem. Anal.** (%): Calculated for $C_{35}H_{46}AlN_2O_2P$: C, 70.68; H, 9.49; N, 4.71. Found: C, 69.57; H, 9.19; N, 4.91.

Concentration Dependence of 1,2,3,4-tetrafluorobenzene in the Production of III-14

In a typical experiment, the desired quantity of 1,2,3,4-tetrafluorobenzene (8-12 equivalents, 0.0116-0.0174 mL, 0.1080-0.1619 mmol) was added to 0.6 mL of a stock solution of **III-1** dissolved in toluene-d_8 (0.0135 mmol) at room temperature. The sample was shaken and quickly inserted into the NMR probe. The progress of the reaction was monitored by integration of the backbone proton in **III-1** and **III-14** in the ^{1}H NMR spectrum. The reaction was followed until 95% completion.

Activation Parameters in the Production of III-14

In a typical experiment, 1,2,3,4-tetrafluorobenzene (0.0145 mL, 0.1350 mmol) was added to 0.6 mL of a stock solution of **III-1** dissolved in toluene-d_8 (0.0135 mmol) at room temperature. The sample was shaken and quickly inserted into the NMR probe, at which time it was given 5 minutes to equilibrate to the specified temperature. The progress of the reaction was monitored by integration of the backbone proton in **III-1** and **III-14** in the ^{1}H NMR spectrum. The reaction was followed until 95% completion.

VI.5 Experimental Procedures Pertaining to Chapter IV

Preparation of [$^{Me}I_2PGeCl][GeCl_4$] (IV-1)

A flask containing $^{Me}I_2P$ (0.500 g, 1.038 mmol) and $GeCl_2$·dioxane (0.481 g, 2.076 mmol) was charged with dichloromethane (25 mL). The reaction was stirred overnight at room temperature to yield a dark orange solution. Volatiles were removed under vacuo and the orange solid was washed twice with benzene (10 mL) to yield 0.678 g (0.882 mmol, 85%) of **IV-1**.

^{1}H NMR (300 MHz, chloroform-d_1): δ 9.13 (t, 1H, *p-H* Py, $^3J_{H–H}$ = 8.0 Hz), 8.85 (d, 2H, *m-H* Py, $^3J_{H–H}$ = 7.9 Hz), 7.30 (m, 6H, C_6H_3), 2.79 (hept, 4H, C*H*$(CH_3)_2$, $^3J_{H–H}$ = 6.8 Hz), 2.69 (s, 6H, NCC*H*$_3$), 1.22 (d, 6H, CH(C*H*$_3$)$_2$, $^3J_{H–H}$ = 6.6 Hz), 1.14 (d, 6H, CH(C*H*$_3$)$_2$, $^3J_{H–H}$ = 6.8 Hz). **^{13}C{^{1}H} NMR** (75 MHz, chloroform-d_1): δ 166.9 (N*C*CH$_3$), 149.3 (*o-C* Py), 147.7 (*p-C* Py), 140.2 (*o-C* Ph), 136.3 (*ipso-C* Ph), 130.6 (*m-C* Py), 128.4 (*p-C* Ph), 124.8 (*m-C* Ph), 29.0 (*C*H$(CH_3)_2$), 25.0 (CH(*C*H$_3$)$_2$), 19.0 (NC*C*H$_3$). **IR** (nujol): ν = 1658 cm^{-1} (N=C). **Elem. Anal.** (%): Calculated for $C_{33}H_{43}Cl_4Ge_2N_3$·0.2CH_2Cl_2: C, 50.75; H, 5.57; N, 5.35. Found: C, 50.66; H, 5.52; N, 5.36.

Preparation of [$^{Me}I_2PGeCl][BCl_4$] (IV-2)

Boron trichloride (1.0 M in heptane, 0.83 mL, 0.830 mmol) was added to a suspension of $GeCl_2$·dioxane (0.192 g, 0.830 mmol) in dichloromethane (10 mL). A solution of $^{Me}I_2P$ (0.400 g, 0.830 mmol) in dichloromethane (15 mL) was added to the mixture at room temperature and stirred overnight. Solvent was removed from the resulting orange solution and the residue was dissolved in a 1:1 mixture of dichloromethane and hexanes. Cooling the solution to −30 °C afforded orange crystals of **IV-2** (0.370 g, 0.498 mmol, 60%).

^{1}H NMR (300 MHz, chloroform-d_1): δ 9.08 (t, 1H, *p-H* Py, $^{3}J_{H–H}$ = 8.0 Hz), 8.84 (d, 2H, *m-H* Py, $^{3}J_{H–H}$ = 8.0 Hz), 7.28 (m, 6H, C_6H_3), 2.75 (hept, 4H, C*H*$(CH_3)_2$, $^{3}J_{H–H}$ = 6.8 Hz), 2.66 (s, 6H, NCC*H*$_3$), 1.22 (d, 6H, CH(C*H*$_3)_2$, $^{3}J_{H–H}$ = 6.7 Hz), 1.14 (d, 6H, CH(C*H*$_3)_2$, $^{3}J_{H–H}$ = 6.8 Hz). **^{13}C{^{1}H} NMR** (75 MHz, chloroform-d_1): δ 166.8 (N*C*CH$_3$), 149.5 (*o-C* Py), 147.6 (*p-C* Py), 140.2 (*o-C* Ph), 136.2 (*ipso-C* Ph), 130.4 (*m-C* Py), 128.4 (*p-C* Ph), 124.9 (*m-C* Ph), 29.1 (*C*H$(CH_3)_2$), 25.0 (CH(*C*H$_3)_2$), 18.9 (NC*C*H$_3$). **^{11}B NMR** (96 MHz, chloroform-d_1): δ 6.8 (s, *B*Cl$_4$). **IR** (nujol): ν = 1655 cm^{-1} (N=C). **Elem. Anal.** (%): Calculated for $C_{33}H_{43}BCl_5GeN_3$: C, 53.39; H, 5.84; N, 5.66. Found C, 53.44; H, 5.87; N, 5.73.

Preparation of [^{Me}I$_2$PGeCl][BF$_3$Cl] (IV-3)

To a suspension of $GeCl_2$·dioxane (0.240 g, 1.038 mmol) in dichloromethane (10 mL) was added boron trifluoride diethyl etherate (0.128 mL, 1.038 mmol). To this mixture a solution of $^{Me}I_2P$ (0.500 g, 1.038 mmol) in dichloromethane (15 mL) was added at room temperature and stirred overnight. Removal of the solvent in vacuo yielded an orange solid. The product was recrystallized in a 1:2 mixture of dichloromethane and hexanes at −30 °C to give orange crystals of **IV-3** (0.425 g, 0.613 mmol, 59%).

^{1}H NMR (300 MHz, chloroform-d_1): δ 9.05 (t, 1H, *p-H* Py, $^{3}J_{H–H}$ = 7.3 Hz), 8.88 (d, 2H, *m-H* Py, $^{3}J_{H–H}$ = 8.0 Hz), 7.28 (m, 6H, C_6H_3), 2.78 (hept, 4H, C*H*$(CH_3)_2$, $^{3}J_{H–H}$ = 6.7 Hz), 2.66 (s, 6H, NCC*H*$_3$), 1.22 (d, 6H, CH(C*H*$_3)_2$, $^{3}J_{H–H}$ = 6.7 Hz), 1.13 (d, 6H, CH(C*H*$_3)_2$, $^{3}J_{H–H}$ = 6.8 Hz). **^{13}C{^{1}H} NMR** (75 MHz, chloroform-d_1): δ 166.6 (N*C*CH$_3$), 149.5 (*o-C* Py), 147.5 (*p-C* Py), 140.2 (*o-C* Ph), 136.4 (*ipso-C* Ph), 130.5 (*m-C* Py), 128.4 (*p-C* Ph), 124.7 (*m-C* Ph), 29.1 (*C*H$(CH_3)_2$), 25.0 (CH(*C*H$_3)_2$), 18.9 (NC*C*H$_3$). **^{11}B NMR** (96 MHz, chloroform-d_1): δ −1.1 (s, *B*F$_3$Cl). **^{19}F NMR** (282 MHz, chloroform-d_1): δ −152.3 (s,

B*F*$_3$Cl). **IR** (nujol): ν = 1653 cm^{-1} (N=C). **Elem. Anal.** (%): Calculated for $C_{33}H_{43}BCl_2F_3GeN_3 \cdot 0.3C_6H_{14}$: C, 58.14; H, 6.62; N, 5.85. Found: C, 58.03; H, 6.58; N, 5.65.

Preparation of $^{Me}I_2PGe$ (IV-4)

Benzene (30 mL) was added to a flask containing **IV-1** (0.425 g, 0.553 mmol) and KC_8 (0.157 g, 1.161 mmol) and stirred for 2 hours at room temperature. The dark green mixture was filtered and the residue was washed with benzene (3 x 5 mL). Volatiles were removed from the combined filtrate to give **IV-4** as a green solid (0.196 g, 0.354 mmol, 64%).

^{1}H NMR (300 MHz, benzene-d_6): δ 7.18 (m, 8H, C_6H_3, *m-H* Py), 6.35 (t, 1H, *p-H* Py, $^3J_{H–H}$ = 7.6 Hz), 2.66 (hept, 4H, C*H*(CH$_3$)$_2$, $^3J_{H–H}$ = 6.9 Hz), 2.04 (s, 6H, NCC*H*$_3$), 1.16 (d, 6H, CH(C*H*$_3$)$_2$, $^3J_{H–H}$ = 6.8 Hz), 1.08 (d, 6H, CH(C*H*$_3$)$_2$, $^3J_{H–H}$ = 7.0 Hz). **^{13}C{^{1}H} NMR** (75 MHz, benzene-d_6): δ 146.1 (N*C*CH$_3$), 141.7 (*ipso-C* Ph), 141.3 (*o-C* Ph), 137.4 (*o-C* Py), 125.9 (*p-C* Ph), 124.1 (*m-C* Py), 123.3 (*m-C* Ph), 113.9 (*p-C* Py), 28.4 (*C*H(CH$_3$)$_2$), 25.9, 23.4 (CH(*C*H$_3$)$_2$), 15.0 (NC*C*H$_3$). **IR** (nujol): ν = 1575 cm^{-1} (N=C). **Elem. Anal.** (%): Calculated for $C_{33}H_{43}GeN_3$: C, 71.50; H, 7.82; N, 7.58. Found: C, 70.89; H, 7.96; N, 7.15.

Preparation of $^{Me}I_2PH_2$ (IV-5)

Degassed water (0.003 mL, 0.153 mmol) was added to a solution of **IV-4** (0.085 g, 0.153 mmol) in benzene (4 mL). The dark green solution immediately turned colorless and left to stir for an hour. Volatiles were removed to give a white solid and the product was recrystallized from hexanes at −30 °C to give colorless needles of **IV-5** (0.031 g, 0.064 mmol, 42%).

^{1}H NMR (400 MHz, benzene-d_6): δ 8.35 (d, 1H, *m-H* Py, $^{3}J_{H–H}$ = 7.9 Hz), 7.15 (m, 6H, C_6H_3), 7.03 (t, 1H, *p-H* Py, $^{3}J_{H–H}$ = 7.7 Hz), 6.60 (d, 1H, *m-H* Py, $^{3}J_{H–H}$ = 7.6 Hz), 4.41 (s, 1H, N*H*), 4.31 (q, 1H, NC*H*CH$_3$, $^{3}J_{H–H}$ = 6.7 Hz), 3.46 (hept, 2H, C*H*(CH$_3$)$_2$, $^{3}J_{H–H}$ = 6.9 Hz), 2.92 (m, 2H, C*H*(CH$_3$)$_2$), 2.30 (s, 6H, NCC*H*$_3$), 1.53 (d, 3H, NCHC*H*$_3$, $^{3}J_{H–H}$ = 6.6 Hz), 1.18 (m, 24H, CH(C*H*$_3$)$_2$). **^{13}C{^{1}H} NMR** (101 MHz, benzene-d_6): δ 167.2 (N*C*CH$_3$), 162.7, 156.4 (*o-C* Py), 147.2, 142.6, 136.0, 124.3, 124.0, 123.6 (*C*$_6$H$_3$), 136.8 (*p-C* Py), 123.0, 119.8 (*m-C* Py), 61.1 (N*C*HCH$_3$), 28.8, 28.1 (*C*H(CH$_3$)$_2$), 24.4, 24.3, 23.6, 23.5, 23.5, 23.1, 23.0, 22.9 (CH(*C*H$_3$)$_2$), 22.2 (NCH*C*H$_3$), 17.2 (NC*C*H$_3$). **IR** (nujol): ν = 1644 cm^{-1} (N=C). **Elem. Anal.** (%): Calculated for $C_{33}H_{45}N_3$: C, 81.94; H, 9.38; N, 8.69. Found: C, 81.89; H, 9.36; N, 8.75.

Preparation of ^{Me}I$_2$PZnCl (IV-6)

Benzene (50 mL) was added to a flask containing ^{Me}I$_2$PZnCl$_2$ (0.917 g, 1.483 mmol) and KC_8 (0.200 g, 1.483 mmol) and stirred for 2 hours. The dark green-red mixture was filtered and the residue was washed with benzene (4 x 10 mL). Volatiles were removed from the combined filtrate to give the product as a dark green solid that was washed with hexanes (2 x 10 mL) to give **IV-6** (0.671 g, 1.152 mmol, 77%). Crystals suitable for X-ray diffraction were grown by slow evaporation of a benzene solution.

IR (nujol): ν = 1597 cm^{-1} (N=C). **Elem. Anal.** (%): Calculated for $C_{33}H_{43}ClN_3Zn$: C, 68.04; H, 7.44; N, 7.21. Found: C, 68.41; H, 7.26; N, 7.44. This compound is paramagnetic and NMR silent.

Preparation of ^{Me}I$_2$PZnCl(DMAP) (IV-7)

A vial containing **IV-6** (0.200 g, 0.343 mmol) and 4-dimethylaminopyridine (0.042 g, 0.343 mmol) was charged with benzene (20 mL). The reaction was stirred for 2 hours to

yield a dark red solution. Volatiles were removed under vacuo and the dark red-green solid was washed with hexanes (2 x 10 mL) to yield 0.169 g (0.240 mmol, 70%) of **IV-7**. Single crystals suitable for X-ray diffraction were grown by slow evaporation of a benzene solution.

IR (nujol): ν = 1595 cm^{-1} (N=C). **Elem. Anal.** (%): Calculated for $C_{40}H_{53}ClN_5Zn$: C, 68.17; H, 7.58; N, 9.94. Found: C, 68.38; H, 7.30; N, 9.67. This compound is paramagnetic and NMR silent.

Preparation of $^{Me}I_2PZnMe$ (IV-8)

To a dark green solution of **IV-6** (0.126 g, 0.216 mmol) in benzene (10 mL) was added 0.14 mL of a 1.6 M methyllithium solution in diethyl ether at room temperature. The mixture was stirred for 2 hours and the dark red solution was filtered and the residue washed with benzene (3 x 5 mL). Solvent was removed from the combined filtrate and the product was dissolved in toluene (5 mL) then filtered. Upon cooling to −30 °C, dark red crystals of **IV-8** were obtained (0.066 g, 0.117 mmol, 54%).

IR (nujol): ν = 1598 cm^{-1} (N=C). **Elem. Anal.** (%): Calculated for $C_{34}H_{46}N_3Zn$: C, 72.65; H, 8.25; N, 7.48. Found: C, 72.33; H, 8.28; N, 7.50. This compound is paramagnetic and NMR silent.

Preparation of $^{Me}I_2PZn(DMAP)_2$ (IV-9)

Method A. A solution of **IV-7** (0.050 g, 0.071 mmol) in benzene (5 mL) was stirred with 4-dimethylaminopyridine (0.009 g, 0.071 mmol) and KC_8 (0.011 g, 0.078 mmol) for 2 hours. The dark green mixture was filtered and the residue washed with benzene (2 x 5 mL). The combined filtrate was evaporated to dryness then extracted into toluene. Dark

green needles of **IV-9** were obtained upon cooling to −30 °C (0.017 g, 0.021 mmol, 30 %).

Method B. To a dark green solution of **IV-6** (0.201 g, 0.345 mmol) in benzene (10 mL) was added 4-dimethylaminopyridine (0.084 g, 0.690 mmol). The solution was stirred for an hour then added to a separate vial containing KC_8 (0.051 g, 0.380 mmol) and stirred for 2 hours then filtered and the residue was rinsed with benzene (2 x 10 mL). Solvent was removed and the solid dissolved in toluene which afforded dark green needles of **IV-9** upon cooling to −30 °C. A second crop of product is obtained by cooling the mother liquor to −30 °C for a combined yield of 0.123 g (0.155 mmol, 45 %).

^{1}H NMR (400 MHz, benzene-d_6): δ 8.28 (br s, 2H, *o*-*H* py–NMe_2), 5.97 (br s, 2H, *m*-*H* py–NMe_2), 3.32 (hept, 4H, C*H*$(CH_3)_2$, $^3J_{H–H}$ = 6.9 Hz), 2.06 (br s, 18H, NCC*H*$_3$ and py–N*Me*$_2$), 1.21 (d, 12H, CH(C*H*$_3$)$_2$, $^3J_{H–H}$ = 6.9 Hz), 0.97 (d, 6H, CH(C*H*$_3$)$_2$, $^3J_{H–H}$ = 6.5 Hz). **^{13}C{^{1}H} NMR** (101 MHz, benzene-d_6): 38.3 (py–N*Me*$_2$), 27.6 (*C*H$(CH_3)_2$), 24.4, 23.9 (CH(*C*H$_3$)$_2$), 17.1 (NC*C*H$_3$). **IR** (nujol): ν = 1610, 1596 cm^{-1} (N=C). **Elem. Anal.** Calculated for $C_{47}H_{63}N_7Zn$: C, 71.33; H, 8.02; N, 12.39. Found: C, 71.54; H, 8.13; N, 12.35.

Activation Parameters in the Exchange Between Amido and Methine Proton in IV-5

In a typical experiment, a solution of **IV-5** (0.015 g, 0.031 mmol) in benzene-d_6 (0.5 mL) was prepared at room temperature. The sample was then inserted into the NMR spectrometer and given 5 minutes to equilibrate to the specified temperature. A series of 1D ^{1}H EXSY NMR experiments (irradiation applied to the resonance of the methine proton) with different mixing times (t_m = 0–0.6 s) were performed and the rate constant of the exchange process was extracted.

VII. Appendix

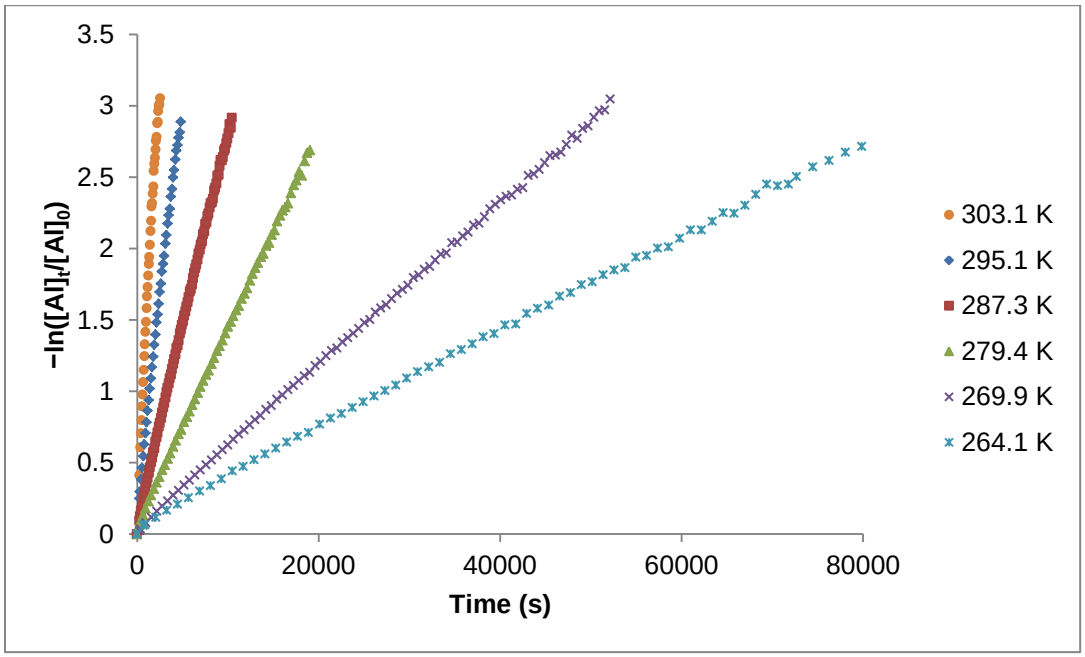

Figure 41. Plot of $-\ln([Al]_t/[Al]_0)$ versus time for reactions of **III-1** with 1,2,3,4-tetrafluorobenzene under pseudo 1st order conditions at different temperatures.

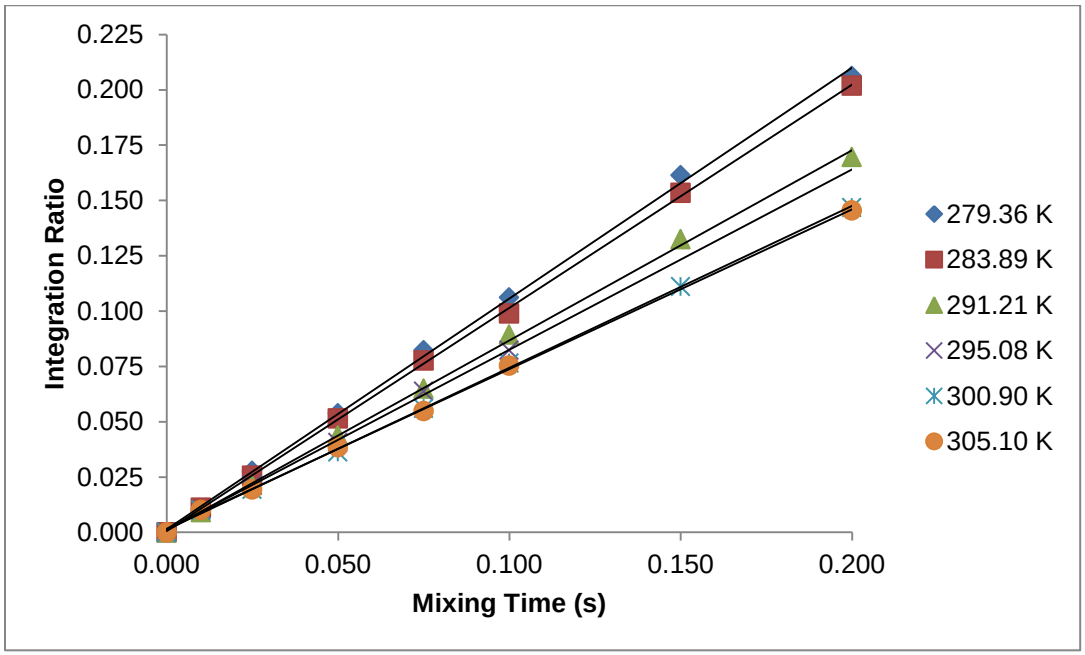

Figure 42. Plot of integration ratio versus mixing time for the intramolecular proton exchange in **IV-5** obtained via 1D ^{1}H EXSY NMR experiments.

^{1}H NMR Spectrum (600 MHz, C_6D_6)

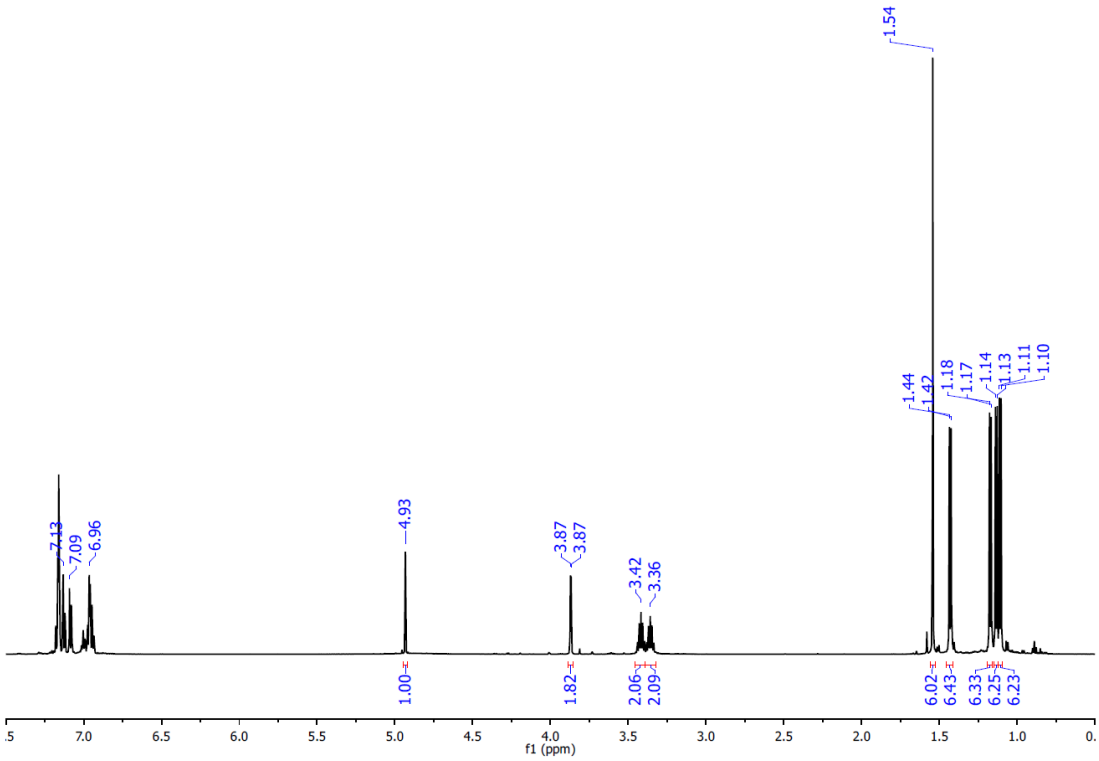

$^{13}C\{^{1}H\}$ NMR Spectrum (151 MHz, C_6D_6)

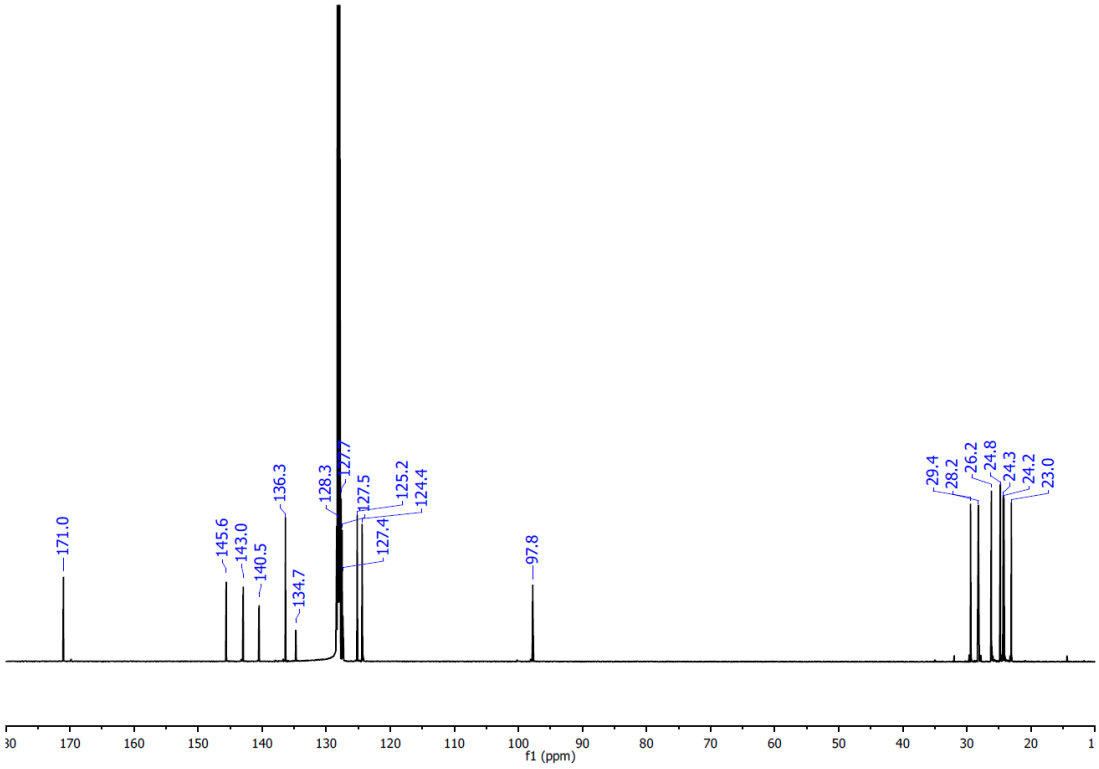

^{29}Si INEPT+ NMR Spectrum (119 MHz, C_6D_6)

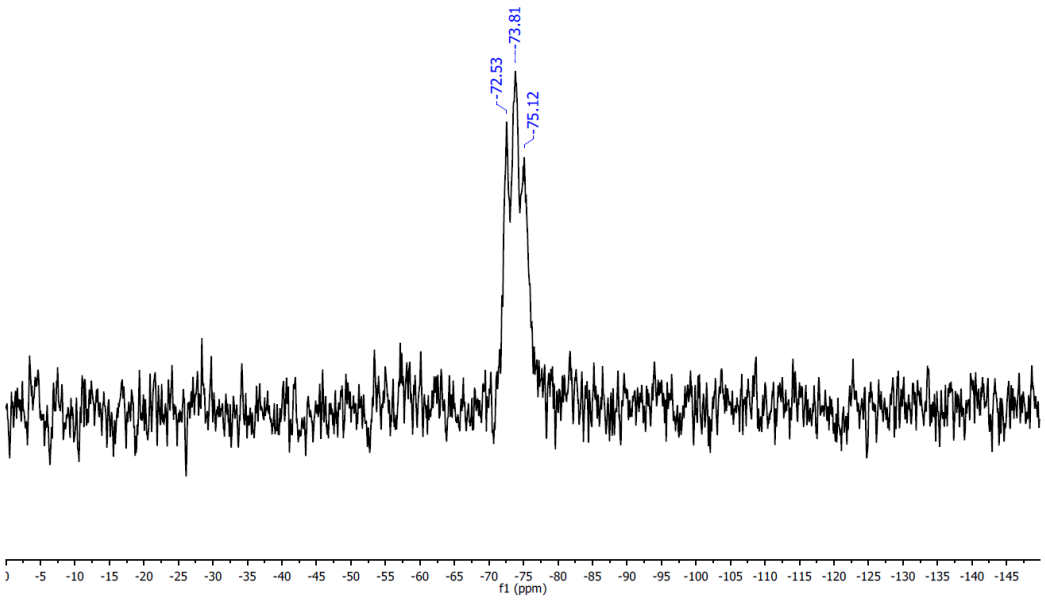

Figure 43. ^{1}H, ^{13}C{^{1}H}, and ^{29}Si INEPT+ NMR spectra of **III-3**.

^{1}H NMR Spectrum (300 MHz, C_6D_6)

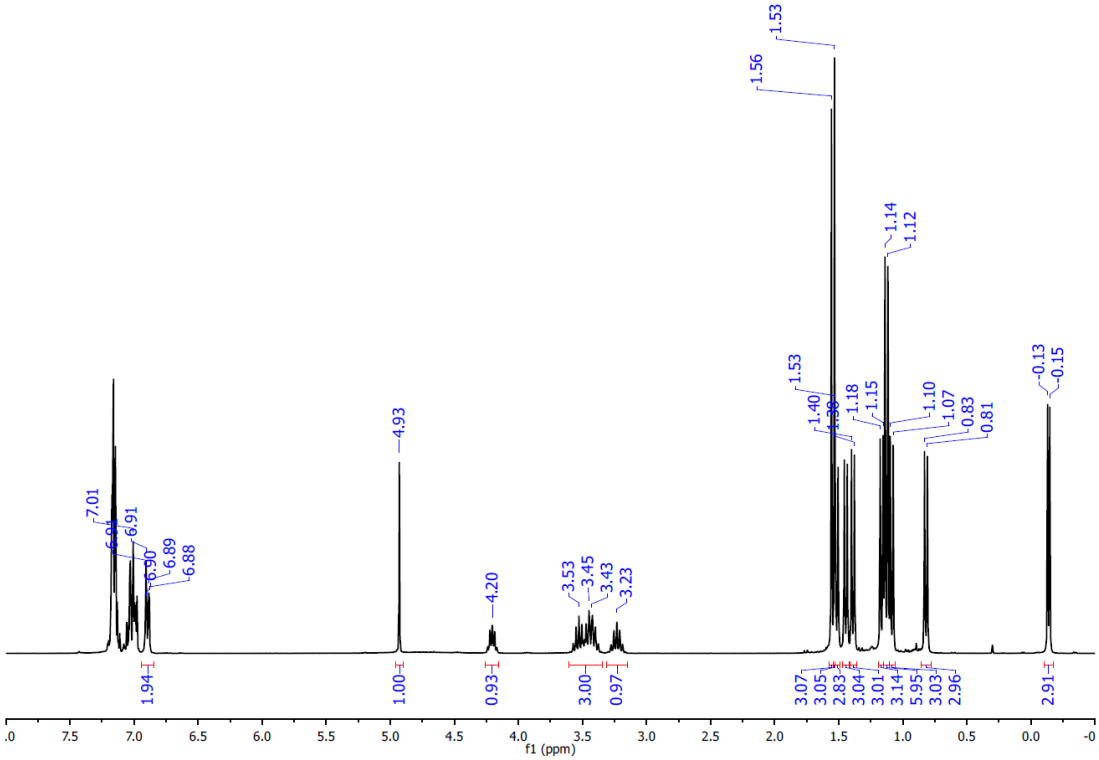

$^{13}C\{^{1}H\}$ NMR Spectrum (75 MHz, C_6D_6)

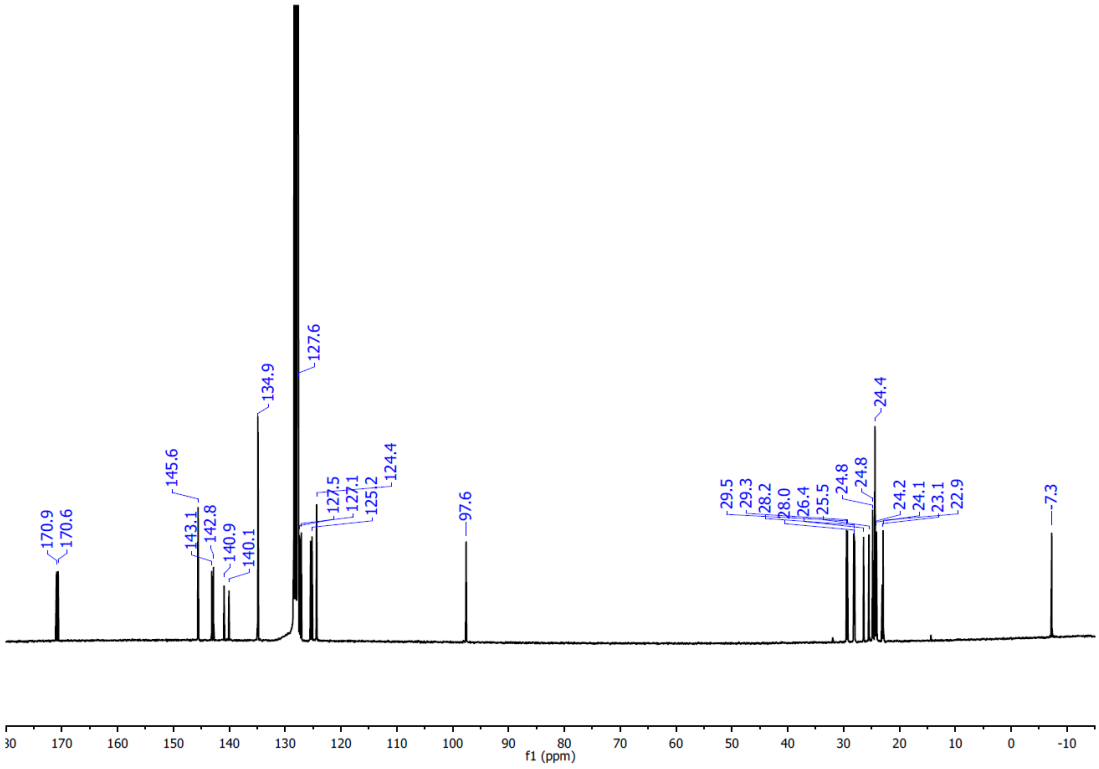

^{29}Si INEPT+ NMR Spectrum (119 MHz, C_6D_6)

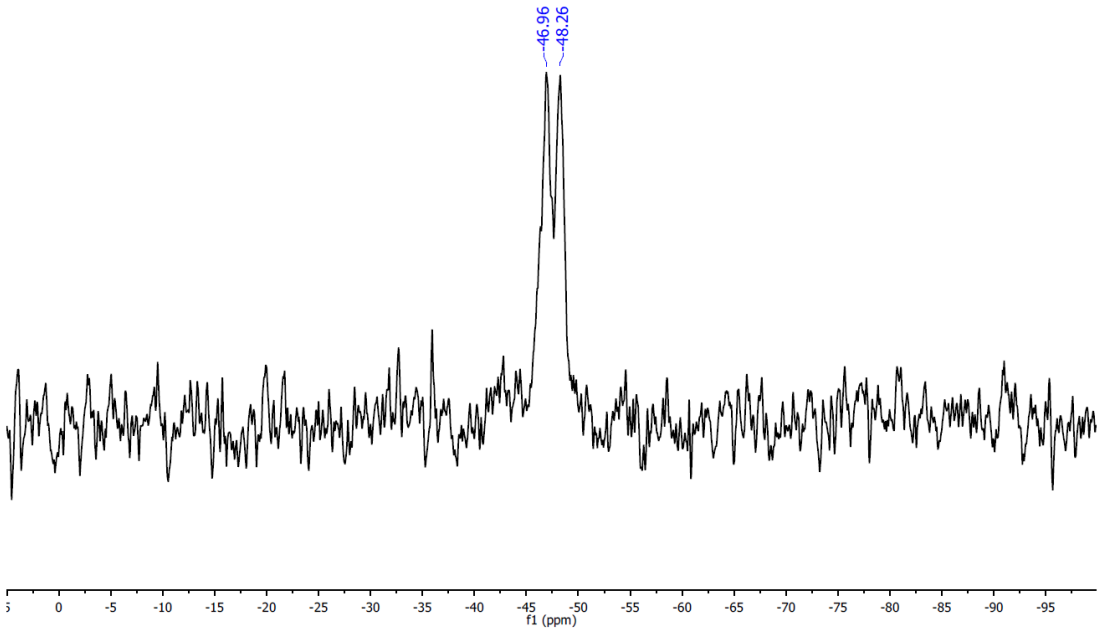

Figure 44. ^{1}H, ^{13}C{^{1}H}, and ^{29}Si INEPT+ NMR spectra of **III-4**.

^{1}H NMR Spectrum (300 MHz, C_6D_6)

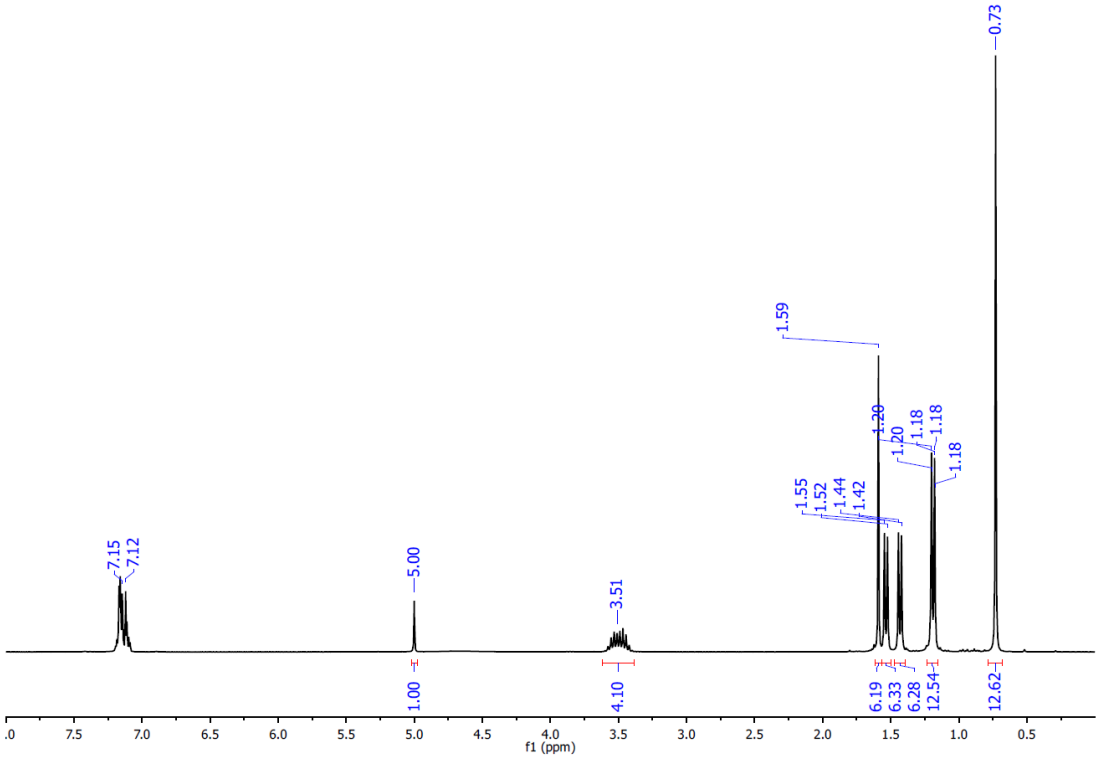

$^{13}C\{^{1}H\}$ NMR Spectrum (75 MHz, C_6D_6)

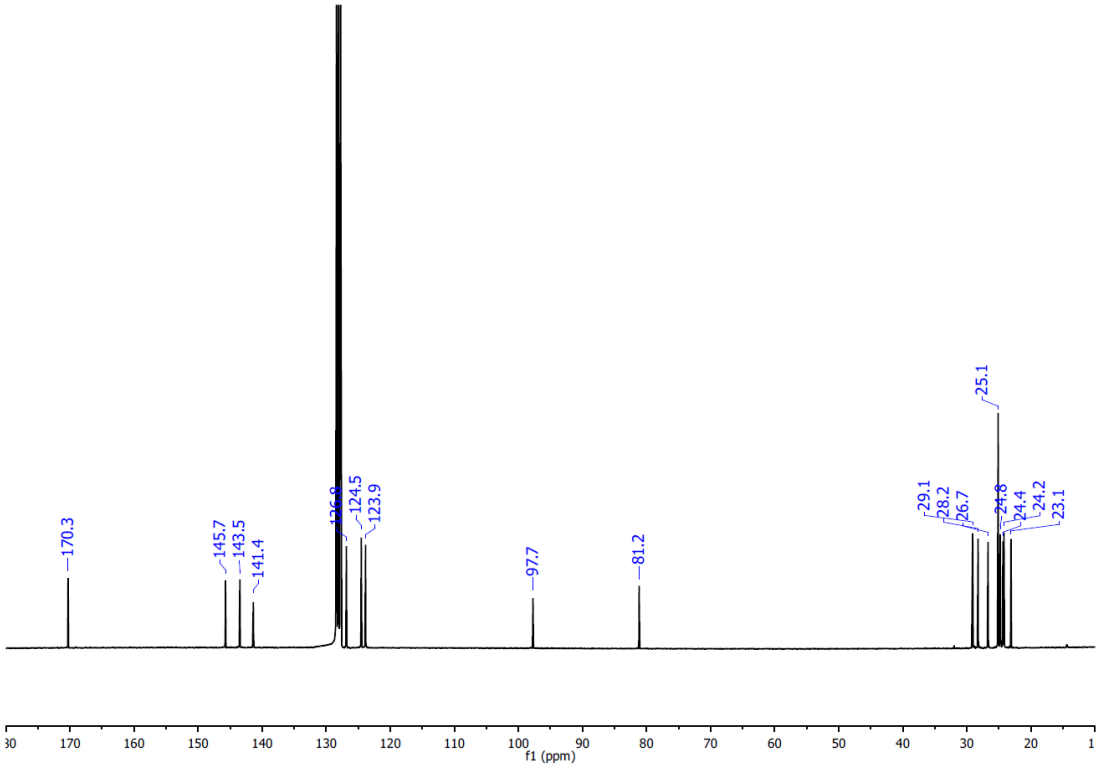

^{11}B NMR Spectrum (96 MHz, C_6D_6)

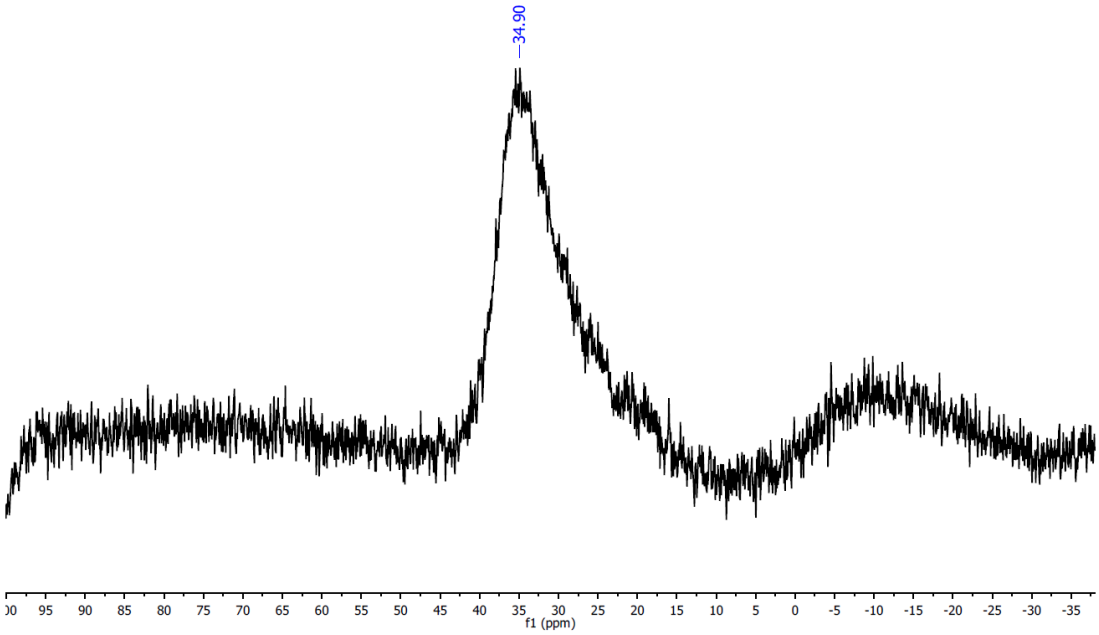

Figure 45. ^{1}H, $^{13}C\{^{1}H\}$, and ^{11}B NMR spectra of **III-5**.

^{1}H NMR Spectrum (600 MHz, C_6D_6)

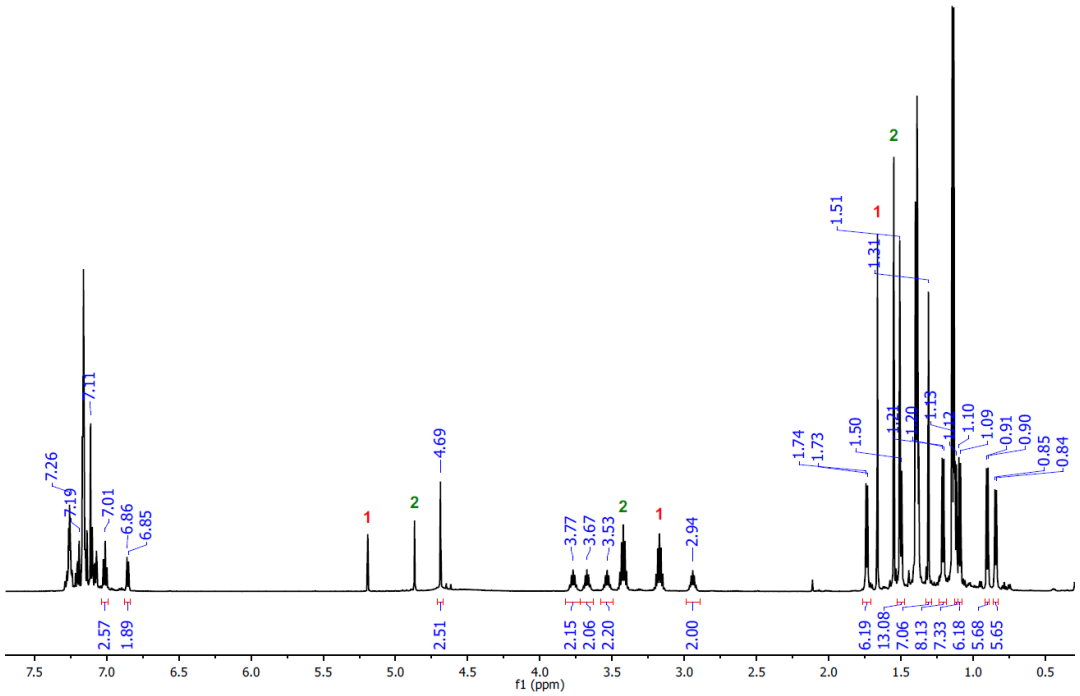

$^{13}C\{^{1}H\}$ NMR Spectrum (151 MHz, C_6D_6)

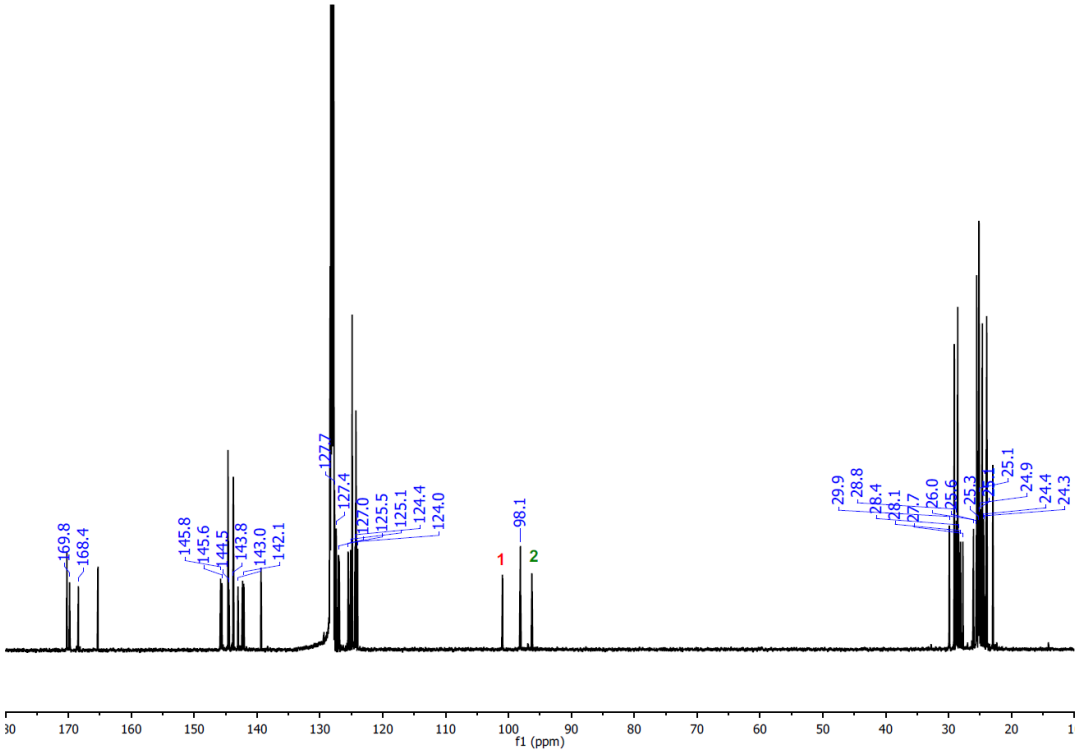

Figure 46. ^{1}H and $^{13}C\{^{1}H\}$ NMR spectra of **III-6**. The labels denote signals that belong to **III-1** (1) and **III-2** (2).

^{1}H NMR Spectrum (300 MHz, C_6D_6)

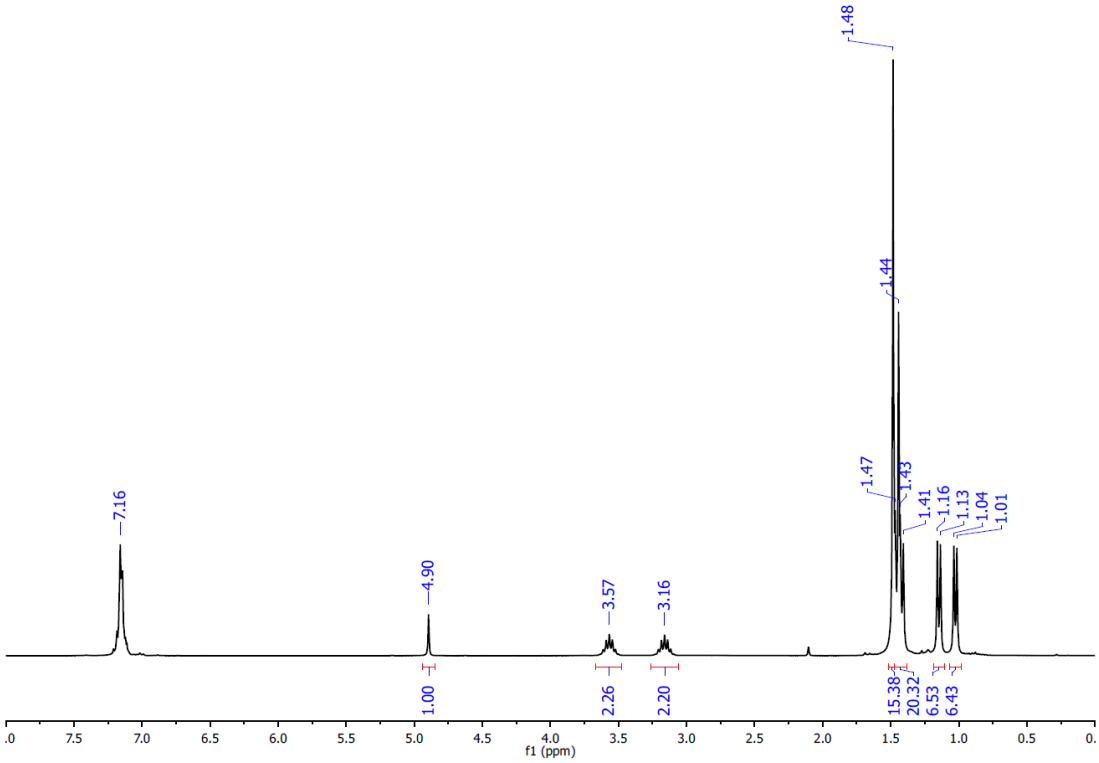

$^{13}C\{^{1}H\}$ NMR Spectrum (75 MHz, C_6D_6)

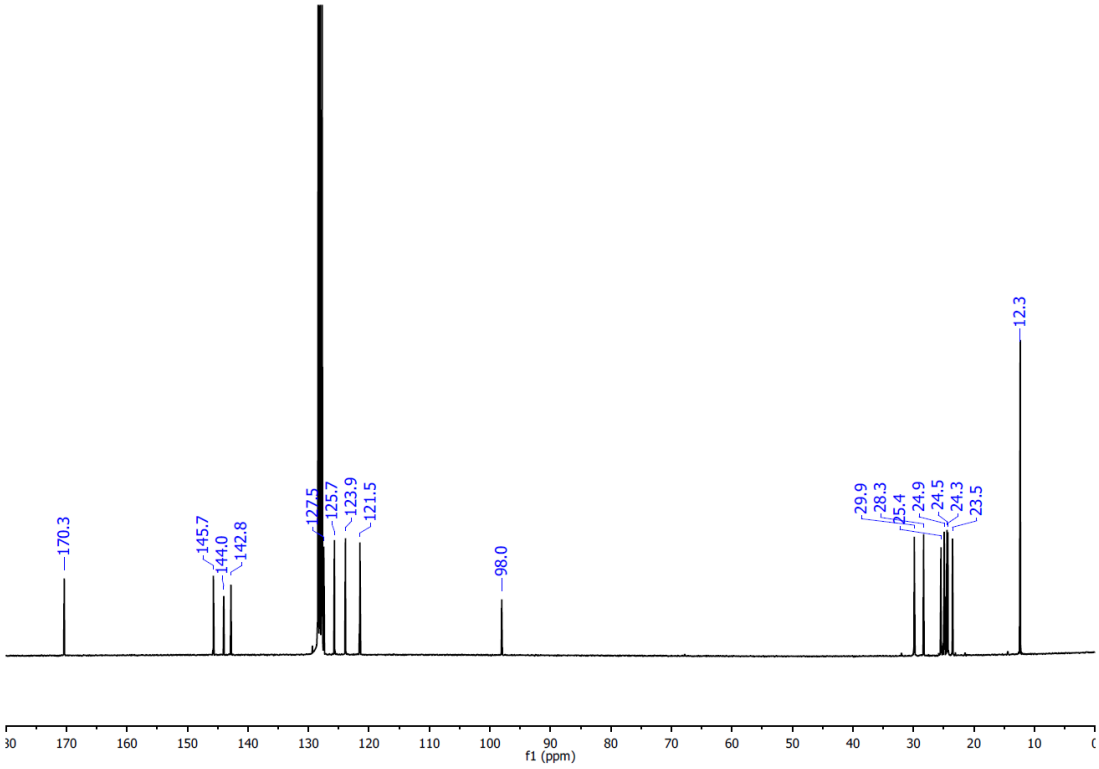

Figure 47. ^{1}H and $^{13}C\{^{1}H\}$ NMR spectra of **III-7**.

^{1}H NMR Spectrum (300 MHz, C_6D_6)

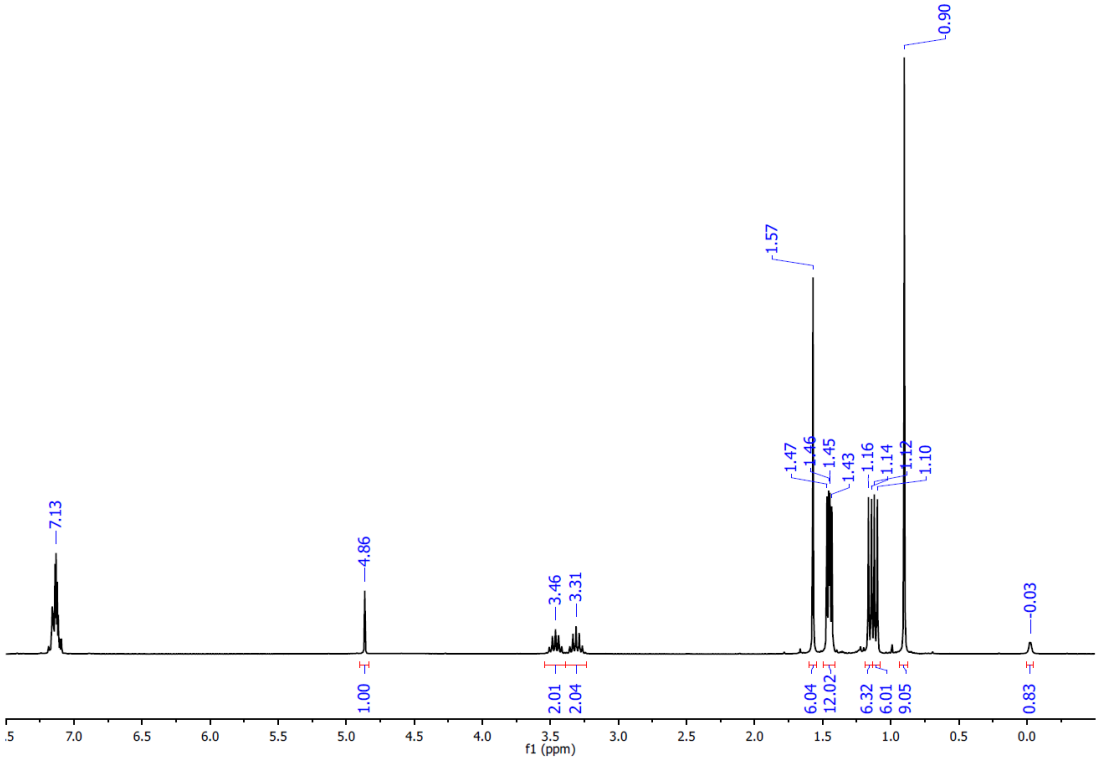

$^{13}C\{^{1}H\}$ NMR Spectrum (75 MHz, C_6D_6)

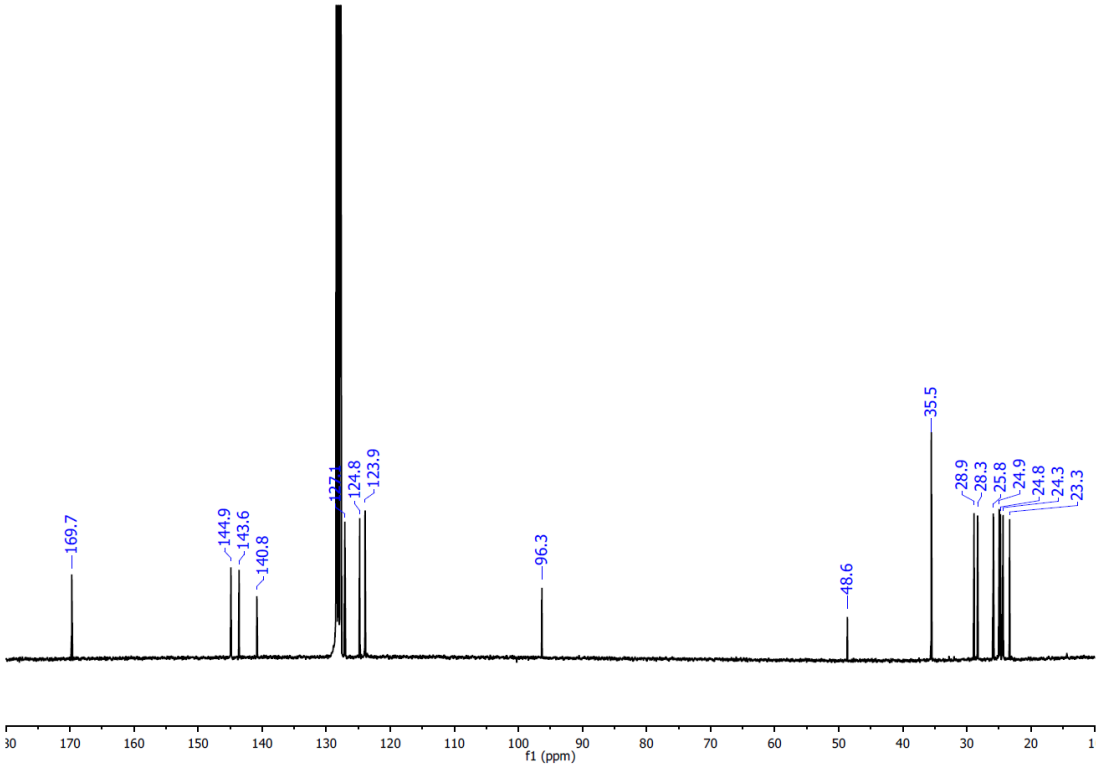

Figure 48. ^{1}H and $^{13}C\{^{1}H\}$ NMR spectra of **III-8**.

^{1}H NMR Spectrum (300 MHz, C_6D_6)

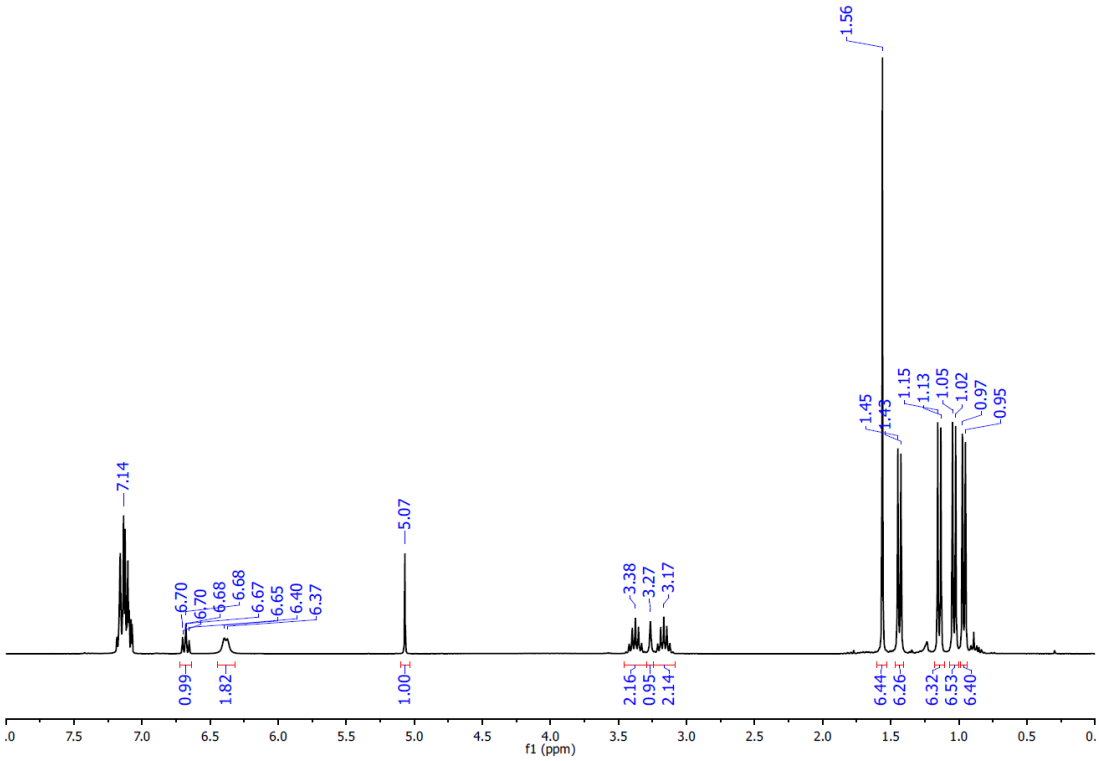

$^{13}C\{^{1}H\}$ NMR Spectrum (75 MHz, C_6D_6)

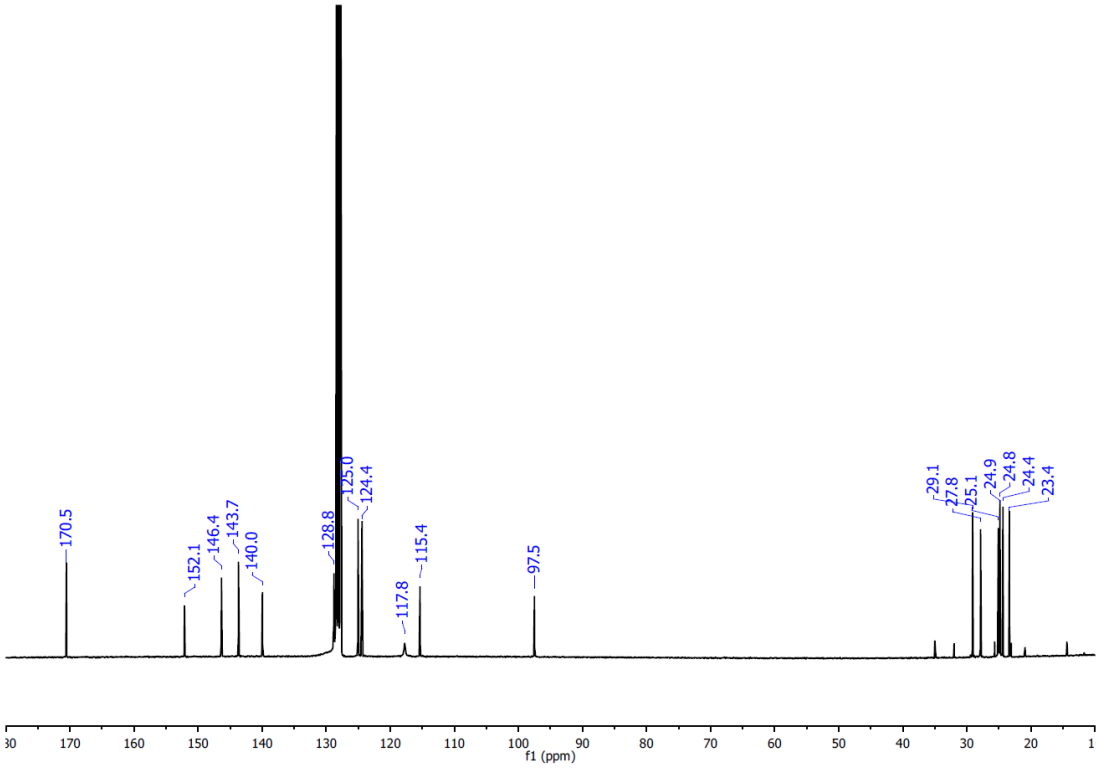

Figure 49. ^{1}H and $^{13}C\{^{1}H\}$ NMR spectra of **III-9**.

^{1}H NMR Spectrum (300 MHz, C_6D_6)

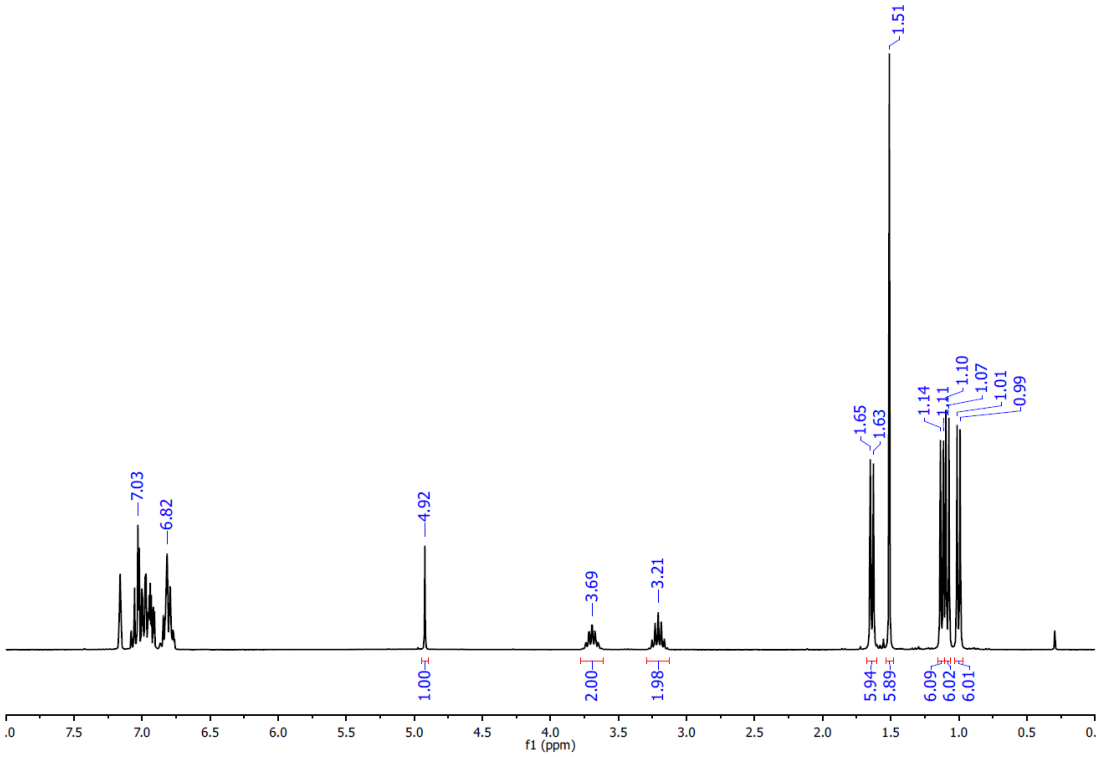

$^{13}C\{^{1}H\}$ NMR Spectrum (75 MHz, C_6D_6)

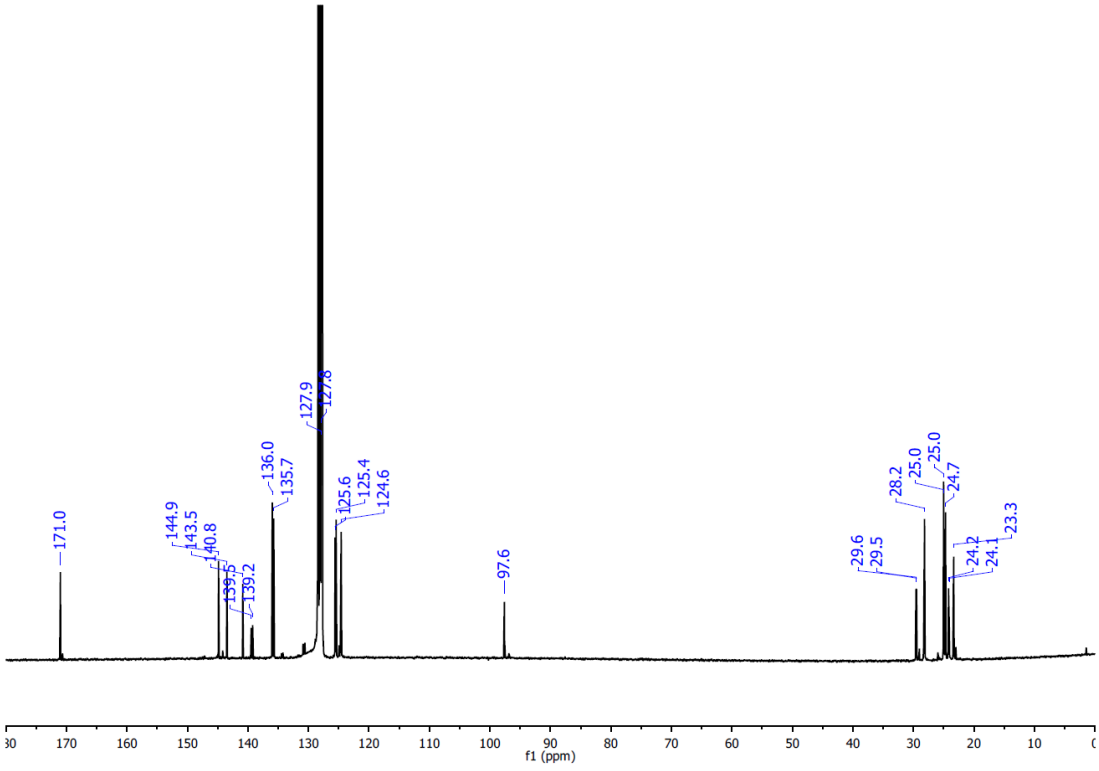

$^{31}P\{^{1}H\}$ NMR Spectrum (121 MHz, C_6D_6)

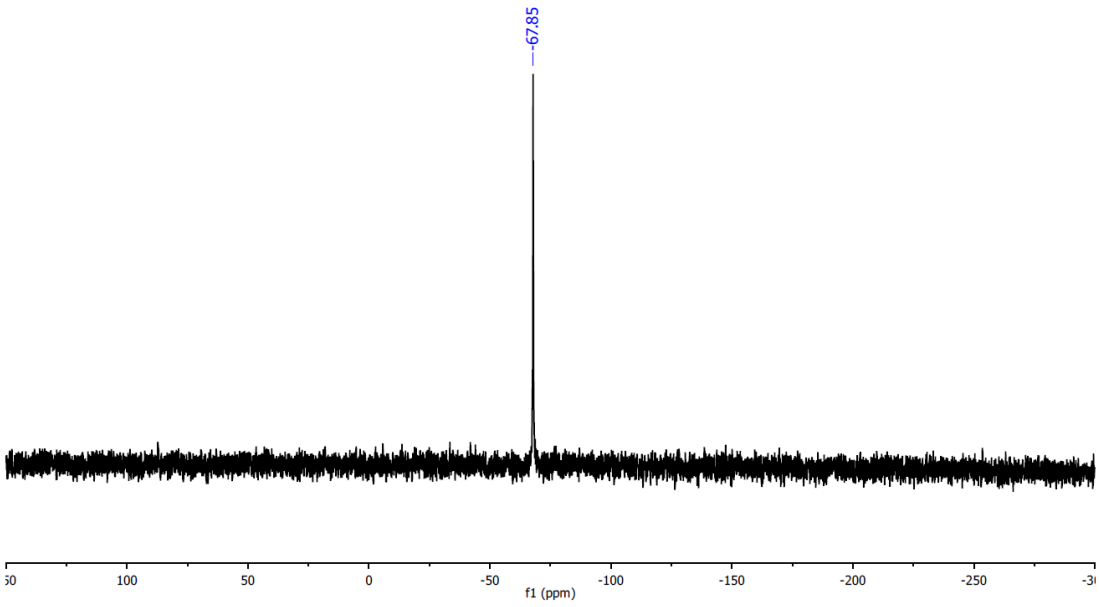

Figure 50. ^{1}H, $^{13}C\{^{1}H\}$, and $^{31}P\{^{1}H\}$ NMR spectra of **III-10**.

^{1}H NMR Spectrum (300 MHz, C_6D_6)

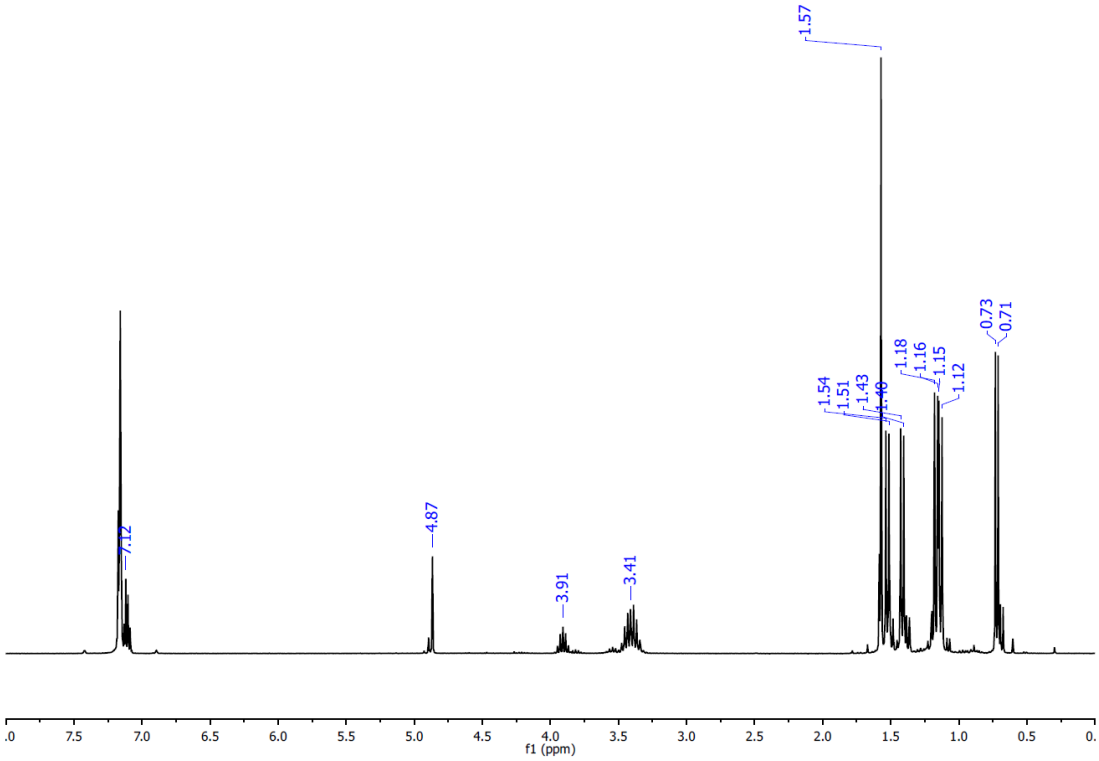

$^{13}C\{^{1}H\}$ NMR Spectrum (75 MHz, C_6D_6)

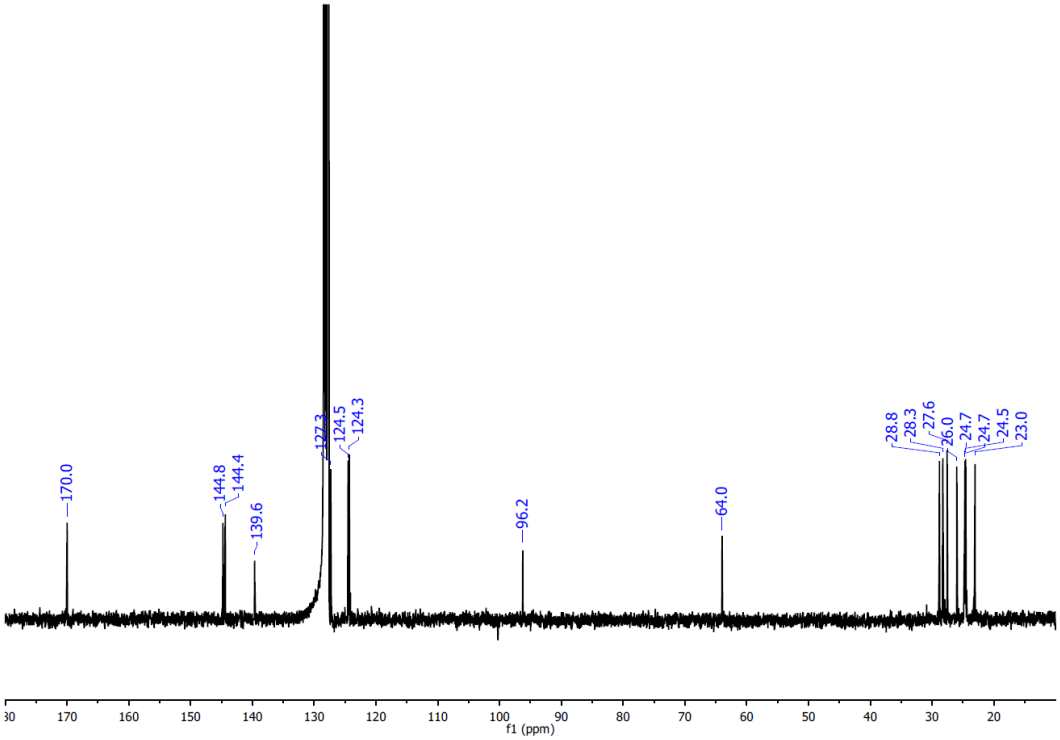

Figure 51. ^{1}H and $^{13}C\{^{1}H\}$ NMR spectra of **III-11**.

^{1}H NMR Spectrum (400 MHz, C_6D_6)

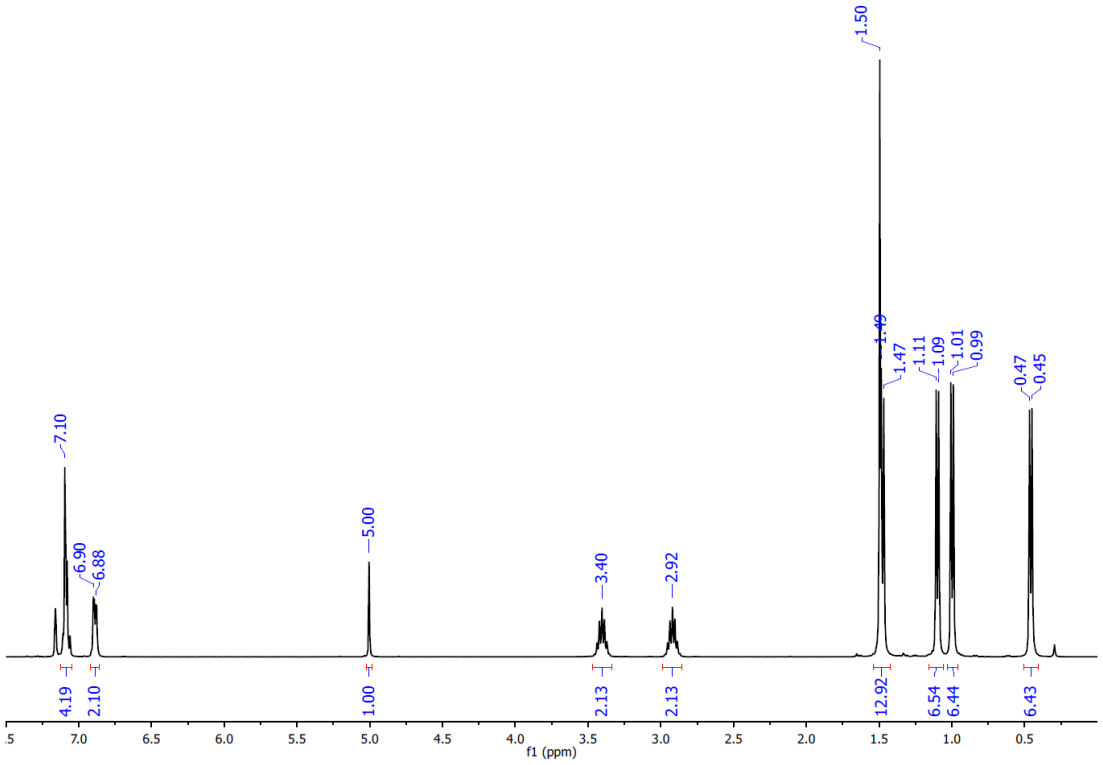

$^{13}C\{^{1}H\}$ NMR Spectrum (101 MHz, C_6D_6)

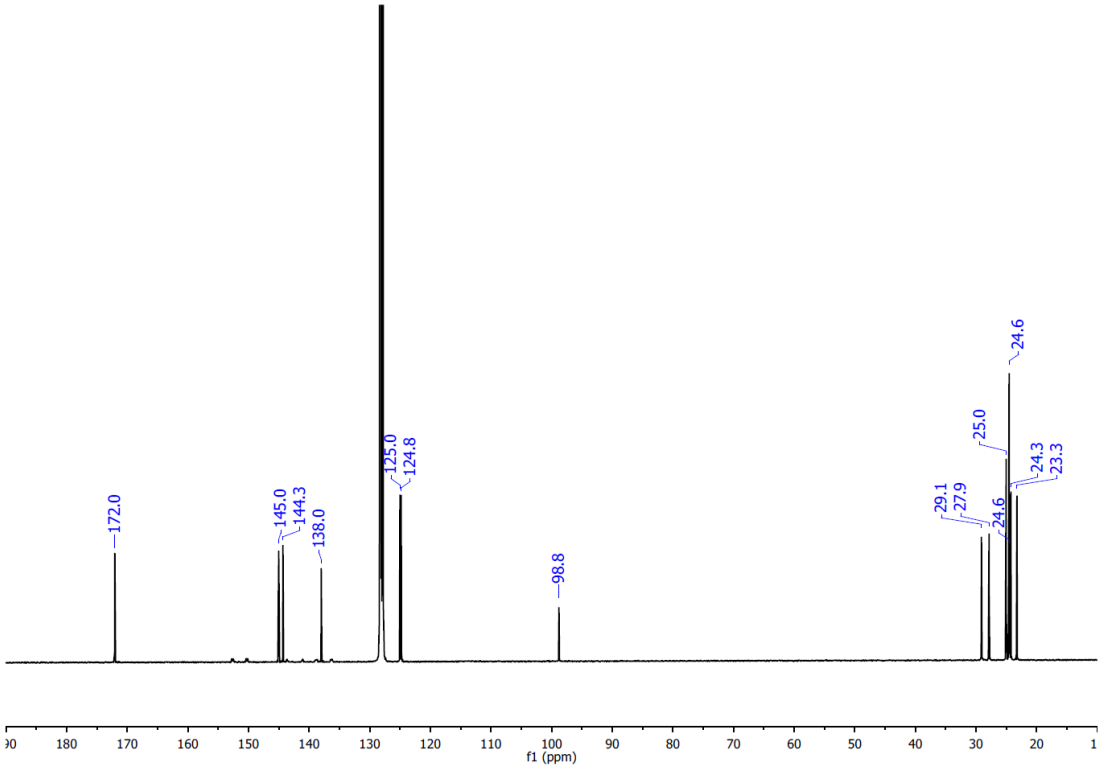

^{19}F NMR Spectrum (377 MHz, C_6D_6)

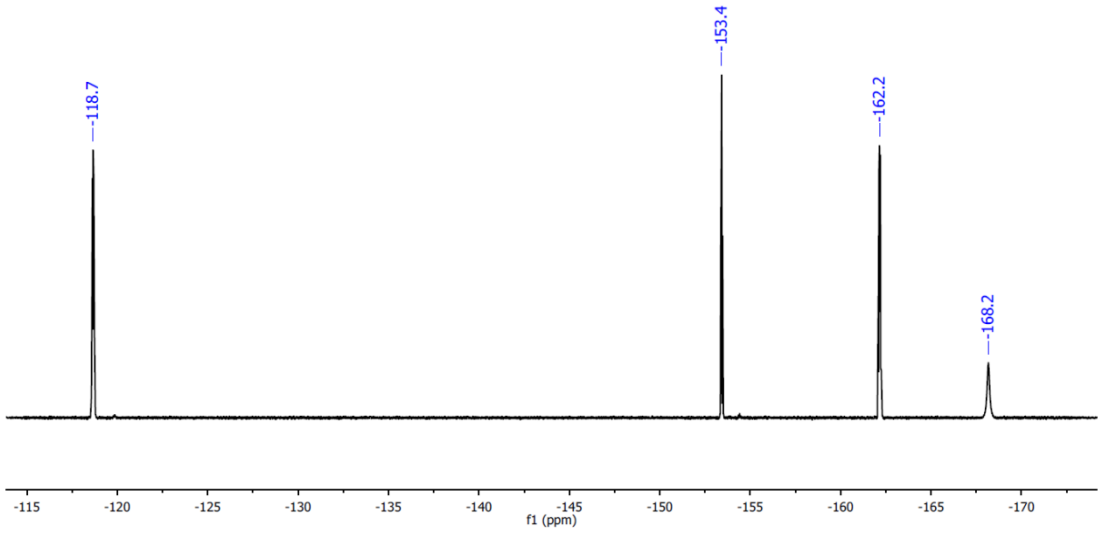

Figure 52. ^{1}H, $^{13}C\{^{1}H\}$, and ^{19}F NMR spectra of **III-12**.

^{1}H NMR Spectrum (400 MHz, C_6D_6)

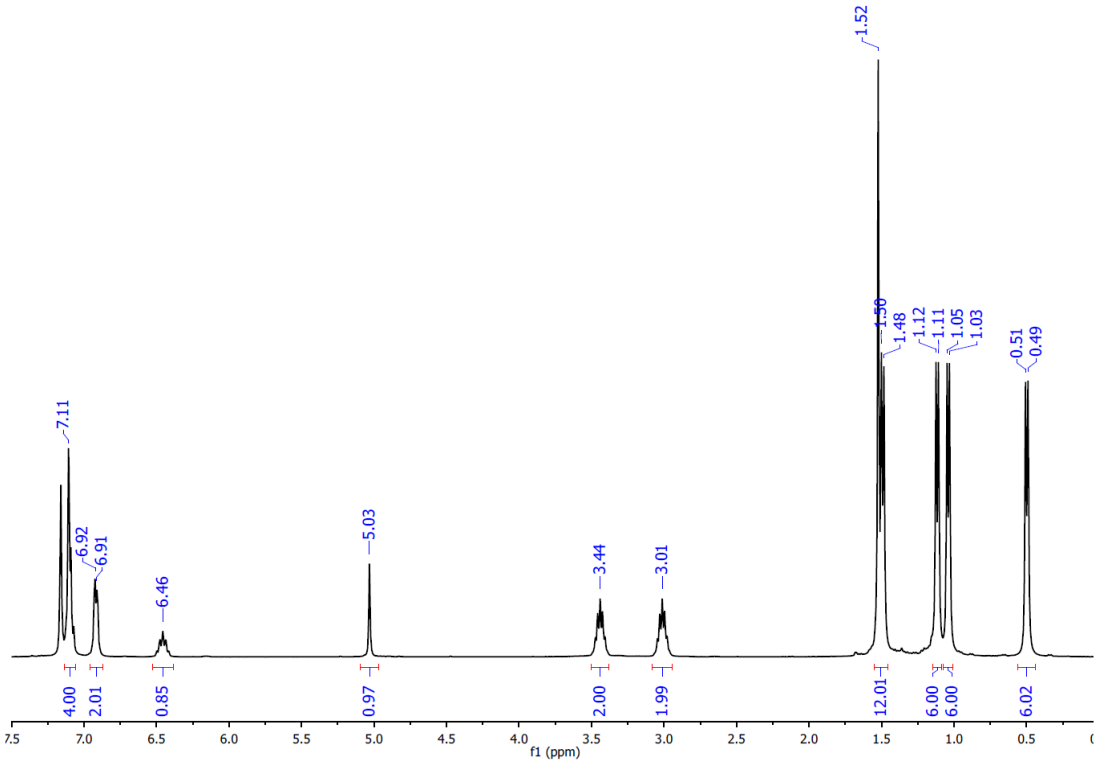

$^{13}C\{^{1}H\}$ NMR Spectrum (101 MHz, C_6D_6)

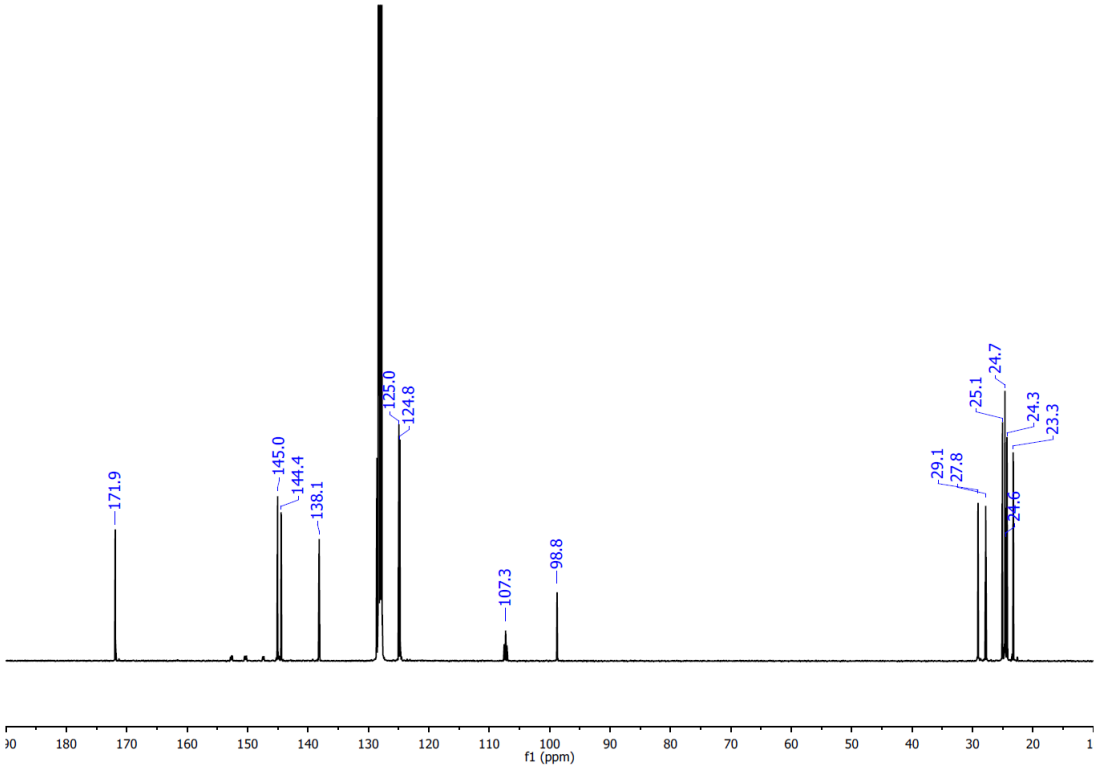

^{19}F NMR Spectrum (377 MHz, C_6D_6)

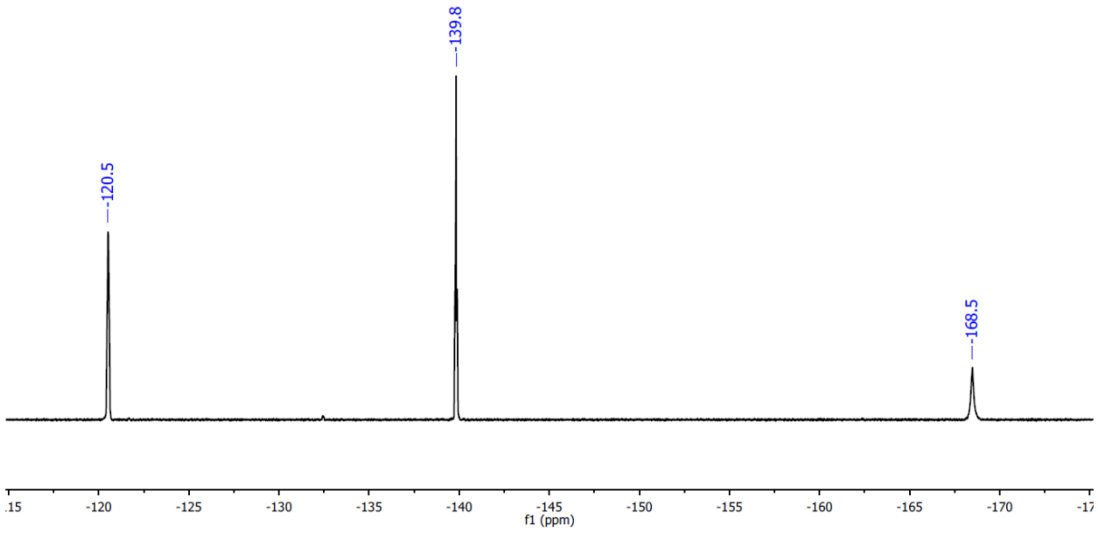

Figure 53. ^{1}H, $^{13}C\{^{1}H\}$, and ^{19}F NMR spectra of **III-13**.

^{1}H NMR Spectrum (400 MHz, C_6D_6)

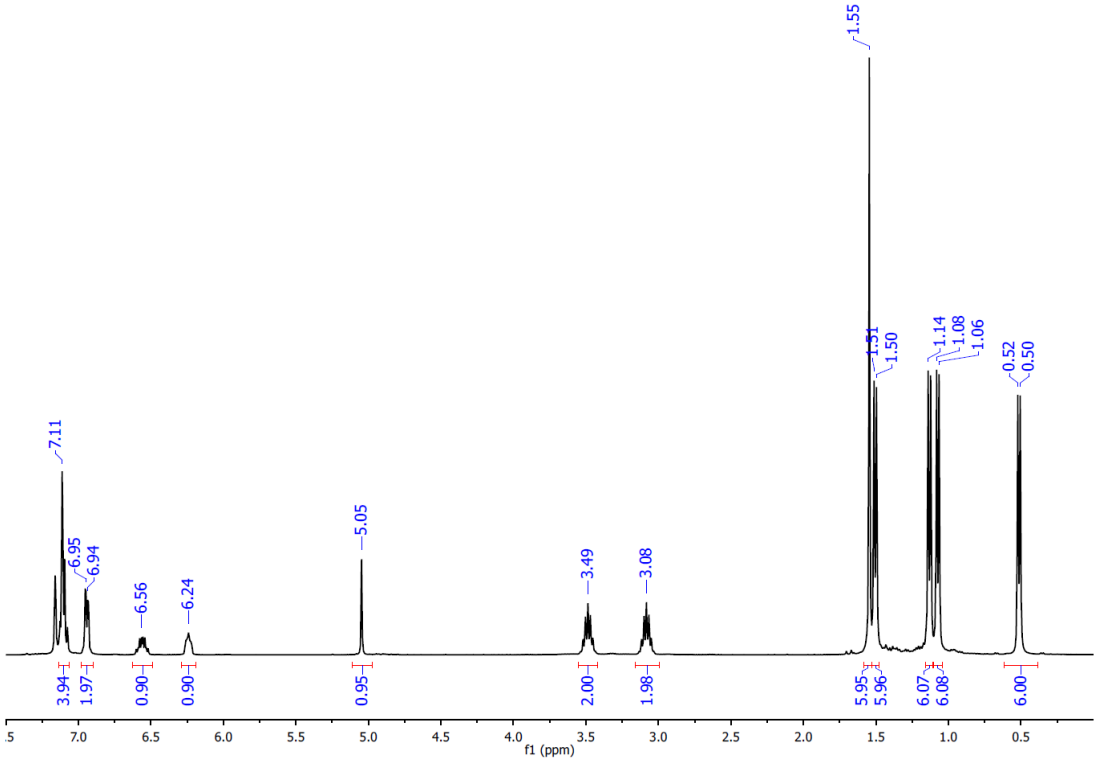

$^{13}C\{^{1}H\}$ NMR Spectrum (101 MHz, C_6D_6)

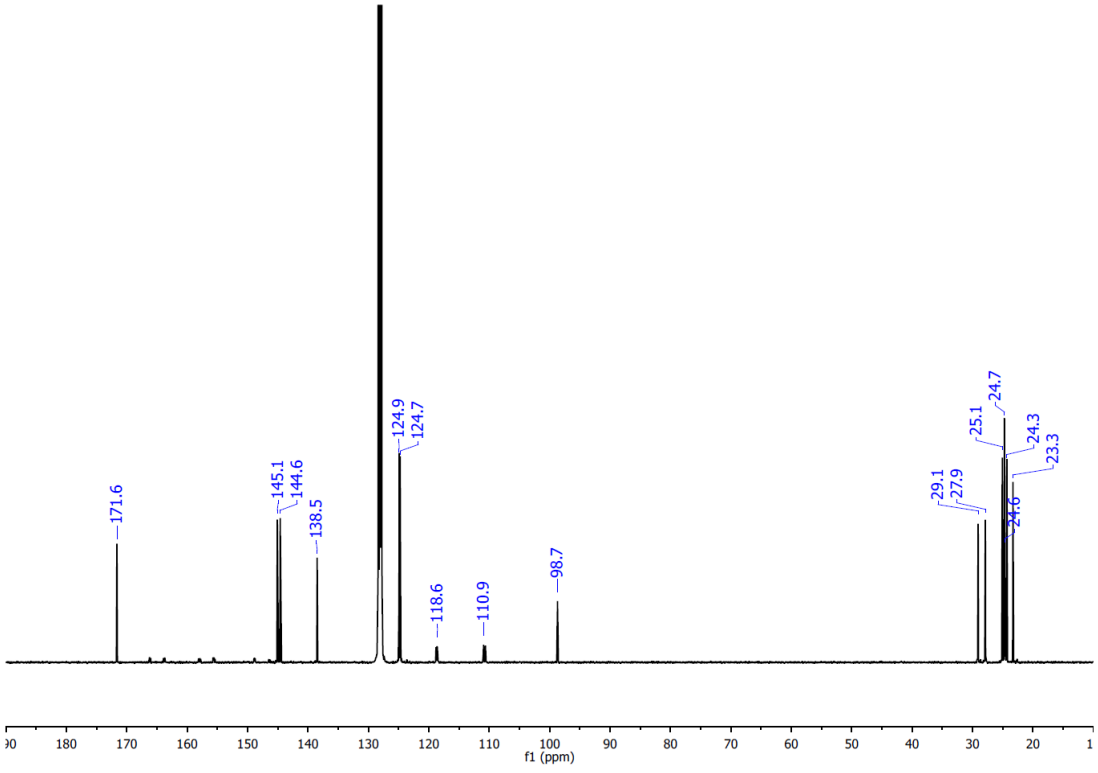

^{19}F NMR Spectrum (377 MHz, C_6D_6)

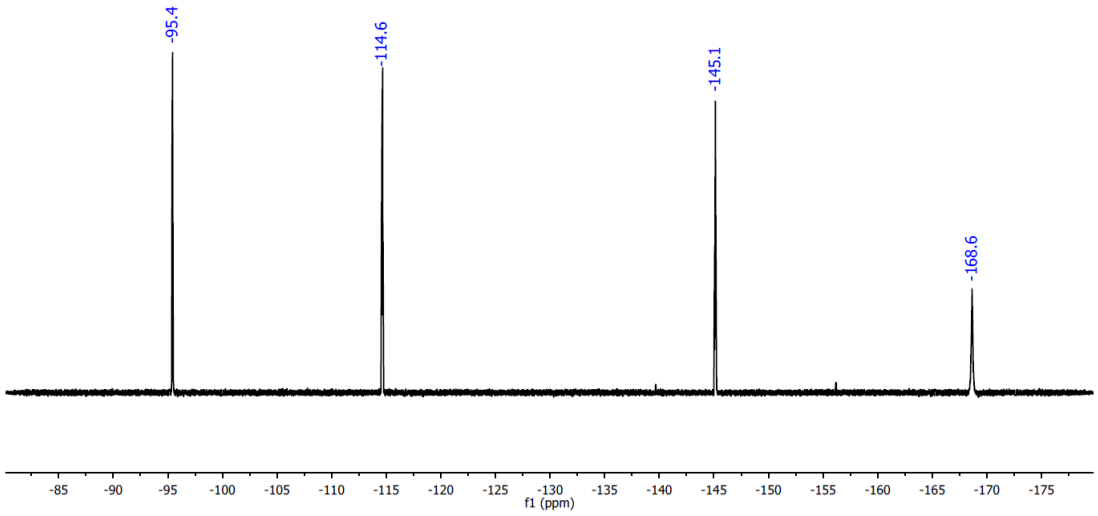

Figure 54. ^{1}H, $^{13}C\{^{1}H\}$, and ^{19}F NMR spectra of **III-14**.

^{1}H NMR Spectrum (400 MHz, C_6D_6)

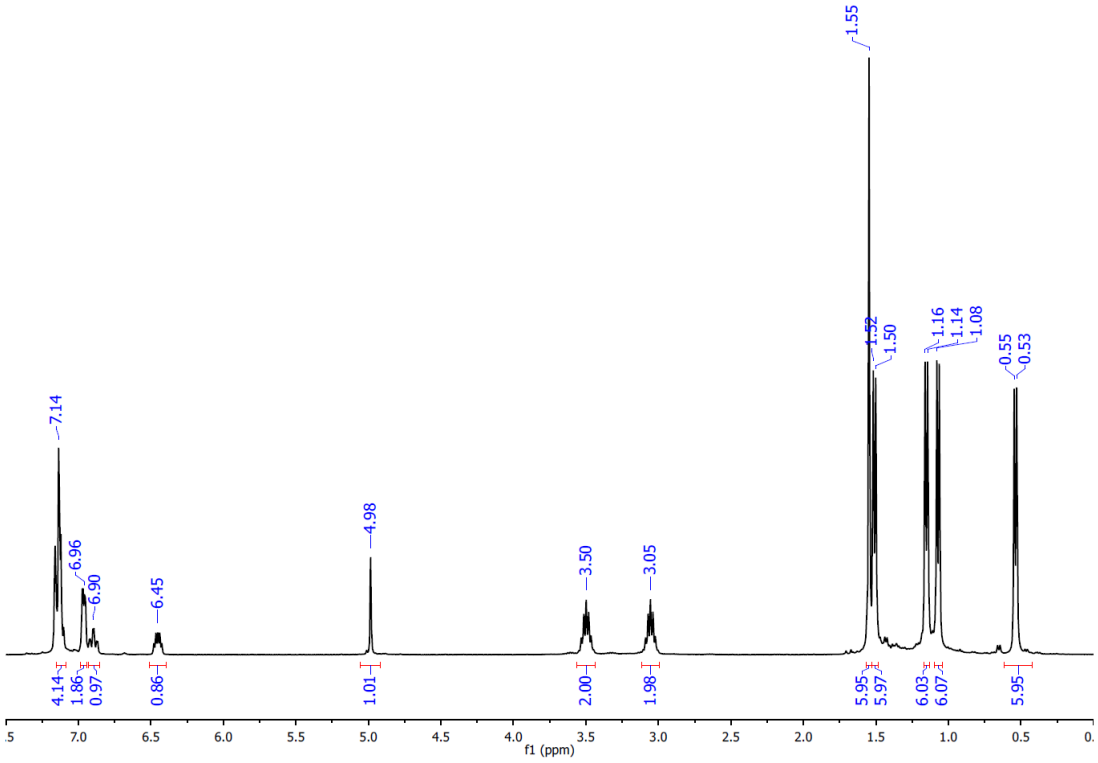

$^{13}C\{^{1}H\}$ NMR Spectrum (101 MHz, C_6D_6)

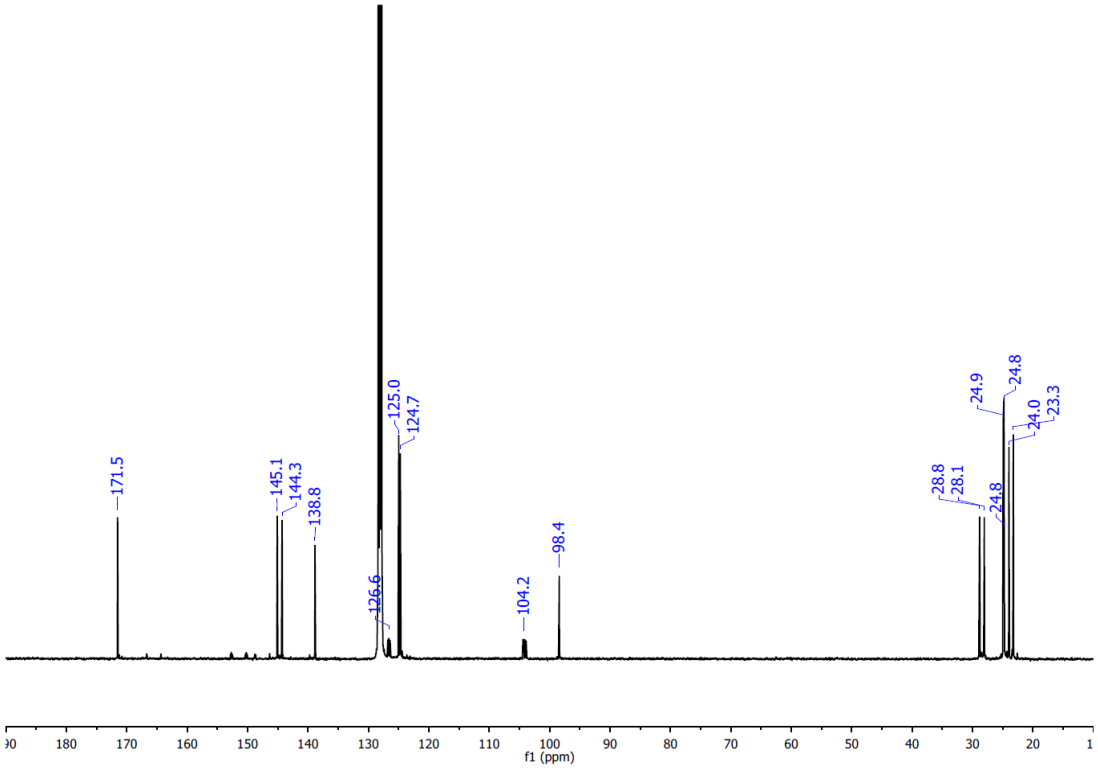

^{19}F NMR Spectrum (377 MHz, C_6D_6)

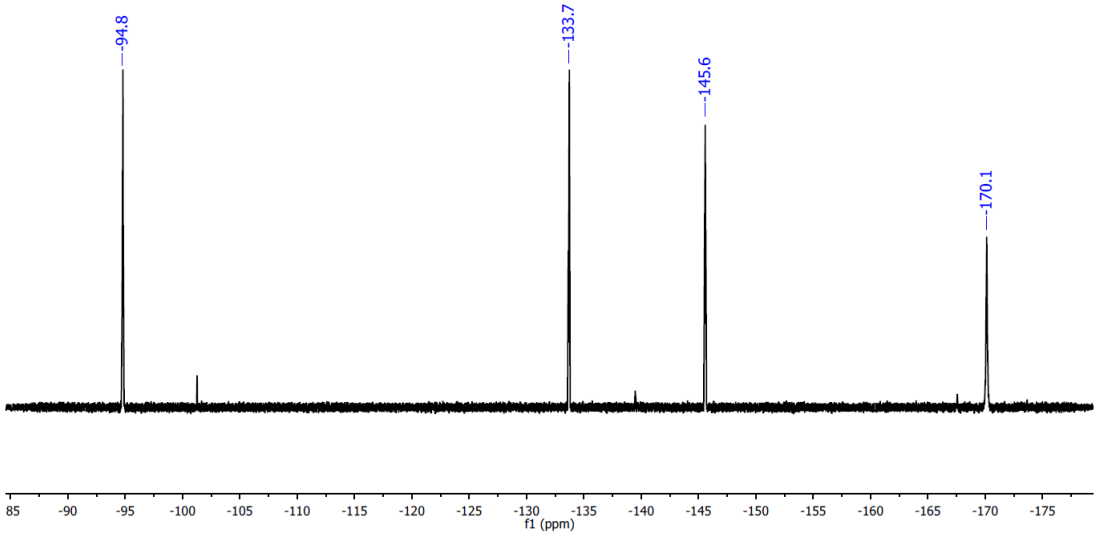

Figure 55. ^{1}H, $^{13}C\{^{1}H\}$, and ^{19}F NMR spectra of **III-15**.

^{1}H NMR Spectrum (400 MHz, C_6D_6)

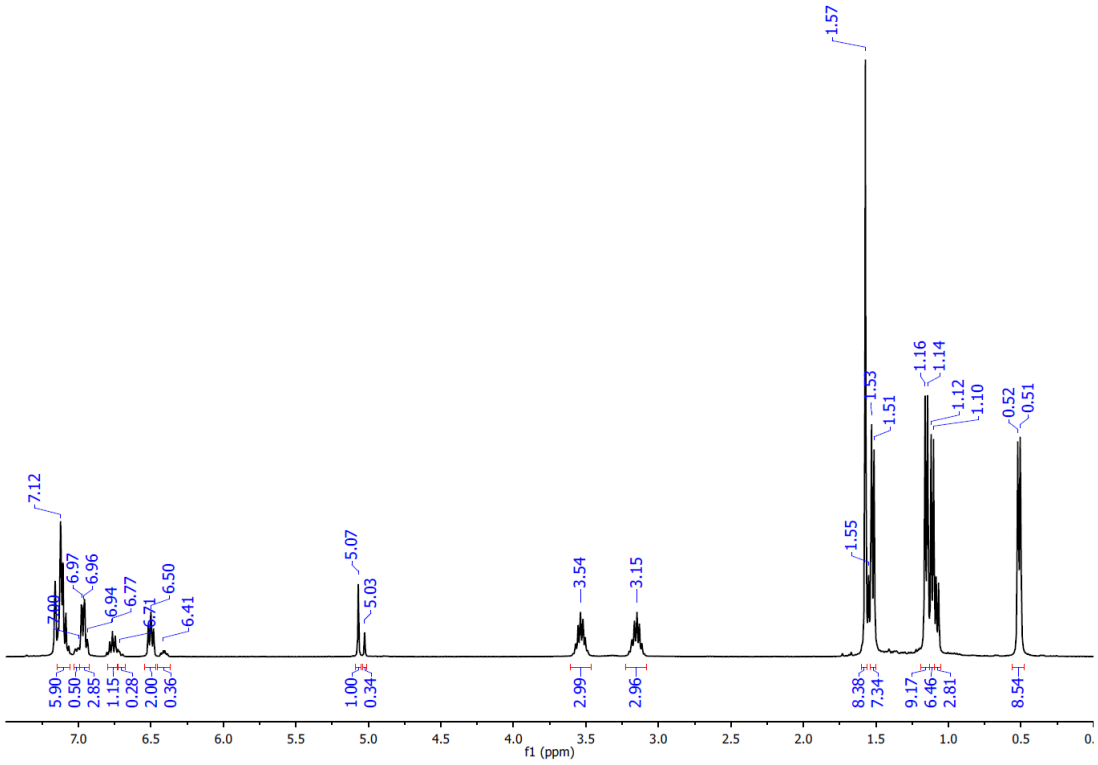

$^{13}C\{^{1}H\}$ NMR Spectrum (101 MHz, C_6D_6)

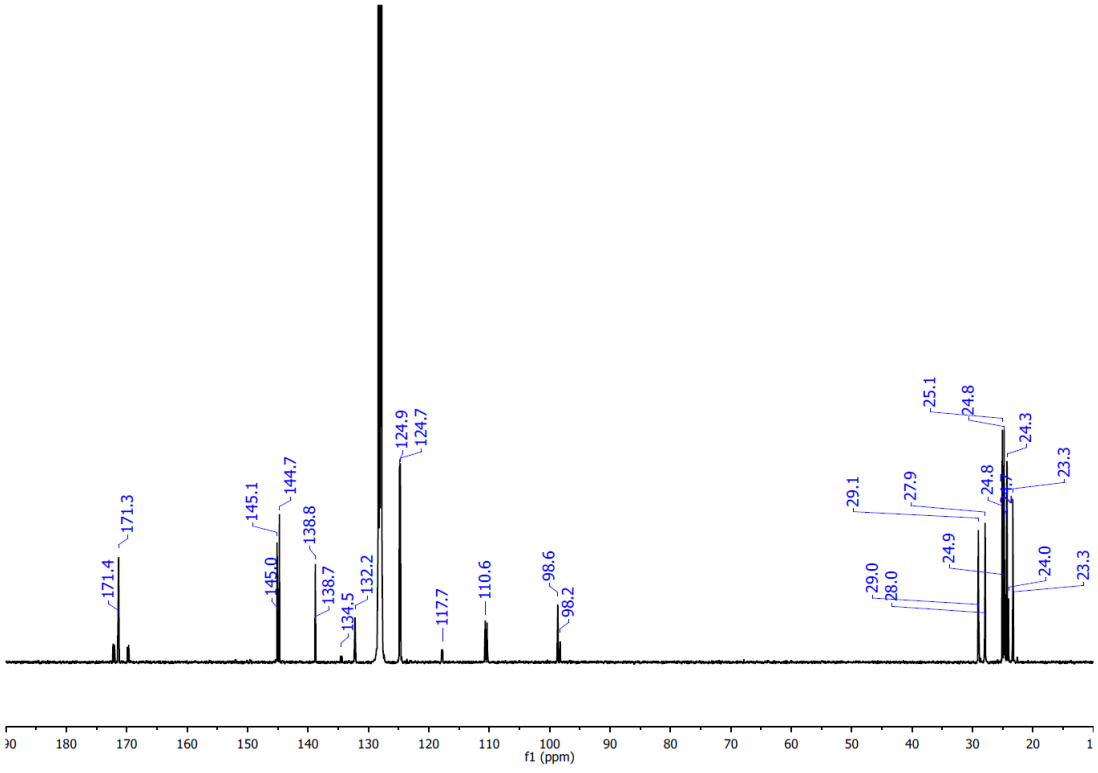

^{19}F NMR Spectrum (377 MHz, C_6D_6)

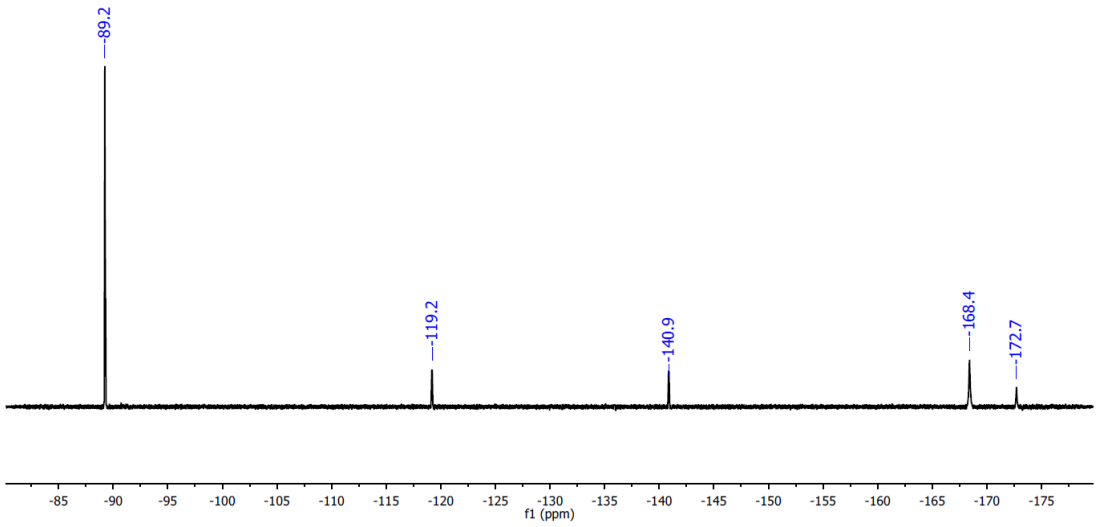

Figure 56. ^{1}H, $^{13}C\{^{1}H\}$, and ^{19}F NMR spectra of **III-16-1** and **III-16-2**.

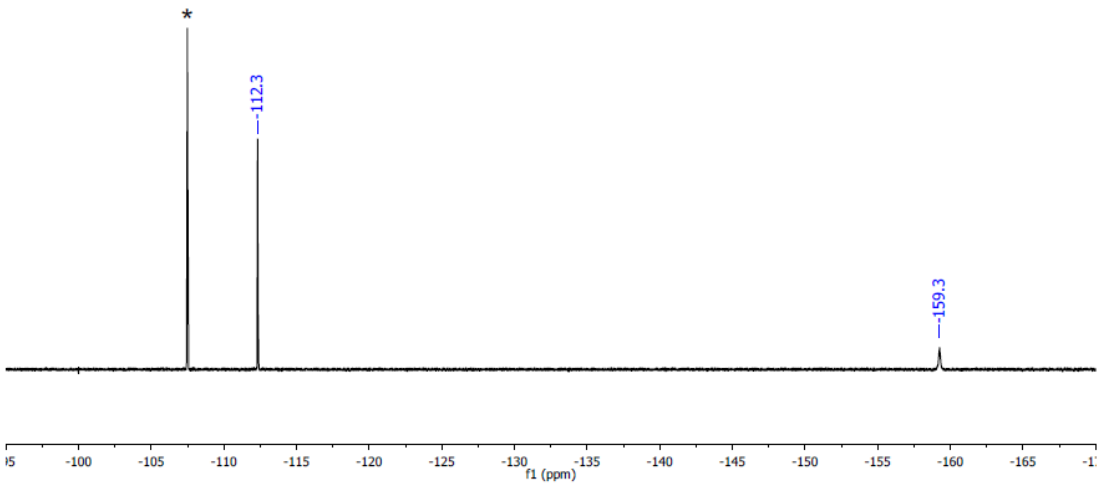

Figure 57. ^{19}F NMR spectrum (377 MHz, C_6D_6) of **III-17**. * denotes unreacted 1,3,5-trifluorobenzene.

^{1}H NMR Spectrum (400 MHz, C_6D_6)

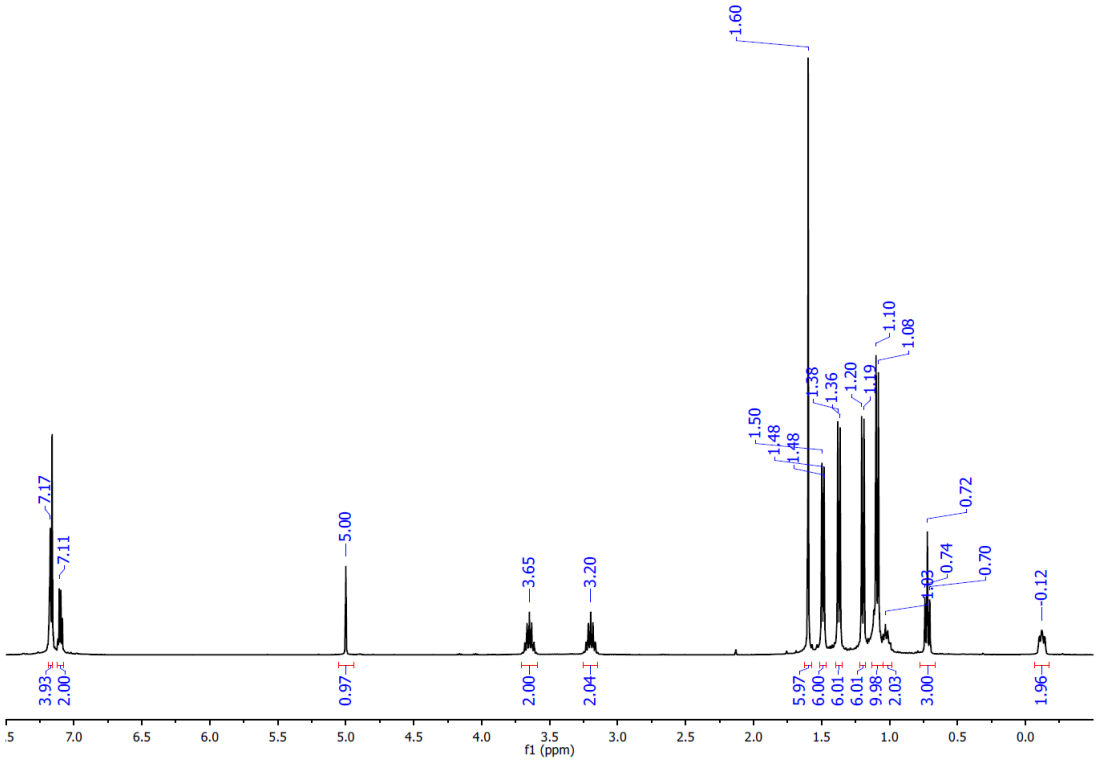

$^{13}C\{^{1}H\}$ NMR Spectrum (101 MHz, C_6D_6)

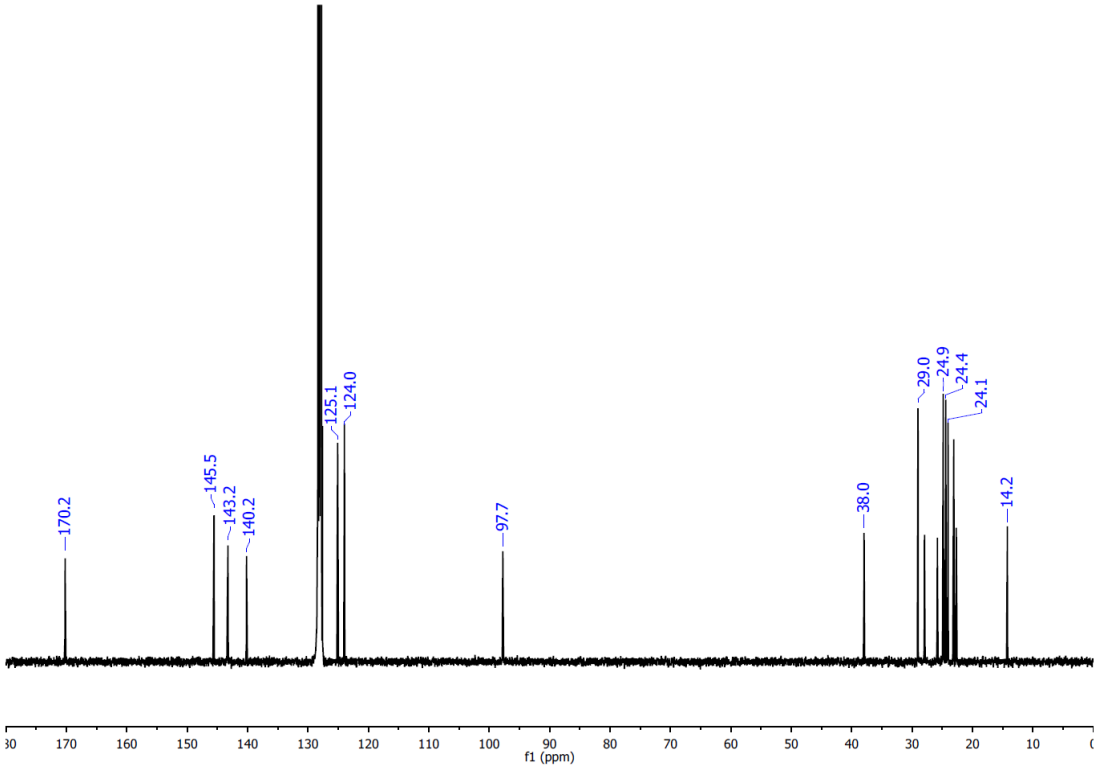

^{19}F NMR Spectrum (377 MHz, C_6D_6)

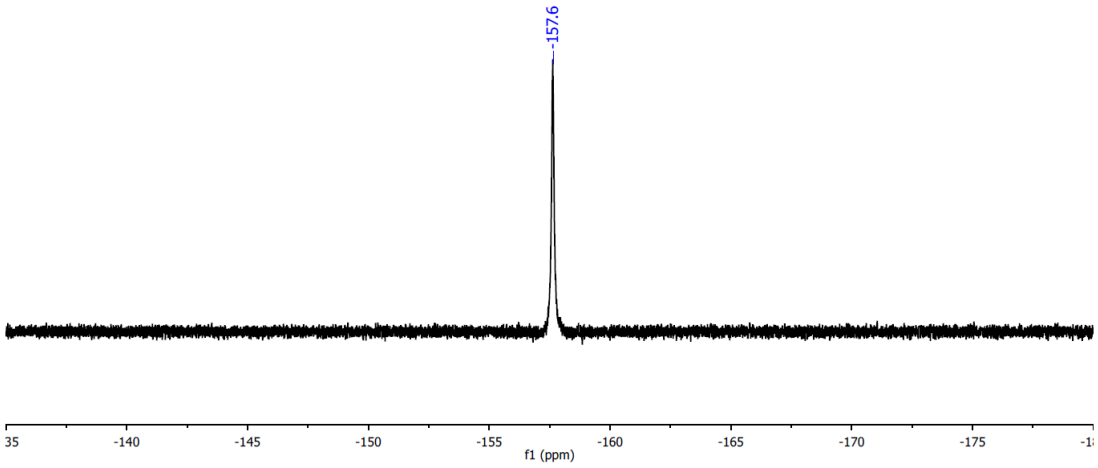

Figure 58. ^{1}H, $^{13}C\{^{1}H\}$, and ^{19}F NMR spectra of **III-18**.

^{1}H NMR Spectrum (400 MHz, C_6D_6)

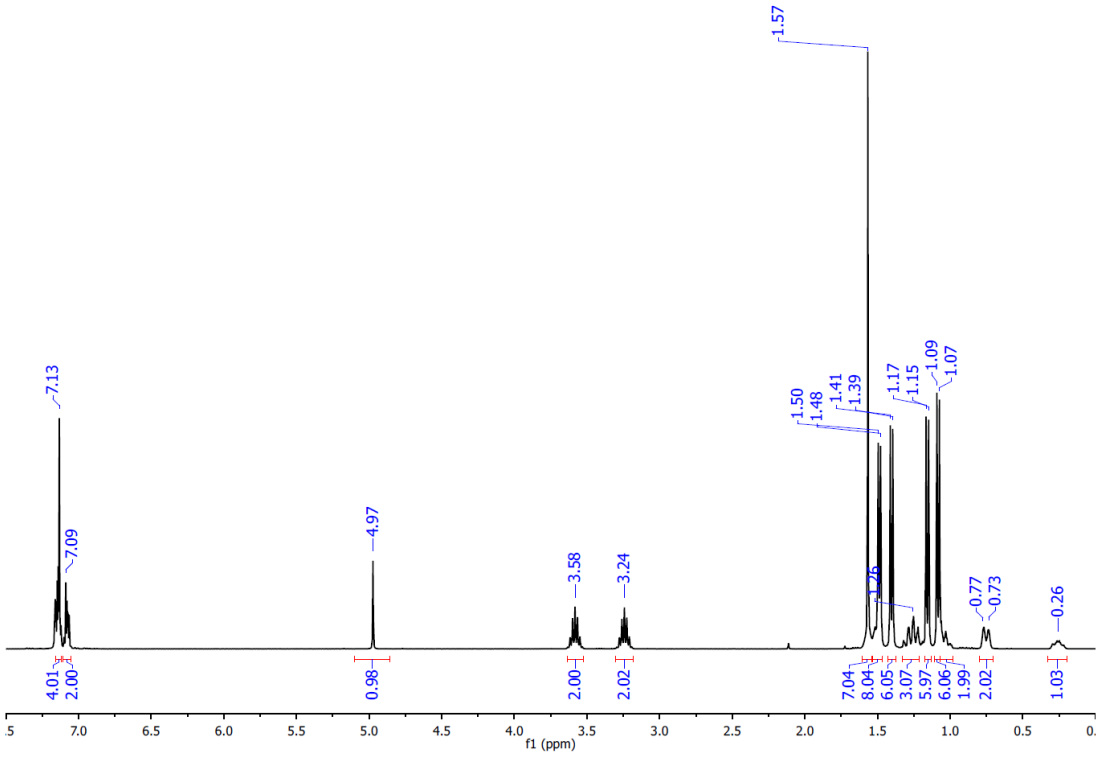

$^{13}C\{^{1}H\}$ NMR Spectrum (101 MHz, C_6D_6)

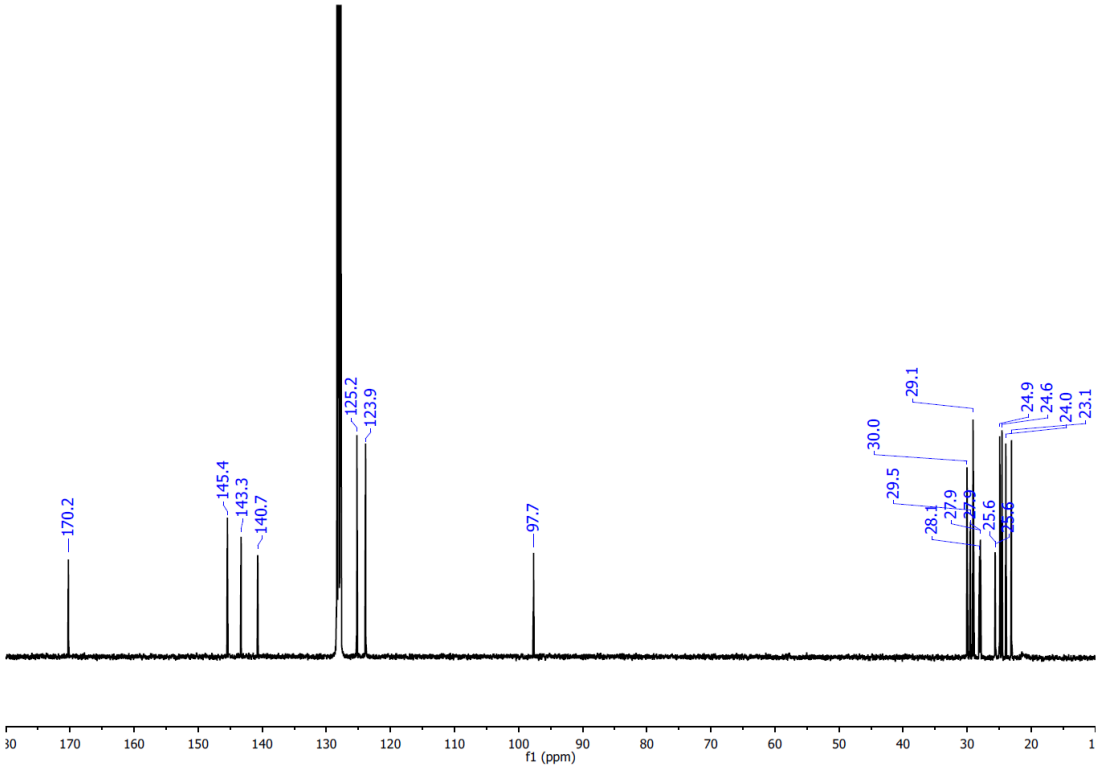

^{19}F NMR Spectrum (377 MHz, C_6D_6)

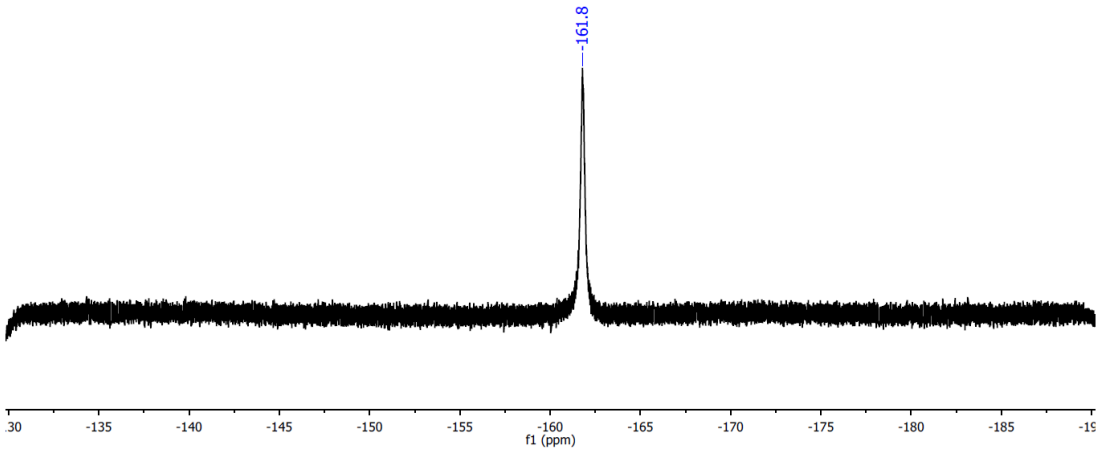

Figure 59. ^{1}H, $^{13}C\{^{1}H\}$, and ^{19}F NMR spectra of **III-19**.

^{1}H NMR Spectrum (400 MHz, C_6D_6)

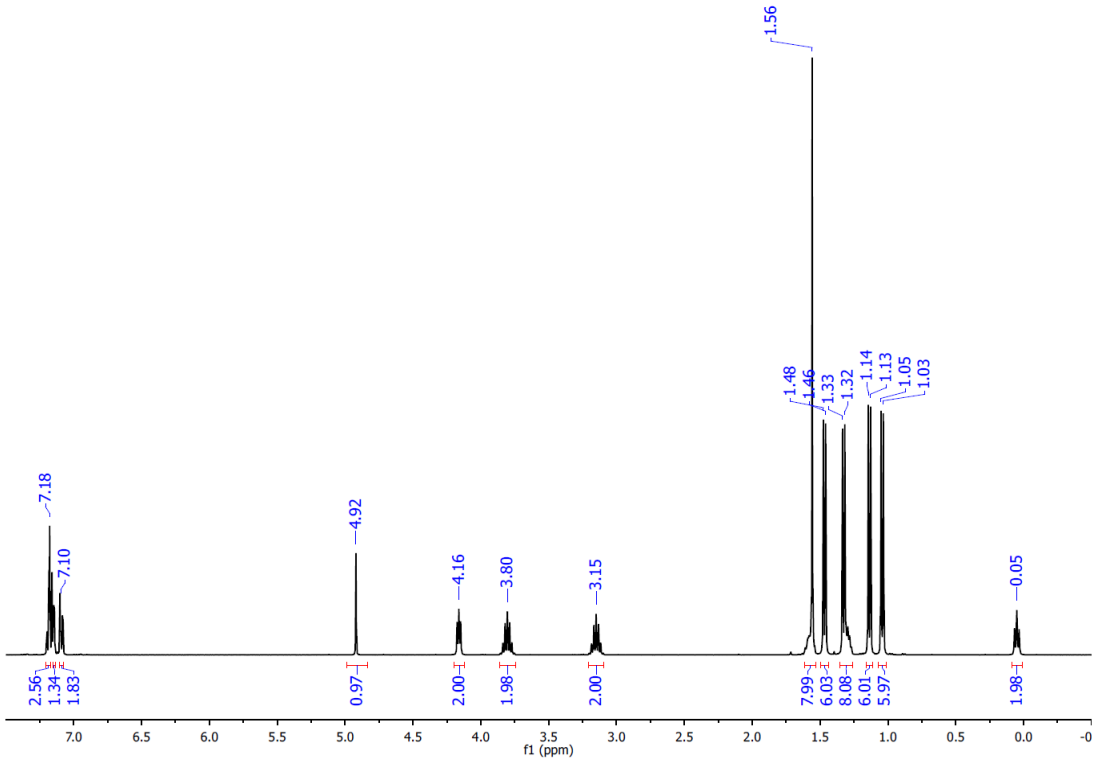

$^{13}C\{^{1}H\}$ NMR Spectrum (101 MHz, C_6D_6)

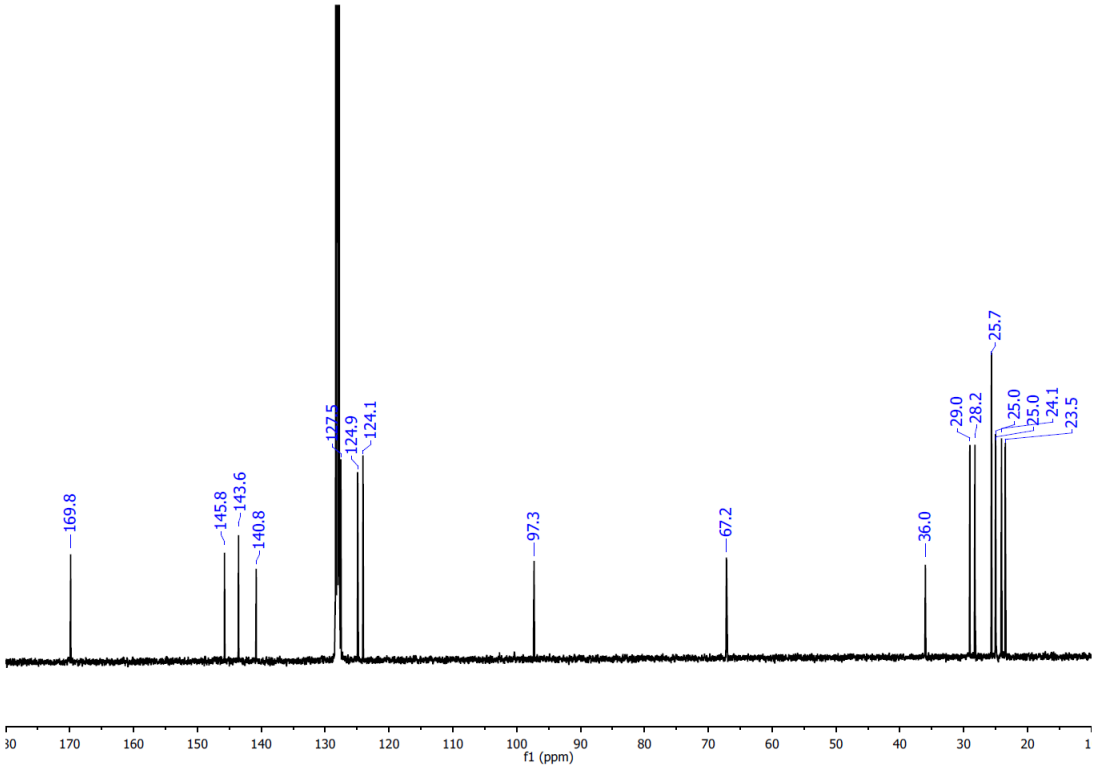

Figure 60. ^{1}H and $^{13}C\{^{1}H\}$ NMR spectra of **III-20**.

^{1}H NMR Spectrum (400 MHz, C_6D_6)

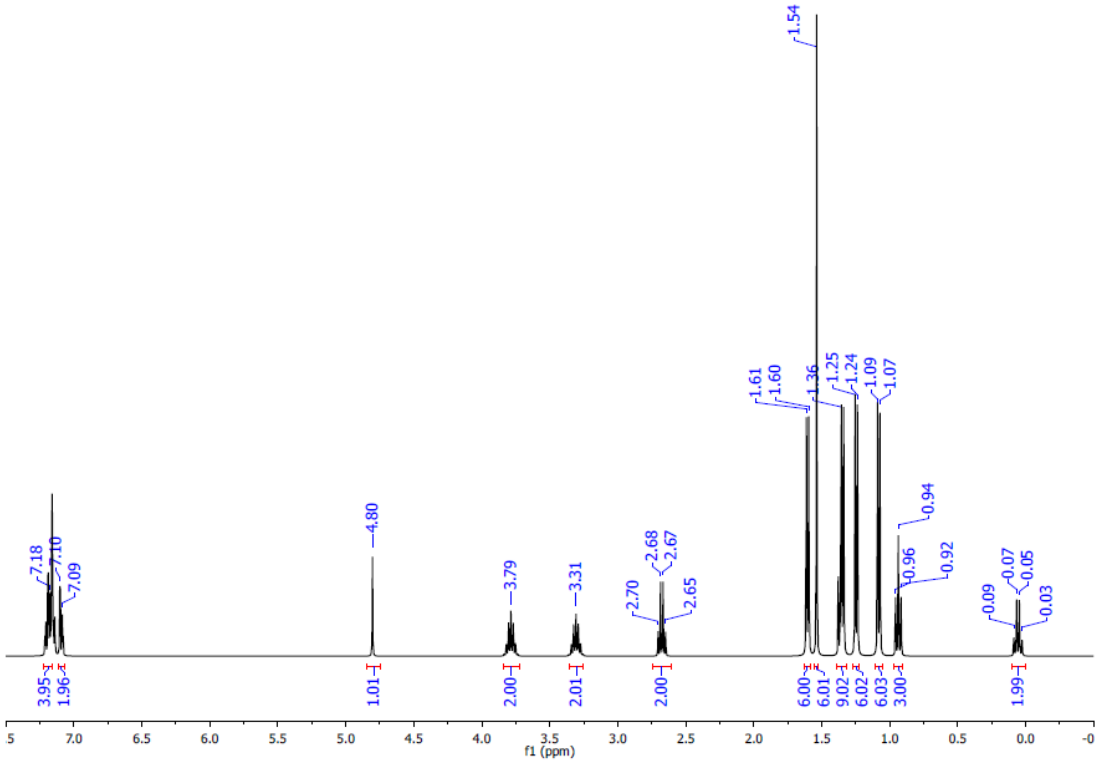

$^{13}C\{^{1}H\}$ NMR Spectrum (101 MHz, C_6D_6)

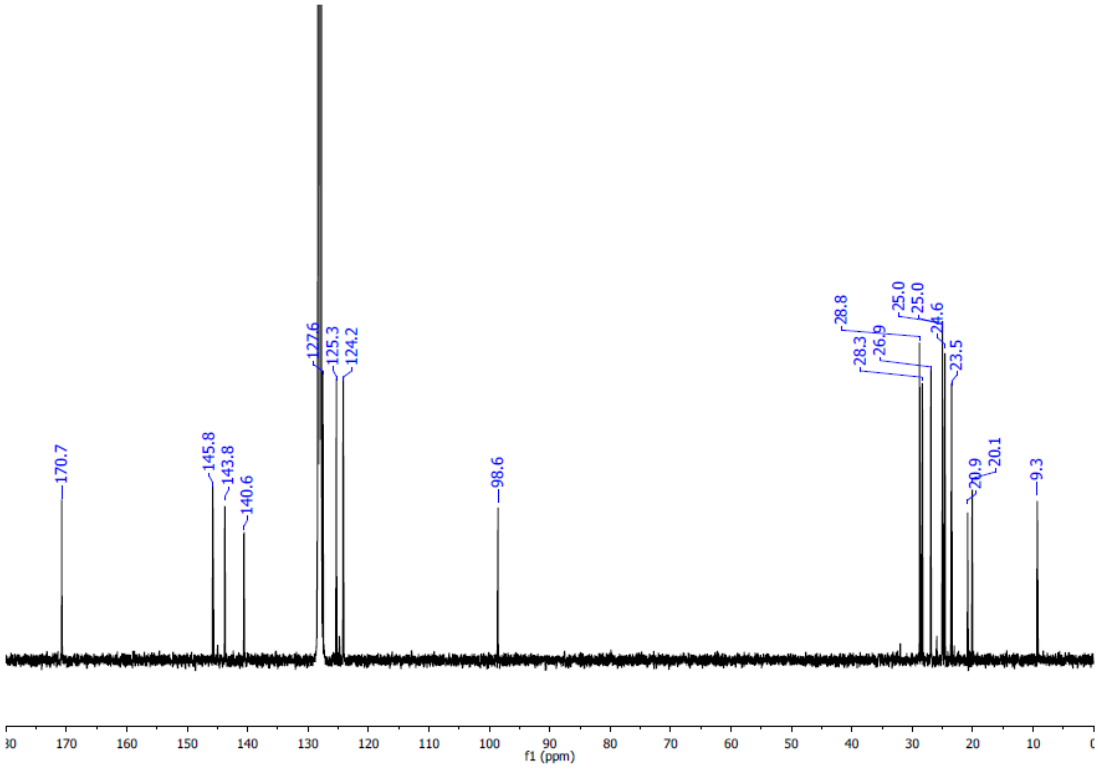

Figure 61. ^{1}H and $^{13}C\{^{1}H\}$ NMR spectra of **III-21**.

^{1}H NMR Spectrum (400 MHz, C_6D_6)

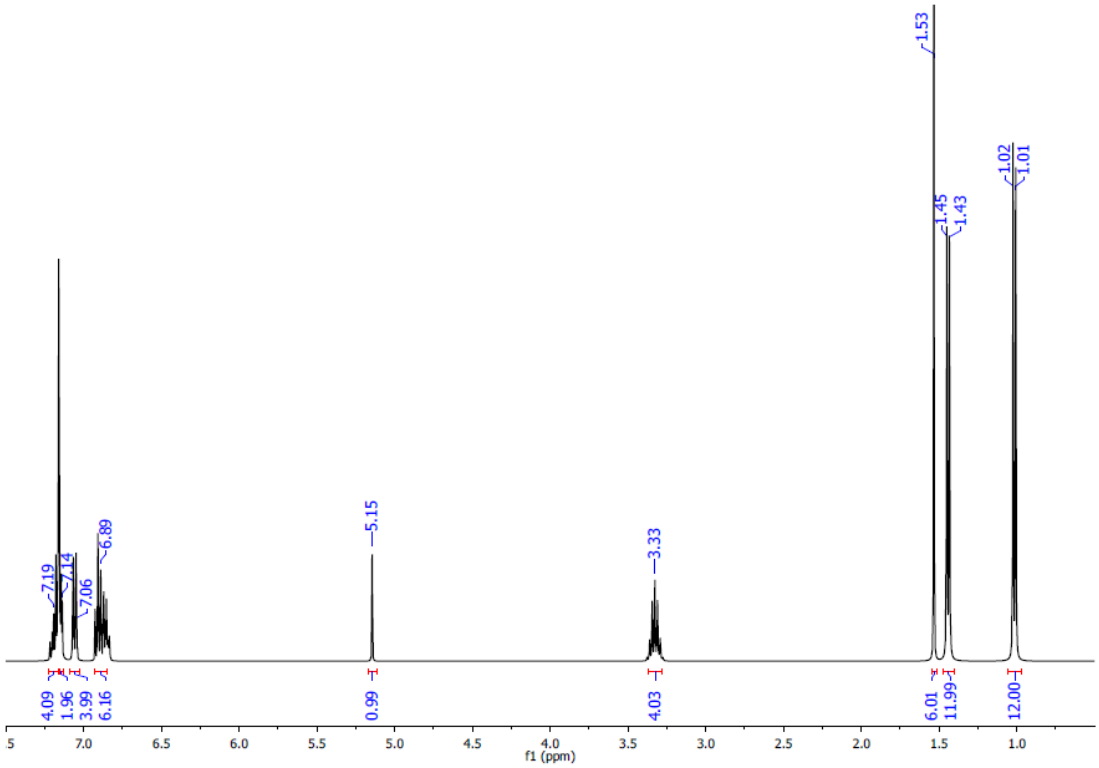

$^{13}C\{^{1}H\}$ NMR Spectrum (101 MHz, C_6D_6)

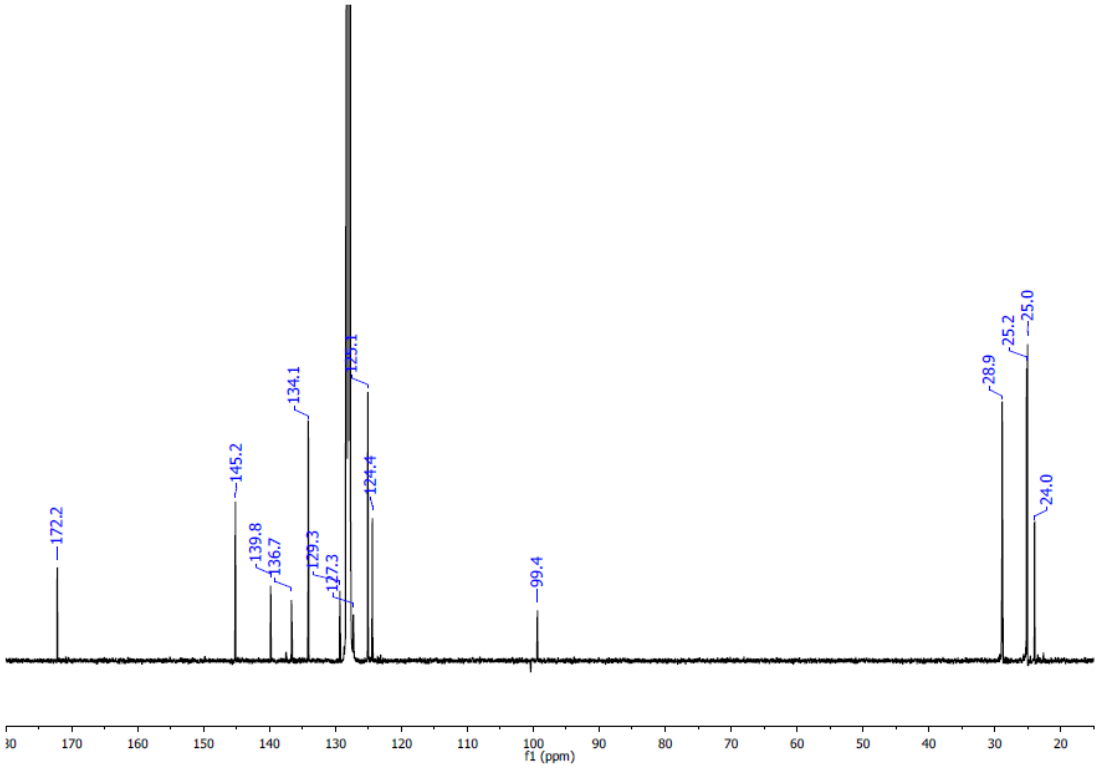

Figure 62. ^{1}H and $^{13}C\{^{1}H\}$ NMR spectra of **III-22**.

^{1}H NMR Spectrum (400 MHz, C_6D_6)

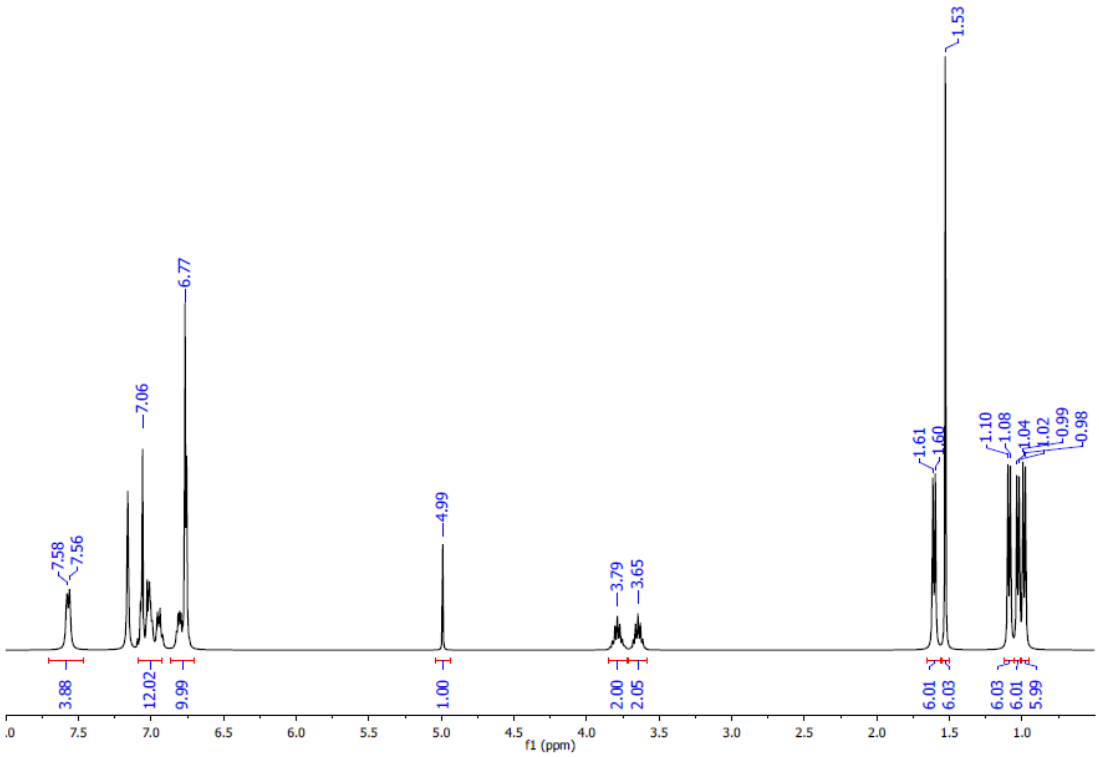

$^{13}C\{^{1}H\}$ NMR Spectrum (101 MHz, C_6D_6)

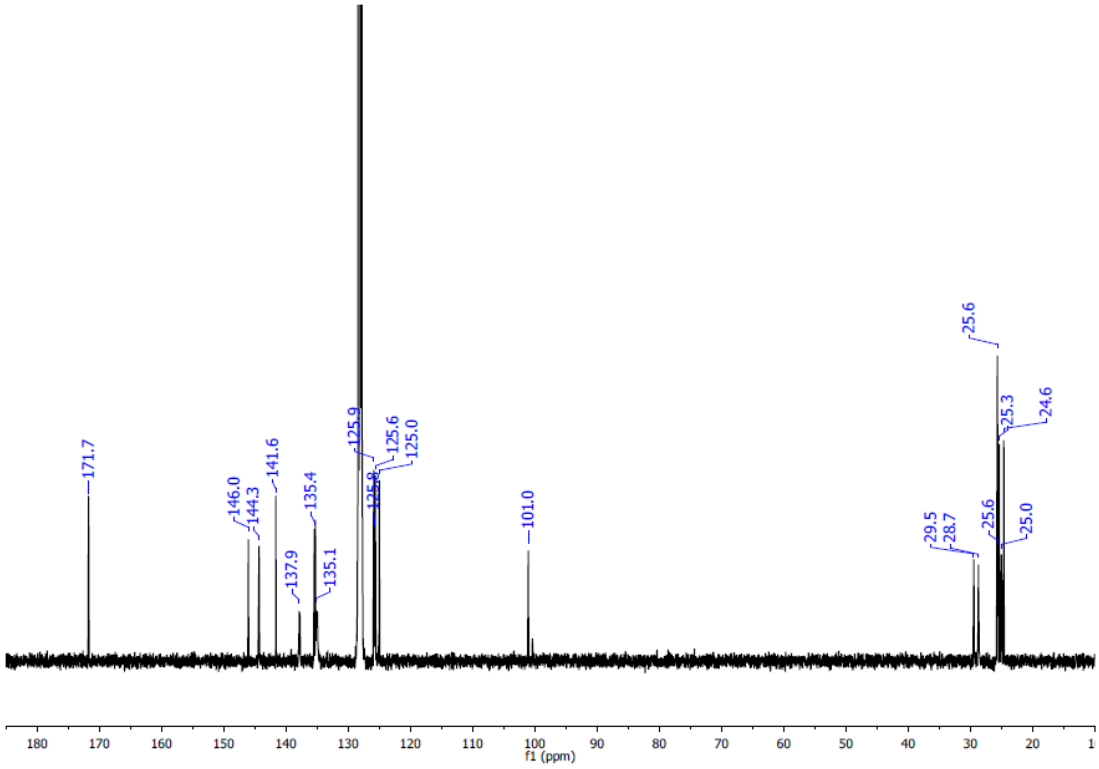

$^{31}P\{^{1}H\}$ NMR Spectrum (162 MHz, C_6D_6)

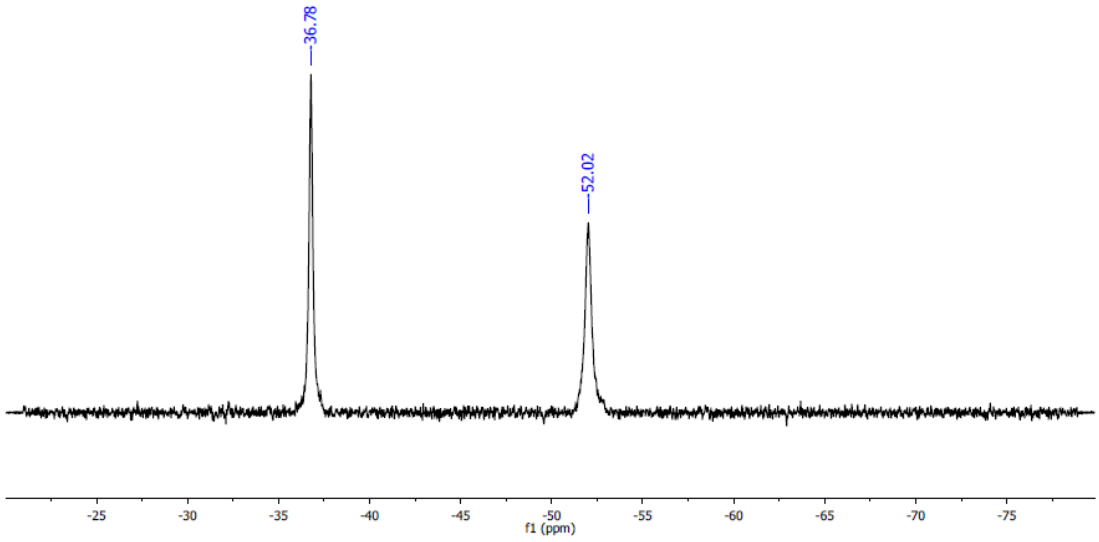

Figure 63. ^{1}H, $^{13}C\{^{1}H\}$, and $^{31}P\{^{1}H\}$ NMR spectra of **III-23**.

^{1}H NMR Spectrum (600 MHz, toluene-d_8, −20 °C)

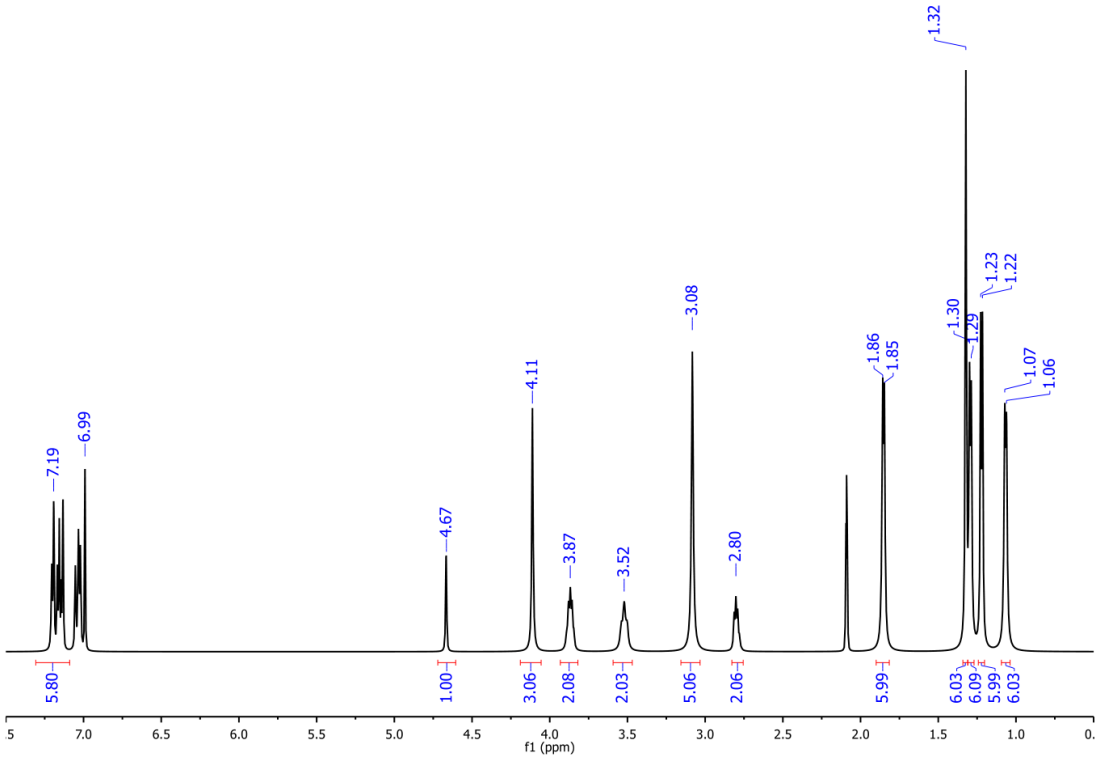

$^{13}C\{^{1}H\}$ NMR Spectrum (151 MHz, toluene-d_8, −20 °C)

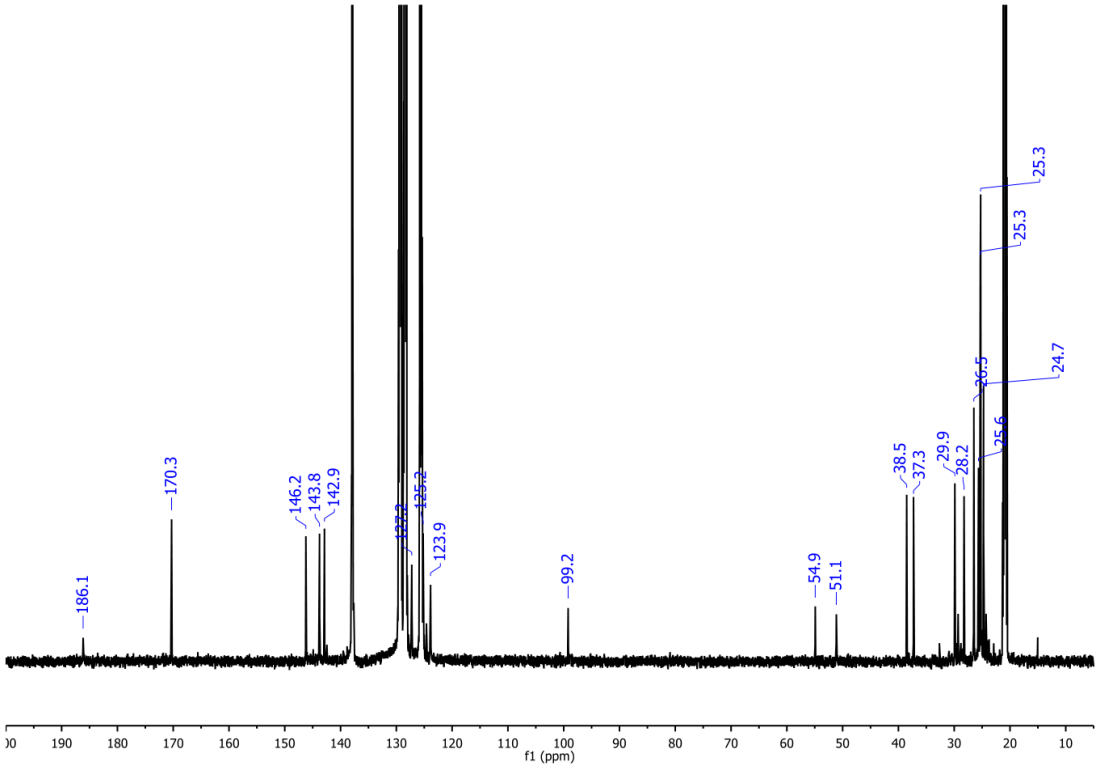

Figure 64. ^{1}H and $^{13}C\{^{1}H\}$ NMR spectra of **III-24**.

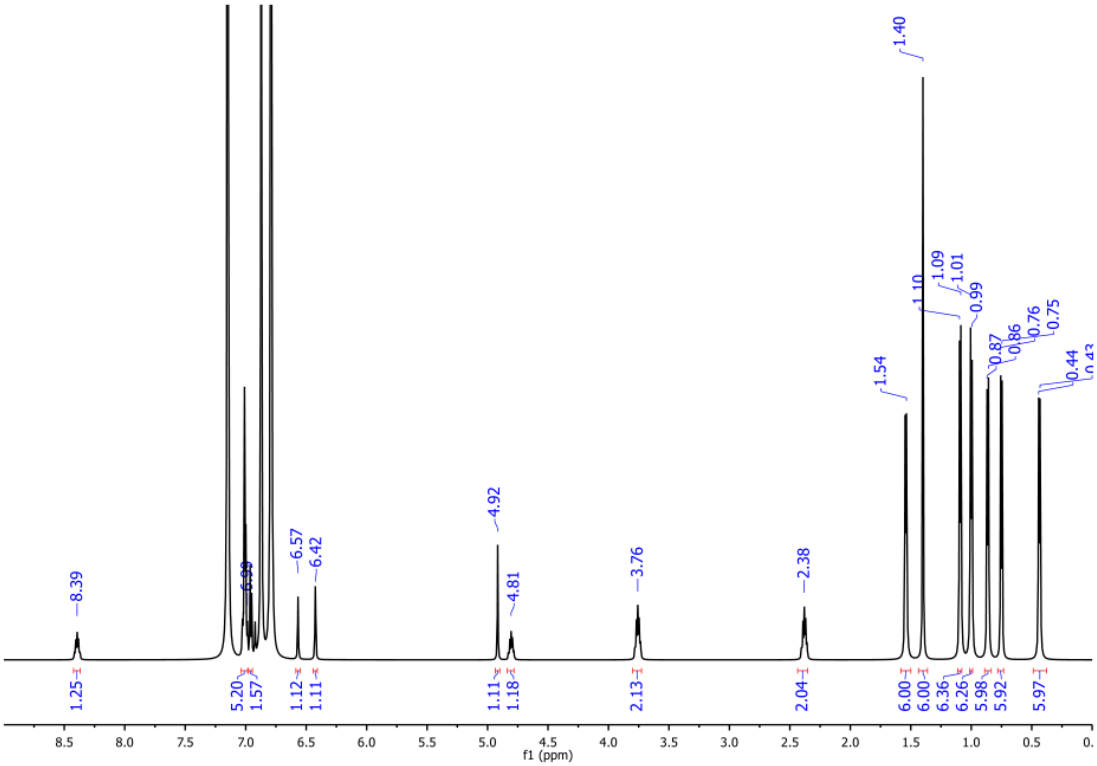

Figure 65. ^{1}H NMR spectrum (600 MHz, bromobenzene-d_5) of **III-25**.

^{1}H NMR Spectrum (400 MHz, toluene-d_8)

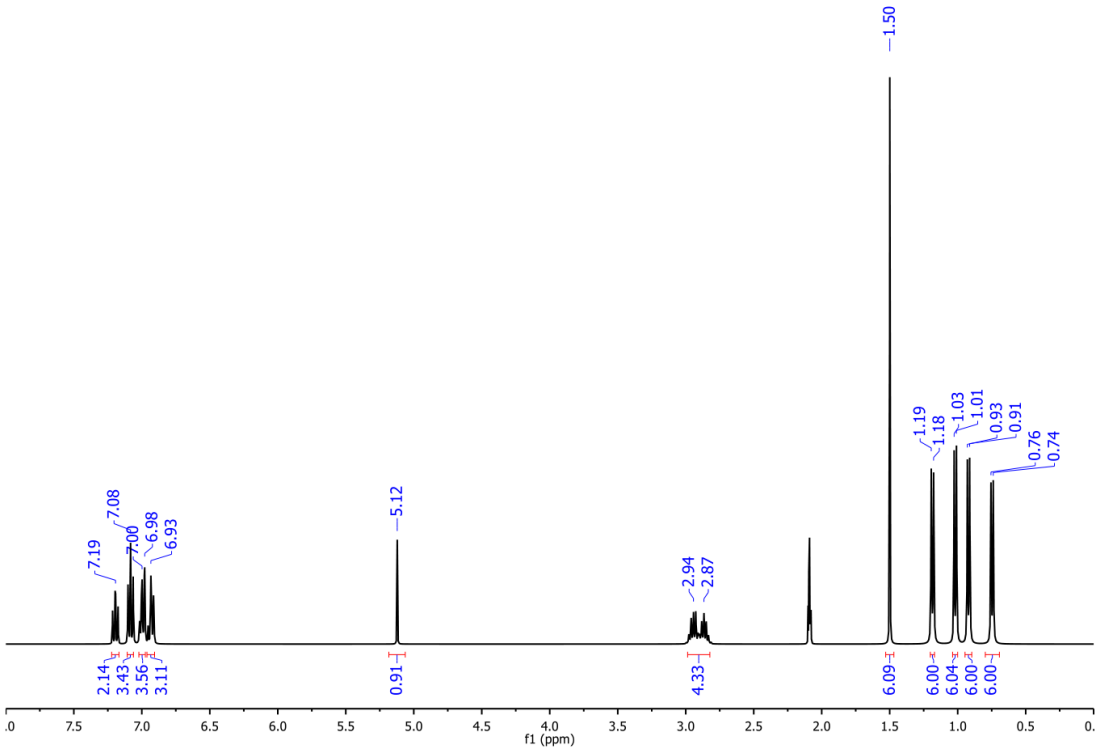

$^{13}C\{^{1}H\}$ NMR Spectrum (101 MHz, toluene-d_8)

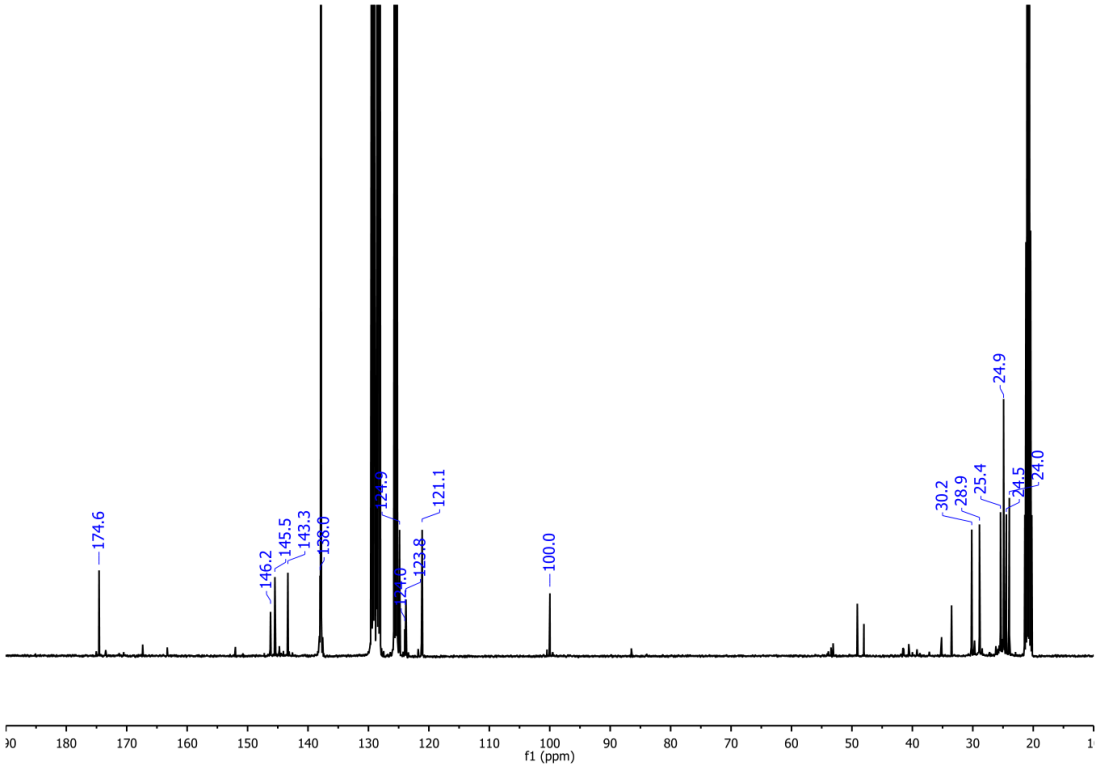

Figure 66. ^{1}H and $^{13}C\{^{1}H\}$ NMR spectra of **III-26**.

^{1}H NMR Spectrum (400 MHz, CD_2Cl_2)

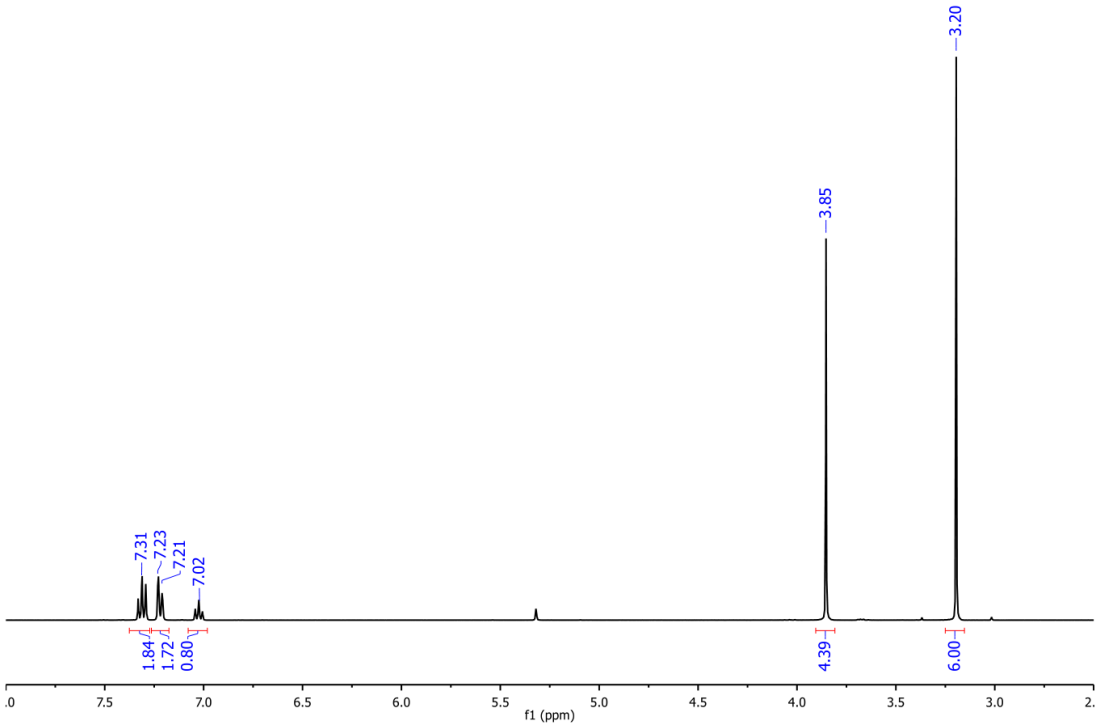

$^{13}C\{^{1}H\}$ NMR Spectrum (101 MHz, CD_2Cl_2)

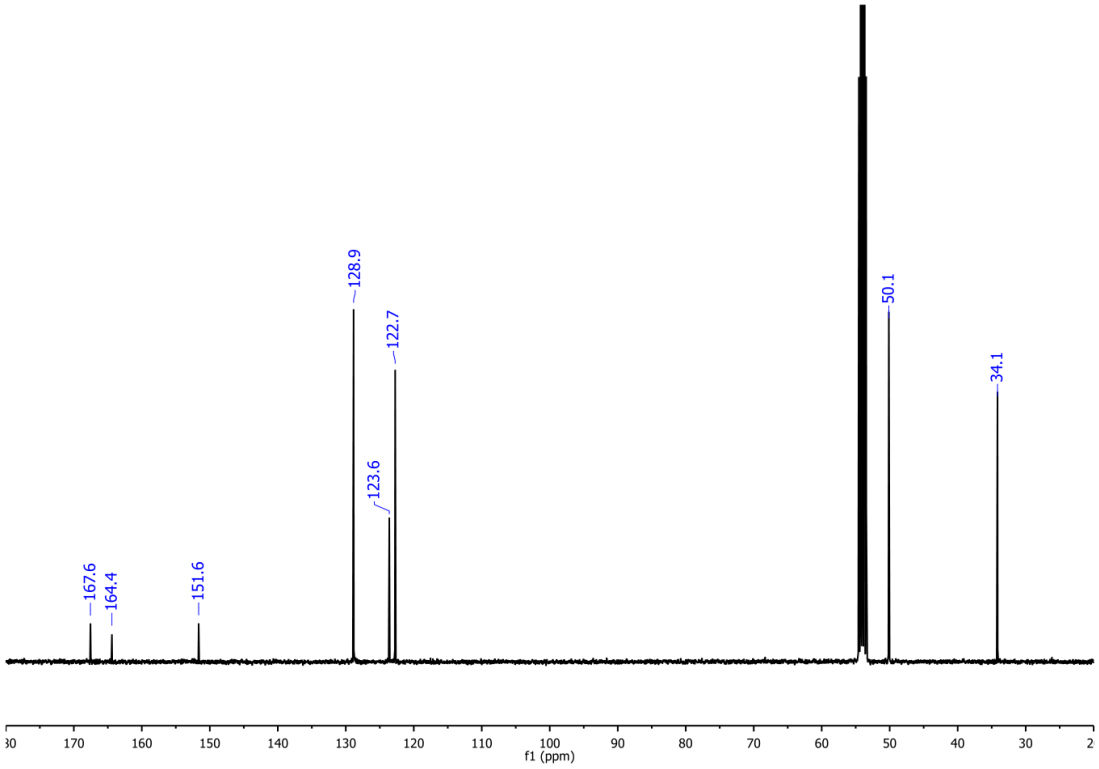

Figure 67. ^{1}H and $^{13}C\{^{1}H\}$ NMR spectra of **III-27**.

^{1}H NMR Spectrum (600 MHz, toluene-d_8, −60 °C)

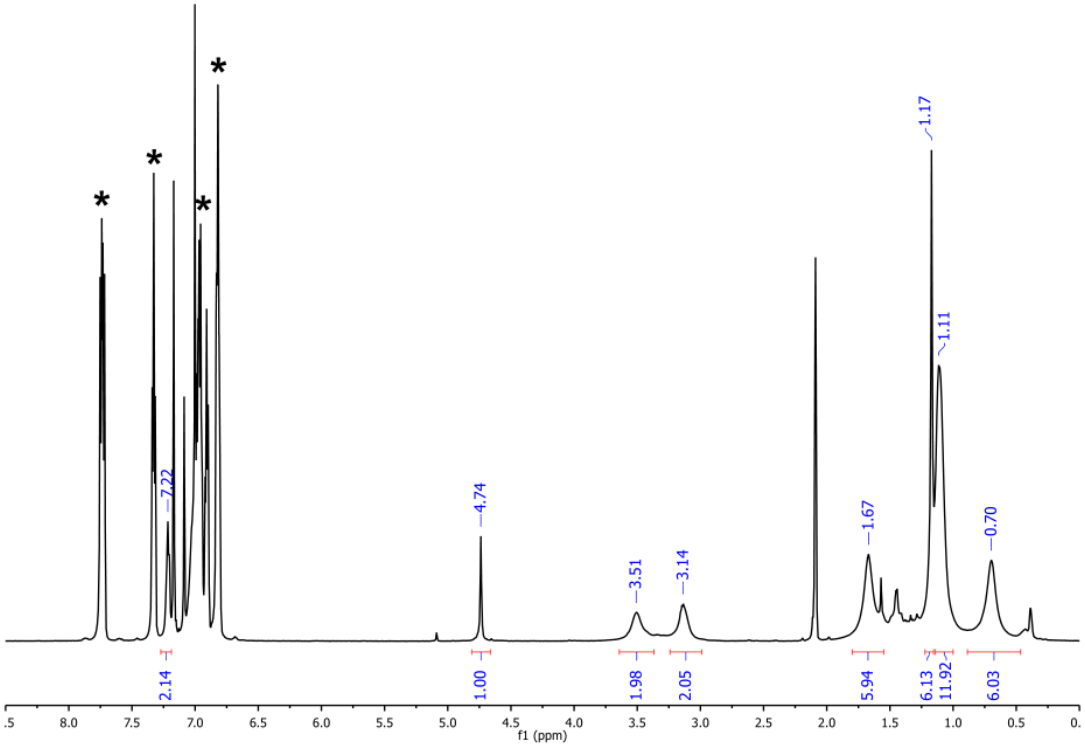

$^{13}C\{^{1}H\}$ NMR Spectrum (151 MHz, toluene-d_8, −60 °C)

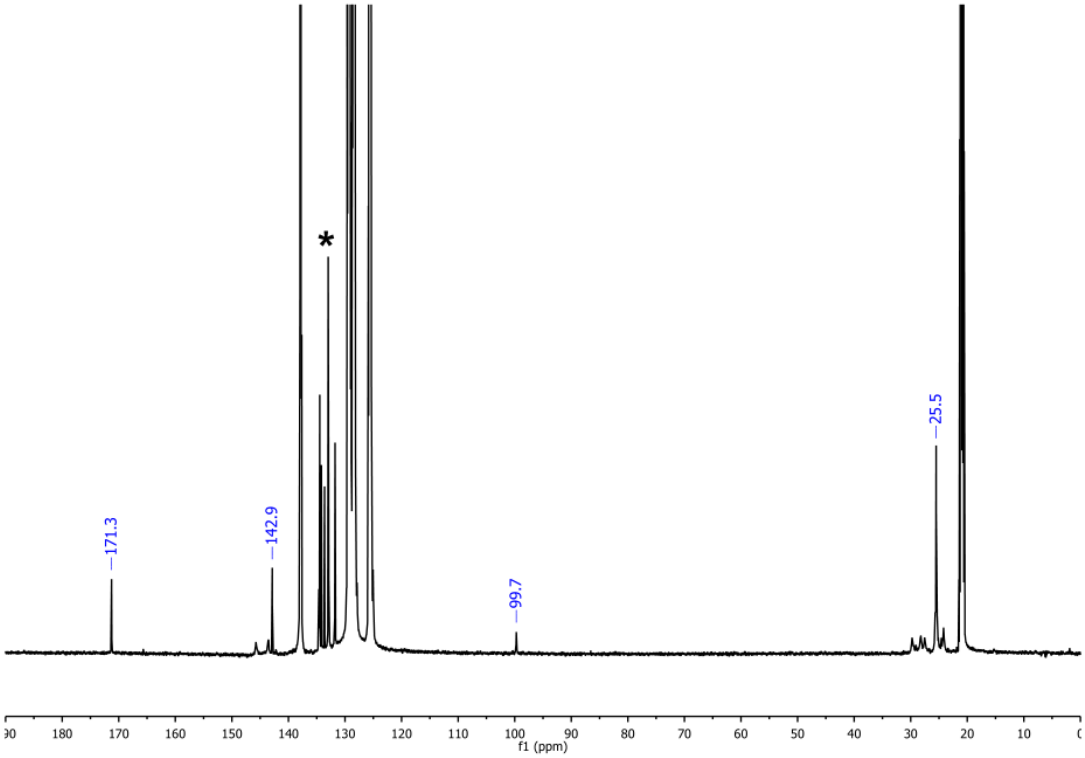

Figure 68. ^{1}H and $^{13}C\{^{1}H\}$ NMR spectra of **III-28**. * denotes signals for triphenylphosphine and triphenylphosphine sulfide.

^{1}H NMR Spectrum (400 MHz, C_6D_6)

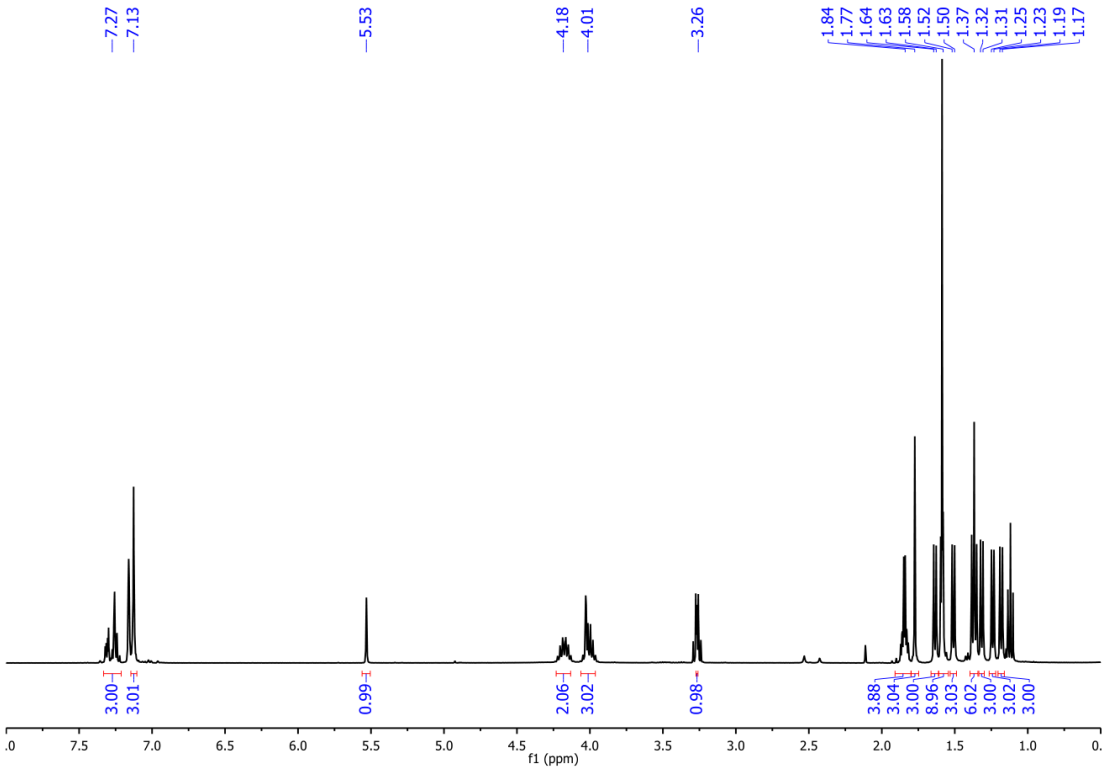

$^{13}C\{^{1}H\}$ NMR Spectrum (101 MHz, C_6D_6)

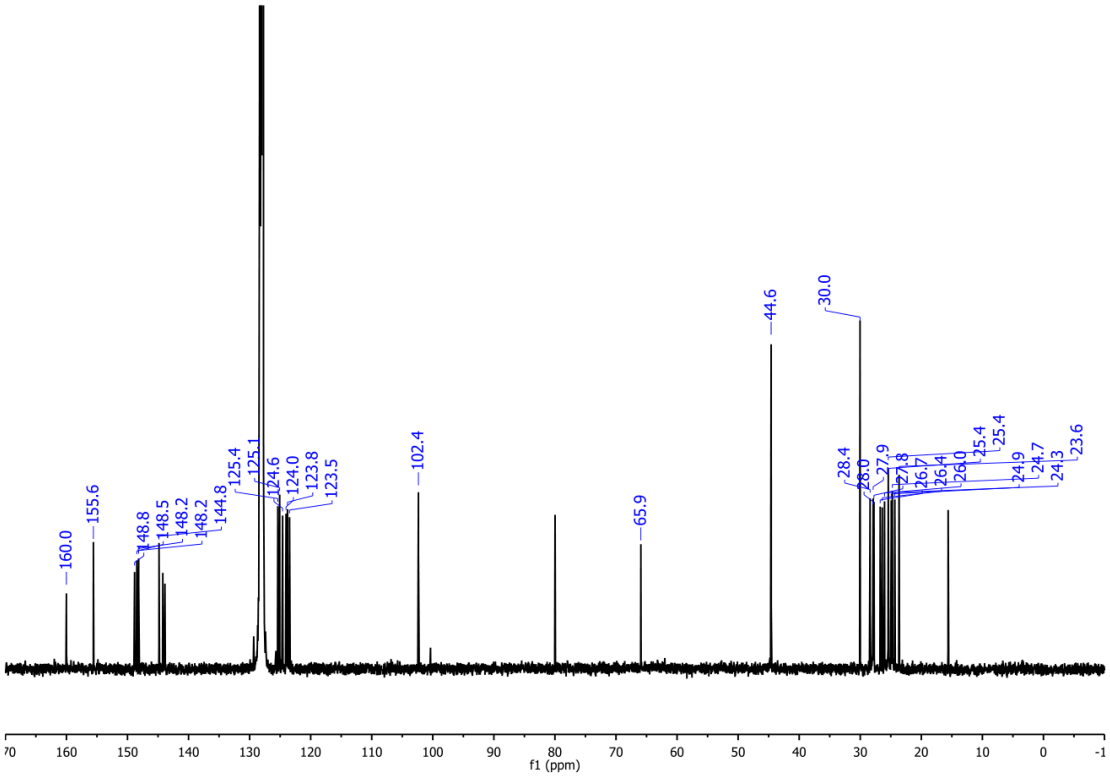

Figure 69. ^{1}H and $^{13}C\{^{1}H\}$ NMR spectra of **III-29**.

^{1}H NMR Spectrum (400 MHz, C_6D_6)

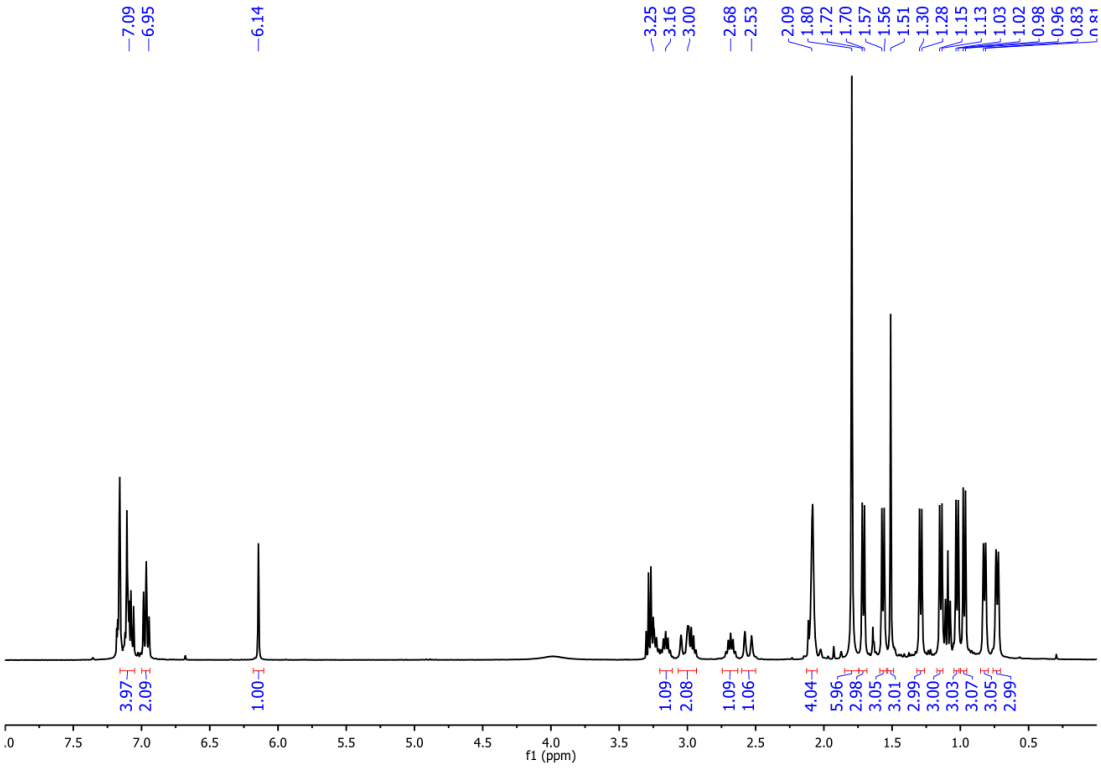

$^{13}C\{^{1}H\}$ NMR Spectrum (101 MHz, C_6D_6)

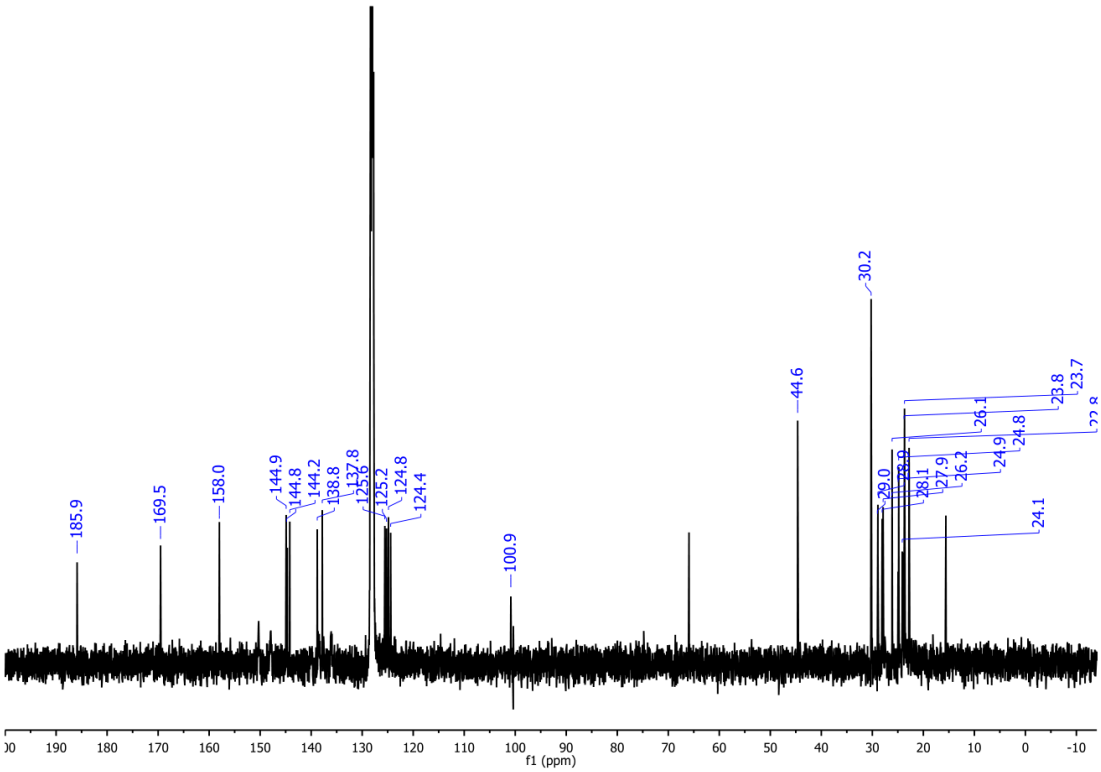

$^{11}B\{^{1}H\}$ NMR Spectrum (128 MHz, C_6D_6)

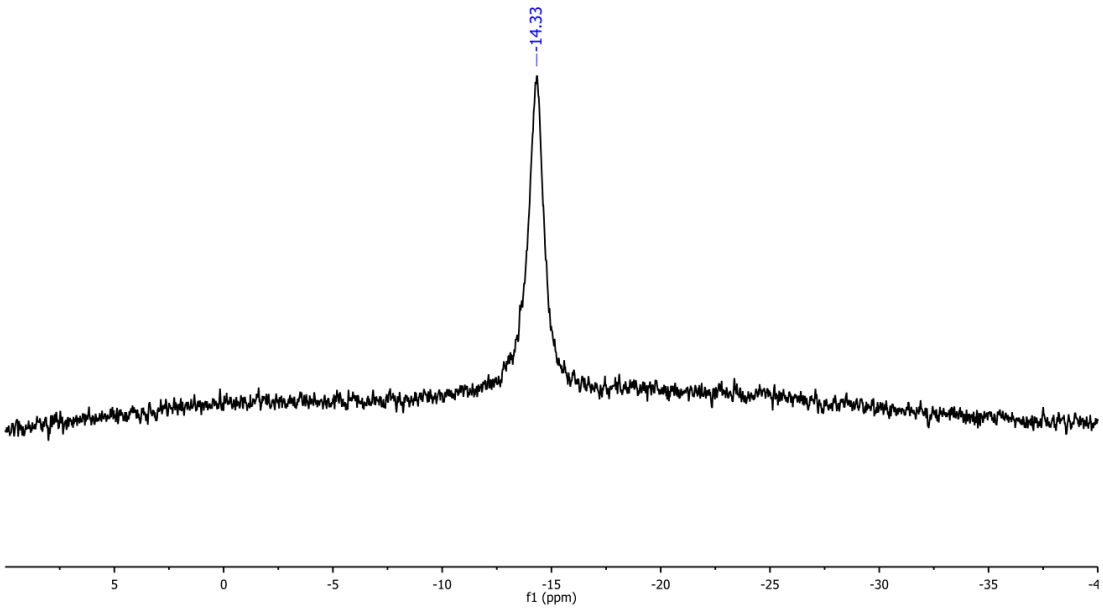

$^{19}F\{^{1}H\}$ NMR Spectrum (377 MHz, C_6D_6)

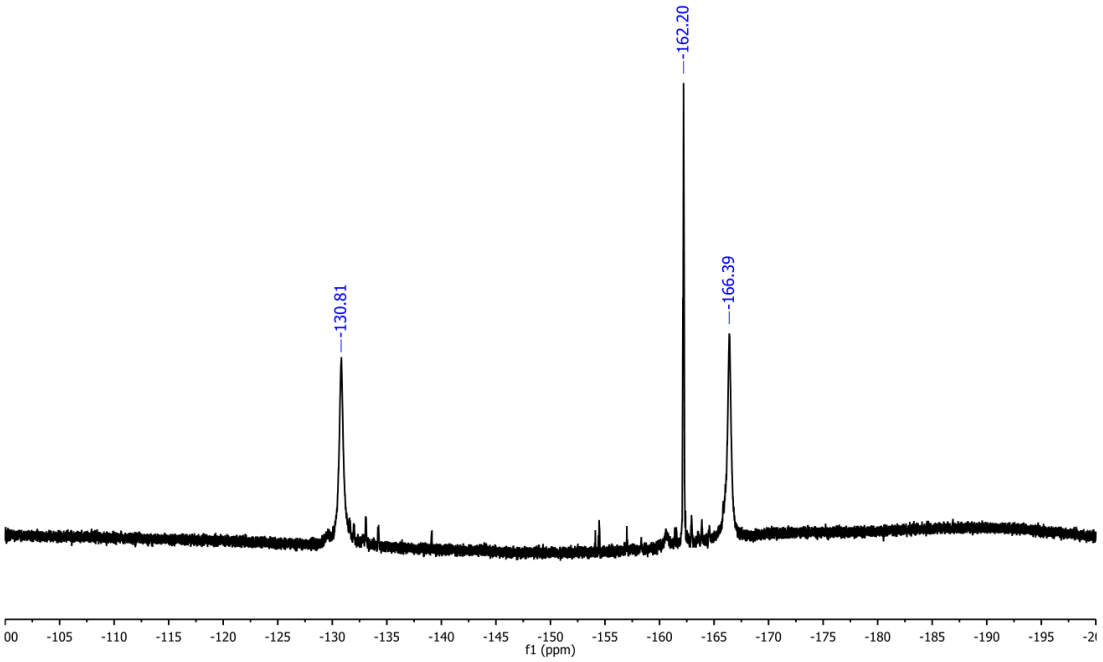

Figure 70. ^{1}H, $^{13}C\{^{1}H\}$, $^{11}B\{^{1}H\}$, and $^{19}F\{^{1}H\}$ NMR spectra of **III-30**.

^{1}H NMR Spectrum (400 MHz, C_6D_6)

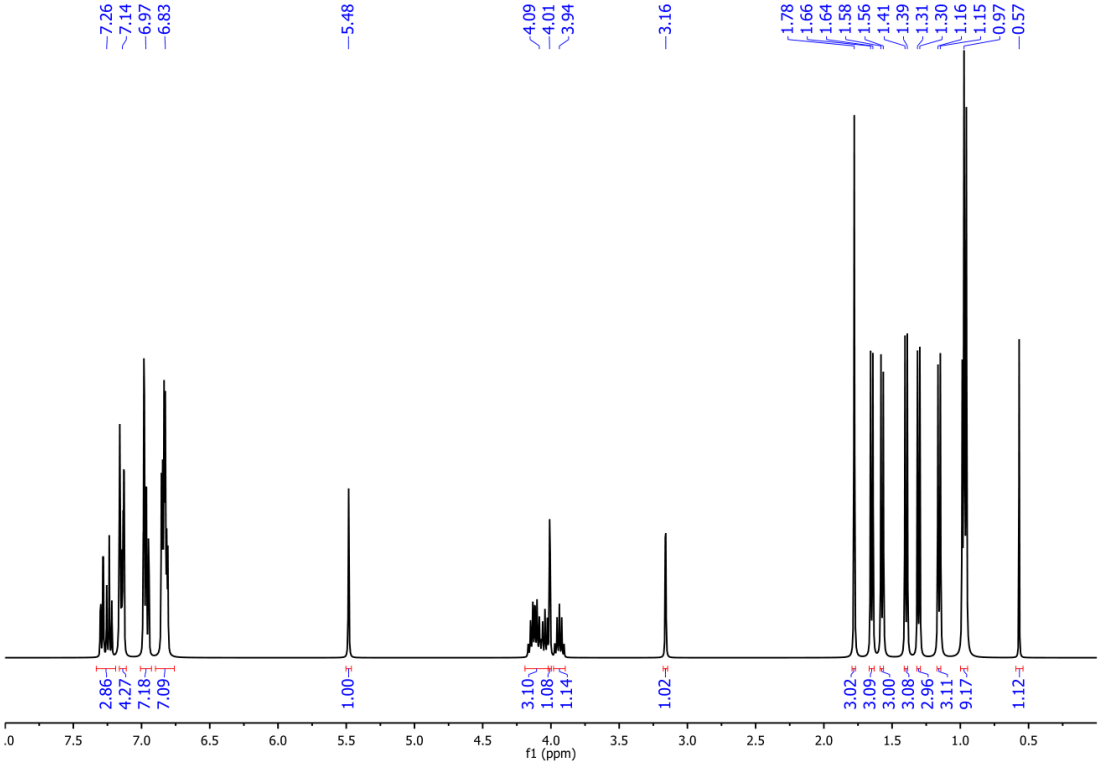

$^{13}C\{^{1}H\}$ NMR Spectrum (101 MHz, C_6D_6)

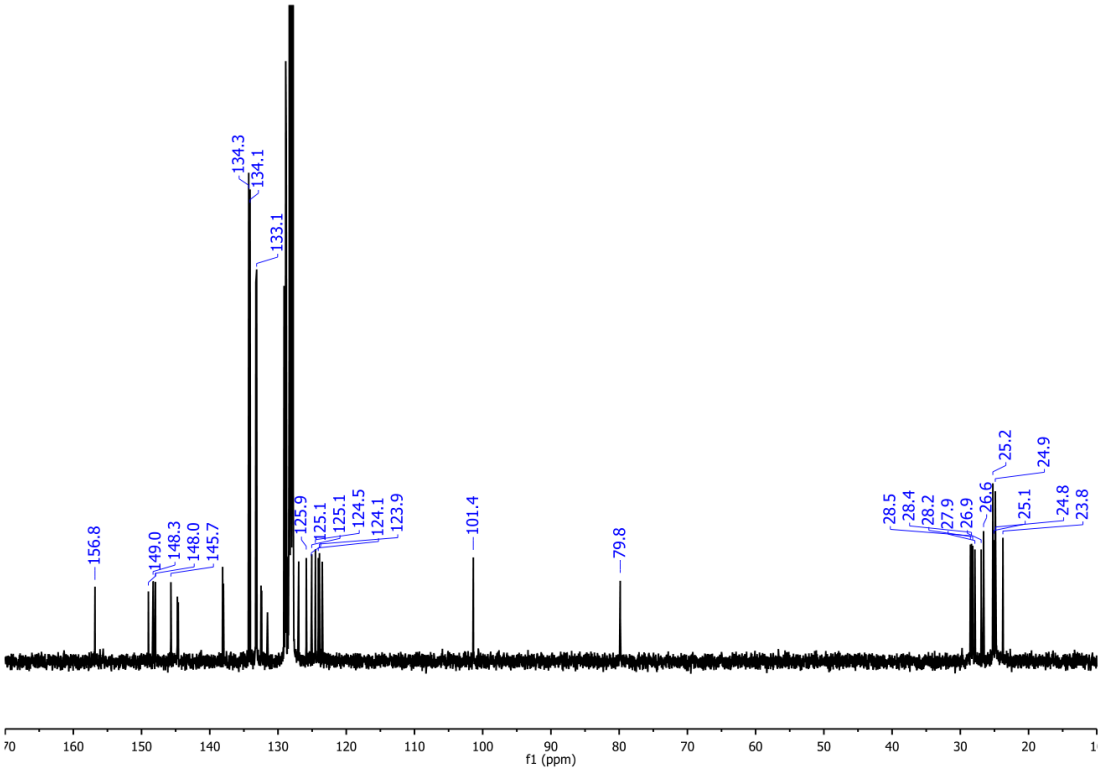

$^{31}P\{^{1}H\}$ NMR Spectrum (162 MHz, C_6D_6)

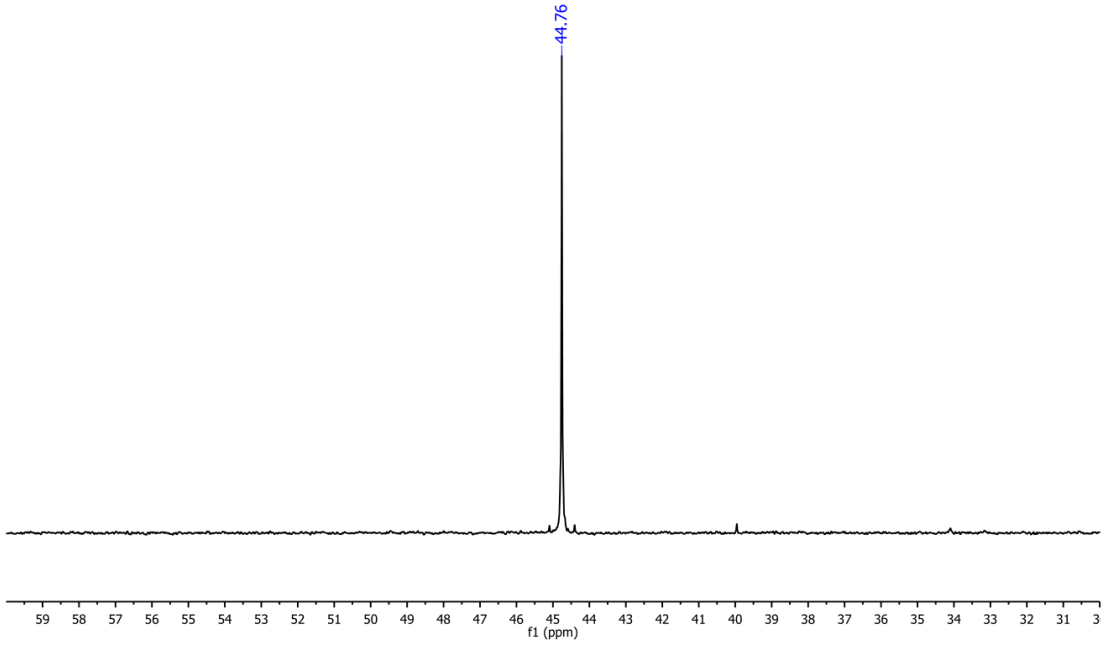

Figure 71. ^{1}H, $^{13}C\{^{1}H\}$, and $^{31}P\{^{1}H\}$ NMR spectra of **III-31**.

^{1}H NMR Spectrum (400 MHz, C_6D_6)

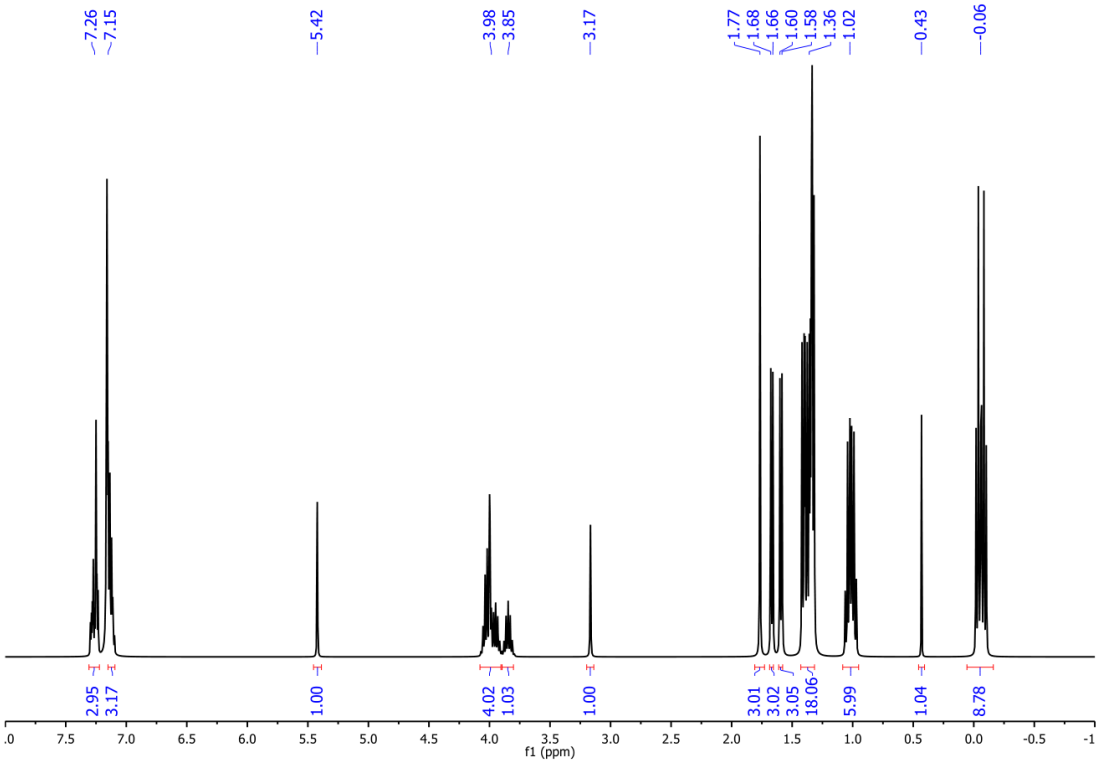

$^{13}C\{^{1}H\}$ NMR Spectrum (101 MHz, C_6D_6)

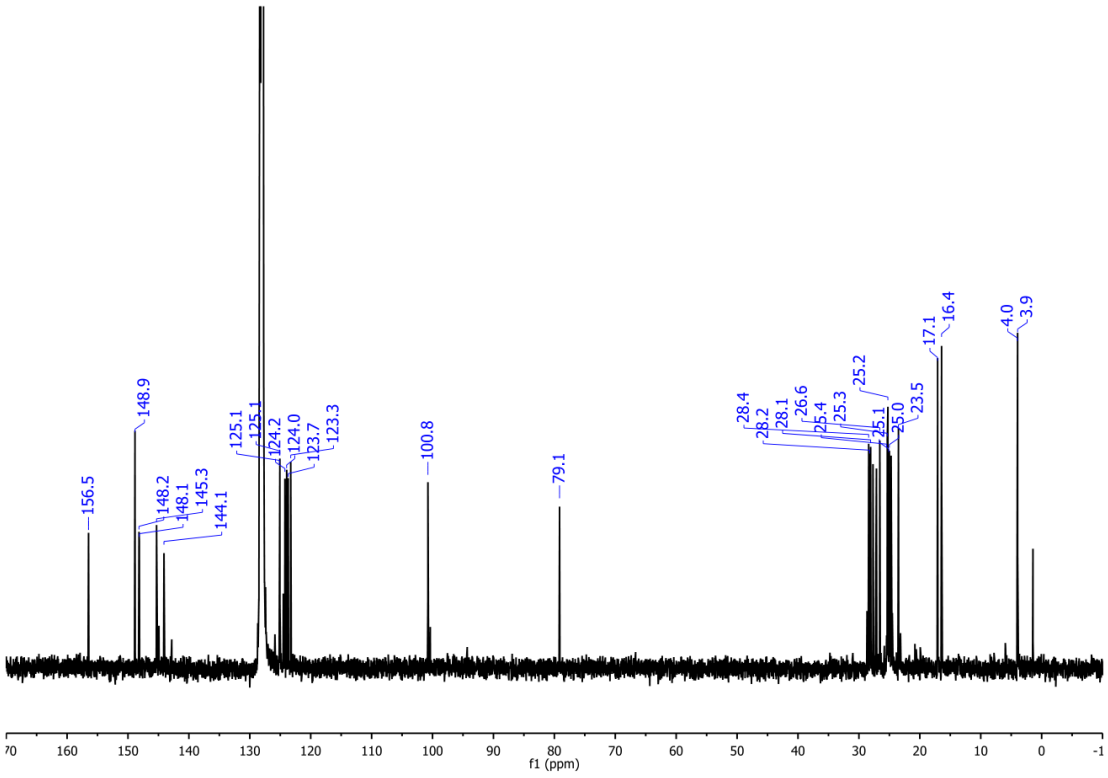

$^{31}P\{^{1}H\}$ NMR Spectrum (162 MHz, C_6D_6)

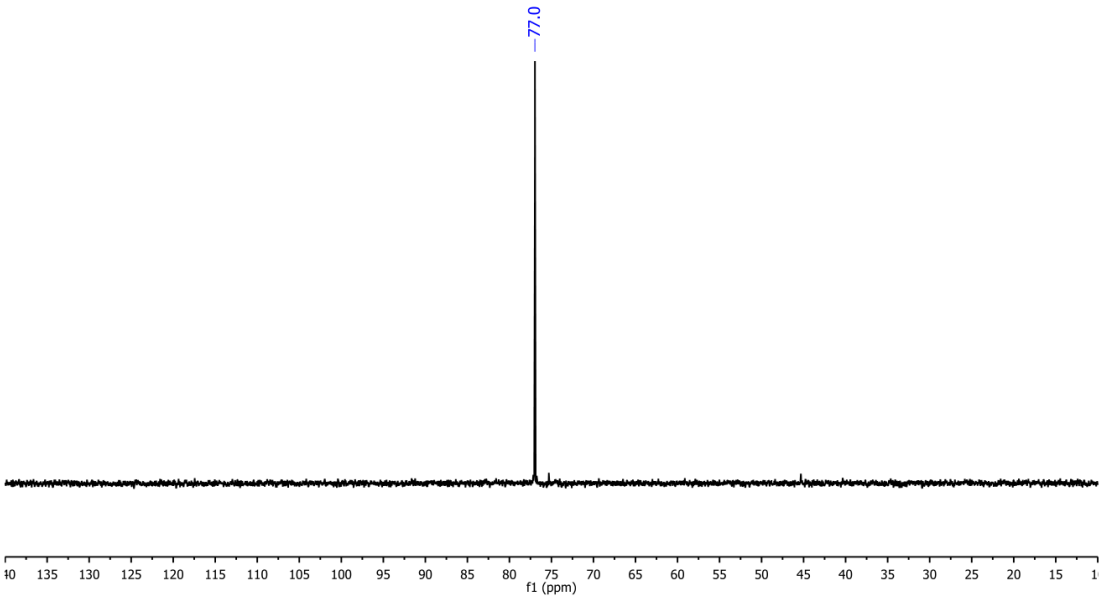

Figure 72. ^{1}H, $^{13}C\{^{1}H\}$, and $^{31}P\{^{1}H\}$ NMR spectra of **III-32**.

^{1}H NMR Spectrum (300 MHz, $CDCl_3$)

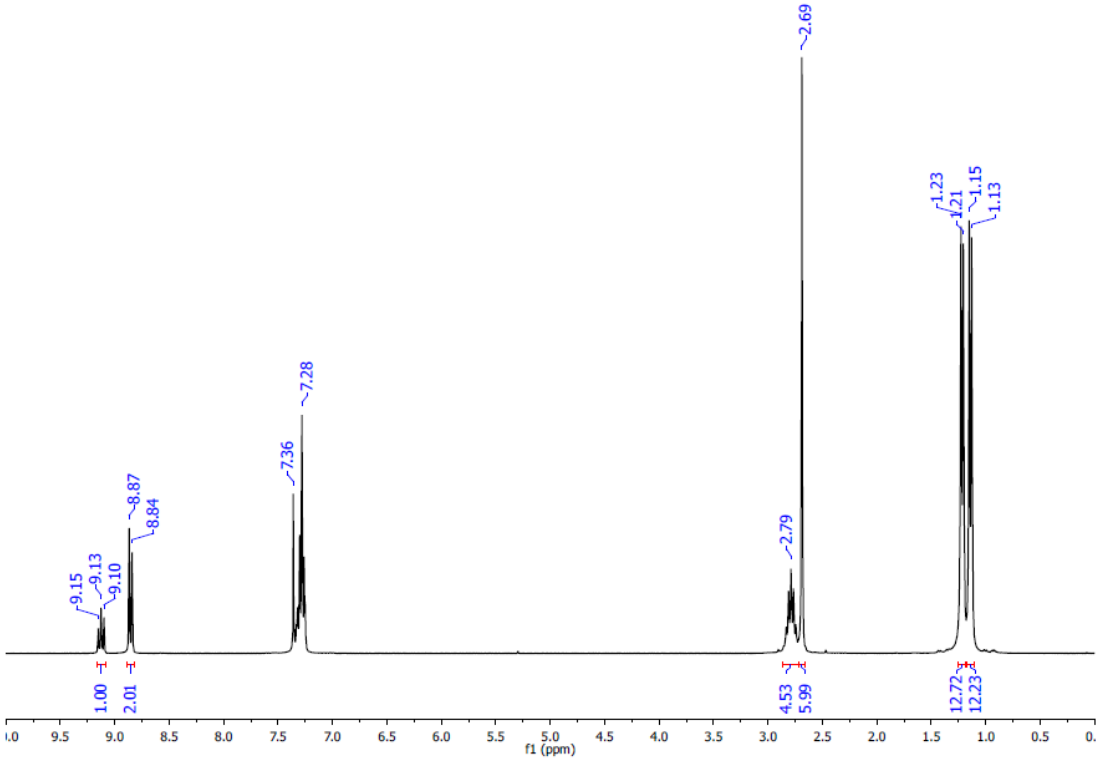

$^{13}C\{^{1}H\}$ NMR Spectrum (75 MHz, $CDCl_3$)

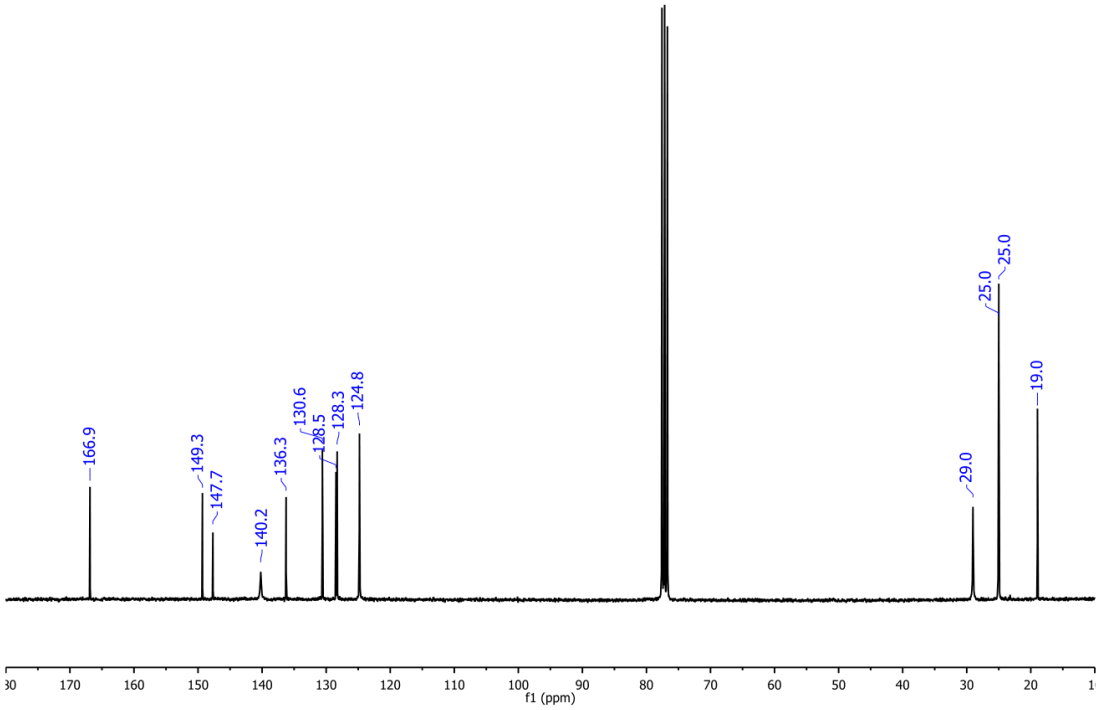

Figure 73. ^{1}H and $^{13}C\{^{1}H\}$ NMR spectra of **IV-1**.

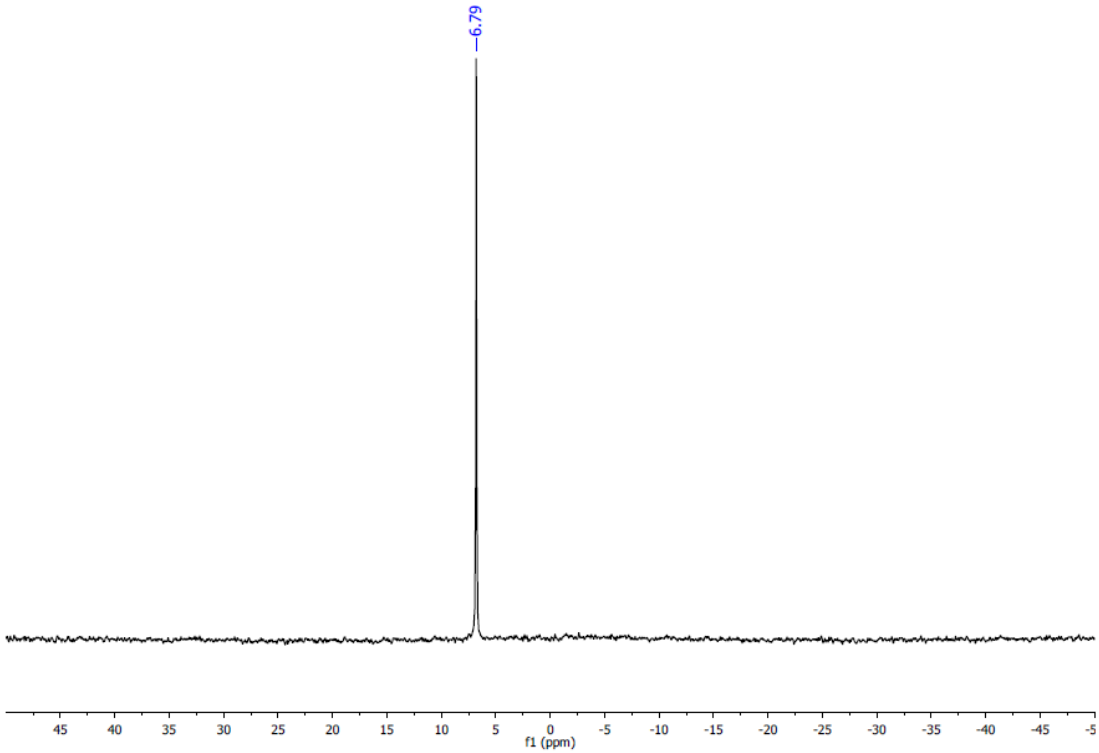

Figure 74. ^{11}B NMR spectrum (96 MHz, $CDCl_3$) of **IV-2**.

^{11}B NMR Spectrum (96 MHz, $CDCl_3$)

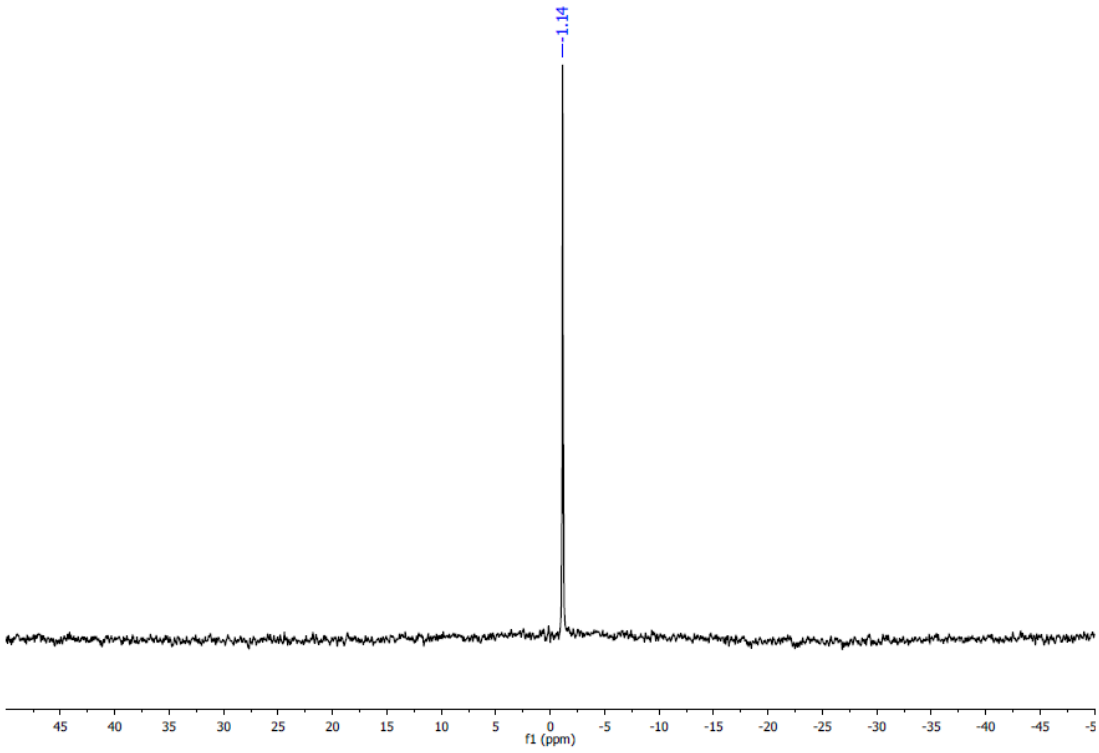

^{19}F NMR Spectrum (282 MHz, $CDCl_3$)

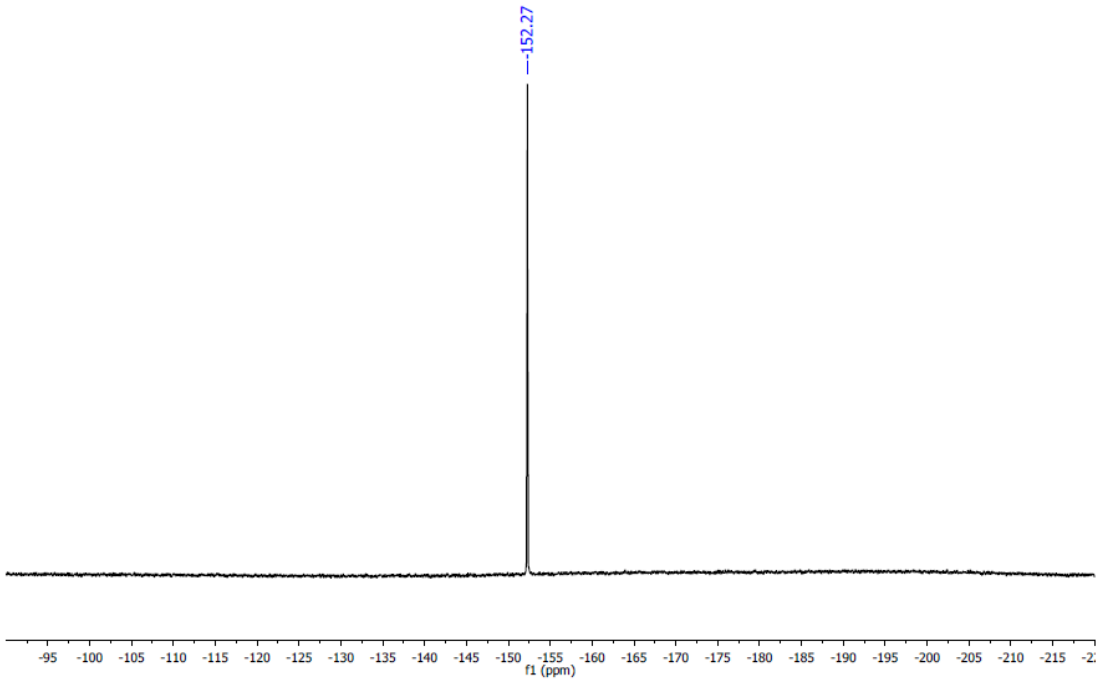

Figure 75. ^{11}B and ^{19}F NMR spectra of **IV-3**.

^{1}H NMR Spectrum (300 MHz, C_6D_6)

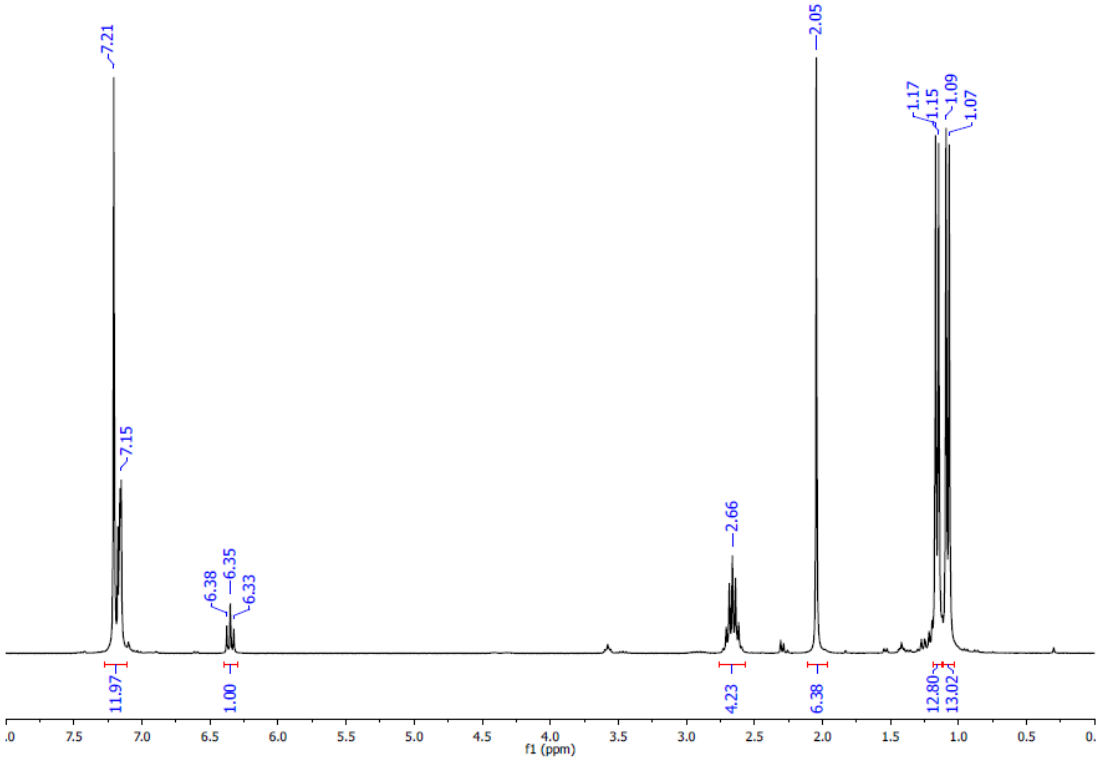

$^{13}C\{^{1}H\}$ NMR Spectrum (75 MHz, C_6D_6)

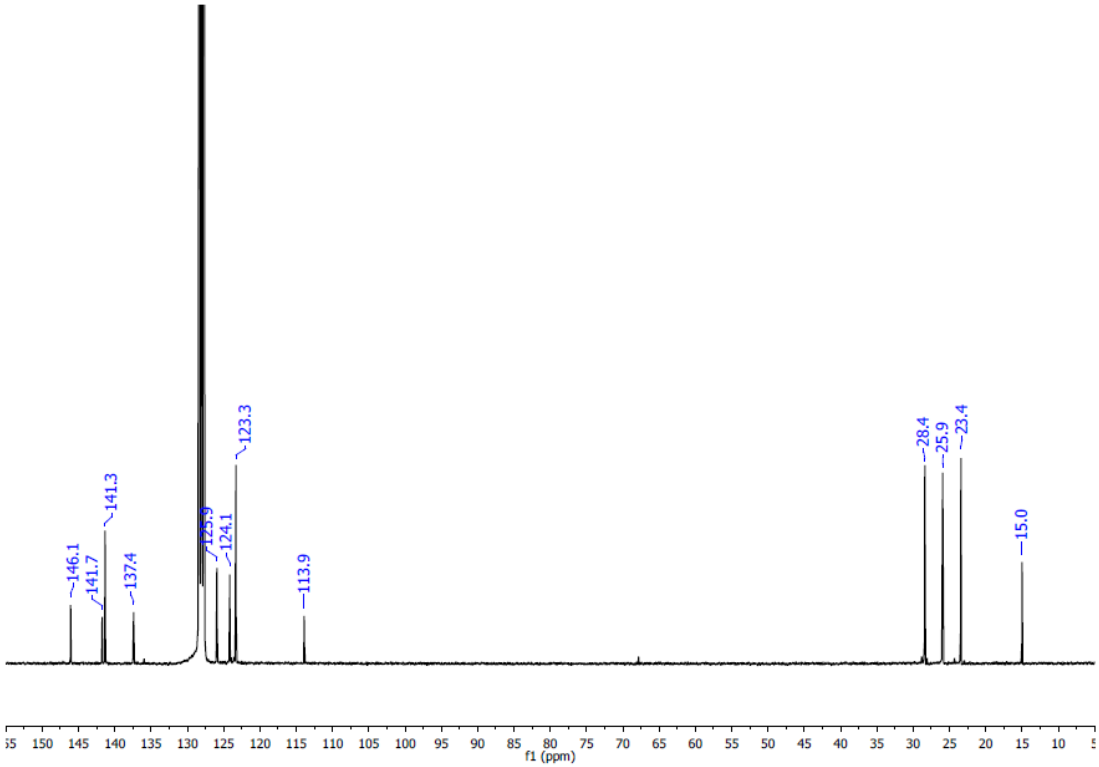

Figure 76. ^{1}H and $^{13}C\{^{1}H\}$ NMR spectra of **IV-4**.

^{1}H NMR Spectrum (400 MHz, C_6D_6)

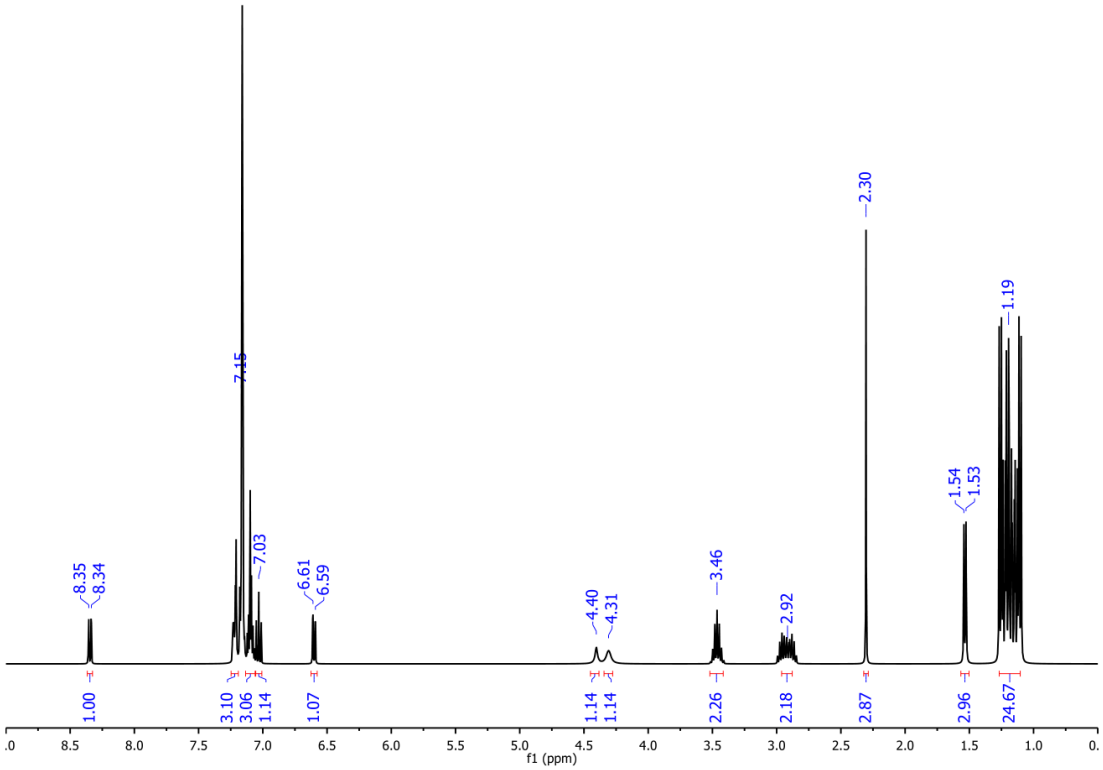

$^{13}C\{^{1}H\}$ NMR Spectrum (101 MHz, C_6D_6)

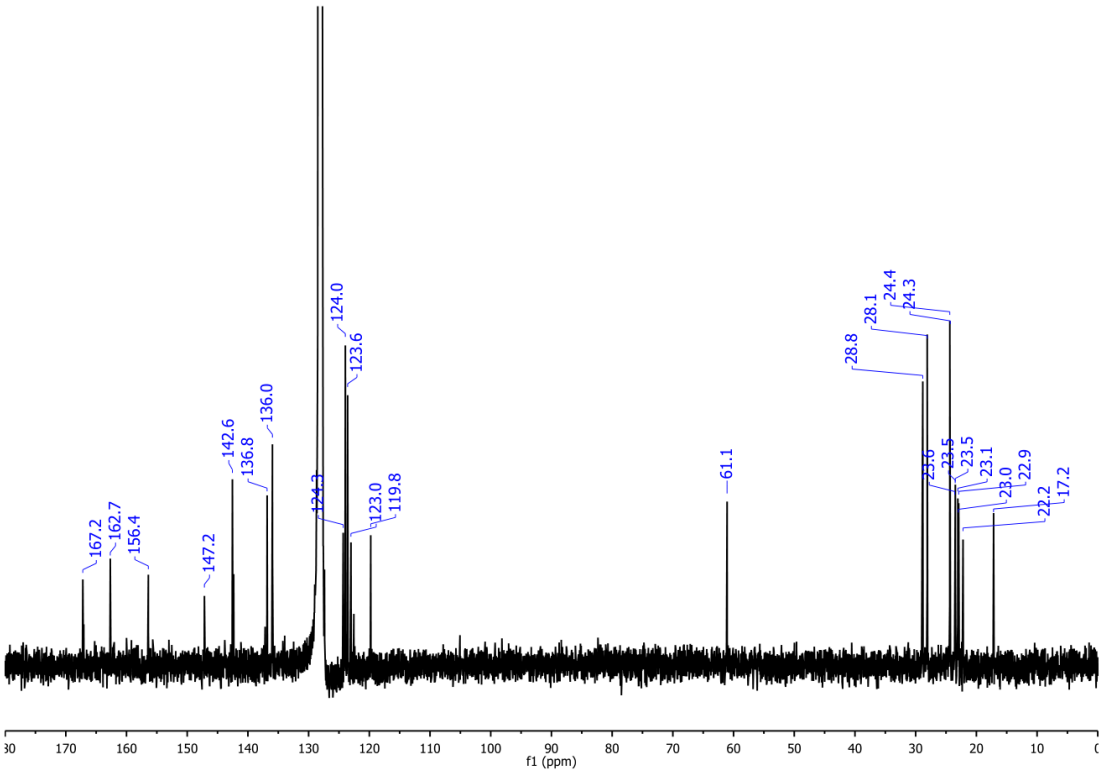

Figure 77. ^{1}H and $^{13}C\{^{1}H\}$ NMR spectra of **IV-5**.

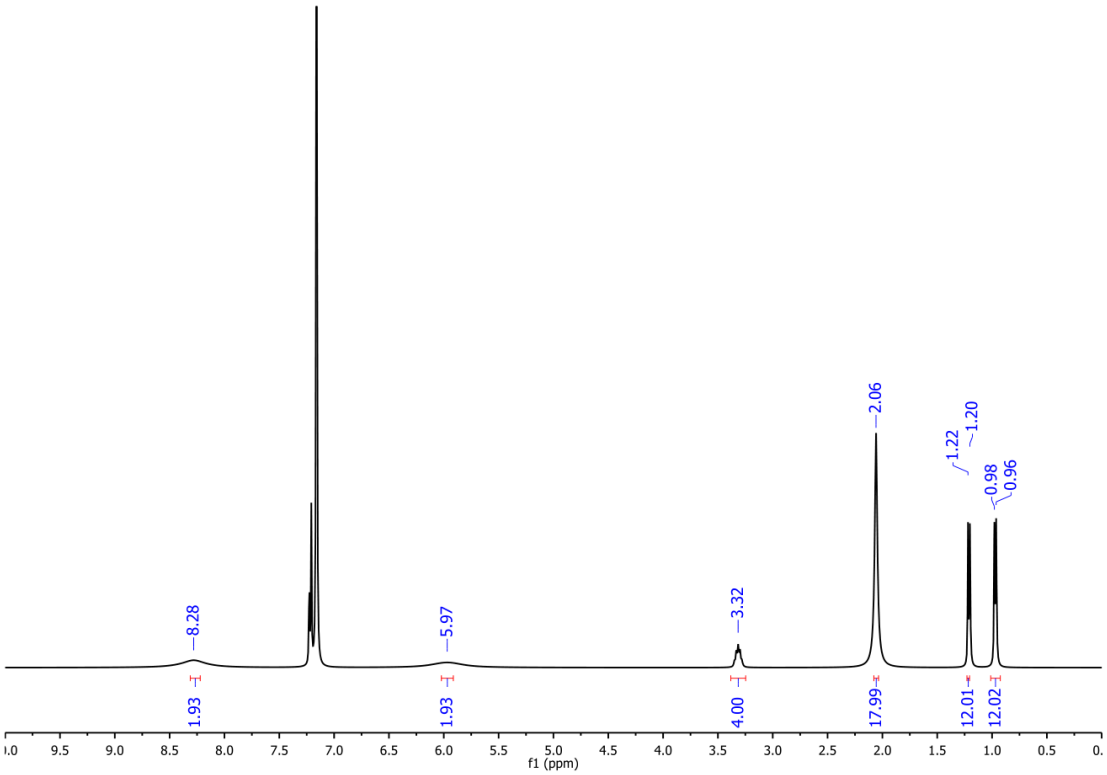

Figure 78. ^{1}H NMR spectrum (400 MHz, C_6D_6) of **IV-9**.

Table 24. Crystal structure determination parameters for **III-3**.

Empirical formula		$C_{35}H_{49}AlN_2O_{0.25}Si$	
Formula weight		556.83	
Crystal habit		block	
Crystal color		colorless	
Temperature		200(2) K	
Wavelength		0.71073 Å	
Crystal system		Monoclinic	
Space group		P2(1)/n	
Unit cell dimensions:			
a	9.6330(5) Å	α	90°
b	16.9749(8) Å	β	93.418(3)°
c	20.9503(10) Å	γ	90°
Volume		3419.7(3) $Å^3$	
Z		4	
Density (calc)		1.082 Mg/m^3	
Absorption coefficient		0.119 mm^{-1}	
F(000)		1208	
Crystal size		0.190 x 0.140 x 0.120 mm^3	
Theta range for data collection		2.278 to 28.312°	
Index ranges		-12<=h<=12, -22<=k<=22, -27<=l<=27	
Reflections collected		26467	
Independent reflections		8338 [R(int) = 0.0406]	
Completeness to theta = 25.242°		99.2 %	
Absorption correction		Semi-empirical from equivalents	
Max. and min. transmission		0.7457 and 0.6834	
Refinement method		Full-matrix least-squares on F^2	
Data / restraints / parameters		8338 / 26 / 377	
Goodness-of-fit on F^2		1.039	
Final R indices [I>2sigma(I)]		R1 = 0.0488, wR2 = 0.1168	
R indices (all data)		R1 = 0.0898, wR2 = 0.1326	
Largest diff. peak and hole		0.306 and -0.173 $e.Å^{-3}$	

Table 25. Crystal structure determination parameters for **III-4**.

Empirical formula		$C_{18}H_{25.5}Al_{0.5}NSi_{0.5}$	
Formula weight		283.43	
Crystal habit		block	
Crystal color		colorless	
Temperature		200(2) K	
Wavelength		0.71073 Å	
Crystal system		Triclinic	
Space group		P-1	
Unit cell dimensions:			
a	12.0366(12) Å	α	70.633(6)°
b	12.3508(13) Å	β	87.367(6)°
c	12.6164(13) Å	γ	79.059(6)°
Volume		1737.0(3) $Å^3$	
Z		4	
Density (calc)		1.084 Mg/m^3	
Absorption coefficient		0.118 mm^{-1}	
F(000)		616	
Crystal size		0.24 x 0.15 x 0.14 mm^3	
Theta range for data collection		1.71 to 26.43°	
Index ranges		-15<=h<=14, -15<=k<=15, -15<=l<=15	
Reflections collected		22062	
Independent reflections		7090 [R(int) = 0.0251]	
Completeness to theta = 25.242°		99.3 %	
Absorption correction		None	
Max. and min. transmission		0.9837 and 0.9723	
Refinement method		Full-matrix least-squares on F^2	
Data / restraints / parameters		7090 / 0 / 369	
Goodness-of-fit on F^2		1.064	
Final R indices [I>2sigma(I)]		R1 = 0.0507, wR2 = 0.1247	
R indices (all data)		R1 = 0.0672, wR2 = 0.1344	
Largest diff. peak and hole		0.413 and -0.314 e.$Å^{-3}$	

Table 26. Crystal structure determination parameters for **III-5**.

Empirical formula		$C_{35}H_{54}AlBN_2O_2$	
Formula weight		572.59	
Crystal habit		block	
Crystal color		colorless	
Temperature		200(2) K	
Wavelength		0.71073 Å	
Crystal system		Triclinic	
Space group		P-1	
Unit cell dimensions:			
a	9.3319(3) Å	α	80.3490(10)°
b	11.6691(3) Å	β	75.2380(10)°
c	17.0064(5) Å	γ	88.0350(10)°
Volume		1765.37(9) $Å^3$	
Z		2	
Density (calc)		1.077 Mg/m^3	
Absorption coefficient		0.088 mm^{-1}	
F(000)		624	
Crystal size		0.22 x 0.17 x 0.15 mm^3	
Theta range for data collection		1.77 to 28.32°	
Index ranges		-12<=h<=12, -15<=k<=15, -22<=l<=22	
Reflections collected		26594	
Independent reflections		8702 [R(int) = 0.0197]	
Completeness to theta = 28.32°		98.7 %	
Absorption correction		Semi-empirical from equivalents	
Max. and min. transmission		0.9869 and 0.9809	
Refinement method		Full-matrix least-squares on F^2	
Data / restraints / parameters		8702 / 0 / 371	
Goodness-of-fit on F^2		1.032	
Final R indices [I>2sigma(I)]		R1 = 0.0506, wR2 = 0.1412	
R indices (all data)		R1 = 0.0641, wR2 = 0.1532	
Largest diff. peak and hole		0.555 and -0.354 $e.Å^{-3}$	

Table 27. Crystal structure determination parameters for **III-7**.

Empirical formula		$C_{80}H_{100}Al_2N_2$	
Formula weight		1143.58	
Crystal habit		block	
Crystal color		colorless	
Temperature		200(2) K	
Wavelength		0.71073 Å	
Crystal system		Orthorhombic	
Space group		Ibam	
Unit cell dimensions:			
a	16.3923(4) Å	α	90°
b	19.8520(6) Å	β	90°
c	21.4153(6) Å	γ	90°
Volume		6969.0(3) $Å^3$	
Z		4	
Density (calc)		1.090 Mg/m^3	
Absorption coefficient		0.085 mm^{-1}	
F(000)		2480	
Crystal size		0.23 x 0.19 x 0.16 mm^3	
Theta range for data collection		1.61 to 28.32°	
Index ranges		-21<=h<=21, -26<=k<=23, -28<=l<=27	
Reflections collected		47830	
Independent reflections		4465 [R(int) = 0.0485]	
Completeness to theta = 25.242°		98.6 %	
Absorption correction		None	
Max. and min. transmission		0.9865 and 0.9807	
Refinement method		Full-matrix least-squares on F^2	
Data / restraints / parameters		4465 / 0 / 209	
Goodness-of-fit on F^2		1.042	
Final R indices [I>2sigma(I)]		R1 = 0.0447, wR2 = 0.1171	
R indices (all data)		R1 = 0.0644, wR2 = 0.1323	
Largest diff. peak and hole		0.456 and -0.254 $e.Å^{-3}$	

Table 28. Crystal structure determination parameters for **III-8**.

Empirical formula		$C_{30}H_{30}AlN_3$	
Formula weight		459.55	
Crystal habit		block	
Crystal color		colorless	
Temperature		200(2) K	
Wavelength		0.71073 Å	
Crystal system		Monoclinic	
Space group		P2(1)/m	
Unit cell dimensions:			
a	8.9717(3) Å	α	90°
b	19.8654(7) Å	β	113.658(2)°
c	10.1194(4) Å	γ	90°
Volume		1651.97(10) $Å^3$	
Z		4	
Density (calc)		1.848 Mg/m^3	
Absorption coefficient		0.158 mm^{-1}	
F(000)		976	
Crystal size		0.19 x 0.15 x 0.10 mm^3	
Theta range for data collection		2.05 to 28.32°	
Index ranges		-11<=h<=11, -25<=k<=26, -13<=l<=13	
Reflections collected		22744	
Independent reflections		4213 [R(int) = 0.0299]	
Completeness to theta = 25.242°		98.4 %	
Absorption correction		None	
Max. and min. transmission		0.9844 and 0.9706	
Refinement method		Full-matrix least-squares on F^2	
Data / restraints / parameters		4213 / 0 / 204	
Goodness-of-fit on F^2		1.043	
Final R indices [I>2sigma(I)]		R1 = 0.0456, wR2 = 0.1204	
R indices (all data)		R1 = 0.0624, wR2 = 0.1308	
Largest diff. peak and hole		0.258 and -0.219 $e.Å^{-3}$	

Table 29. Crystal structure determination parameters for **III-9**.

Empirical formula		$C_{72}H_{100}Al_2N_6O_{0.50}$	
Formula weight		1111.54	
Crystal habit		block	
Crystal color		colorless	
Temperature		200(2) K	
Wavelength		0.71073 Å	
Crystal system		Triclinic	
Space group		P-1	
Unit cell dimensions:			
a	11.9759(9) Å	α	104.188(3)°
b	12.3948(8) Å	β	93.639(4)°
c	24.9637(17) Å	γ	90.242(4)°
Volume		3584.6(4) $Å^3$	
Z		2	
Density (calc)		1.030 Mg/m^3	
Absorption coefficient		0.083 mm^{-1}	
F(000)		1208	
Crystal size		0.18 x 0.13 x 0.11 mm^3	
Theta range for data collection		2.38 to 24.81°	
Index ranges		-14<=h<=14, -14<=k<=14, -29<=l<=23	
Reflections collected		24915	
Independent reflections		12063 [R(int) = 0.0516]	
Completeness to theta = 24.81°		97.5 %	
Absorption correction		Semi-empirical from equivalents	
Max. and min. transmission		0.9910 and 0.9853	
Refinement method		Full-matrix least-squares on F^2	
Data / restraints / parameters		12063 / 18 / 746	
Goodness-of-fit on F^2		1.011	
Final R indices [I>2sigma(I)]		R1 = 0.0689, wR2 = 0.1628	
R indices (all data)		R1 = 0.1329, wR2 = 0.1955	
Largest diff. peak and hole		0.418 and -0.316 $e.Å^{-3}$	

Table 30. Crystal structure determination parameters for **III-10**.

Empirical formula		$C_{27.33}H_{34.67}Al_{0.67}N_{1.33}P_{0.67}$	
Formula weight		420.53	
Crystal habit		block	
Crystal color		yellow	
Temperature		200(2) K	
Wavelength		0.71073 Å	
Crystal system		Monoclinic	
Space group		P2(1)/c	
Unit cell dimensions:			
a	17.2991(7) Å	α	90°
b	12.1331(6) Å	β	100.282(2)°
c	18.0903(8) Å	γ	90°
Volume		3736.0(3) $Å^3$	
Z		6	
Density (calc)		1.121 Mg/m^3	
Absorption coefficient		0.127 mm^{-1}	
F(000)		1360	
Crystal size		0.23 x 0.17 x 0.13 mm^3	
Theta range for data collection		2.03 to 28.33°	
Index ranges		-23<=h<=23, -16<=k<=15, -24<=l<=23	
Reflections collected		52628	
Independent reflections		9241 [R(int) = 0.0242]	
Completeness to theta = 28.33°		99.3 %	
Absorption correction		Semi-empirical from equivalents	
Max. and min. transmission		0.9837 and 0.9715	
Refinement method		Full-matrix least-squares on F^2	
Data / restraints / parameters		9241 / 0 / 407	
Goodness-of-fit on F^2		1.012	
Final R indices [I>2sigma(I)]		R1 = 0.0500, wR2 = 0.1387	
R indices (all data)		R1 = 0.0631, wR2 = 0.1516	
Largest diff. peak and hole		0.525 and -0.364 $e.Å^{-3}$	

Table 31. Crystal structure determination parameters for **III-11**.

Empirical formula		$C_{40}H_{50}AlN_4O_4$	
Formula weight		677.82	
Crystal habit		block	
Crystal color		colorless	
Temperature		200(2) K	
Wavelength		0.71073 Å	
Crystal system		Monoclinic	
Space group		P2(1)/c	
Unit cell dimensions:			
a	13.2522(3) Å	α	90°
b	16.5975(4) Å	β	107.7689(12)°
c	15.2587(3) Å	γ	90°
Volume		3196.09(12) $Å^3$	
Z		4	
Density (calc)		1.409 Mg/m^3	
Absorption coefficient		0.116 mm^{-1}	
F(000)		1452	
Crystal size		0.18 x 0.14 x 0.12 mm^3	
Theta range for data collection		1.79 to 28.32°	
Index ranges		-17<=h<=14, -22<=k<=20, -20<=l<=20	
Reflections collected		35266	
Independent reflections		7879 [R(int) = 0.0321]	
Completeness to theta = 25.242°		99.1 %	
Absorption correction		None	
Max. and min. transmission		0.9862 and 0.9794	
Refinement method		Full-matrix least-squares on F^2	
Data / restraints / parameters		7879 / 0 / 337	
Goodness-of-fit on F^2		1.027	
Final R indices [I>2sigma(I)]		R1 = 0.0595, wR2 = 0.1575	
R indices (all data)		R1 = 0.0908, wR2 = 0.1782	
Largest diff. peak and hole		0.596 and -0.278 $e.Å^{-3}$	

Table 32. Crystal structure determination parameters for **III-15**.

Empirical formula		$C_{35}H_{43}AlF_4N_2$	
Formula weight		594.69	
Crystal habit		block	
Crystal color		colorless	
Temperature		200(2) K	
Wavelength		0.71073 Å	
Crystal system		Monoclinic	
Space group		P2(1)/c	
Unit cell dimensions:			
a	12.1958(3) Å	α	90°
b	22.3860(5) Å	β	109.4383(11)°
c	12.5990(3) Å	γ	90°
Volume		3243.66(13) $Å^3$	
Z		4	
Density (calc)		1.218 Mg/m^3	
Absorption coefficient		0.111 mm^{-1}	
F(000)		1264	
Crystal size		0.37 x 0.29 x 0.25 mm^3	
Theta range for data collection		1.941 to 28.333°	
Index ranges		-16<=h<=16, -29<=k<=29, -16<=l<=16	
Reflections collected		41754	
Independent reflections		8048 [R(int) = 0.0208]	
Completeness to theta = 25.242°		99.5 %	
Absorption correction		Semi-empirical from equivalents	
Max. and min. transmission		0.7457 and 0.6956	
Refinement method		Full-matrix least-squares on F^2	
Data / restraints / parameters		8048 / 0 / 381	
Goodness-of-fit on F^2		1.036	
Final R indices [I>2sigma(I)]		R1 = 0.0376, wR2 = 0.1033	
R indices (all data)		R1 = 0.0439, wR2 = 0.1094	
Largest diff. peak and hole		0.296 and -0.203 $e.Å^{-3}$	

Table 33. Crystal structure determination parameters for **III-18**.

Empirical formula		$C_{34}H_{51.50}AlFN_2$	
Formula weight		534.25	
Crystal habit		block	
Crystal color		colorless	
Temperature		200(2) K	
Wavelength		0.71073 Å	
Crystal system		Monoclinic	
Space group		P2(1)/c	
Unit cell dimensions:			
a	13.8480(4) Å	α	90°
b	14.7791(4) Å	β	98.8140(15)°
c	16.4335(5) Å	γ	90°
Volume		3323.58(17) $Å^3$	
Z		4	
Density (calc)		1.068 Mg/m^3	
Absorption coefficient		0.089 mm^{-1}	
F(000)		1166	
Crystal size		0.24 x 0.22 x 0.19 mm^3	
Theta range for data collection		1.863 to 28.334°	
Index ranges		-18<=h<=17, -12<=k<=19, -21<=l<=21	
Reflections collected		8152	
Independent reflections		5782 [R(int) = 0.0369]	
Completeness to theta = 25.242°		99.2 %	
Absorption correction		Multi-scan	
Max. and min. transmission		0.6720 and 0.7457	
Refinement method		Full-matrix least-squares on F^2	
Data / restraints / parameters		5782/ 76 / 363	
Goodness-of-fit on F^2		1.031	
Final R indices [I>2sigma(I)]		R1 = 0.0494, wR2 = 0.0781	
R indices (all data)		R1 = 0.1203, wR2 = 0.1374	
Largest diff. peak and hole		0.329 and -0.213 $e.Å^{-3}$	

Table 34. Crystal structure determination parameters for **III-19**.

Empirical formula		$C_{35}H_{52}AlFN_2$	
Formula weight		546.76	
Crystal habit		block	
Crystal color		colorless	
Temperature		200(2) K	
Wavelength		0.71073 Å	
Crystal system		Monoclinic	
Space group		P2(1)/m	
Unit cell dimensions:			
a	8.9145(6) Å	α	90°
b	19.8791(12) Å	β	114.2542(17)°
c	10.0955(6) Å	γ	90°
Volume		1631.13(18) $Å^3$	
Z		2	
Density (calc)		1.113 Mg/m^3	
Absorption coefficient		0.093 mm^{-1}	
F(000)		596	
Crystal size		0.35x 0.26 x 0.23 mm^3	
Theta range for data collection		2.049 to 28.354°	
Index ranges		-11<=h<=5, -26<=k<=24, -13<=l<=13	
Reflections collected		14090	
Independent reflections		4169 [R(int) = 0.0154]	
Completeness to theta = 25.242°		99.6 %	
Absorption correction		Semi-empirical from equivalents	
Max. and min. transmission		0.7457 and 0.6211	
Refinement method		Full-matrix least-squares on F^2	
Data / restraints / parameters		4169 / 0 / 185	
Goodness-of-fit on F^2		1.049	
Final R indices [I>2sigma(I)]		R1 = 0.0398, wR2 = 0.1105	
R indices (all data)		R1 = 0.0457, wR2 = 0.1164	
Largest diff. peak and hole		0.357 and -0.170 $e.Å^{-3}$	

Table 35. Crystal structure determination parameters for **III-20**.

Empirical formula		$C_{33}H_{49}AlN_2O$	
Formula weight		516.72	
Crystal habit		block	
Crystal color		colorless	
Temperature		200(2) K	
Wavelength		0.71073 Å	
Crystal system		Monoclinic	
Space group		P2(1)/c	
Unit cell dimensions:			
a	10.9788(2) Å	α	90°
b	12.4374(3) Å	β	98.9370(10)°
c	22.7307(5) Å	γ	90°
Volume		3066.14(11) $Å^3$	
Z		4	
Density (calc)		1.119 Mg/m^3	
Absorption coefficient		0.093 mm^{-1}	
F(000)		1128	
Crystal size		0.24 x 0.22 x 0.18 mm^3	
Theta range for data collection		1.814 to 28.330°	
Index ranges		-14<=h<=14, -16<=k<=16, -30<=l<=28	
Reflections collected		33869	
Independent reflections		7407 [R(int) = 0.0195]	
Completeness to theta = 25.242°		99.6 %	
Absorption correction		Semi-empirical from equivalents	
Max. and min. transmission		0.7457 and 0.7022	
Refinement method		Full-matrix least-squares on F^2	
Data / restraints / parameters		7407 / 0 / 336	
Goodness-of-fit on F^2		1.019	
Final R indices [I>2sigma(I)]		R1 = 0.0423, wR2 = 0.1132	
R indices (all data)		R1 = 0.0528, wR2 = 0.1219	
Largest diff. peak and hole		0.300 and -0.241 $e.Å^{-3}$	

Table 36. Crystal structure determination parameters for **III-21**.

Empirical formula		$C_{33}H_{50}AlN_2S$	
Formula weight		533.79	
Crystal habit		block	
Crystal color		colorless	
Temperature		200(2) K	
Wavelength		0.71073 Å	
Crystal system		Orthorhombic	
Space group		Pnma	
Unit cell dimensions:			
a	16.4471(5) Å	α	90°
b	20.3617(5) Å	β	90°
c	9.8161(2) Å	γ	90°
Volume		3287.32(14) $Å^3$	
Z		4	
Density (calc)		1.079 Mg/m^3	
Absorption coefficient		0.147 mm^{-1}	
F(000)		1164	
Crystal size		0.36 x 0.25 x 0.22 mm^3	
Theta range for data collection		2.00 to 28.37°	
Index ranges		-10<=h<=21, -27<=k<=27, -12<=l<=13	
Reflections collected		27846	
Independent reflections		4198 [R(int) = 0.0215]	
Completeness to theta = 25.242°		99.8 %	
Absorption correction		SADABS	
Max. and min. transmission		0.7457 and 0.6567	
Refinement method		Full-matrix least-squares on F^2	
Data / restraints / parameters		4198 / 0 / 184	
Goodness-of-fit on F^2		1.090	
Final R indices [I>2sigma(I)]		R1 = 0.0499, wR2 = 0.1539	
R indices (all data)		R1 = 0.0578, wR2 = 0.1637	
Largest diff. peak and hole		0.65 and -0.34 $e.Å^{-3}$	

Table 37. Crystal structure determination parameters for **III-22**.

Empirical formula		$C_{41}H_{51}AlN_2S_2$	
Formula weight		662.94	
Crystal habit		block	
Crystal color		colorless	
Temperature		200(2) K	
Wavelength		0.71073 Å	
Crystal system		Monoclinic	
Space group		P2(1)/c	
Unit cell dimensions:			
a	9.6103(7) Å	α	90°
b	22.3119(15) Å	β	95.512(2)°
c	17.1718(12) Å	γ	90°
Volume		3665.0(4) $Å^3$	
Z		4	
Density (calc)		1.2015 Mg/m^3	
Absorption coefficient		0.200 mm^{-1}	
F(000)		1424	
Crystal size		0.36 x 0.34 x 0.28 mm^3	
Theta range for data collection		2.18 to 29.00°	
Index ranges		-13<=h<=13, -31<=k<=31, -24<=l<=24	
Reflections collected		51462	
Independent reflections		9713 [R(int) = 0.0735]	
Completeness to theta = 26.0000°		99.5 %	
Absorption correction		SADABS	
Max. and min. transmission		0.76135 and 0.64321	
Refinement method		Full-matrix least-squares on F^2	
Data / restraints / parameters		9713 / 0 / 425	
Goodness-of-fit on F^2		1.067	
Final R indices [I>2sigma(I)]		R1 = 0.0668, wR2 = 0.1628	
R indices (all data)		R1 = 0.0799, wR2 = 0.1736	
Largest diff. peak and hole		0.75 and -0.38 e.$Å^{-3}$	

Table 38. Crystal structure determination parameters for **III-23**.

Empirical formula		$C_{53}H_{61}AlN_2P_2$	
Formula weight		814.96	
Crystal habit		block	
Crystal color		colorless	
Temperature		200(2) K	
Wavelength		0.71073 Å	
Crystal system		Monoclinic	
Space group		P2(1)/n	
Unit cell dimensions:			
a	14.6691(8) Å	α	90°
b	18.0515(10) Å	β	92.0975(15)°
c	17.5329(9) Å	γ	90°
Volume		4639.6(4) $Å^3$	
Z		4	
Density (calc)		1.750 Mg/m^3	
Absorption coefficient		0.224 mm^{-1}	
F(000)		2616	
Crystal size		0.26 x 0.16 x 0.14 mm^3	
Theta range for data collection		1.62 to 30.59°	
Index ranges		-20<=h<=21, -25<=k<=25, -24<=l<=24	
Reflections collected		14218	
Independent reflections		11797 [R(int) = 0.0205]	
Completeness to theta = 25.242°		99.9 %	
Absorption correction		SADABS	
Max. and min. transmission		0.7461 and 0.6723	
Refinement method		Full-matrix least-squares on F^2	
Data / restraints / parameters		14218 / 1 / 495	
Goodness-of-fit on F^2		1.033	
Final R indices [I>2sigma(I)]		R1 = 0.0459, wR2 = 0.1192	
R indices (all data)		R1 = 0.0570, wR2 = 0.1289	
Largest diff. peak and hole		0.74 and -0.69 e.$Å^{-3}$	

Table 39. Crystal structure determination parameters for **III-25**.

Empirical formula		$C_{45}H_{65}AlN_4S$	
Formula weight		721.05	
Crystal habit		block	
Crystal color		yellow	
Temperature		200(2) K	
Wavelength		0.71073 Å	
Crystal system		Monoclinic	
Space group		P2(1)/c	
Unit cell dimensions:			
a	12.1184(10) Å	α	90°
b	16.2978(13) Å	β	102.7380(10)°
c	22.5340(18) Å	γ	90°
Volume		4341.0(6) $Å^3$	
Z		4	
Density (calc)		1.103 Mg/m^3	
Absorption coefficient		0.129 mm^{-1}	
F(000)		1568	
Crystal size		0.684 x 0.608 x 0.388 mm^3	
Theta range for data collection		1.723 to 28.004°	
Index ranges		-15<=h<=15, -21<=k<=21, -29<=l<=29	
Reflections collected		48561	
Independent reflections		10405 [R(int) = 0.0275]	
Completeness to theta = 28.00°		99.5 %	
Absorption correction		Semi-empirical from equivalents	
Max. and min. transmission		0.7456 and 0.7134	
Refinement method		Full-matrix least-squares on F^2	
Data / restraints / parameters		10405 / 0 / 464	
Goodness-of-fit on F^2		1.031	
Final R indices [I>2sigma(I)]		R1 = 0.0501, wR2 = 0.1288	
R indices (all data)		R1 = 0.0672, wR2 = 0.1424	
Largest diff. peak and hole		0.566 and -0.280 $e.Å^{-3}$	

Table 40. Crystal structure determination parameters for **III-26**.

Empirical formula		$C_{43}H_{54}AlN_3S_2$	
Formula weight		703.99	
Crystal habit		block	
Crystal color		colorless	
Temperature		200(2) K	
Wavelength		0.71073 Å	
Crystal system		Monoclinic	
Space group		C2/c	
Unit cell dimensions:			
a	25.402(7) Å	α	90°
b	17.788(5) Å	β	123.514(10)°
c	21.029(10) Å	γ	90°
Volume		7922(5) $Å^3$	
Z		8	
Density (calc)		1.180 Mg/m^3	
Absorption coefficient		0.190 mm^{-1}	
F(000)		3024	
Crystal size		0.621 x 0.296 x 0.154 mm^3	
Theta range for data collection		2.040 to 28.099°	
Index ranges		-33<=h<=33, -23<=k<=23, -27<=l<=27	
Reflections collected		51115	
Independent reflections		9576 [R(int) = 0.0636]	
Completeness to theta = 28.10°		99.1 %	
Absorption correction		Semi-empirical from equivalents	
Max. and min. transmission		0.7456 and 0.6546	
Refinement method		Full-matrix least-squares on F^2	
Data / restraints / parameters		9576 / 0 / 446	
Goodness-of-fit on F^2		1.044	
Final R indices [I>2sigma(I)]		R1 = 0.0666, wR2 = 0.1585	
R indices (all data)		R1 = 0.1137, wR2 = 0.1884	
Largest diff. peak and hole		0.472 and -0.495 e.$Å^{-3}$	

Table 41. Crystal structure determination parameters for **III-27**.

Empirical formula		$C_{12}H_{15}N_3S$	
Formula weight		233.33	
Crystal habit		block	
Crystal color		colorless	
Temperature		200(2) K	
Wavelength		0.71073 Å	
Crystal system		Monoclinic	
Space group		P2(1)/c	
Unit cell dimensions:			
a	8.8344(14) Å	α	90°
b	10.2720(17) Å	β	99.426(12)°
c	13.913(3) Å	γ	90°
Volume		1245.5(4) $Å^3$	
Z		4	
Density (calc)		1.244 Mg/m^3	
Absorption coefficient		0.237 mm^{-1}	
F(000)		496	
Crystal size		0.44 x 0.31 x 0.1 mm^3	
Theta range for data collection		2.34 to 28.32°	
Index ranges		-11<=h<=11, -13<=k<=13, -18<=l<=18	
Reflections collected		19869	
Independent reflections		3090 [R(int) = 0.064]	
Completeness to theta = 28.32°		99.6 %	
Absorption correction		Semi-empirical from equivalents	
Max. and min. transmission		0.9039 and 0.9758	
Refinement method		Full-matrix least-squares on F^2	
Data / restraints / parameters		3090 / 0 / 145	
Goodness-of-fit on F^2		0.998	
Final R indices [I>2sigma(I)]		R1 = 0.0501, wR2 = 0.1261	
R indices (all data)		R1 = 0.0794, wR2 = 0.1474	
Largest diff. peak and hole		0.349 and -0.303 e.$Å^{-3}$	

Table 42. Crystal structure determination parameters for **III-29**.

Empirical formula		$C_{1.53}H_{2.34}Al_{0.09}N_{0.17}O_{0.06}$	
Formula weight		26.46	
Crystal habit		block	
Crystal color		colorless	
Temperature		200(2) K	
Wavelength		0.71073 Å	
Crystal system		Monoclinic	
Space group		P2(1)	
Unit cell dimensions:			
a	8.9776(18) Å	α	90°
b	35.496(7) Å	β	98.931(2)°
c	11.535(2) Å	γ	90°
Volume		3631.3(13) $Å^3$	
Z		47	
Density (calc)		0.569 Mg/m^3	
Absorption coefficient		0.057 mm^{-1}	
F(000)		674	
Crystal size		0.44 x 0.31 x 0.1 mm^3	
Theta range for data collection		1.88 to 28.31°	
Index ranges		-11<=h<=11, -45<=k<=47, -14<=l<=15	
Reflections collected		44072	
Independent reflections		17365 [R(int) = 0.042]	
Completeness to theta = 28.31°		98.5 %	
Absorption correction		Semi-empirical from equivalents	
Max. and min. transmission		0.9039 and 0.9758	
Refinement method		Full-matrix least-squares on F^2	
Data / restraints / parameters		17365 / 1 / 790	
Goodness-of-fit on F^2		0.939	
Final R indices [I>2sigma(I)]		R1 = 0.0531, wR2 = 0.1326	
R indices (all data)		R1 = 0.0814, wR2 = 0.1510	
Largest diff. peak and hole		0.276 and -0.246 e.$Å^{-3}$	

Table 43. Crystal structure determination parameters for **III-32**.

Empirical formula		$C_{35}H_{56}AlN_2O_2P$	
Formula weight		233.33	
Crystal habit		block	
Crystal color		colorless	
Temperature		200(2) K	
Wavelength		0.71073 Å	
Crystal system		Orthorhombic	
Space group		Pnma	
Unit cell dimensions:			
a	16.400(5) Å	α	90°
b	21.773(6) Å	β	90°
c	9.744(3) Å	γ	90°
Volume		3749.5(17) $Å^3$	
Z		4	
Density (calc)		1.135 Mg/m^3	
Absorption coefficient		0.136 mm^{-1}	
F(000)		1296	
Crystal size		0.26 x 0.21 x 0.12 mm^3	
Theta range for data collection		1.87 to 28.32°	
Index ranges		-21<=h<=21, -28<=k<=29, -12<=l<=12	
Reflections collected		40494	
Independent reflections		4421 [R(int) = 0.044]	
Completeness to theta = 28.32°		99.8 %	
Absorption correction		Semi-empirical from equivalents	
Max. and min. transmission		0.9658 and 0.9836	
Refinement method		Full-matrix least-squares on F^2	
Data / restraints / parameters		4421 / 0 / 215	
Goodness-of-fit on F^2		1.063	
Final R indices [I>2sigma(I)]		R1 = 0.0412, wR2 = 0.1022	
R indices (all data)		R1 = 0.0698, wR2 = 0.1218	
Largest diff. peak and hole		0.380 and -0.353 $e.Å^{-3}$	

Table 44. Crystal structure determination parameters for **IV-1**.

Empirical formula		$C_{33.75}H_{44.50}Cl_{5.50}Ge_2N_3$	
Formula weight		832.38	
Crystal habit		block	
Crystal color		orange	
Temperature		200(2) K	
Wavelength		0.71073 Å	
Crystal system		Triclinic	
Space group		P-1	
Unit cell dimensions:			
a	10.3253(2) Å	α	102.5690(10)°
b	12.6550(3) Å	β	92.9670(10)°
c	16.4056(4) Å	γ	106.9180(10)°
Volume		1986.48(8) $Å^3$	
Z		2	
Density (calc)		1.392 Mg/m^3	
Absorption coefficient		1.909 mm^{-1}	
F(000)		851	
Crystal size		0.230 x 0.170 x 0.120 mm^3	
Theta range for data collection		1.889 to 28.347°	
Index ranges		-13<=h<=13, -16<=k<=16, -21<=l<=21	
Reflections collected		28878	
Independent reflections		9729 [R(int) = 0.0193]	
Completeness to theta = 25.242°		99.2 %	
Absorption correction		Semi-empirical from equivalents	
Max. and min. transmission		0.7457 and 0.6174	
Refinement method		Full-matrix least-squares on F^2	
Data / restraints / parameters		9729 / 34 / 412	
Goodness-of-fit on F^2		0.976	
Final R indices [I>2sigma(I)]		R1 = 0.0427, wR2 = 0.1237	
R indices (all data)		R1 = 0.0503, wR2 = 0.1309	
Largest diff. peak and hole		1.617 and -0.855 e.$Å^{-3}$	

Table 45. Crystal structure determination parameters for **IV-4**.

Empirical formula		$C_{33}H_{43}GeN_3$	
Formula weight		554.29	
Crystal habit		block	
Crystal color		green	
Temperature		200(2) K	
Wavelength		0.71073 Å	
Crystal system		Monoclinic	
Space group		C2/c	
Unit cell dimensions:			
a	23.2465(9) Å	α	90°
b	8.5300(3) Å	β	104.746(2)°
c	15.8674(7) Å	γ	90°
Volume		3042.8(2) $Å^3$	
Z		4	
Density (calc)		1.210 Mg/m^3	
Absorption coefficient		1.031 mm^{-1}	
F(000)		1176	
Crystal size		0.180 x 0.110 x 0.100 mm^3	
Theta range for data collection		1.812 to 28.305°	
Index ranges		-30<=h<=30, -11<=k<=11, -21<=l<=19	
Reflections collected		17133	
Independent reflections		3737 [R(int) = 0.0315]	
Completeness to theta = 25.242°		99.2 %	
Absorption correction		Semi-empirical from equivalents	
Max. and min. transmission		0.7457 and 0.5705	
Refinement method		Full-matrix least-squares on F^2	
Data / restraints / parameters		3737 / 0 / 170	
Goodness-of-fit on F^2		1.008	
Final R indices [I>2sigma(I)]		R1 = 0.0349, wR2 = 0.0796	
R indices (all data)		R1 = 0.0681, wR2 = 0.0914	
Largest diff. peak and hole		0.335 and -0.339 $e.Å^{-3}$	

Table 46. Crystal structure determination parameters for **IV-5**.

Empirical formula		$C_{33}H_{45}N_3$	
Formula weight		483.72	
Crystal habit		needle	
Crystal color		colorless	
Temperature		200(2) K	
Wavelength		0.71073 Å	
Crystal system		Orthorhombic	
Space group		Pbca	
Unit cell dimensions:			
a	16.5977(5) Å	α	90°
b	11.5560(3) Å	β	90°
c	31.1594(9) Å	γ	90°
Volume		5976.5(3) $Å^3$	
Z		8	
Density (calc)		1.075 Mg/m^3	
Absorption coefficient		0.062 mm^{-1}	
F(000)		2112	
Crystal size		0.150 x 0.090 x 0.060 mm^3	
Theta range for data collection		1.793 to 24.758°	
Index ranges		-19<=h<=19, -13<=k<=12, -36<=l<=36	
Reflections collected		49767	
Independent reflections		5114 [R(int) = 0.0900]	
Completeness to theta = 24.758°		99.8 %	
Absorption correction		Semi-empirical from equivalents	
Max. and min. transmission		0.7451 and 0.5524	
Refinement method		Full-matrix least-squares on F^2	
Data / restraints / parameters		5114 / 21 / 327	
Goodness-of-fit on F^2		1.018	
Final R indices [I>2sigma(I)]		R1 = 0.0630, wR2 = 0.1508	
R indices (all data)		R1 = 0.1202, wR2 = 0.1837	
Largest diff. peak and hole		0.443 and -0.178 $e.Å^{-3}$	

Table 47. Crystal structure determination parameters for **IV-6**.

Empirical formula		$C_{33}H_{43}ClN_3Zn$	
Formula weight		582.52	
Crystal habit		block	
Crystal color		green	
Temperature		200(2) K	
Wavelength		0.71073 Å	
Crystal system		Monoclinic	
Space group		P2(1)/n	
Unit cell dimensions:			
a	8.6852(2) Å	α	90°
b	13.9641(4) Å	β	92.0765(12)°
c	25.8243(7) Å	γ	90°
Volume		3129.94(14) $Å^3$	
Z		4	
Density (calc)		1.236 Mg/m^3	
Absorption coefficient		0.895 mm^{-1}	
F(000)		1236	
Crystal size		0.13 x 0.11 x 0.10 mm^3	
Theta range for data collection		1.578 to 28.245°	
Index ranges		-11<=h<=10, -17<=k<=18, -27<=l<=30	
Reflections collected		30834	
Independent reflections		6787 [R(int) = 0.0427]	
Completeness to theta = 25.242°		98.6 %	
Absorption correction		Semi-empirical from equivalents	
Max. and min. transmission		0.7457 and 0.6493	
Refinement method		Full-matrix least-squares on F^2	
Data / restraints / parameters		6787 / 0 / 343	
Goodness-of-fit on F^2		1.025	
Final R indices [I>2sigma(I)]		R1 = 0.0394, wR2 = 0.0937	
R indices (all data)		R1 = 0.0671, wR2 = 0.1048	
Largest diff. peak and hole		0.730 and -0.391 $e.Å^{-3}$	

Table 48. Crystal structure determination parameters for **IV-7**.

Empirical formula		$C_{40}H_{53}ClN_5Zn$	
Formula weight		704.69	
Crystal habit		block	
Crystal color		red	
Temperature		200(2) K	
Wavelength		0.71073 Å	
Crystal system		Triclinic	
Space group		P-1	
Unit cell dimensions:			
a	8.8613(4) Å	α	108.539(2)°
b	12.6319(6) Å	β	90.012(2)°
c	17.9583(8) Å	γ	93.205(2)°
Volume		1905.28(15) $Å^3$	
Z		2	
Density (calc)		1.228 Mg/m^3	
Absorption coefficient		0.748 mm^{-1}	
F(000)		750	
Crystal size		0.19 x 0.12 x 0.10 mm^3	
Theta range for data collection		1.741 to 28.349°	
Index ranges		-11<=h<=11, -16<=k<=15, 0<=l<=23	
Reflections collected		28106	
Independent reflections		28106 [R(int) = 0.0292]	
Completeness to theta = 25.242°		99.2 %	
Absorption correction		Semi-empirical from equivalents	
Max. and min. transmission		0.745685 and 0.649428	
Refinement method		Full-matrix least-squares on F^2	
Data / restraints / parameters		9342 / 21 / 425	
Goodness-of-fit on F^2		0.863	
Final R indices [I>2sigma(I)]		R1 = 0.0465, wR2 = 0.1223	
R indices (all data)		R1 = 0.0676, wR2 = 0.1397	
Largest diff. peak and hole		0.543 and -0.625 $e.Å^{-3}$	

Table 49. Crystal structure determination parameters for **IV-8**.

Empirical formula		$C_{34}H_{46}N_3Zn$	
Formula weight		562.11	
Crystal habit		block	
Crystal color		red	
Temperature		200(2) K	
Wavelength		0.71073 Å	
Crystal system		Monoclinic	
Space group		P2(1)/n	
Unit cell dimensions:			
a	14.328(2) Å	α	90°
b	8.7698(13) Å	β	93.489(7)°
c	25.005(4) Å	γ	90°
Volume		3136.3(8) $Å^3$	
Z		4	
Density (calc)		1.190 Mg/m^3	
Absorption coefficient		0.808 mm^{-1}	
F(000)		1204	
Crystal size		0.20 x 0.16 x 0.12 mm^3	
Theta range for data collection		1.579 to 28.338°	
Index ranges		-19<=h<=19, 0<=k<=11, 0<=l<=33	
Reflections collected		11644	
Independent reflections		11644 [R(int) = 0.0499]	
Completeness to theta = 25.242°		89.0 %	
Absorption correction		Semi-empirical from equivalents	
Max. and min. transmission		0.745686 and 0.601014	
Refinement method		Full-matrix least-squares on F^2	
Data / restraints / parameters		5714 / 0 / 354	
Goodness-of-fit on F^2		1.073	
Final R indices [I>2sigma(I)]		R1 = 0.0591, wR2 = 0.1723	
R indices (all data)		R1 = 0.0703, wR2 = 0.1768	
Largest diff. peak and hole		0.843 and -0.424 $e.Å^{-3}$	

Table 50. Crystal structure determination parameters for **IV-9**.

Empirical formula		$C_{20}H_{20}N_3Zn$	
Formula weight		367.76	
Crystal habit		block	
Crystal color		green	
Temperature		200(2) K	
Wavelength		0.71073 Å	
Crystal system		Triclinic	
Space group		P-1	
Unit cell dimensions:			
a	14.5172(4) Å	α	90.5750(17)°
b	18.2605(5) Å	β	109.8856(15)°
c	19.9983(5) Å	γ	97.8222(16)°
Volume		4929.8(2) $Å^3$	
Z		12	
Density (calc)		1.486 Mg/m^3	
Absorption coefficient		1.500 mm^{-1}	
F(000)		2292	
Crystal size		0.24 x 0.21 x 0.21 mm^3	
Theta range for data collection		1.988 to 30.555°	
Index ranges		-20<=h<=19, -25<=k<=25, 0<=l<=28	
Reflections collected		40318	
Independent reflections		27446 [R(int) = 0.0482]	
Completeness to theta = 25.242°		99.6 %	
Absorption correction		Semi-empirical from equivalents	
Max. and min. transmission		0.746068 and 0.651904	
Refinement method		Full-matrix least-squares on F^2	
Data / restraints / parameters		27446 / 85 / 1109	
Goodness-of-fit on F^2		0.999	
Final R indices [I>2sigma(I)]		R1 = 0.0697, wR2 = 0.1682	
R indices (all data)		R1 = 0.1519, wR2 = 0.2078	
Largest diff. peak and hole		0.736 and -1.020 e.$Å^{-3}$	

VIII. References

(1) Power, P. P. *Chem. Rev.* **2003**, *103*, 789.
(2) Breher, F. *Coord. Chem. Rev.* **2007**, *251*, 1007.
(3) Power, P. P. *Organometallics* **2007**, *26*, 4362.
(4) Rivard, E.; Power, P. P. *Inorg. Chem.* **2007**, *46*, 10047.
(5) Nagendran, S.; Roesky, H. W. *Organometallics* **2008**, *27*, 457.
(6) Asay, M.; Jones, C.; Driess, M. *Chem. Rev.* **2011**, *111*, 354.
(7) Power, P. P. *Nature* **2010**, *463*, 171.
(8) Cui, C.; Roesky, H. W.; Schmidt, H.-G.; Noltemeyer, M.; Hao, H.; Cimpoesu, F. *Angew. Chem., Int. Ed.* **2000**, *39*, 4274.
(9) Xiong, Y.; Yao, S.; Tan, G.; Inoue, S.; Driess, M. *J. Am. Chem. Soc.* **2013**, *135*, 5004.
(10) Li, Y.; Mondal, K. C.; Roesky, H. W.; Zhu, H.; Stollberg, P.; Herbst-Irmer, R.; Stalke, D.; Andrada, D. M. *J. Am. Chem. Soc.* **2013**, *135*, 12422.
(11) Hartwig, J. F. *Organotransition Metal Chemistry: From Bonding to Catalysis*; University Science Books: Sausalito, California, 2010.
(12) Welch, G. C.; San Juan, R. R.; Masuda, J. D.; Stephan, D. W. *Science* **2006**, *314*, 1124.
(13) Welch, G. C.; Stephan, D. W. *J. Am. Chem. Soc.* **2007**, *129*, 1880.
(14) Stephan, D. W. *Acc. Chem. Res.* **2015**, *48*, 306.
(15) Stephan, D. W. *J. Am. Chem. Soc.* **2015**, *137*, 10018.
(16) Stephan, D. W.; Erker, G. *Angew. Chem., Int. Ed.* **2015**, *54*, 6400.
(17) Mas-Ballesté, R.; Lledós, A. In *Comprehensive Inorganic Chemistry II*; 2 ed.; Poeppelmeier, K., Ed.; Elsevier: Amsterdam, 2013; Vol. 9, p 727.
(18) Himmel, H.-J. *Dalton Trans.* **2003**, 3639.
(19) Xiao, Z. L.; Hauge, R. H.; Margrave, J. L. *Inorg. Chem.* **1993**, *32*, 642.
(20) Himmel, H.-J.; Vollet, J. *Organometallics* **2002**, *21*, 5972.
(21) Spikes, G. H.; Fettinger, J. C.; Power, P. P. *J. Am. Chem. Soc.* **2005**, *127*, 12232.
(22) Fan, C.; Mercier, L. G.; Piers, W. E.; Tuononen, H. M.; Parvez, M. *J. Am. Chem. Soc.* **2010**, *132*, 9604.
(23) Houghton, A. Y.; Karttunen, V. A.; Fan, C.; Piers, W. E.; Tuononen, H. M. *J. Am. Chem. Soc.* **2013**, *135*, 941.
(24) Dahcheh, F.; Martin, D.; Stephan, D. W.; Bertrand, G. *Angew. Chem., Int. Ed.* **2014**, *53*, 13159.
(25) Zhu, Z.; Wang, X.; Peng, Y.; Lei, H.; Fettinger, J. C.; Rivard, E.; Power, P. P. *Angew. Chem., Int. Ed.* **2009**, *48*, 2031.
(26) Caputo, C. A.; Koivistoinen, J.; Moilanen, J.; Boynton, J. N.; Tuononen, H. M.; Power, P. P. *J. Am. Chem. Soc.* **2013**, *135*, 1952.
(27) Seifert, A.; Scheid, D.; Linti, G.; Zessin, T. *Chem. - Eur. J.* **2009**, *15*, 12114.
(28) Abdalla, J. A. B.; Riddlestone, I. M.; Tirfoin, R.; Aldridge, S. *Angew. Chem., Int. Ed.* **2015**, *54*, 5098.
(29) Frey, G. D.; Lavallo, V.; Donnadieu, B.; Schoeller, W. W.; Bertrand, G. *Science* **2007**, *316*, 439.

(30) Protchenko, A. V.; Birjkumar, K. H.; Dange, D.; Schwarz, A. D.; Vidovic, D.; Jones, C.; Kaltsoyannis, N.; Mountford, P.; Aldridge, S. *J. Am. Chem. Soc.* **2012**, *134*, 6500.
(31) Protchenko, A. V.; Schwarz, A. D.; Blake, M. P.; Jones, C.; Kaltsoyannis, N.; Mountford, P.; Aldridge, S. *Angew. Chem., Int. Ed.* **2013**, *52*, 568.
(32) Li, J.; Schenk, C.; Goedecke, C.; Frenking, G.; Jones, C. *J. Am. Chem. Soc.* **2011**, *133*, 18622.
(33) Hermann, M.; Goedecke, C.; Jones, C.; Frenking, G. *Organometallics* **2013**, *32*, 6666.
(34) Hadlington, T. J.; Hermann, M.; Li, J.; Frenking, G.; Jones, C. *Angew. Chem., Int. Ed.* **2013**, *52*, 10199.
(35) Hermann, M.; Jones, C.; Frenking, G. *Inorg. Chem.* **2014**, *53*, 6482.
(36) Peng, Y.; Guo, J.-D.; Ellis, B. D.; Zhu, Z.; Fettinger, J. C.; Nagase, S.; Power, P. P. *J. Am. Chem. Soc.* **2009**, *131*, 16272.
(37) Peng, Y.; Brynda, M.; Ellis, B. D.; Fettinger, J. C.; Rivard, E.; Power, P. P. *Chem. Commun.* **2008**, 6042.
(38) Zhao, L.; Huang, F.; Lu, G.; Wang, Z.-X.; Schleyer, P. v. R. *J. Am. Chem. Soc.* **2012**, *134*, 8856.
(39) Hadlington, T. J.; Jones, C. *Chem. Commun.* **2014**, *50*, 2321.
(40) Peng, Y.; Ellis, B. D.; Wang, X.; Power, P. P. *J. Am. Chem. Soc.* **2008**, *130*, 12268.
(41) Protchenko, A. V.; Bates, J. I.; Saleh, L. M. A.; Blake, M. P.; Schwarz, A. D.; Kolychev, E. L.; Thompson, A. L.; Jones, C.; Mountford, P.; Aldridge, S. *J. Am. Chem. Soc.* **2016**, *138*, 4555.
(42) Vasko, P.; Wang, S.; Tuononen, H. M.; Power, P. P. *Angew. Chem., Int. Ed.* **2015**, *54*, 3802.
(43) Longobardi, L. E.; Russell, C. A.; Green, M.; Townsend, N. S.; Wang, K.; Holmes, A. J.; Duckett, S. B.; McGrady, J. E.; Stephan, D. W. *J. Am. Chem. Soc.* **2014**, *136*, 13453.
(44) Zhao, J.; Goldman, A. S.; Hartwig, J. F. *Science* **2005**, *307*, 1080.
(45) Herrmann, W. A.; Elison, M.; Fischer, J.; Köcher, C.; Artus, G. R. J. *Chem. - Eur. J.* **1996**, *2*, 772.
(46) Moerdyk, J. P.; Blake, G. A.; Chase, D. T.; Bielawski, C. W. *J. Am. Chem. Soc.* **2013**, *135*, 18798.
(47) Teator, A. J.; Tian, Y.; Chen, M.; Lee, J. K.; Bielawski, C. W. *Angew. Chem., Int. Ed.* **2015**, *54*, 11559.
(48) Hudnall, T. W.; Moerdyk, J. P.; Bielawski, C. W. *Chem. Commun.* **2010**, *46*, 4288.
(49) Moerdyk, J. P.; Bielawski, C. W. *Chem. Commun.* **2014**, *50*, 4551.
(50) Jana, A.; Schulzke, C.; Roesky, H. W. *J. Am. Chem. Soc.* **2009**, *131*, 4600.
(51) Alberto, M. E.; Russo, N.; Sicilia, E. *Chem. - Eur. J.* **2013**, *19*, 7835.
(52) Jana, A.; Roesky, H. W.; Schulzke, C.; Samuel, P. P. *Organometallics* **2009**, *28*, 6574.
(53) Meltzer, A.; Inoue, S.; Präsang, C.; Driess, M. *J. Am. Chem. Soc.* **2010**, *132*, 3038.

(54) Xiong, Y.; Yao, S.; Müller, R.; Kaupp, M.; Driess, M. *J. Am. Chem. Soc.* **2010**, *132*, 6912.
(55) Jana, A.; Objartel, I.; Roesky, H. W.; Stalke, D. *Inorg. Chem.* **2009**, *48*, 798.
(56) Jana, A.; Roesky, H. W.; Schulzke, C.; Samuel, P. P.; Döring, A. *Inorg. Chem.* **2010**, *49*, 5554.
(57) Wang, W.; Inoue, S.; Yao, S.; Driess, M. *Organometallics* **2011**, *30*, 6490.
(58) Brown, Z. D.; Guo, J.-D.; Nagase, S.; Power, P. P. *Organometallics* **2012**, *31*, 3768.
(59) McCarthy, S. M.; Lin, Y.-C.; Devarajan, D.; Chang, J. W.; Yennawar, H. P.; Rioux, R. M.; Ess, D. H.; Radosevich, A. T. *J. Am. Chem. Soc.* **2014**, *136*, 4640.
(60) Arduengo, A. J.; Stewart, C. A. *Chem. Rev.* **1994**, *94*, 1215.
(61) Cui, J.; Li, Y.; Ganguly, R.; Inthirarajah, A.; Hirao, H.; Kinjo, R. *J. Am. Chem. Soc.* **2014**, *136*, 16764.
(62) Zhao, W.; McCarthy, S. M.; Lai, T. Y.; Yennawar, H. P.; Radosevich, A. T. *J. Am. Chem. Soc.* **2014**, *136*, 17634.
(63) Robinson, T. P.; De Rosa, D. M.; Aldridge, S.; Goicoechea, J. M. *Angew. Chem., Int. Ed.* **2015**, *54*, 13758.
(64) Yao, S.; Brym, M.; van Wüllen, C.; Driess, M. *Angew. Chem., Int. Ed.* **2007**, *46*, 4159.
(65) Lappert, M. F.; Miles, S. J.; Atwood, J. L.; Zaworotko, M. J.; Carty, A. J. *J. Organomet. Chem.* **1981**, *212*, C4.
(66) Erickson, J. D.; Vasko, P.; Riparetti, R. D.; Fettinger, J. C.; Tuononen, H. M.; Power, P. P. *Organometallics* **2015**, *34*, 5785.
(67) Jana, A.; Nekoueishahraki, B.; Roesky, H. W.; Schulzke, C. *Organometallics* **2009**, *28*, 3763.
(68) Schager, F.; Goddard, R.; Seevogel, K.; Pörschke, K.-R. *Organometallics* **1998**, *17*, 1546.
(69) Goldberg, K. I.; Goldman, A. S. *Activation and Functionalization of C—H Bonds*; American Chemical Society, 2004; Vol. 885.
(70) Tan, G.; Szilvási, T.; Inoue, S.; Blom, B.; Driess, M. *J. Am. Chem. Soc.* **2014**, *136*, 9732.
(71) Jones, C.; Mills, D. P.; Rose, R. P. *J. Organomet. Chem.* **2006**, *691*, 3060.
(72) Arduengo III, A. J.; Calabrese, J. C.; Davidson, F.; Rasika Dias, H. V.; Goerlich, J. R.; Krafczyk, R.; Marshall, W. J.; Tamm, M.; Schmutzler, R. *Helv. Chim. Acta* **1999**, *82*, 2348.
(73) Iglesias, M.; Beetstra, D. J.; Knight, J. C.; Ooi, L.-L.; Stasch, A.; Coles, S.; Male, L.; Hursthouse, M. B.; Cavell, K. J.; Dervisi, A.; Fallis, I. A. *Organometallics* **2008**, *27*, 3279.
(74) Holdroyd, R. S.; Page, M. J.; Warren, M. R.; Whittlesey, M. K. *Tetrahedron Lett.* **2010**, *51*, 557.
(75) Korotkikh, N. I.; Rayenko, G. F.; Shvaika, O. P.; Pekhtereva, T. M.; Cowley, A. H.; Jones, J. N.; Macdonald, C. L. B. *J. Org. Chem.* **2003**, *68*, 5762.
(76) Solé, S.; Gornitzka, H.; Schoeller, W. W.; Bourissou, D.; Bertrand, G. *Science* **2001**, *292*, 1901.
(77) Vignolle, J.; Asay, M.; Miqueu, K.; Bourissou, D.; Bertrand, G. *Org. Lett.* **2008**, *10*, 4299.

(78) Hudnall, T. W.; Bielawski, C. W. *J. Am. Chem. Soc.* **2009**, *131*, 16039.
(79) Moerdyk, J. P.; Bielawski, C. W. *Chem. - Eur. J.* **2013**, *19*, 14773.
(80) McCarty, Z. R.; Lastovickova, D. N.; Bielawski, C. W. *Chem. Commun.* **2016**, *52*, 5447.
(81) Yao, S.; van Wüllen, C.; Sun, X.-Y.; Driess, M. *Angew. Chem., Int. Ed.* **2008**, *47*, 3250.
(82) Jana, A.; Samuel, P. P.; Tavčar, G.; Roesky, H. W.; Schulzke, C. *J. Am. Chem. Soc.* **2010**, *132*, 10164.
(83) Xiong, Y.; Yao, S.; Driess, M. *Chem. - Asian J.* **2010**, *5*, 322.
(84) Agou, T.; Sugiyama, Y.; Sasamori, T.; Sakai, H.; Furukawa, Y.; Takagi, N.; Guo, J.-D.; Nagase, S.; Hashizume, D.; Tokitoh, N. *J. Am. Chem. Soc.* **2012**, *134*, 4120.
(85) Yao, S.; van Wullen, C.; Driess, M. *Chem. Commun.* **2008**, 5393.
(86) Jana, A.; Objartel, I.; Roesky, H. W.; Stalke, D. *Inorg. Chem.* **2009**, *48*, 7645.
(87) Summerscales, O. T.; Fettinger, J. C.; Power, P. P. *J. Am. Chem. Soc.* **2011**, *133*, 11960.
(88) Peng, Y.; Ellis, B. D.; Wang, X.; Fettinger, J. C.; Power, P. P. *Science* **2009**, *325*, 1668.
(89) Summerscales, O. T.; Caputo, C. A.; Knapp, C. E.; Fettinger, J. C.; Power, P. P. *J. Am. Chem. Soc.* **2012**, *134*, 14595.
(90) Hadlington, T. J.; Li, J.; Hermann, M.; Davey, A.; Frenking, G.; Jones, C. *Organometallics* **2015**, *34*, 3175.
(91) Brown, Z. D.; Vasko, P.; Fettinger, J. C.; Tuononen, H. M.; Power, P. P. *J. Am. Chem. Soc.* **2012**, *134*, 4045.
(92) Braunschweig, H.; Damme, A.; Hörl, C.; Kupfer, T.; Wahler, J. *Organometallics* **2013**, *32*, 6800.
(93) Frey, G. D.; Masuda, J. D.; Donnadieu, B.; Bertrand, G. *Angew. Chem., Int. Ed.* **2010**, *49*, 9444.
(94) Schmidt, D.; Berthel, J. H. J.; Pietsch, S.; Radius, U. *Angew. Chem., Int. Ed.* **2012**, *51*, 8881.
(95) Lastovickova, D. N.; Moerdyk, J. P.; Kelley, A. R.; Bielawski, C. W. *J. Phys. Org. Chem.* **2015**, *28*, 75.
(96) Heuclin, H.; Ho, S. Y. F.; Le Goff, X. F.; So, C.-W.; Mézailles, N. *J. Am. Chem. Soc.* **2013**, *135*, 8774.
(97) Lastovickova, D. N.; Bielawski, C. W. *Organometallics* **2016**, *35*, 706.
(98) Xiong, Y.; Yao, S.; Driess, M. *Chem. - Eur. J.* **2012**, *18*, 3316.
(99) Chase, D. T.; Moerdyk, J. P.; Bielawski, C. W. *Org. Lett.* **2014**, *16*, 812.
(100) Präsang, C.; Stoelzel, M.; Inoue, S.; Meltzer, A.; Driess, M. *Angew. Chem., Int. Ed.* **2010**, *49*, 10002.
(101) Dube, J. W.; Brown, Z. D.; Caputo, C. A.; Power, P. P.; Ragogna, P. J. *Chem. Commun.* **2014**, *50*, 1944.
(102) Ung, G.; Bertrand, G. *Chem. - Eur. J.* **2012**, *18*, 12955.
(103) Styra, S.; Melaimi, M.; Moore, C. E.; Rheingold, A. L.; Augenstein, T.; Breher, F.; Bertrand, G. *Chem. - Eur. J.* **2015**, *21*, 8441.
(104) Junold, K.; Nutz, M.; Baus, J. A.; Burschka, C.; Fonseca Guerra, C.; Bickelhaupt, F. M.; Tacke, R. *Chem. - Eur. J.* **2014**, *20*, 9319.

(105) Samuel, P. P.; Singh, A. P.; Sarish, S. P.; Matussek, J.; Objartel, I.; Roesky, H. W.; Stalke, D. *Inorg. Chem.* **2013**, *52*, 1544.
(106) Azhakar, R.; Roesky, H. W.; Wolf, H.; Stalke, D. *Chem. Commun.* **2013**, *49*, 1841.
(107) Kempter, A.; Gemel, C.; Fischer, R. A. *Inorg. Chem.* **2008**, *47*, 7279.
(108) Hill, M. S.; Hitchcock, P. B.; Pongtavornpinyo, R. *Inorg. Chem.* **2007**, *46*, 3783.
(109) Xiong, Y.; Yao, S.; Driess, M. *Organometallics* **2009**, *28*, 1927.
(110) Driess, M.; Yao, S.; Brym, M.; van Wüllen, C.; Lentz, D. *J. Am. Chem. Soc.* **2006**, *128*, 9628.
(111) Gynane, M. J. S.; Lappert, M. F.; Miles, S. J.; Carty, A. J.; Taylor, N. J. *J. Chem. Soc., Dalton Trans.* **1977**, 2009.
(112) Eaborn, C.; Hill, M. S.; Hitchcock, P. B.; Patel, D.; Smith, J. D.; Zhang, S. *Organometallics* **2000**, *19*, 49.
(113) Asadi, A.; Eaborn, C.; Hill, M. S.; Hitchcock, P. B.; Meehan, M. M.; Smith, J. D. *Organometallics* **2002**, *21*, 2430.
(114) Aldridge, S. In *The Group 13 Metals Aluminium, Gallium, Indium and Thallium: Chemical Patterns and Peculiarities*; John Wiley & Sons, Ltd: 2011, p 75.
(115) Aldridge, S.; Downs, A. J.; Kays, D. L. In *The Group 13 Metals Aluminium, Gallium, Indium and Thallium: Chemical Patterns and Peculiarities*; John Wiley & Sons, Ltd: 2011, p 148.
(116) Klemm, W.; Voss, E.; Geiersberger, K. *Z. Anorg. Chem.* **1948**, *256*, 15.
(117) Dohmeier, C.; Loos, D.; Schnöckel, H. *Angew. Chem., Int. Ed.* **1996**, *35*, 129.
(118) Dohmeier, C.; Robl, C.; Tacke, M.; Schnöckel, H. *Angew. Chem., Int. Ed. Engl.* **1991**, *30*, 564.
(119) Schulz, S.; Roesky, H. W.; Koch, H. J.; Sheldrick, G. M.; Stalke, D.; Kuhn, A. *Angew. Chem., Int. Ed. Engl.* **1993**, *32*, 1729.
(120) Gauss, J.; Schneider, U.; Ahlrichs, R.; Dohmeier, C.; Schnoeckel, H. *J. Am. Chem. Soc.* **1993**, *115*, 2402.
(121) Sitzmann, H.; Lappert, M. F.; Dohmeier, C.; Üffing, C.; Schnöckel, H. *J. Organomet. Chem.* **1998**, *561*, 203.
(122) Haaland, A.; Martinsen, K.-G.; Shlykov, S. A.; Volden, H. V.; Dohmeier, C.; Schnoeckel, H. *Organometallics* **1995**, *14*, 3116.
(123) Purath, A.; Dohmeier, C.; Ecker, A.; Schnöckel, H.; Amelunxen, K.; Passler, T.; Wiberg, N. *Organometallics* **1998**, *17*, 1894.
(124) Purath, A.; Schnöckel, H. *J. Organomet. Chem.* **1999**, *579*, 373.
(125) Schnitter, C.; Roesky, H. W.; Röpken, C.; Herbst-Irmer, R.; Schmidt, H.-G.; Noltemeyer, M. *Angew. Chem., Int. Ed.* **1998**, *37*, 1952.
(126) Linti, G.; Schnöckel, H. *Coord. Chem. Rev.* **2000**, *206–207*, 285.
(127) Sudheendra Rao, M. N.; Roesky, H. W.; Anantharaman, G. *J. Organomet. Chem.* **2002**, *646*, 4.
(128) Roesky, H. W.; Kumar, S. S. *Chem. Commun.* **2005**, 4027.
(129) Li, X.; Cheng, X.; Song, H.; Cui, C. *Organometallics* **2007**, *26*, 1039.
(130) Yang, Z.; Ma, X.; Oswald, R. B.; Roesky, H. W.; Zhu, H.; Schulzke, C.; Starke, K.; Baldus, M.; Schmidt, H.-G.; Noltemeyer, M. *Angew. Chem., Int. Ed.* **2005**, *44*, 7072.

(131) Zhu, H.; Chai, J.; Jancik, V.; Roesky, H. W.; Merrill, W. A.; Power, P. P. *J. Am. Chem. Soc.* **2005**, *127*, 10170.
(132) Peng, Y.; Fan, H.; Jancik, V.; Roesky, H. W.; Herbst-Irmer, R. *Angew. Chem., Int. Ed.* **2004**, *43*, 6190.
(133) Peng, Y.; Fan, H.; Zhu, H.; Roesky, H. W.; Magull, J.; Hughes, C. E. *Angew. Chem., Int. Ed.* **2004**, *43*, 3443.
(134) Hardman, N. J.; Cui, C.; Roesky, H. W.; Fink, W. H.; Power, P. P. *Angew. Chem., Int. Ed.* **2001**, *40*, 2172.
(135) Zhu, H.; Chai, J.; Chandrasekhar, V.; Roesky, H. W.; Magull, J.; Vidovic, D.; Schmidt, H.-G.; Noltemeyer, M.; Power, P. P.; Merrill, W. A. *J. Am. Chem. Soc.* **2004**, *126*, 9472.
(136) Cui, C.; Roesky, H. W.; Schmidt, H.-G.; Noltemeyer, M. *Angew. Chem., Int. Ed.* **2000**, *39*, 4531.
(137) Zhu, H.; Yang, Z.; Magull, J.; Roesky, H. W.; Schmidt, H.-G.; Noltemeyer, M. *Organometallics* **2005**, *24*, 6420.
(138) Zhu, H.; Chai, J.; Stasch, A.; Roesky, Herbert W.; Blunck, T.; Vidovic, D.; Magull, J.; Schmidt, H.-G.; Noltemeyer, M. *Eur. J. Inorg. Chem.* **2004**, *2004*, 4046.
(139) Zhu, H.; Chai, J.; Fan, H.; Roesky, H. W.; Nehete, U. N.; Schmidt, H.-G.; Noltemeyer, M. *Eur. J. Inorg. Chem.* **2005**, *2005*, 2147.
(140) Zhu, H.; Chai, J.; Fan, H.; Roesky, H. W.; He, C.; Jancik, V.; Schmidt, H.-G.; Noltemeyer, M.; Merrill, W. A.; Power, P. P. *Angew. Chem., Int. Ed.* **2005**, *44*, 5090.
(141) Zhu, H.; Oswald, R. B.; Fan, H.; Roesky, H. W.; Ma, Q.; Yang, Z.; Schmidt, H.-G.; Noltemeyer, M.; Starke, K.; Hosmane, N. S. *J. Am. Chem. Soc.* **2006**, *128*, 5100.
(142) Cui, C.; Köpke, S.; Herbst-Irmer, R.; Roesky, H. W.; Noltemeyer, M.; Schmidt, H.-G.; Wrackmeyer, B. *J. Am. Chem. Soc.* **2001**, *123*, 9091.
(143) Li, J.; Li, X.; Huang, W.; Hu, H.; Zhang, J.; Cui, C. *Chem. - Eur. J.* **2012**, *18*, 15263.
(144) Yang, Z.; Ma, X.; Oswald, R. B.; Roesky, H. W.; Noltemeyer, M. *J. Am. Chem. Soc.* **2006**, *128*, 12406.
(145) Kong, L.; Ganguly, R.; Li, Y.; Kinjo, R. *Chem. - Eur. J.* **2016**, *22*, 1922.
(146) Ganesamoorthy, C.; Blaser, D.; Wolper, C.; Schulz, S. *Chem. Commun.* **2014**, *50*, 12382.
(147) Ganesamoorthy, C.; Bläser, D.; Wölper, C.; Schulz, S. *Angew. Chem., Int. Ed.* **2014**, *53*, 11587.
(148) Wang, Y.; Xie, Y.; Wei, P.; King, R. B.; Schaefer, H. F.; von R. Schleyer, P.; Robinson, G. H. *Science* **2008**, *321*, 1069.
(149) Sidiropoulos, A.; Jones, C.; Stasch, A.; Klein, S.; Frenking, G. *Angew. Chem., Int. Ed.* **2009**, *48*, 9701.
(150) Jones, C.; Sidiropoulos, A.; Holzmann, N.; Frenking, G.; Stasch, A. *Chem. Commun.* **2012**, *48*, 9855.
(151) Mondal, K. C.; Roy, S.; Dittrich, B.; Andrada, D. M.; Frenking, G.; Roesky, H. W. *Angew. Chem., Int. Ed.* **2016**, *55*, 3158.
(152) Shan, Y.-L.; Yim, W.-L.; So, C.-W. *Angew. Chem., Int. Ed.* **2014**, *53*, 13155.

(153) Tonner, R.; Frenking, G. *Angew. Chem., Int. Ed.* **2007**, *46*, 8695.
(154) Tonner, R.; Frenking, G. *Chem. - Eur. J.* **2008**, *14*, 3260.
(155) Tonner, R.; Frenking, G. *Chem. - Eur. J.* **2008**, *14*, 3273.
(156) Dyker, C. A.; Lavallo, V.; Donnadieu, B.; Bertrand, G. *Angew. Chem., Int. Ed.* **2008**, *47*, 3206.
(157) Fürstner, A.; Alcarazo, M.; Goddard, R.; Lehmann, C. W. *Angew. Chem., Int. Ed.* **2008**, *47*, 3210.
(158) Takagi, N.; Shimizu, T.; Frenking, G. *Chem. - Eur. J.* **2009**, *15*, 3448.
(159) Takagi, N.; Shimizu, T.; Frenking, G. *Chem. - Eur. J.* **2009**, *15*, 8593.
(160) Takagi, N.; Tonner, R.; Frenking, G. *Chem. - Eur. J.* **2012**, *18*, 1772.
(161) Ishida, S.; Iwamoto, T.; Kabuto, C.; Kira, M. *Nature* **2003**, *421*, 725.
(162) Iwamoto, T.; Masuda, H.; Kabuto, C.; Kira, M. *Organometallics* **2005**, *24*, 197.
(163) Iwamoto, T.; Abe, T.; Kabuto, C.; Kira, M. *Chem. Commun.* **2005**, 5190.
(164) Wiberg, N.; Lerner, H.-W.; Vasisht, S.-K.; Wagner, S.; Karaghiosoff, K.; Nöth, H.; Ponikwar, W. *Eur. J. Inorg. Chem.* **1999**, *1999*, 1211.
(165) Kira, M.; Iwamoto, T.; Ishida, S.; Masuda, H.; Abe, T.; Kabuto, C. *J. Am. Chem. Soc.* **2009**, *131*, 17135.
(166) Mondal, K. C.; Roesky, H. W.; Schwarzer, M. C.; Frenking, G.; Niepötter, B.; Wolf, H.; Herbst-Irmer, R.; Stalke, D. *Angew. Chem., Int. Ed.* **2013**, *52*, 2963.
(167) Niepötter, B.; Herbst-Irmer, R.; Kratzert, D.; Samuel, P. P.; Mondal, K. C.; Roesky, H. W.; Jerabek, P.; Frenking, G.; Stalke, D. *Angew. Chem., Int. Ed.* **2014**, *53*, 2766.
(168) Roy, S.; Mondal, K. C.; Krause, L.; Stollberg, P.; Herbst-Irmer, R.; Stalke, D.; Meyer, J.; Stückl, A. C.; Maity, B.; Koley, D.; Vasa, S. K.; Xiang, S. Q.; Linser, R.; Roesky, H. W. *J. Am. Chem. Soc.* **2014**, *136*, 16776.
(169) Xiong, Y.; Yao, S.; Inoue, S.; Epping, J. D.; Driess, M. *Angew. Chem., Int. Ed.* **2013**, *52*, 7147.
(170) Xiong, Y.; Yao, S.; Müller, R.; Kaupp, M.; Driess, M. *Angew. Chem., Int. Ed.* **2015**, *54*, 10254.
(171) Su, B.; Ganguly, R.; Li, Y.; Kinjo, R. *Angew. Chem., Int. Ed.* **2014**, *53*, 13106.
(172) Su, B.; Ganguly, R.; Li, Y.; Kinjo, R. *Chem. Commun.* **2016**, *52*, 613.
(173) Power, P. P. *Acc. Chem. Res.* **2011**, *44*, 627.
(174) Power, P. P. *Chem. Rec.* **2012**, *12*, 238.
(175) Altman, A. B.; Pemmaraju, C. D.; Camp, C.; Arnold, J.; Minasian, S. G.; Prendergast, D.; Shuh, D. K.; Tyliszczak, T. *J. Am. Chem. Soc.* **2015**, *137*, 10304.
(176) Zhang, X.; Cao, Z. *Dalton Trans.* **2016**, *45*, 10355.
(177) Cui, C.; Roesky, H. W.; Hao, H.; Schmidt, H.-G.; Noltemeyer, M. *Angew. Chem., Int. Ed.* **2000**, *39*, 1815.
(178) Corey, J. Y. *Chem. Rev.* **2011**, *111*, 863.
(179) Dettenrieder, N.; Dietrich, H. M.; Schädle, C.; Maichle-Mössmer, C.; Törnroos, K. W.; Anwander, R. *Angew. Chem., Int. Ed.* **2012**, *51*, 4461.
(180) Beachley, O. T.; Simmons, R. G. *Inorg. Chem.* **1980**, *19*, 3042.
(181) Beachley, O. T.; Rusinko, R. N. *Inorg. Chem.* **1981**, *20*, 1367.
(182) Hallock, R. B.; Beachley, O. T.; Li, Y. J.; Sanders, W. M.; Churchill, M. R.; Hunter, W. E.; Atwood, J. L. *Inorg. Chem.* **1983**, *22*, 3683.

(183) Ganesamoorthy, C.; Loerke, S.; Gemel, C.; Jerabek, P.; Winter, M.; Frenking, G.; Fischer, R. A. *Chem. Commun.* **2013**, *49*, 2858.
(184) Gorden, J. D.; Voigt, A.; Macdonald, C. L. B.; Silverman, J. S.; Cowley, A. H. *J. Am. Chem. Soc.* **2000**, *122*, 950.
(185) Romero, P. E.; Piers, W. E.; Decker, S. A.; Chau, D.; Woo, T. K.; Parvez, M. *Organometallics* **2003**, *22*, 1266.
(186) Uhl, W.; Jana, B. *Chem. - Eur. J.* **2008**, *14*, 3067.
(187) Uhl, W.; Jana, B. *J. Organomet. Chem.* **2009**, *694*, 1101.
(188) Atwood, D. A.; Contreras, L.; Cowley, A. H.; Jones, R. A.; Mardones, M. A. *Organometallics* **1993**, *12*, 17.
(189) Janik, J. F.; Wells, R. L.; White, P. S. *Inorg. Chem.* **1998**, *37*, 3561.
(190) Andrews, P. C.; Raston, C. L.; Roberts, B. A. *Chem. Commun.* **2000**, 1961.
(191) Vogel, U.; Timoshkin, A. Y.; Scheer, M. *Angew. Chem., Int. Ed.* **2001**, *40*, 4409.
(192) Vogel, U.; Timoshkin, A. Y.; Schwan, K.-C.; Bodensteiner, M.; Scheer, M. *J. Organomet. Chem.* **2006**, *691*, 4556.
(193) Bodensteiner, M.; Vogel, U.; Timoshkin, A. Y.; Scheer, M. *Angew. Chem., Int. Ed.* **2009**, *48*, 4629.
(194) Melton, C. E.; Dube, J. W.; Ragogna, P. J.; Fettinger, J. C.; Power, P. P. *Organometallics* **2014**, *33*, 329.
(195) Janik, J. F.; Wells, R. L.; White, P. S. *Organometallics* **1998**, *17*, 2361.
(196) von Hänisch, C.; Rolli, B. *Z. Anorg. Allg. Chem.* **2004**, *630*, 1987.
(197) Healy, M. D.; Mason, M. R.; Gravelle, P. W.; Bott, S. G.; Barron, A. R. *J. Chem. Soc., Dalton Trans.* **1993**, 441.
(198) Campbell, J. P.; Gladfelter, W. L. *Inorg. Chem.* **1997**, *36*, 4094.
(199) Shekar, S.; Taylor, M. M.; Twamley, B.; Wehmschulte, R. J. *Dalton Trans.* **2009**, 9322.
(200) Nöth, H.; Schlegel, A.; Knizek, J.; Krossing, I.; Ponikwar, W.; Seifert, T. *Chem. - Eur. J.* **1998**, *4*, 2191.
(201) Hiyama, T. *Organofluorine Compounds: Chemistry and Applications*; Springer Berlin Heidelberg, 2010.
(202) Macgregor, S. A.; McKay, D.; Panetier, J. A.; Whittlesey, M. K. *Dalton Trans.* **2013**, *42*, 7386.
(203) Johnson, S. A.; Hatnean, J. A.; Doster, M. E. In *Progress in Inorganic Chemistry*; John Wiley & Sons, Inc.: Hoboken, 2011; Vol. 57, p 255.
(204) Crimmin, M. R.; Butler, M. J.; White, A. J. P. *Chem. Commun.* **2015**, *51*, 15994.
(205) Yow, S.; Gates, S. J.; White, A. J. P.; Crimmin, M. R. *Angew. Chem., Int. Ed.* **2012**, *51*, 12559.
(206) Choi, J.; Wang, D. Y.; Kundu, S.; Choliy, Y.; Emge, T. J.; Krogh-Jespersen, K.; Goldman, A. S. *Science* **2011**, *332*, 1545.
(207) Barrett, A. G. M.; Crimmin, M. R.; Hill, M. S.; Hitchcock, P. B.; Procopiou, P. A. *Angew. Chem., Int. Ed.* **2007**, *46*, 6339.
(208) Träff, A. M.; Janjetovic, M.; Ta, L.; Hilmersson, G. *Angew. Chem., Int. Ed.* **2013**, *52*, 12073.
(209) Yow, S.; Nako, A. E.; Neveu, L.; White, A. J. P.; Crimmin, M. R. *Organometallics* **2013**, *32*, 5260.

(210) Jancik, V.; Peng, Y.; Roesky, H. W.; Li, J.; Neculai, D.; Neculai, A. M.; Herbst-Irmer, R. *J. Am. Chem. Soc.* **2003**, *125*, 1452.
(211) Khan, S.; Sen, S. S.; Kratzert, D.; Tavčar, G.; Roesky, H. W.; Stalke, D. *Chem. - Eur. J.* **2011**, *17*, 4283.
(212) Mück, F. M.; Baus, J. A.; Burschka, C.; Tacke, R. *Chem. - Eur. J.* **2016**, *22*, 5830.
(213) Foley, S. R.; Yap, G. P. A.; Richeson, D. S. *J. Chem. Soc., Dalton Trans.* **2000**, 1663.
(214) Huang, M.; Kireenko, M. M.; Zaitsev, K. V.; Oprunenko, Y. F.; Churakov, A. V.; Howard, J. A. K.; Lermontova, E. K.; Sorokin, D.; Linder, T.; Sundermeyer, J.; Karlov, S. S.; Zaitseva, G. S. *Eur. J. Inorg. Chem.* **2012**, *2012*, 3712.
(215) Huang, M.; Kireenko, M. M.; Zaitsev, K. V.; Oprunenko, Y. F.; Churakov, A. V.; Howard, J. A. K.; Zabalov, M. V.; Lermontova, E. K.; Sundermeyer, J.; Linder, T.; Karlov, S. S.; Zaitseva, G. S. *J. Organomet. Chem.* **2012**, *706–707*, 66.
(216) Steiniger, P.; Bendt, G.; Blaser, D.; Wolper, C.; Schulz, S. *Chem. Commun.* **2014**, *50*, 15461.
(217) Bendt, G.; Lapsien, S.; Steiniger, P.; Bläser, D.; Wölper, C.; Schulz, S. *Z. Anorg. Allg. Chem.* **2015**, *641*, 797.
(218) Hitchcock, P. B.; Lappert, M. F.; Pierssens, L. J. M.; Protchenko, A. V.; Uiterweerd, P. G. H. *Dalton Trans.* **2009**, 4578.
(219) Wagner, M.; Dietz, C.; Bouška, M.; Dostál, L.; Padělková, Z.; Jambor, R.; Jurkschat, K. *Organometallics* **2013**, *32*, 4973.
(220) Pop, A.; Wang, L.; Dorcet, V.; Roisnel, T.; Carpentier, J.-F.; Silvestru, A.; Sarazin, Y. *Dalton Trans.* **2014**, *43*, 16459.
(221) Šimon, P.; Jambor, R.; Růžička, A.; Dostál, L. *J. Organomet. Chem.* **2013**, *740*, 98.
(222) Šimon, P.; Jambor, R.; Růžička, A.; Dostál, L. *Organometallics* **2013**, *32*, 239.
(223) Dureen, M. A.; Welch, G. C.; Gilbert, T. M.; Stephan, D. W. *Inorg. Chem.* **2009**, *48*, 9910.
(224) Inés, B.; Holle, S.; Goddard, R.; Alcarazo, M. *Angew. Chem., Int. Ed.* **2010**, *49*, 8389.
(225) Knabel, K.; Krossing, I.; Nöth, H.; Schwenk-Kircher, H.; Schmidt-Amelunxen, M.; Seifert, T. *Eur. J. Inorg. Chem.* **1998**, *1998*, 1095.
(226) Myers, T. W.; Holmes, A. L.; Berben, L. A. *Inorg. Chem.* **2012**, *51*, 8997.
(227) Jancik, V.; Moya Cabrera, Monica M.; Roesky, Herbert W.; Herbst-Irmer, R.; Neculai, D.; Neculai, Ana M.; Noltemeyer, M.; Schmidt, H.-G. *Eur. J. Inorg. Chem.* **2004**, *2004*, 3508.
(228) Scheer, M.; Balázs, G.; Seitz, A. *Chem. Rev.* **2010**, *110*, 4236.
(229) Giffin, N. A.; Masuda, J. D. *Coord. Chem. Rev.* **2011**, *255*, 1342.
(230) Khan, S.; Sen, S. S.; Roesky, H. W. *Chem. Commun.* **2012**, *48*, 2169.
(231) Baker, R. T.; Whitney, J. F.; Wreford, S. S. *Organometallics* **1983**, *2*, 1049.
(232) Hayes, P. G.; Piers, W. E.; Lee, L. W. M.; Knight, L. K.; Parvez, M.; Elsegood, M. R. J.; Clegg, W. *Organometallics* **2001**, *20*, 2533.
(233) Herrmann, W. A.; Köcher, C. *Angew. Chem., Int. Ed. Engl.* **1997**, *36*, 2162.
(234) Denk, M. K.; Thadani, A.; Hatano, K.; Lough, A. J. *Angew. Chem., Int. Ed. Engl.* **1997**, *36*, 2607.

(235) Jancik, V.; Roesky, H. W.; Neculai, D.; Neculai, A. M.; Herbst-Irmer, R. *Angew. Chem., Int. Ed.* **2004**, *43*, 6192.
(236) Jancik, V.; Roesky, H. W. *Inorg. Chem.* **2005**, *44*, 5556.
(237) Gómora-Figueroa, A. P.; Jancik, V.; Cea-Olivares, R.; Toscano, R. A. *Inorg. Chem.* **2007**, *46*, 10749.
(238) Xiong, Y.; Yao, S.; Driess, M. *J. Am. Chem. Soc.* **2009**, *131*, 7562.
(239) Kennedy, A. R.; Mulvey, R. E.; Robertson, S. D. *Dalton Trans.* **2010**, *39*, 9091.
(240) Schmitt, A.-L.; Schnee, G.; Welter, R.; Dagorne, S. *Chem. Commun.* **2010**, *46*, 2480.
(241) Mayer, I. *Chem. Phys. Lett.* **1983**, *97*, 270.
(242) Mayer, I. *Int. J. Quantum Chem.* **1984**, *26*, 151.
(243) Wiberg, K. B. *Tetrahedron* **1968**, *24*, 1083.
(244) Reed, A. E.; Weinstock, R. B.; Weinhold, F. *J. Chem. Phys.* **1985**, *83*, 735.
(245) Liu, M.-F.; Wang, B.; Cheng, Y. *Chem. Commun.* **2006**, 1215.
(246) Bittner, A.; Männig, D.; Nöth, H. *Z. Naturforsch., B* **1986**, *41*, 587.
(247) Driess, M.; Yao, S.; Brym, M.; van Wüllen, C. *Angew. Chem., Int. Ed.* **2006**, *45*, 6730.
(248) Stennett, T. E.; Pahl, J.; Zijlstra, H. S.; Seidel, F. W.; Harder, S. *Organometallics* **2016**, *35*, 207.
(249) Chirik, P. J. *Inorg. Chem.* **2011**, *50*, 9737.
(250) Kaim, W. *Eur. J. Inorg. Chem.* **2012**, *2012*, 343.
(251) Luca, O. R.; Crabtree, R. H. *Chem. Soc. Rev.* **2013**, *42*, 1440.
(252) Bart, S. C.; Chłopek, K.; Bill, E.; Bouwkamp, M. W.; Lobkovsky, E.; Neese, F.; Wieghardt, K.; Chirik, P. J. *J. Am. Chem. Soc.* **2006**, *128*, 13901.
(253) Enright, D.; Gambarotta, S.; Yap, G. P. A.; Budzelaar, P. H. M. *Angew. Chem., Int. Ed.* **2002**, *41*, 3873.
(254) Bart, S. C.; Lobkovsky, E.; Chirik, P. J. *J. Am. Chem. Soc.* **2004**, *126*, 13794.
(255) Russell, S. K.; Darmon, J. M.; Lobkovsky, E.; Chirik, P. J. *Inorg. Chem.* **2010**, *49*, 2782.
(256) Bowman, A. C.; Milsmann, C.; Atienza, C. C. H.; Lobkovsky, E.; Wieghardt, K.; Chirik, P. J. *J. Am. Chem. Soc.* **2010**, *132*, 1676.
(257) Bowman, A. C.; Milsmann, C.; Bill, E.; Lobkovsky, E.; Weyhermüller, T.; Wieghardt, K.; Chirik, P. J. *Inorg. Chem.* **2010**, *49*, 6110.
(258) Trovitch, R. J.; Lobkovsky, E.; Bill, E.; Chirik, P. J. *Organometallics* **2008**, *27*, 1470.
(259) Monfette, S.; Turner, Z. R.; Semproni, S. P.; Chirik, P. J. *J. Am. Chem. Soc.* **2012**, *134*, 4561.
(260) Yu, R. P.; Darmon, J. M.; Hoyt, J. M.; Margulieux, G. W.; Turner, Z. R.; Chirik, P. J. *ACS Catal.* **2012**, *2*, 1760.
(261) Friedfeld, M. R.; Shevlin, M.; Margulieux, G. W.; Campeau, L.-C.; Chirik, P. J. *J. Am. Chem. Soc.* **2016**, *138*, 3314.
(262) Tondreau, A. M.; Atienza, C. C. H.; Weller, K. J.; Nye, S. A.; Lewis, K. M.; Delis, J. G. P.; Chirik, P. J. *Science* **2012**, *335*, 567.
(263) Hojilla Atienza, C. C.; Tondreau, A. M.; Weller, K. J.; Lewis, K. M.; Cruse, R. W.; Nye, S. A.; Boyer, J. L.; Delis, J. G. P.; Chirik, P. J. *ACS Catal.* **2012**, *2*, 2169.

(264) Atienza, C. C. H.; Diao, T.; Weller, K. J.; Nye, S. A.; Lewis, K. M.; Delis, J. G. P.; Boyer, J. L.; Roy, A. K.; Chirik, P. J. *J. Am. Chem. Soc.* **2014**, *136*, 12108.
(265) Obligacion, J. V.; Chirik, P. J. *Org. Lett.* **2013**, *15*, 2680.
(266) Obligacion, J. V.; Chirik, P. J. *J. Am. Chem. Soc.* **2013**, *135*, 19107.
(267) Obligacion, J. V.; Neely, J. M.; Yazdani, A. N.; Pappas, I.; Chirik, P. J. *J. Am. Chem. Soc.* **2015**, *137*, 5855.
(268) Martin, C. D.; Ragogna, P. J. *Dalton Trans.* **2011**, *40*, 11976.
(269) Magdzinski, E.; Gobbo, P.; Martin, C. D.; Workentin, M. S.; Ragogna, P. J. *Inorg. Chem.* **2012**, *51*, 8425.
(270) Flock, J.; Suljanovic, A.; Torvisco, A.; Schoefberger, W.; Gerke, B.; Pöttgen, R.; Fischer, R. C.; Flock, M. *Chem. - Eur. J.* **2013**, *19*, 15504.
(271) Myers, T. W.; Berben, L. A. *J. Am. Chem. Soc.* **2013**, *135*, 9988.
(272) Thompson, E. J.; Myers, T. W.; Berben, L. A. *Angew. Chem., Int. Ed.* **2014**, *53*, 14132.
(273) Thompson, E. J.; Berben, L. A. *Angew. Chem., Int. Ed.* **2015**, *54*, 11642.
(274) Parkin, G. *Chem. Rev.* **2004**, *104*, 699.
(275) Li, T.; Schulz, S.; Roesky, P. W. *Chem. Soc. Rev.* **2012**, *41*, 3759.
(276) Oda, A.; Torigoe, H.; Itadani, A.; Ohkubo, T.; Yumura, T.; Kobayashi, H.; Kuroda, Y. *J. Am. Chem. Soc.* **2013**, *135*, 18481.
(277) Hicks, J.; Underhill, E. J.; Kefalidis, C. E.; Maron, L.; Jones, C. *Angew. Chem., Int. Ed.* **2015**, *54*, 10000.
(278) Banh, H.; Dilchert, K.; Schulz, C.; Gemel, C.; Seidel, R. W.; Gautier, R.; Kahlal, S.; Saillard, J.-Y.; Fischer, R. A. *Angew. Chem., Int. Ed.* **2016**, *55*, 3285.
(279) Wei, L.; Yang, Y.; Fan, R.; Wang, P.; Li, L.; Yu, J.; Yang, B.; Cao, W. *RSC Adv.* **2013**, *3*, 25908.
(280) Singh, A. P.; Roesky, H. W.; Carl, E.; Stalke, D.; Demers, J.-P.; Lange, A. *J. Am. Chem. Soc.* **2012**, *134*, 4998.
(281) Davidson, P. J.; Hudson, A.; Lappert, M. F.; Lednor, P. W. *J. Chem. Soc., Chem. Commun.* **1973**, 829.
(282) Lee, V. Y.; Sekiguchi, A. *Acc. Chem. Res.* **2007**, *40*, 410.
(283) Woodul, W. D.; Carter, E.; Müller, R.; Richards, A. F.; Stasch, A.; Kaupp, M.; Murphy, D. M.; Driess, M.; Jones, C. *J. Am. Chem. Soc.* **2011**, *133*, 10074.
(284) Fukuzumi, S.; Ohkubo, K.; Tokuda, Y.; Suenobu, T. *J. Am. Chem. Soc.* **2000**, *122*, 4286.
(285) Fukuzumi, S.; Endo, Y.; Imahori, H. *J. Am. Chem. Soc.* **2002**, *124*, 10974.
(286) Yoder, J. C.; Roth, J. P.; Gussenhoven, E. M.; Larsen, A. S.; Mayer, J. M. *J. Am. Chem. Soc.* **2003**, *125*, 2629.
(287) Mader, E. A.; Larsen, A. S.; Mayer, J. M. *J. Am. Chem. Soc.* **2004**, *126*, 8066.
(288) Fan, R.; Zhu, D.; Ding, H.; Mu, Y.; Su, Q.; Xia, H. *Synth. Met.* **2005**, *149*, 135.
(289) Myers, T. W.; Sherbow, T. J.; Fettinger, J. C.; Berben, L. A. *Dalton Trans.* **2016**, *45*, 5989.
(290) Yang, L.; Powell, D. R.; Houser, R. P. *Dalton Trans.* **2007**, 955.
(291) Addison, A. W.; Rao, T. N.; Reedijk, J.; van Rijn, J.; Verschoor, G. C. *J. Chem. Soc., Dalton Trans.* **1984**, 1349.
(292) Chai, J.-D.; Head-Gordon, M. *Phys. Chem. Chem. Phys.* **2008**, *10*, 6615.

(293) Minenkov, Y.; Singstad, A.; Occhipinti, G.; Jensen, V. R. *Dalton Trans.* **2012**, *41*, 5526.
(294) Stoll, S.; Schweiger, A. *J. Magn. Reson.* **2006**, *178*, 42.
(295) Lawrence, N. J.; Beynek, H. *Synlett* **1998**, *1998*, 497.
(296) Dai, M.; Wang, C.; Dong, G.; Xiang, J.; Luo, T.; Liang, B.; Chen, J.; Yang, Z. *Eur. J. Org. Chem.* **2003**, *2003*, 4346.
(297) Sauerbrey, S.; Majhi, P. K.; Schnakenburg, G.; Arduengo Iii, A. J.; Streubel, R. *Dalton Trans.* **2012**, *41*, 5368.
(298) Smellie, I. A. In *Inorganic Experiments*; 3 ed.; Woollins, J. D., Ed.; Wiley-VCH Verlag GmbH & Co. KGaA: Weinheim, Germany, 2010, p 81.
(299) Britovsek, G. J. P.; Bruce, M.; Gibson, V. C.; Kimberley, B. S.; Maddox, P. J.; Mastroianni, S.; McTavish, S. J.; Redshaw, C.; Solan, G. A.; Strömberg, S.; White, A. J. P.; Williams, D. J. *J. Am. Chem. Soc.* **1999**, *121*, 8728.
(300) Pinter, B.; Smith, K. T.; Kamitani, M.; Zolnhofer, E. M.; Tran, B. L.; Fortier, S.; Pink, M.; Wu, G.; Manor, B. C.; Meyer, K.; Baik, M.-H.; Mindiola, D. J. *J. Am. Chem. Soc.* **2015**, *137*, 15247.
(301) Chu, C.; Yang, Y.; Zhu, H. *Sci. China Chem.* **2010**, *53*, 1970.